Max-Planck-Institut für Meteorologie
Max Planck Institute for Meteorology

MAX-PLANCK-GESELLSCHAFT

Glacial and interglacial climate during the late Quaternary: global circulation model simulations and comparison with proxy data

Stephan J. Lorenz

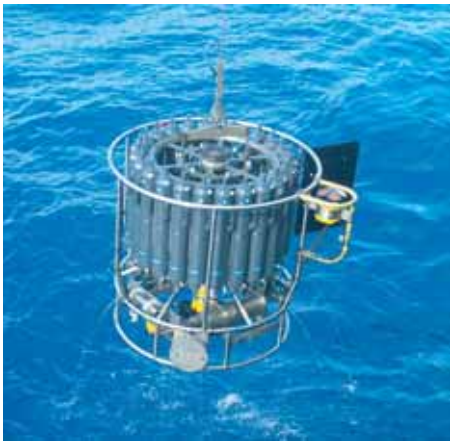

Berichte zur Erdsystemforschung 43/2007

Reports on Earth System Science

Hinweis

Die Berichte zur Erdsytemforschung werden vom Max-Planck-Institut für Meteorologie in Hamburg in unregelmäßiger Abfolge herausgegeben.

Sie enthalten wissenschaftliche und technische Beiträge, inklusive Dissertationen.

Die Beiträge geben nicht notwendigerweise die Auffassung des Instituts wieder.

Die "Berichte zur Erdsystemforschung" führen die vorherigen Reihen "Reports" und "Examensarbeiten" weiter.

Notice

The Reports on Earth System Science are published by the Max Planck Institute for Meteorology in Hamburg. They appear in irregular intervals.

They contain scientific and technical contributions, including Ph. D. theses.

The Reports do not necessarily reflect the opinion of the Institute.

The "Reports on Earth System Science" continue the former "Reports" and "Examensarbeiten" of the Max Planck Institute.

Anschrift / Address

Max-Planck-Institut für Meteorologie
Bundesstrasse 53
20146 Hamburg
Deutschland

Tel.: +49-(0)40-4 11 73-0
Fax: +49-(0)40-4 11 73-298
Web: www.mpimet.mpg.de

Layout:

Bettina Diallo, PR & Grafik

Titelfotos:
vorne:
Christian Klepp - Jochem Marotzke - Christian Klepp
hinten:
Clotilde Dubois - Christian Klepp - Katsumasa Tanaka

Berichte zur Erdsystemforschung 43/2007

Glacial and interglacial climate during the late Quaternary: global circulation model simulations and comparison with proxy data

Dissertation zur Erlangung des Doktorgrades der Naturwissenschaften
im Departement Geowissenschaften der Universität Hamburg
vorgelegt von

Stephan J. Lorenz
aus Tübingen

Hamburg 2007

Reports on Earth System Science 43/2007

ISSN 1614-1199

Stephan J. Lorenz
Max-Planck-Institut für Meteorologie
Bundesstrasse 53
20146 Hamburg
Germany

Als Dissertation angenommen
vom Departement Geowissenschaften der Universität Hamburg

auf Grund der Gutachten von
Prof. Dr. Martin Claußen
und
Prof. Dr. Gerrit Lohmann

Hamburg, den 16. Mai 2006
Prof. Dr. Kay-Christian Emeis
Leiter des Departements für Geowissenschaften

ISSN 1614-1199

Glacial and interglacial climate during the late Quaternary: global circulation model simulations and comparison with proxy data

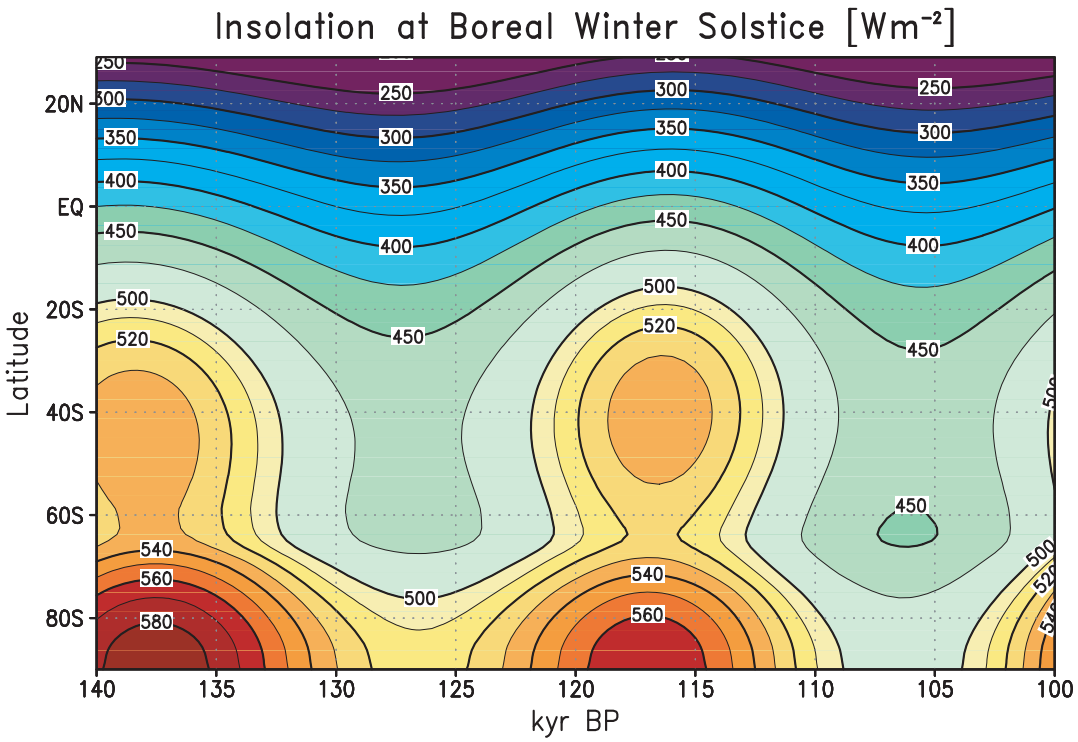

Stephan J. Lorenz

Hamburg 2007

Contents

Abstract

The Earth's climate experienced long-term cycles during the late Quaternary. The climate varied between relatively short warm interglacial climates and longer glacial cold phases, where the Northern Hemisphere was largely covered by continental ice. The last of these glacial cycles spans from the Eemian interglacial phase at 125.000 years ago (125 kyr ago), via the last glacial maximum (LGM, 21 kyr ago), up to the still ongoing interglacial phase, the Holocene (the last 10 kyr). For the understanding of processes that have caused this natural climate variability an integrated model-data approach is proposed: in order to achieve a consistent interpretation of late Quaternary climate variability, a combined assessment of simulations with atmospheric and oceanic general circulation models (GCM) concomitantly with analysis of recent marine and terrestrial proxy data from the Eemian, the LGM, and the Holocene climate is applied.

When investigating the tropical climate of the LGM, a series of atmospheric GCM simulations with varying lower boundary condition are utilised to deduce inversely the best fit with terrestrial temperature proxies derived from glacier debris stemming from the LGM. Such remainders from tropical glaciers suggest, besides others, a much stronger cooling of air temperature at the height of the snowline (near the 0°C level) than at sea level. Motivated by various studies suggesting that the estimates of glacial sea surface temperatures (SST) by the CLIMAP (Climate: Long-Range Investigation, Mapping, and Prediction) project are too warm, simulations of the LGM climate are forced by SSTs that are 3°C colder in the tropical oceans than the CLIMAP distribution. In the Atlantic, the recent reconstruction of SST by the Glacial Atlantic Ocean Mapping Project (GLAMAP) is also used. Due to reduced water vapour in the tropical troposphere when driven by cooler SST, the simulated environmental lapse rate increased. A further cooling occurred in the surface air temperature at the snowline level due to a longer snow coverage and the snow-albedo feedback. The simulations exhibit a possible coexistence of moderately cooler SSTs than supposed by CLIMAP and a tropical snowline lowering of about 900 m during LGM.

For an assessment of the impact of the Earth's orbital parameters on the evolution of long-term climate trends in the late Quaternary, a different model-data approach is applied. A coupled atmosphere-ocean GCM is used in order to simulate surface ocean and air temperatures independently from proxy-derived SST. Combined analysis of climate trend patterns from simulation data and globally distributed alkenone-derived SST trends during the middle to late Holocene can elucidate the role of the orbitally driven insolation forcing. Moreover, imprints of a major atmospheric circulation pattern are deduced in the model simulations and related (1) to temperature patterns in the alkenone-derived trends, and (2) to changes in the seasonal cycle as recorded in two fossil corals from the Eemian and late Holocene periods.

Millennial-scale palaeoclimate simulations are enabled by the application of acceleration factors of 10 and 100 to the orbitally driven insolation forcing. This method can be justified by the explicitly distinct timescales of the involved processes, which are 10 kyr for the orbital parameters and up to several years for the near-surface feedback in the atmosphere-ocean system. Results from the transient simulations with six ensemble members of the mid-Holocene climate at 6 kyr ago depict considerable differences to atmosphere-alone model simulations: at high latitudes, the strongest warming relative

to the present climate takes place in October, when the upper ocean stored the warming of the preceding boreal summer insolation inducing a longer ice-free season and reduced snow cover. This indicates a strong nonlinear response in the atmosphere-ocean-sea ice system to the radiative forcing.

The model results and the reconstructed SST trends derived from the alkenone-method both exhibit a cooling of up to 3°C in high latitudes, and minor warming in low latitudes during the last 7 kyr. These surface temperature trends are driven to a large extent by the astronomical insolation signal. Superimposed on this trend, a temperature pattern related to a change of the modern Arctic/North Atlantic Oscillation (AO/NAO) is found. The signal of a change in this pattern is strong during winter, but is also impressed upon the simulated Holocene annual mean trends in the European and North Atlantic region. This signal can as well be identified in the alkenone-derived SST distribution. It is found that changes in the entire seasonal cycle of insolation played an important role for the temporal evolution of Holocene surface temperatures. In addition to the strong influence of summer insolation on climate in high latitudes, a notable shift in the maximum insolation of the year in low latitudes occurs. For understanding of marine proxy data, such a shift is important, because it can be able to influence timing of phytoplankton production and thus to alter the seasonal origin of temperature signals recorded in the proxies.

Three independent ensemble simulations of the transition from the Eemian interglacial to the onset of the last glaciation have been performed using the acceleration technique for the orbitally driven insolation forcing. In these simulations the AO/NAO pattern is enhanced corresponding to the much stronger eccentricity of more than 4 % during that time. Seasonally resolved temperature reconstructions from fossil corals in the northern Red Sea corroborate the enhanced influence of a positive phase of the AO/NAO-like pattern on the seasonal cycle. Northerly winds lead to an additional winter cooling; simultaneously, warmer winter temperatures in central Europe of more than 5°C exceed the little effect of decreased winter insolation in middle latitudes.

The combined assessment of simulation data as well as marine and terrestrial palaeoclimate data from the Eemian, the Holocene, and the LGM revealed that orbitally driven changes in the seasonal cycle of insolation have substantially contributed to the climate variability during the last glacial cycle. For a comparison of natural climate variability and anthropogenic change of the long-term future by using climate models, the variation of the Earth's orbital parameters have to be taken into account.

Zusammenfassung

Im Spätquatär hat das Klima der Erde regelmäßige Schwankungen zwischen relativ kurzen Warmphasen (Interglazialen) und langen glazialen Kaltphasen, mit großen Inlandeisen auf der Nordhalbkugel durchlaufen. Der letzte dieser Eiszeitzyklen reicht von der Eem-Warmzeit vor 125 000 Jahren über das letzte glaziale Maximum (LGM, vor 21 000 Jahren) bis zum Holozän, der noch heute andauernden Warmzeit (die letzten 10 000 Jahre). Um die Prozesse verstehen zu können, die diese Klimaschwankungen verursacht haben, wird ein integrierter Modell-Daten Ansatz verfolgt: Hierfür werden Simulationen mit Zirkulationsmodellen für Atmosphäre und Ozean (general circulation models, GCM) sowie marine und terrestrische Proxy-Daten aus dem Eem, dem LGM und dem Holozän für eine konsistente Interpretation der natürlichen Klimavariabilität im Spätquartär analysiert.

Für die Untersuchung des tropischen Klimas im LGM wird eine Serie von Simulationen mit einem atmosphärischen GCM mit unterschiedlichen Meeresoberflächentemperaturen (SST) als unterer Randbedingung erstellt. Sie ermöglicht die Auswahl einer Simulation, die am besten mit terrestrischen Temperatur-Rekonstruktionen, abgeleitet von Gletscher-Moränen aus dem LGM, vereinbar ist. Solche Rückstände von tropischen Gletschern lassen eine erheblich stärkere Abkühlung der glazialen Lufttemperatur in Höhe der Schneelinie (nahe der 0° C Isotherme), als in Meereshöhe vermuten. Motiviert durch die vielfach diskutierte Ansicht, dass die vom CLIMAP Projekt (Climate: Long-Range Investigation, Mapping, and Prediction) für das LGM rekonstruierte SST-Verteilung in den Tropen zu warm ausfällt, wurden Simulation des LGM von einer SST-Verteilung angetrieben, die in den niederen Breiten um 3°C abgekühlt wurden. Durch den geringeren Wasserdampfgehalt der kühleren tropischen Atmosphäre ergibt sich ein verstärkter vertikaler Temperaturgradient. Eine zusätzliche Abkühlung wird in der bodennahen Luftschicht in Höhe der tropischen Schneelinie durch eine längere Schneebedeckung ausgelöst. Die Simulationen zeigen, dass moderat kühlere SST und eine Schneelinienabsenkung von etwa einem Kilometer an tropischen Gletschern während des LGM gleichzeitig aufgetreten sein können.

Für eine Beurteilung des Einflusses erdgeschichtlicher Änderungen der astronomischen Erdbahnparameter auf das Klima, werden langfristige Simulationen mit Hilfe eines gekoppelten GCM erstellt, das die Temperaturen an der Grenzschicht zwischen Atmophäre und Ozean unabhängig von Proxydaten berechnet. Die gemeinsame Analyse von Temperaturtends mit ihren typischen Mustern, sowohl aus Simulationsergebnissen, als auch aus global verteilten Rekonstruktionen der Holozänen SST, abgeleitet nach der geochemischen Untersuchung von Alkenonen aus Tiefseebohrkernen, kann den Einfluss der Erdbahnparameter auf das Klima des Holozäns aufklären. Hierbei wird auch das typische Muster der nordhemisphärischen Winterzirkulation im Modell bestimmt und mit den (1) Mustern der aus Alkenonen abgeleiteten Temperaturtrends sowie mit (2) einem veränderten Jahresgang, hergeleitet aus zwei fossilen Korallen aus dem Eem und dem späten Holozän, verknüpft.

Die erforderlichen paläoklimatischen Simulationen über mehrere Jahrtausende wurden dadurch ermöglicht, dass die Änderung der orbitalen Parameter um den Faktor 10 bzw. 100 gegenüber den vom Modell simulierten Klimavariationen beschleunigt wurden. Dies kann durch die eindeutige Trennung der in den Prozessen involvierten Zeitskalen begründet werden, die etwa 10 000 Jahre für die Orbitalparameter und wenige Jahre für die oberflächennahen Wechselwirkungen im System Atmo-

sphäre-Ozean betragen. Ergebnisse aus den transienten Simulationen für das Klima des mittleren Holozäns vor 6 000 Jahren (sechs unabhängige Simulationen) zeigen erhebliche Unterschiede zu den Ergebnissen mit Atmosphäremodellen ohne Kopplung an ein Ozeanmodell. In hohen Breiten tritt die stärkste Erwärmung im Oktober auf, indem die oberste Ozeanschicht die erhöhte Sonneneinstrahlung der Sommermonate gespeichert hat. Dadurch verlängert sich die meereis- und schneefreie Jahreszeit. Dies verdeutlicht die nichtlineare Wechselwirkung des gekoppelten Systems aus Atmosphäre, Ozean und Meereis mit dem Antrieb durch die veränderliche Sonneneinstrahlung.

Der Vergleich von SST-Trends aus Modellergebnissen und Alkenonen zeigt großräumig übereinstimmend eine Abkühlung von bis zu 3°C in hohen Breiten und geringere Erwärmung in den niederen Breiten, die durch den astronomischen Antrieb maßgeblich hervorgerufen werden. Diesen Trends überlagert findet sich ein Temperatur-Muster, das mit einer Änderung der heutigen Arktischen bzw. Nordatlantischen Oszillation (AO/NAO) verbunden ist. Das Muster dieser Änderung ist besonders deutlich im Winter der Nordhemisphäre, es wird jedoch im Europäischen und Nortatlantischen Raum den simulierten Temperatur-Trends auch im Jahresmittel aufgeprägt und findet sich ebenso in der Verteilung der Holozänen SST-Trends aus Alkenonen. Diese Ergebnisse zeigen, dass Änderungen im gesamten Jahresgang der Einstrahlung einen wichtigen Einfluss auf die zeitliche Entwicklung der Holozänen Temperaturtrends ausüben. Neben der wichtigen Rolle der Sommereinstrahlung auf das Klima in hohen Breiten, tritt eine Verschiebung des Maximums der Sonneneinstrahlung auch in den niederen Breiten auf. Für die Interpretation von marinen Proxy-Daten ist diese Verschiebung wichtig, weil sie zu einer Verschiebung in der Jahreszeit der Phytoplankton-Blüte, und damit zu einer neuen Zuordnung einer SST Rekonstruktion zu einer Jahreszeit führen kann.

In drei unabhängigen Modellsimulationen des Überganges von der Eem-Warmzeit zur letzten Eiszeit, die ebenfalls mit beschleunigtem Antrieb durch die astronomischen Parameter angetrieben wurden, tritt das AO/NAO Muster mit erheblich verstärkter positiver Phase während des Eem auf, korrespondierend mit der extremeren Exzentrizität von über 4 %. Saisonal aufgelöste Temperaturrekonstruktionen aus fossilen Korallen im nördlichen Roten Meer bestätigen den Einfluss einer stark positiven Phase des AO/NAO-Musters auf den Jahresgang. Gleichzeitig mit westlicher Strömung und über 5°C wärmeren Wintern in Zentraleuropa, die trotz einer in mittleren Breiten geringeren Sonneneinstrahlung auftreten, führen nördliche Winde zu bis zu 3°C kälteren Wintern im Roten Meer.

Die gemeinsame Interpretation von Modelldaten sowie marinen und terrestrischen Rekonstruktionen des Paläoklimas aus dem Eem, dem Holozän und dem LGM haben gezeigt, dass die astronomisch ausgelösten Änderungen im Jahresgang der Sonneneinstrahlung einen wichtigen Beitrag zu den natürlichen Klimaschwankungen während des letzten Eiszeitzyklusses geliefert haben. Für einen Vergleich von langfristigen natürlichen Klimaschwankungen und der anthropogen beeinflussten Entwicklung unseres Klimas der nächsten Jahrtausende mit Hilfe von Klimamodellen, müssen die bekannten Schwankungen der Orbitalparameter der Erde berücksichtigt werden.

Chapter 1

Introduction

During the late Quaternary, the Earth's climate experienced long-term climate variations. The climate varied between relatively short warm interglacial climates and longer cold phases, where the Northern Hemisphere was largely covered by continental ice [e. g., *Emiliani*, 1955; *Hays et al.*, 1976; *Imbrie et al.*, 1984]. Within at least the last 800,000 years (800 kyr), these variations operate to a large degree on a timescale of 100 kyr. The causes of this long-term climate cycle are not yet fully understood. Figure 1.1 depicts similar global and local climate fluctuations of the last 420 kyr derived from the Vostok ice core in central Antarctica [*Petit et al.*, 1999] and a deep sea core from the equatorial Pacific [*Lea et al.*, 2000]. The most recent of these glacial cycles lasted from the Eemian interglacial phase (125,000 years before the present = 125 kyr BP) via the last glacial maximum (LGM, 21 kyr BP), to the Holocene (the last 10 kyr, see marked periods in Figure 1.1). These time series exhibit natural variability with a wide range of climate extremes that occurred during this time period.

In the discussion on how future environmental conditions will affect mankind, an important problem is whether human industrialisation with growing emissions of greenhouse gases have already caused, or will have the potential, to induce a significant impact on the Earth's climate. To properly address this question it is necessary to separate natural climate variability from the additional anthropogenic signal. This challenge requires detailed knowledge of amplitude and frequency of natural variations of temperature or other temperature-related environmental properties in the ocean, over the continents, and in the cryosphere. The best way to obtain this knowledge would be to analyse historical time series of temperature, precipitation, and other climate-related measurements. Unfortunately, historical records for environmental observational data, which would allow consideration of natural climate variability on a global scale, are too short and already fall within the period of human impact on nature.

Information on earlier times can be obtained mainly from two strategies: on the one hand by deriving proxies that record past climate and environmental conditions, and on the other hand by simulating climate, using comprehensive models of the climate system under appropriate external forcing. Numerical climate models are clearly unrivalled in their ability to simulate a broad suite of variables across the entire world, but their reliability on multi-decadal and longer timescales requires additional evaluation. Only climate records (proxy data) that are derived from palaeoenvironmental climate-related parameters enable the test of these models because they provide records of climate

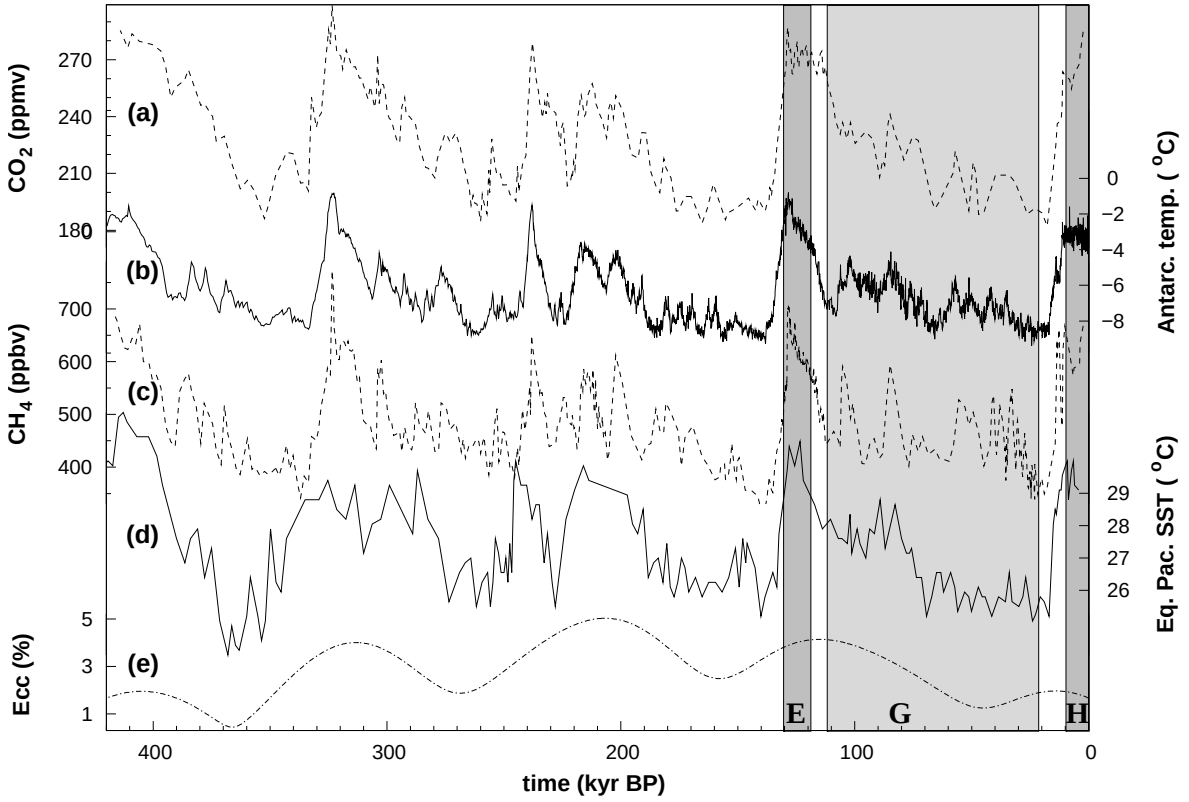

Figure 1.1: *Concentrations of the greenhouse gases CO_2 (a) and CH_4 (c) measured from air bubbles trapped in the Vostok ice core, Antarctica. Also displayed is the surface air temperature (b), reconstructed for Antarctica from the $\delta^{18}O$-record from this core, SST (d) derived from Mg/Ca-ratios in foraminifera shells of core ODP806b from the equatorial Pacific warm pool, and the eccentricity of the Earth's orbit (e), calculated after Berger [1978]. The Eemian (E) and Holocene (H) interglacials and the last glacial period (G) are marked through shading. Data sources are from Petit et al. [1999] (a-c) and Lea et al. [2000] (d). Data are plotted on the "natural" modellers time axis (running from left to right), in contrast to the geological timescale where age increases to the right.*

variations that have actually occurred in the past. Even if well-known uncertainties in the proxy-derived palaeoclimate records exist, e. g., age control, signal formation, and calibration issues, proxy records are a valuable source of information against which models can be tested.

1.1 Synthesis of model simulations and data reconstruction

An important step in palaeoclimate research is the combination of climate modelling and proxy-based reconstruction. In order to conduct a data-model synthesis, various perspectives are possible. One kind of approach is to utilise a model simulation as a consistency-test for independent proxy data that are available at different locations or vertical levels. For instance, an atmospheric general circulation model (GCM) has the potential to test marine geological proxy data against climate reconstructions from terrestrial sites. The atmospheric GCM could be forced by a distribution of marine palaeoclimate

data (mainly sea surface temperatures, SST in the following), where its results could then be compared with terrestrial climates, e. g. borehole temperatures or fossil pollen findings. In turn, a combination of marine and terrestrial palaeoclimate data have the potential to be used for the validation of GCMs, as long as their performance in simulating climate states that are strongly differing from the modern one is not well known. In practise, both paths are often conducted in combination because a clearly divided approach — validation of the model or consistency test of the proxy data — is often not possible due to uncertainties in the models, as well as in the proxy data.

A further step could be an inverse modelling approach: different or inconsistent reconstructions motivate to conduct a series of simulations using diverging or contradictory sets of palaeoclimate data as boundary conditions for the same model. Comparing results from the different simulations with independent terrestrial data can give clues to which marine and terrestrial geological conditions best fit together with the picture of a particular palaeoclimate. Such consistency-tests help to improve the understanding of discrepancies between proxy data derived with different methodologies and to suggest how these could be reconciled. In Section 1.1.2, a particular problem is introduced where an atmospheric GCM can be used in the sense of a consistency-test for marine and terrestrial data. The following Sections (1.1.3, 1.1.4, and 1.1.5) then explain the approach of combining coupled atmosphere-ocean GCM simulations with relevant proxy data for the interpretation of Holocene and Eemian climate change.

1.1.1 The CLIMAP project: global mapping of proxy data

Atmospheric as well as oceanic circulation models need boundary conditions at the atmosphere-ocean interface. For past climates, these boundary conditions are not generally available on a global scale. In order to derive a marine data set applicable as boundary condition for a palaeoclimate simulation, accurately dated proxy-records of the same time frame have to be collected from as many deep sea cores as possible. Up to now, only a few such globally compiled data sets of a palaeoclimate time slice exist: the first one is the reconstruction of SST, albedo and other surface parameters for the LGM. This extensive work was conducted by the Climate: Long-Range Investigation, Mapping, and Prediction (CLIMAP) project during the seventies [*CLIMAP Project Members*, 1976]. In this project, uniformly utilised reconstruction methods were defined and results were provided as global and gridded digital data sets. The CLIMAP reconstruction of the marine climate was based on transfer functions to connect assemblages of planktic foraminifera from a large number of available deep sea cores with near surface water temperature. One of the results of CLIMAP was that the decrease in tropical SST during LGM was only moderate when compared with the decrease of SST in middle and high latitudes (see Figures 1.2 and 2.1, p. 29).

An obvious limitation that is common to marine (as well as terrestrial) palaeoclimate records is visible in Figure 1.2: their scarce distribution over the open oceans (see also distribution of Holocene alkenone-derived temperature trends, Figure 4.4, p. 90). In Figure 1.2, the cores and their locations as used for the CLIMAP reconstruction for the LGM are depicted. One reason for this is that the deep sea floor falls below the lysocline (more exactly, below the calcite compensation depth, CCD) for large parts of the oceans, especially in the Pacific, where no analogue to the Atlantic ridge exists. The lysocline is the level of onset of dissolution of calcium carbonate, CCD is the depth at which

calcite does not accumulate because the rate of carbonate supply is equal to the rate of carbonate dissolution. Therefore, the carbonate shells of marine microfossils (e. g. foraminifera), which are the most common marine proxy-recorders, are dissolved before they reach the sediment top at the ocean floor.

A number of more recent climate reconstructions conflict with the CLIMAP result for tropical SST. Colder glacial tropics have been detected from marine as well as from terrestrial sites [see *Anderson and Webb*, 1994; *Crowley*, 2000a]: analyses of noble gases from groundwater in tropical lowlands [*Stute et al.*, 1995; *Weyhenmeyer et al.*, 2000], isotopic measurements from tropical mountain glaciers [*Thompson et al.*, 1995], and analysis of strontium to calcium ratios (Sr/Ca) in Caribbean corals [*Guilderson et al.*, 1994], indicate surface temperatures that are 5 K (Kelvin) colder compared with today. Furthermore, newly calculated transfer functions [*Lee and Slowey*, 1999; *Mix et al.*, 2001] as well as SST-reconstructions from alkenones result in 3–4 K tropical temperature difference between LGM and today [*Bard et al.*, 1997; *Rühlemann et al.*, 1999]. This is remarkably or moderately lower than CLIMAP in some tropical areas, respectively. In summary, different proxy methods (alkenones,

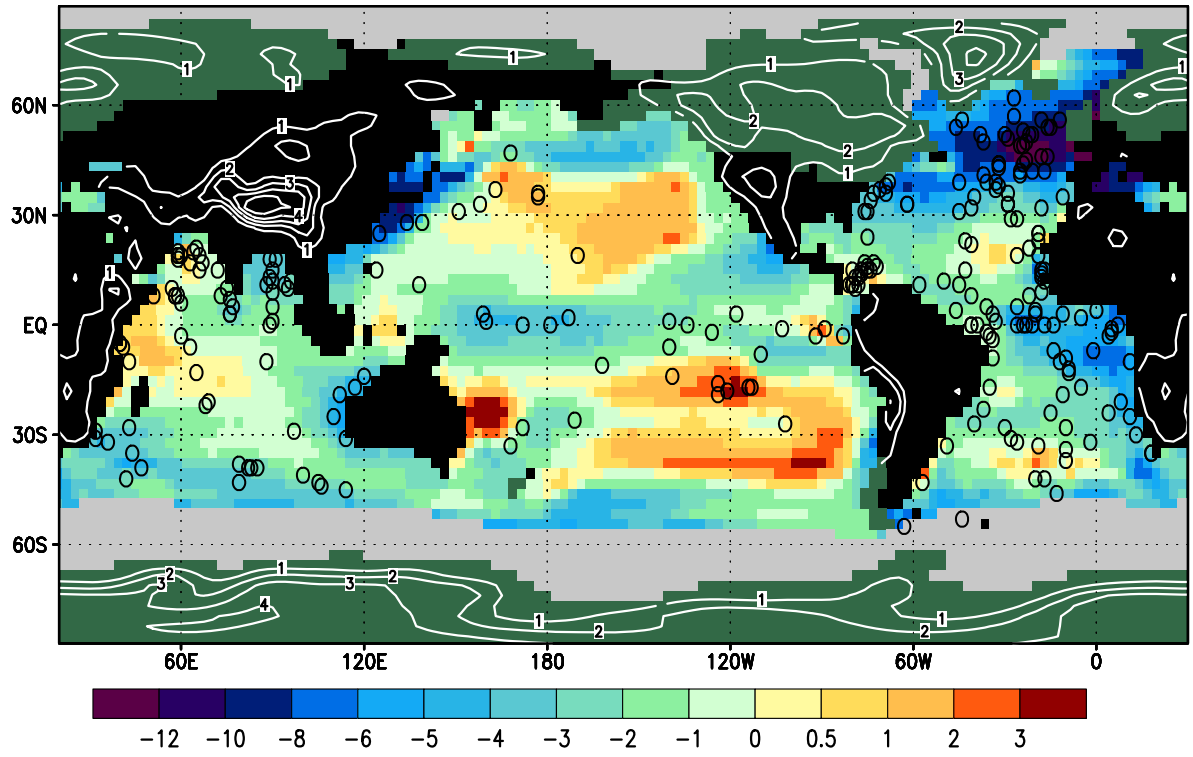

Figure 1.2: *Position of a large part of the deep sea cores (marked by circles) used for the reconstruction of the climate of the LGM by CLIMAP (data compiled by Prell [1985]). The figure also depicts the glacial SST difference to the present climate and the sea ice distribution for boreal summer (August) as provided by the Glacial Atlantic Ocean Mapping Project (GLAMAP, [Sarnthein et al., 2003]) for the Atlantic, and by CLIMAP Project Members [1981] for the Indian and Pacific Oceans, which are displayed on the grid of the ECHAM model in T42 resolution (Section 1.2.1). Furthermore, continental ice caps (green), distribution and topography (contour level interval of 1 km) of continents during LGM are marked (see Figure 2.1, p. 29 for different boundary conditions for the LGM).*

magnesium and Sr/Ca ratios, oxygen isotopes, transfer functions) reveal discrepancies of a few Kelvin in LGM temperature reconstructions [*Bard*, 2001; *Mix et al.*, 2001].

1.1.2 Tropical snowlines and CLIMAP SST: atmospheric modelling of the LGM

Another indication that is thought to contradict the marginal tropical cooling at sea level during LGM is the reconstructed height of the snowline of tropical mountain glaciers during LGM. The height above sea level of the "equilibrium-line altitude" (ELA) of a glacier, where the glacier mass balance equals zero, divides the accumulation from the ablation zone. On temperate and tropical glaciers the ELA and the snowline are very similar in height and are in close vicinity to the zero-degree (0°C) isotherm. The ELA can be deduced from reconstructed extent and height of palaeoclimatic moraines. Such moraines are built by deposit of detritus during periods of waxing glaciers. They are left over after glacier retreat and can easily be observed, even though they are much harder to date. In most palaeoclimate studies using snowline reconstructions, a change in ELA is translated into a temperature variation by assuming a constant vertical temperature gradient, the environmental lapse

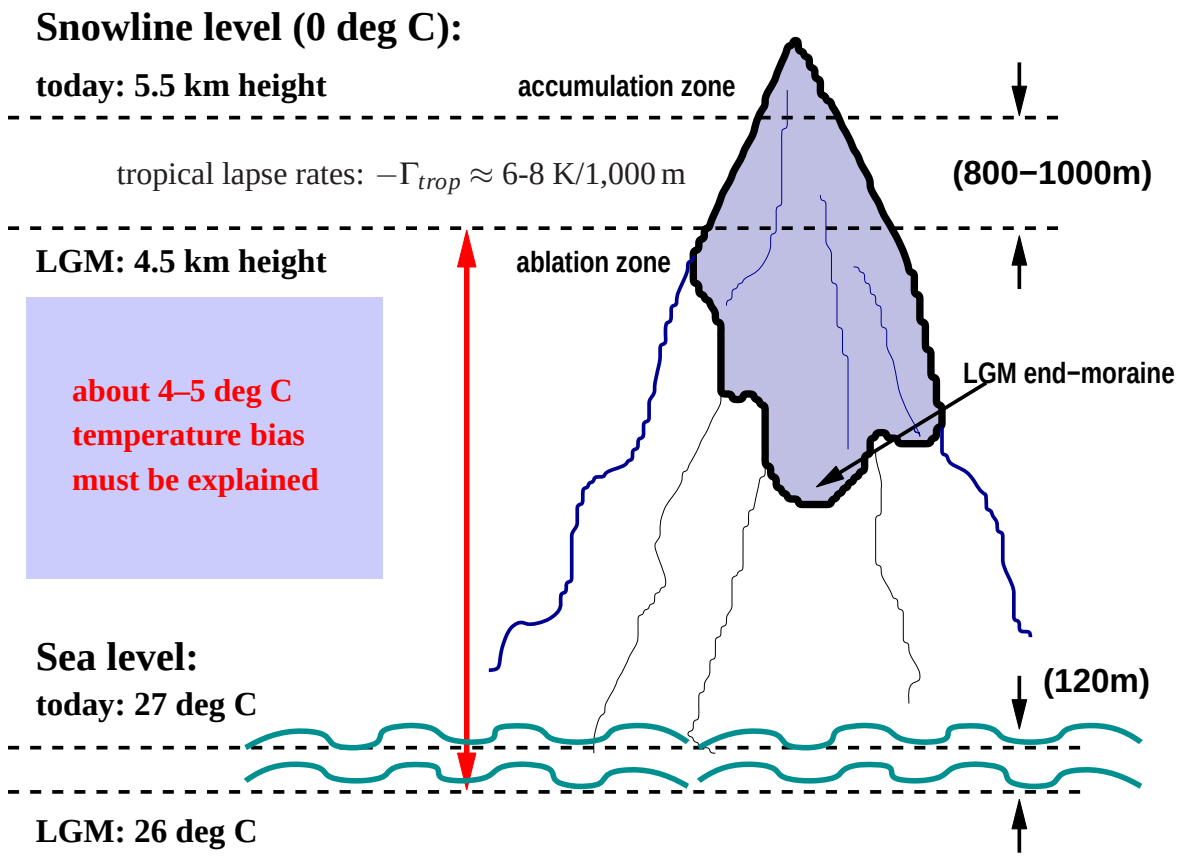

Figure 1.3: *On the discrepancy of tropical glacial SST and air temperature at the snowline level: the vertical temperature gradient is between the dry adiabatic lapse rate ($-\Gamma_d = \frac{g}{c_p} = 9.8$ K/1,000 m) and the moist adiabatic lapse rate ($-\Gamma_m \approx 5-7$ K/1,000 m). The estimated net vertical lowering of the snowline during LGM (900 ± 135 m, [Porter, 2001] minus the sea level change of 120 m [Fairbanks, 1989]) leads to a temperature reduction of ≈5-7 K at the snowline level, whereas the SST reduction at the sea level was estimated to be only 1 K. Therefore, a discrepancy of about 4 to 5 K remains.*

rate, which is typical for the large scale climate of the respective region.

Based on the evidence from tropical mountain sites in Africa, America, and the Pacific islands, *Porter* [2001] concluded that glacial snowlines were 800 to 1,000 m lower than today. Taking into account the glacial change in sea level of 120 m [*Fairbanks*, 1989; *Rohling et al.*, 1998], the 900 ± 135 m change in ELA translates into a 780 m drop of the 0°C isoline. Tropical lapse rates in the free atmosphere lie between the dry adiabatic and the moist adiabatic lapse rate. Furthermore, near surface temperatures over tropical mountains are anticipated to be colder than the free atmosphere [*Farrera et al.*, 1999]. Using a simplistic lapse rate approach, the snowline depression corresponds to a $\sim$5–7 K mean annual temperature drop, which may at least provide a first-order approximation of regional and global tropical temperature reduction at the LGM [*Seltzer*, 2001]. This leads to an inconsistency of at least 4 K between tropical ocean temperature reconstruction at the surface by CLIMAP (1 K colder than today) and the cooling at the height of the tropical snowline during LGM (Figure 1.3). The apparent discrepancy between tropical SST reconstructed by CLIMAP and the depression of tropical snowlines leads to the following question:

(1) *What is the most probable scenario for tropical air temperatures at sea level in coexistence with those at the level of the tropical snowline? How can the inconsistency between tropical SST and air temperature at the snowline be explained?*

For an independent comparison with these palaeo-reconstructions, the simulation of the atmosphere with a GCM enables the investigation of its vertical structure under the boundary conditions of the LGM. In Chapter 2, a synthesis of atmospheric GCM simulations, marine SST reconstructions, and terrestrial evidence for glacial snowlines is discussed [*Lorenz and Lohmann*, 2006].

1.1.3 Coupled atmosphere-ocean modelling of the LGM time slice

A step forward in a model-data synthesis is to overcome the strong dependence of atmospheric and oceanic GCMs on surface boundary conditions at the atmosphere-ocean interface. In order to derive independent simulation data, an integrated model for the circulation of both atmosphere and ocean is necessary. Coupled atmosphere-ocean general circulation models (AOGCMs) have the potential to make boundary conditions at their interface superfluous. Driven by palaeoclimatic boundary conditions apart from the ocean surface (e. g. solar radiation and land surface characteristics) coupled models should be able to generate independent sea surface data (temperature and salinity). This, however, requires an accurate calculation of the exchange fluxes between atmosphere and ocean (heat, water, momentum) for a reasonable simulation of the coupled atmosphere-ocean system under different palaeoclimate forcing. The quality of model results and globally distributed proxy data, such as the CLIMAP reconstruction or alkenone-derived SST, can be assessed.

1.1.4 Orbital forcing of late Quaternary climate: transient modelling

Coupled atmosphere-ocean models are able to simulate transient climate change driven by internal or external forcing mechanisms, such as changes in greenhouse gas concentrations and astronomical parameters (Figure 1.1). But which forcing mechanisms could have contributed to the extreme climates

of the late Quaternary glacial cycles? To address this question, long-term simulations of changing climate running over at least several thousand years are necessary.

One of the most prominent candidates for triggering changes between the cold glacial phases and the warm interglacials during the late Quaternary is the astronomical or "Milankovitch-forcing" of the climate system [*Milankovič*, 1941; *Imbrie et al.*, 1992]. It is caused by the varying parameters of the Earth's orbit around the Sun. On multi-millennial timescales, the forcing provides for large imbalances in the seasonal distribution of sunlight. The change in orbital parameters have even been regarded as the pacemaker of ice ages [*Hays et al.*, 1976; *Imbrie et al.*, 1992, 1993].

The astronomical or orbitally driven solar radiation (insolation) forcing is controlled by three main parameters of the Earth's orbit (Figure 1.4): the eccentricity, the time of the Earth's passage through its perihelion, and the tilt of its rotational axis. The eccentricity (today 1.67 %) has cycles with periods near 100 kyr and exceeds 5 % during the late Quaternary (Figure 1.1). The precession of the rotation axis through the fixed stars is caused by the gravitational force of mainly the Moon. This leads to a change in the angle of the perihelion (the point on the orbit that is nearest to the Sun in one of the foci of the ellipse, Figure 1.4) with respect to the moving vernal equinox (the so-called longitude of perihelion, or true longitude) [*Berger*, 1978; *Berger et al.*, 1993]. Therefore, the precession determines the time during the year when the average insolation of the whole Earth is at a maximum (today, this is during austral summer, Figure 1.5). Moreover, the precessional effect is

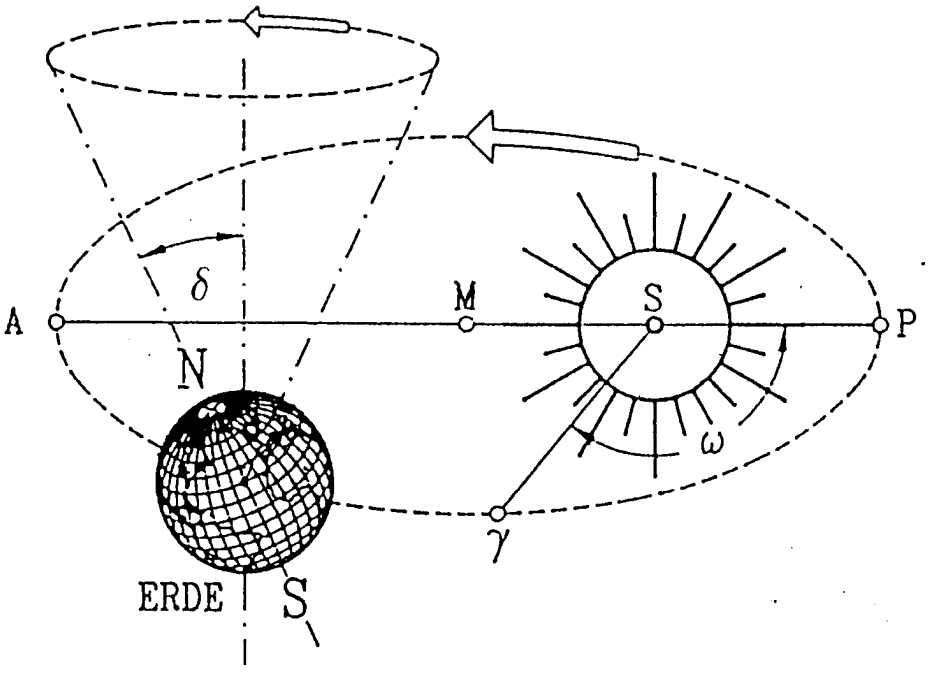

Figure 1.4: *On the definition of the parameters of the Earth's orbit around the Sun: the obliquity is the angle of the Earth's rotation axis with the normal of the orbit (δ); the precession of the rotation axis in space (arrow) leads to the precession of the perihelion (P) relative to the vernal equinox (γ), measured with the angle ω, the "longitude of perihelion"; the eccentricity of the Earth's orbit (ε) is defined by using the two axes ($a = \overline{MP}$, the semi-major axis, b: semi-minor axis perpendicular to a) of the elliptic orbit: $\varepsilon = \sqrt{a^2 - b^2}$. Figure adapted from Herterich [1990].*

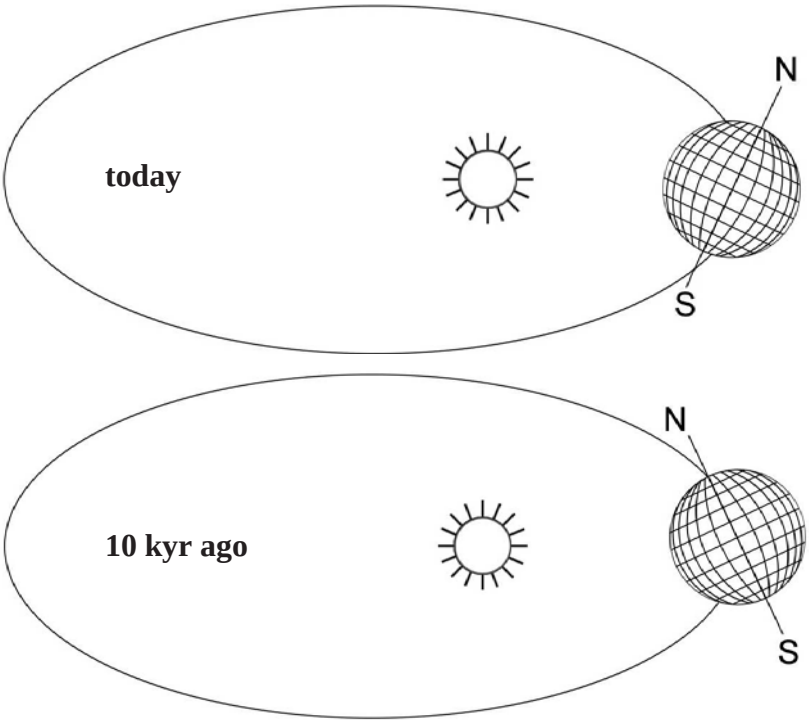

Figure 1.5: *Orbital configuration through a half precessional cycle: Today (upper panel) the Earth is at its perihelion with minimum distance to the Sun in January (near the winter solstice). Therefore, austral summers are warm, whereas the insolation on the Northern Hemisphere during boreal summer is relatively low. At about 10 kyr ago (lower panel), the opposite situation occurred and the Northern Hemisphere insolation was at its maximum during boreal summer. Figure adapted from Hertlerich [1990].*

proportional to the eccentricity, i. e. the difference in the distance to the Sun between the perihelion and the opposite aphelion is zero with vanishing eccentricity. It has its main effect in the tropics, with cycles near 20 kyr (Figure 1.6). During the last million years, the Earth's axis tilt (obliquity) varies between 22 and 24.5° and has a main long-term cycle with a period of approximately 40,000 years. It affects the amplitude of the seasonal cycle of both hemispheres, simultaneously (Figures 1.4 and 1.6).

The variation of these parameters in the Quaternary can easily be calculated with sufficient accuracy using the algorithm described by *Berger* [1978], [see also *Berger and Loutre*, 1991; *Berger et al.*, 1993, 2006]. Newer calculations span much longer timescales, beyond millions of years [*Berger and Loutre*, 1991; *Laskar et al.*, 2004], or take into account short-term variability [*Loutre et al.*, 1992], which is generally far beyond the requirements of simulations of long-term palaeoclimate variability. During the period from the Eemian interglacial to the onset of glaciation (130 kyr BP to 115 kyr BP) when eccentricity was at about 4 %, the seasonal insolation changes reached a maximum of 100 Wm^{-2} (Figures 1.7 and 1.8). The insolation in its annual mean depends to only a small fraction on the orbital parameters. The annual mean insolation integrated over the Earth's surface is affected by less than 1 % in periods with high eccentricity during the late Quaternary. The anomaly with respect to today of the seasonal cycle for specific time slices is shown in Figure 1.8.

A direct comparison of natural climate trends during the Holocene as well as the Eemian climates with marine and terrestrial temperature reconstructions can be accomplished through a series of transient model simulations including a part of the relevant forcing mechanisms. This permits the direct relation of a well-known climate forcing mechanism, the astronomical forcing, to proxy-derived Holocene temperature trends. In Chapter 3, ensemble simulations of Holocene temperature trends

with a coupled AOGCM are introduced. They use an acceleration factor for the orbital forcing (Section 1.2.2) that enables the simulation of long-term palaeoclimate temperature trends [*Lorenz and Lohmann*, 2004].

1.1.5 Seasonal cycle of insolation and interpretation of proxy data

Palaeoclimate simulations using AOGCMs supply climate-related results with monthly or daily resolution over the whole globe. For Holocene and Eemian climates, difficulties arise from coarse temporal resolution of deep sea cores, depending on relatively low sedimentation rates that limit the resolution to be far beyond single years. Seasonally-resolving proxies are generally difficult to extract. Here, annually-banded coral data from the last interglacial and the late Holocene as well as SST trends derived with the alkenone-method are taken into consideration for a combined analysis with the model-derived results.

Recently, two fossil coral colonies (Porites) have been collected from an uplifted shore at the Jordanian coast of the Gulf of Aqaba. They have been dated to 2.9 kyr BP (late Holocene) and 122 kyr BP, which is near the warm peak of the Eemian interglacial in that area [*Felis et al.*, 2004]. The Holocene and Eemian coral provide climate data with seasonal resolution on a multi-decadal time window. This allows for the extraction of seasonal signals, such as the amplitude of the annual cycle and relative temperature shifts of the different seasons (Chapter 5).

Long-term surface temperature trends for the Holocene have recently been derived [*Kim et al.*, 2004; *Rimbu et al.*, 2004] from a number of deep sea cores, using the alkenone method [*Brassell et al.*, 1986; *Prahl and Wakeham*, 1987] (Section 1.2.3). These trends are suitable for a direct comparison with the results of the AOGCM, using the acceleration technique for the orbital forcing. The temporal resolution of ocean cores analysed with the alkenone method is relatively coarse. However, a considerable number of core series are available for the late Quaternary.

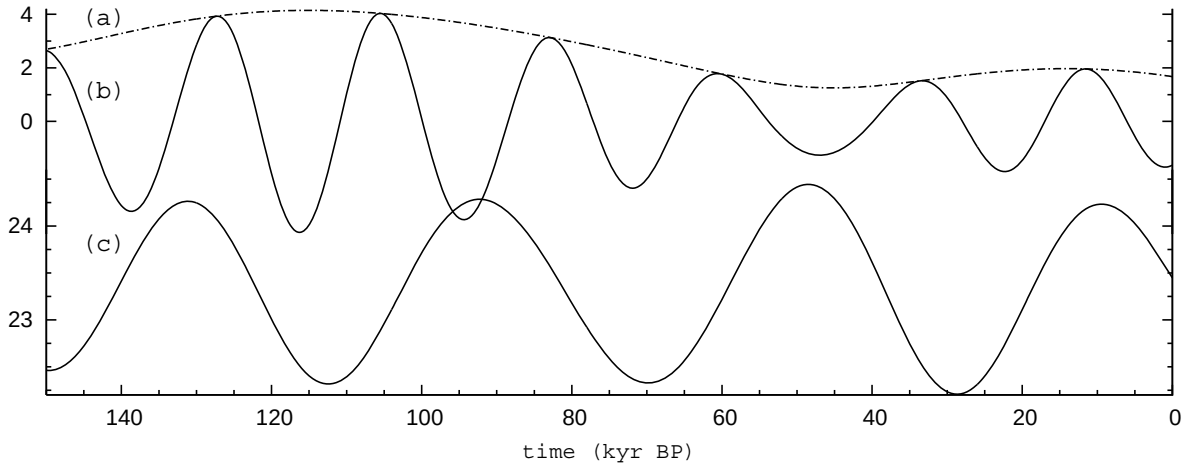

Figure 1.6: *Evolution of the orbital parameters over the last 150 kyr calculated following Berger [1978]: (a) eccentricity* ε *(in %), (b) the precessional parameter (in %) defined as* $p = \varepsilon \sin(\omega)$ *with* ω *the longitude of the perihelion measured from the moving vernal equinox, (c) the obliquity of the Earth's rotation axis (in degrees), compare Figure 1.4.*

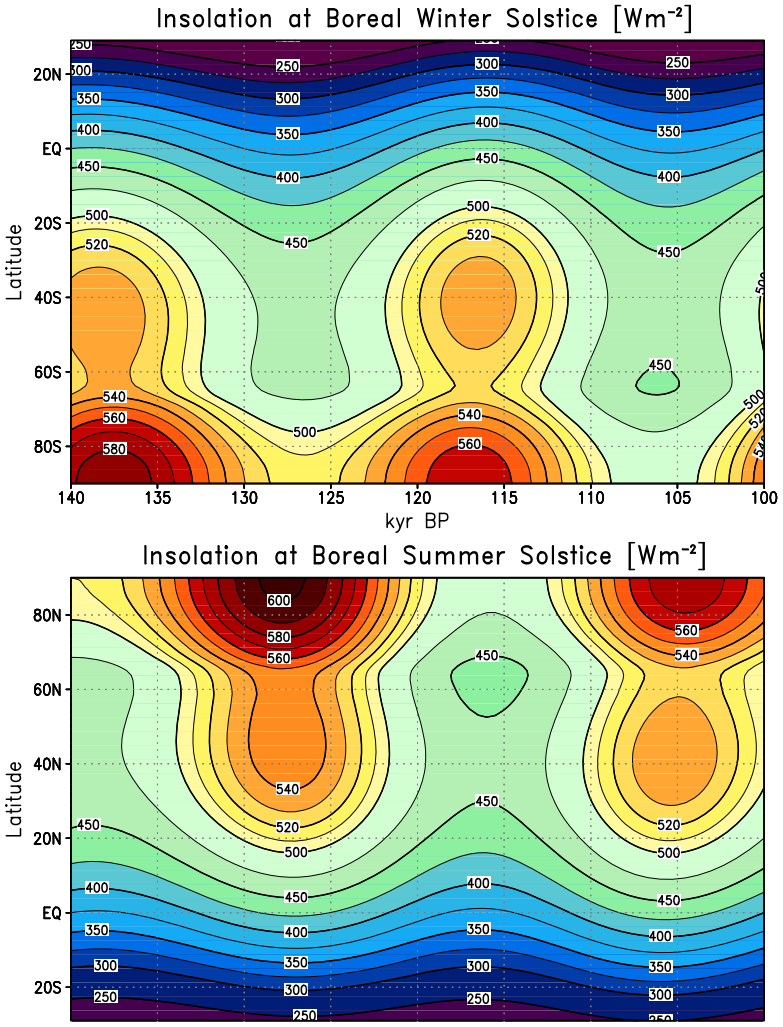

Figure 1.7: *Solar radiation (insolation) forcing as an upper boundary condition for the Earth's climate, resulting from changing orbital parameters: Insolation (Wm^{-2}) at boreal winter and summer solstice during the latest period with high eccentricity (see Figures 1.1 and 1.6). Note the complementary latitude ranges with respect to the hemisphere with insolation at its maximum. An extended series of insolation data and figures (including the time series shown here) has recently be collected in Berger et al. [2006]; see also Figures 3.1 (p. 57) and 4.2 (p. 85) for Holocene insolation, and Figure 1.8 for changes in the entire annual cycle.*

Since the development of the unsaturated alkenone index as a temperature proxy in the late 1980s, the seasonal origin of alkenone-derived temperature signals in different latitudes remains an open question. In high latitudes, maximum coccolithophorid production is observed during late spring to early summer [*Baumann et al.*, 1997]. This suggests that alkenone-derived SSTs should reflect summer temperatures [*Rosell-Melé et al.*, 1995; *Sikes et al.*, 1997], but may be biased towards the annual mean. In tropical to subtropical regions, seasonality in phytoplankton production is generally less pronounced [*Jickells et al.*, 1996] and alkenone-derived SSTs are more likely to record annual mean values [*Müller and Fischer*, 2001]. During the Holocene, the orbital parameters provide for shifts in the timing of the maximum insolation in the tropics as well as in middle to high latitudes. Changes in the seasonal cycle of insolation could possibly influence the timing of phytoplankton blooming, and can therefore be of interest for the interpretation of proxy data. With the simulated and the proxy-derived temperature estimates the following questions are addressed:

(2) *How does the orbitally driven insolation forcing affect the long-term climate trends from the middle to the late Holocene? Are changes in the seasonal cycle of insolation reflected in Holocene and Eemian proxy data?*

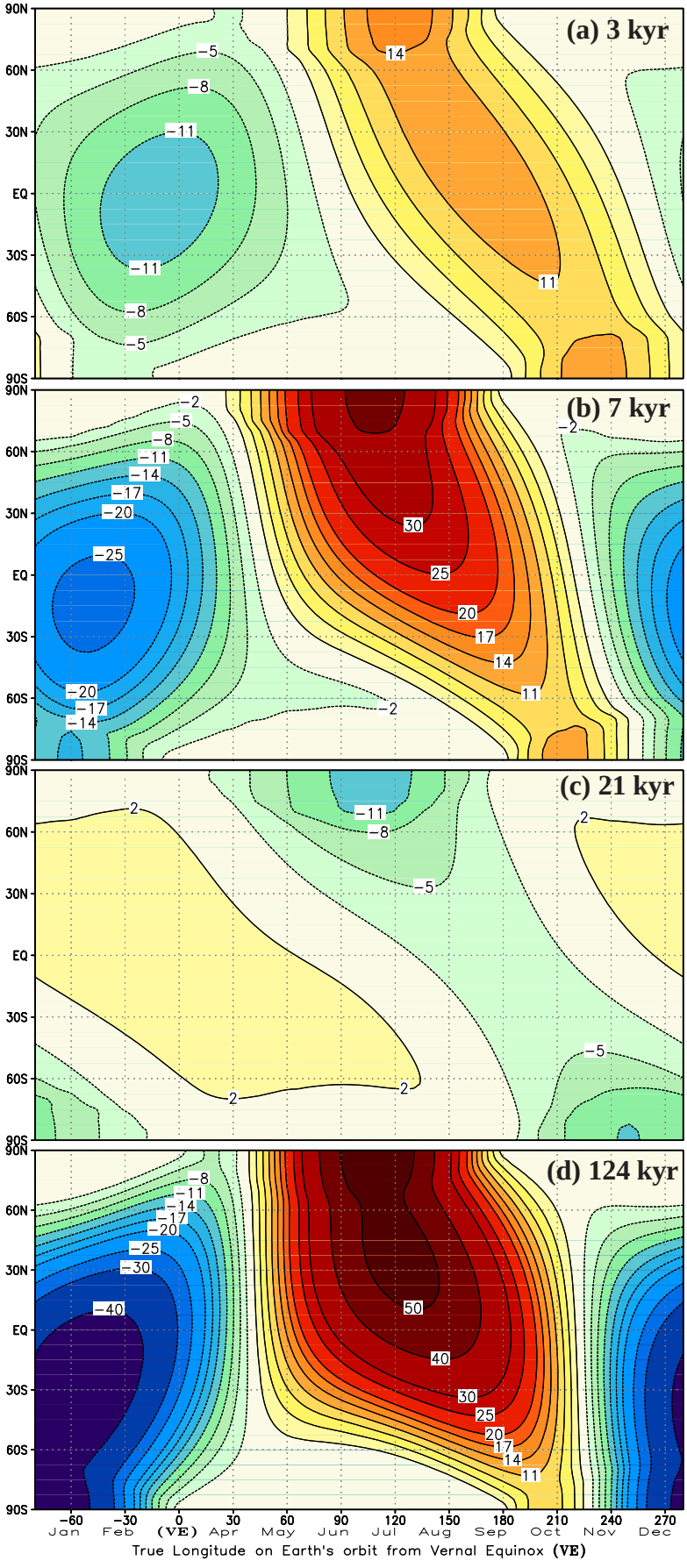

Figure 1.8: *Annual insolation cycle for distinct time slices during the last glacial cycle. Seasonal distribution of insolation anomaly relative to modern conditions for (a) 3 kyr ago (late Holocene), (b) 7 kyr ago (middle Holocene), (c) 21 kyr ago (LGM), and (d) 124 kyr ago (Eemian), calculated after Berger [1978]. Shown is the latitudinal distribution with respect to the true longitude (angle between perihelion and vernal equinox on the Earths orbit). Note that following Keplers Law the track speed on the elliptical orbit varies.*

1.1.6 Orbital forcing of the AO/NAO circulation pattern

Investigation of teleconnection patterns and their underlying internal dynamic processes, such as the Arctic Oscillation/North Atlantic Oscillation (AO/NAO), or the El Niño/Southern Oscillation (ENSO), is a common approach when analysing results of GCMs. In order to understand these mechanisms, the analysis of a series of parameters that are able to produce a complex mechanism with global or continental imprint is essential. For palaeoclimate times it is difficult to identify the signature of their teleconnection patterns, because proxy-parameters of different quantities (air and water temperature, precipitation, air pressure) should be concomitantly available at high resolution in time and space. Moreover, information on particular seasons is necessary.

Surface air temperature and related climatic parameters over the Northern Hemisphere during winter time are strongly influenced by the AO/NAO circulation pattern. The Arctic Oscillation, also known as the northern annular mode, is the dominant mode of the atmospheric circulation variability in the northern extratropics [*Thompson and Wallace*, 1998]. This mode is characterised by a meridional dipole in atmospheric sea level pressure between the polar regions and the mid-latitudes. The North Atlantic Oscillation (NAO) can be regarded as a more regional pattern of a similar phenomenon [*Thompson and Wallace*, 2001]. Conventionally, the NAO-index is defined as the normalised pressure difference between the subtropical high over the Azores or Portugal, and the low over Greenland or Iceland, respectively. This index has been used to characterise the atmospheric winter circulation in the North Atlantic region. When the index is high (positive), strong westerly winds advect mild and moist air over western and central Europe.

The AO/NAO circulation pattern with its short-term (interannual) variability and its impact on the Atlantic/European climate has been studied intensively [e. g., *Thompson and Wallace*, 2001; *Rimbu et al.*, 2001; *Franzke et al.*, 2001]. Most studies are based on instrumental records over the last 100 years. The relevance of this circulation pattern on long-term (orbital) timescales is difficult to acquire in model simulations, since at least an atmospheric GCM is necessary to capture the internal feedbacks involved. Recently, AO/NAO related patterns on centennial to millennial timescales based on alkenone-derived SST during the Holocene have been investigated [*Rimbu et al.*, 2003]. One possible step is the analysis of GCM simulations under astronomical forcing, resolving internal feedback mechanisms on intraseasonal as well as on interannual and longer timescales. With the combined interpretation of temperature-related records from GCM simulations as well as alkenone and coral data the following question is addressed:

(3) *In what way are regional temperatures of the Eemian and Holocene periods governed by changes in atmospheric circulation patterns?*

1.2 Methods and design

1.2.1 Atmospheric modelling of the LGM time slice

In order to follow the proposed approach of a consistency-test for marine and terrestrial data in terms of atmospheric modelling, a general circulation model is necessary. The investigation of the vertical

structure of the atmosphere under the boundary conditions of the LGM needs a sufficient vertical resolution. For the series of numerical experiments, the ECHAM atmospheric GCM [*Roeckner et al.*, 1992] is applied using an intermediate horizontal resolution (T42, corresponding with a 128×64 longitude-latitude grid) with 19 vertical layers. The model uses the primitive equations and includes calculation of radiation and a hydrological cycle with transport of water vapour and cloud water. The insolation at the outer boundary of the atmosphere is prescribed to the respective seasonal cycle of the LGM, which is relatively similar to the present insolation (Figure 1.8c). The calculation of radiation transport through the atmosphere occurs with respect to the glacial level of atmospheric greenhouse gases. The equivalent concentration of carbon dioxide, including the effect of other greenhouse gases like methane, used for the glacial experiments is 200 ppm. Motivated by the differing reconstructions of tropical glacial SST [*Mix et al.*, 2001], a series of model simulations are conducted by applying different SST boundary conditions, as discussed by *Lohmann and Lorenz* [2000].

1.2.2 Acceleration techniques for transient simulations

For modelling the Eemian and Holocene periods, the following model requirements are essential in order to elucidate the questions stated above. The model has to be able to

- resolve teleconnection patterns and their underlying processes,
- generate SST by incorporating atmosphere-ocean feedback mechanisms,
- simulate long-term palaeoclimate trends including the seasonal cycle,
- include multi-millennial scale impact of orbitally driven insolation changes.

The first two requirements together can only be solved by means of utilising a coupled general circulation model for atmosphere and ocean. An attempt to use a modern coupled AOGCM for a transient simulation of a palaeoclimatic time period is hampered by the limited computer resources to run such a model. An atmospheric model with a time step in the range of minutes is too expensive in computational terms to extend the length of a model run to the range of several thousand simulation years (Figure 1.9a). A substantial reduction in computing time is required when simulating long-term palaeoclimatic changes.

In order to reduce the excessive computing time required for running a synchronously coupled model, the method of periodically-synchronous coupling, first suggested by Gates [*Schlesinger*, 1979], can be applied to a coupled AOGCM [e. g., *Voss et al.*, 1998]. In this method, short periods of synchronous coupling alternate with long ocean-only periods, where the atmospheric model is switched off. During the latter periods, the ocean is forced by the surface boundary conditions generated during previous synchronously coupled periods (Figure 1.9b). Due to the much longer time step of the ocean model, the computing time is significantly reduced. The method is predominantly applicable to simulate an equilibrium response of the atmosphere-ocean system within reasonable computing time, forced by constant palaeoclimate boundary conditions. A short discussion of this method can be found in Appendix A.

Another possible technique to reduce the computing time of an AOGCM is to accelerate the timescale of a slowly evolving boundary condition, such as the orbital forcing. As long as the timescales of the boundary conditions are clearly distinct by at least one order of magnitude from

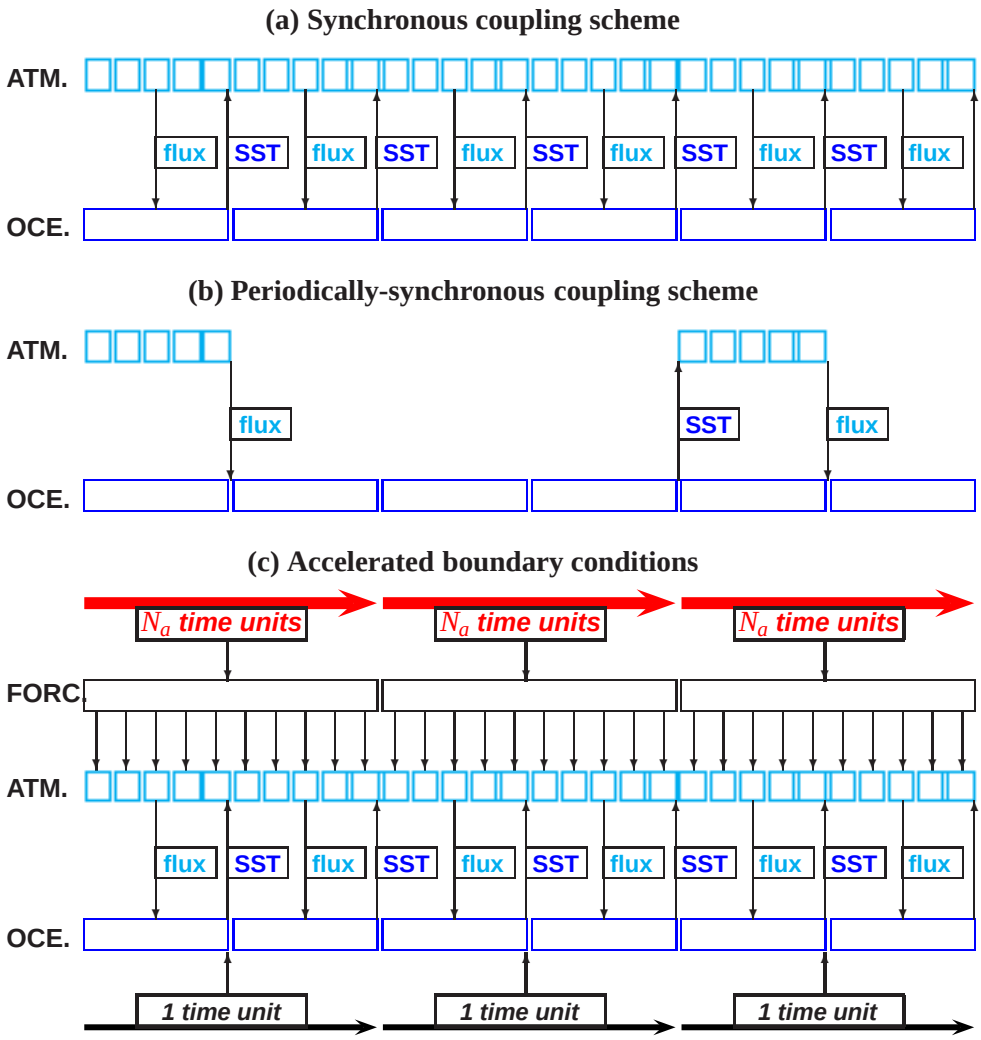

Figure 1.9: *Different methods for palaeoclimate simulations utilising coupled AOGCMs: the synchronous coupling (a) is limited by the extensive computational costs due to the timestep in the range of minutes of the atmospheric GCM. The periodically-synchronous coupling technique (b) saves computing time by running the ocean model without the atmospheric GCM for long periods, where the ocean model is driven by surface boundary conditions generated during previous synchronously coupled periods. The externally prescribed forcing, e. g. orbitally-driven insolation, continental ice caps, etc., may be accelerated by a factor N_a (c) if the simulated system is considered to be in permanent equilibrium with the slowly evolving forcing. An appropriate time unit that is suitable to be accelerated has to be chosen. For example, this time unit may be one year (accelerated to 10 or 100 years) for the orbital parameters and 10 years (accelerated to 100 or 1,000 years) for the continental ice distribution, respectively.*

the timescales of the simulated climate components, the climate system can be regarded as being in "quasi-equilibrium" with the external forcing. Thus, the climate components with their inherent feedbacks can be analysed on all timescales shorter than that of the external forcing (Figure 1.9c). The timescales of the astronomical or "Milankovitch type" forcing are separated from the much shorter timescales of the atmosphere, including the mixed layer of the ocean, by several orders of magnitude. This motivated the idea of accelerating the astronomical forcing, which renders possible multi-millennial integrations with a fully coupled AOGCM and relatively low computational costs. This

method can be used to investigate long-term effects of the atmosphere-sea ice-ocean system induced by the astronomical forcing. The method has been applied to the coupled AOGCM, called ECHO-G, developed in Hamburg [*Legutke and Voss*, 1999]. The application of the acceleration technique in this model enabled transient ensemble integrations of the Holocene and the Eemian periods [*Lorenz and Lohmann*, 2004] that are subject to Chapters 3, 4, and 5.

The atmospheric part of this model is ECHAM4, whose prognostic variables are calculated in the spectral domain using a medium resolution (T30), corresponding to a longitude-latitude grid of approximately $3.8^\circ \times 3.8^\circ$ with 19 levels in the vertical [*Roeckner et al.*, 1996]. The time step of the atmospheric model is 30 minutes. The ECHAM4 model is coupled to the HOPE ocean general circulation model [*Wolff et al.*, 1997], which includes a dynamic-thermodynamic sea ice model with snow cover. Its horizontal grid has a resolution of approximately $2.8^\circ \times 2.8^\circ$ (0.5° resolution in the tropics, 20 vertical levels) and the model has a time step of two hours. The model utilises annual mean flux corrections for heat and freshwater. These fluxes are constant in time and have no sources or sinks of energy or mass.

1.2.3 Alkenone-derived SST

The alkenone method has been established in the late 1980s. It is based on the observation that certain microalgae (e. g. marine coccolithophorids) have the capability to synthesise long-chain unsaturated ketones (alkenones). The extent of unsaturation of the built-in alkenones depends on temperature of the surrounding ocean water in the photic zone (mainly the upper tenth of meters of the mixed layer) during growth of the shells. The relative abundances of methyl alkenones containing two to four double bounds are measured by gas chromatography, often coupled to high resolution mass spectrometry [*Rosell-Melé et al.*, 1995], and used to define slightly varying alkenone unsaturation indices (U^K_{37} [*Brassell et al.*, 1986] and the simplified index without taking into account the tetra-unsaturated alkenone, $U^{K'}_{37}$ [*Prahl and Wakeham*, 1987]). The method consists in converting these indices into annual mean SST [*Brassell et al.*, 1986; *Prahl et al.*, 1988] by applying calibration curves. These are derived from modern empirical relationships between the unsaturation indices and temperature, stemming either from core top calibration or from laboratory culture calibration [*Rosell-Melé et al.*, 1995; *Müller et al.*, 1998; *Rosell-Melé et al.*, 2001]. An updated calibration curve is depicted in Figure 1.10, where analysis of the core tops of deep sea cores distributed over all three ocean basins are employed. The best correlations were obtained using annual mean temperatures from 0 to 10 m water depth. The global error in alkenone-derived temperature from core-top calibration is ± 1.5°C [*Müller et al.*, 1998].

1.2.4 Seasonally-resolving corals

Massive annually-banded corals growing in tropical and subtropical oceans provide a palaeoclimatic archive with a seasonal resolution. Modern reef-building corals live in the upper levels (about 40 to 50 m) of the warm oceans with mean temperatures around 24°C and a minimum not falling below 18°C [*Felis and Pätzold*, 2003]. These corals are able to document past variations in water temperature and ocean circulation. Recent coral-based research mainly in the tropics provided for important

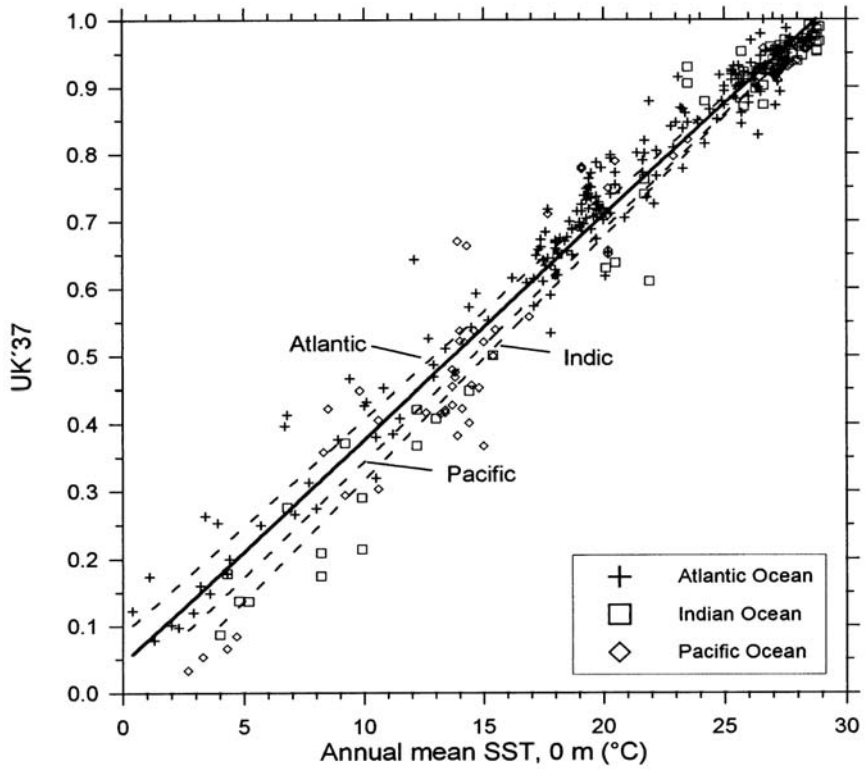

Figure 1.10: *Calibration curve for the alkenone unsaturation index ($U^{K'}_{37}$) derived from analyses of the tops of globally distributed deep sea cores using various microalgae species [Müller et al., 1998]. The obtained global core-top calibration (regression curve: $U^{K'}_{37} = 0.033\,SST + 0.044$, $r^2 = 0.958$, SST is taken from present climatology [Levitus and Boyer, 1994]) is almost identical to that of Prahl and Wakeham [1987], derived from E. huxleyi. The slightly different calibration curves for the three ocean basins are marked.*

implications on past variability of the ENSO phenomenon and decadal tropical climate variability [e. g., *Cole et al.*, 2000; *Rimbu et al.*, 2003]. Furthermore, coral records going back several centuries from rare subtropical key locations (Bermuda, northern Red Sea) have been investigated. Palaeoclimatic records from these coral sites were shown to reflect the oceanic (Bermuda) and atmospheric (northern Red Sea) signature of the NAO variability pattern [*Felis et al.*, 2000; *Rimbu et al.*, 2001]. A principal period of 5.7 years has been analysed in the Red Sea coral, typical for atmospheric forcing by large-scale, primarily Northern Hemisphere Pacific- and Atlantic-based climatic modes [*Felis and Pätzold*, 2003].

Modern corals do not grow older than 100 to 350 years, which limits their direct usage for palaeoclimete research. However, the finding of well-preserved fossil corals can provide limited time window records of climate variability comparable in resolution and quality to those derived from modern corals. In Chapter 5, temperature records with bimonthly resolution derived from two fossil corals from the late Holocene and the Eemian interglacial are investigated. Upper ocean temperatures were derived from isotopic δ^{18}O and Sr/Ca ratios in time windows of 98 and 44 years length for the Holocene and last interglacial coral, respectively [*Felis et al.*, 2004]. The records are related to large-scale atmospheric variability patterns (AO/NAO) analysed from results of the coupled AOGCM forced by the (accelerated) orbital insolation signal.

1.3 Publications

1.3.1 Previous and related work

This thesis is partly based on previous work, where the approach to perform a synthesis in modelling results and geological data has been initialised. The hydrological cycle and the atmospheric transport of water vapour of different climates during the last glacial cycle were examined in *Lohmann and Lorenz* [2000]. This work was based on time slice experiments with the ECHAM model for the climates of the LGM, the climate optimum (6 kyr BP), and the onset of glaciation (115 kyr BP), described in [*Lorenz et al.*, 1996]. These experiments were conducted following the guidelines of the international "Paleoclimate Modeling Intercomparison Project" (PMIP) [*Joussaume and Taylor*, 2000], where the boundary conditions for the LGM and the climate optimum were defined. A part of these simulations were subject to analyses described in Chapter 2. In *Lohmann and Lorenz* [2000], the idea of cooler tropical SST during LGM is discussed and validated through an enhanced comparison of simulated climate parameters with related proxy data; e. g. simulated net precipitation is cross-validated with reconstructed distributions of plant available moisture collected by *Farrera et al.* [1999], and lake level changes as obtained from the Global Lake Status Database [*Kohfeld and Harrison*, 2000]. In addition, *Lorenz et al.* [2004] (in german language) compare the changes of the simulated hydrological cycle of the LGM climate with the ones of a scenario simulation of the climate of the next 100 years under the forcing of increased greenhouse gas concentrations.

The particular role of deep root vegetation, has been studied with a series of ECHAM simulations of the LGM and the present climate [*Kleidon and Lorenz*, 2001]. In the simulation of the LGM including the effect of water storage of deep root vegetation an enhanced altitudinal shift of vegetation zones was found. In contrast to other model studies [e. g., *Crowley and Baum*, 1997], Amazonian rainforest sustained in the LGM simulations due to the availability of moisture from the rainy season to dry periods. Additionally, in a vegetation feedback study, the carbon budget of the glacial terrestrial biosphere has been investigated [*François et al.*, 1999] using results from the ECHAM simulations of the LGM climate.

The question whether a temperature increase in the tropics could initiate the transition from a glacial into an interglacial climate is often discussed [e. g., *Cane*, 1998]. In the LGM experiments with the ECHAM model, surface air temperature over the Laurentide ice sheet is diagnosed to be more than 6 K warmer when tropical SSTs are increased by 3 K. This evidence is discussed by *Rodgers et al.* [2003] in comparison with proxy data indicating a leading role of the tropical warming for initialising a deglaciation [*Lea et al.*, 2000] (see Figure 1.1d). It is explained by extratropical changes in lapse rate and atmospheric moisture, but with only minor circulation change. However, an ice sheet model driven by atmospheric boundary conditions from the ECHAM and two other atmospheric models did not confirm the initiation of ice sheet decay by induced tropical warming [*Rodgers et al.*, 2004].

Another study where changing boundary conditions in an AGCM were related to proxy data, was concerned with rapid ice accumulation in Greenland during the last glacial period [*Kiefer et al.*, 2002]. This study was motivated by evidence of North Pacific warm spells in a northwest Pacific deep sea core [*Kiefer et al.*, 2001] concomitantly with rapid Dansgaard-Oeschger transitions between cold stadials and warmer interstadials as recorded in Greenland as well as in Antarctic ice cores

during the last glacial [*Dansgaard et al.*, 1993; *Grootes et al.*, 1993; *Blunier and Brook*, 2001]. A replenishment of the Greenland ice after severe iceberg outbreaks as recorded in debris-layers is difficult to establish from North Atlantic sources due to cold glacial SST in the vicinity of Greenland. It is suggested that increased ice accumulation may be supplied by moisture sources from the North Pacific. Inducing a warming of 3.5 K to the glacial SST in the Pacific between 49° and 57°N increased the net precipitation (ice accumulation water equivalent) by 40 % in East Greenland [*Kiefer et al.*, 2002].

Recently, teleconnection patterns on centennial to millennial timescales have been analysed in alkenone-derived SST data from the Holocene [*Rimbu et al.*, 2003]. Further studies investigated internal processes that are potentially responsible for detected patterns between the North Atlantic and the North Pacific [*Kim et al.*, 2004] as well as between the North Atlantic and tropical oceans [*Rimbu et al.*, 2004]. This work was based on a statistical analysis of the internal variability derived from the control run of a coupled AOGCM. Moreover, the European winter cooling during the Holocene, as simulated by the transient experiments with this AOGCM [*Schneider et al.*, 2004; *Lorenz et al.*, 2006], is compared and deduced to be in line with a recent regional model study analyzing the oceanic circulation pattern in the Nordic Seas [*Lohmann et al.*, 2005]. In *Groll et al.* [2005], the relationship between regional temperatures and the large-scale circulation, based on quasi-equilibrium time slice simulations of the Eemian and the pre-industrial climate, is discussed. In a recent further analysis of the transient ensemble simulations of the period from the Eemian interglacial to the onset of the last glaciation, *Lohmann and Lorenz* [2006] found a correlation of tropical Pacific convection and the extratropical AO/NAO circulation pattern that is possibly controlled by the orbitally driven insolation signal during this climate transition.

1.3.2 Contents of the thesis

In the following chapters the questions that are introduced and formulated in Section 1.1 are addressed by manuscripts that are mostly published in peer-reviewed journals (Chapters 3, 4, and 5). Chapter 2 contains the revised version of a reviewed article that will be resubmitted in a similar version. A synthesis of this thesis is given in Chapter 6. Furthermore, Appendix A includes the contribution of the author to the cited booklet.

Chapter 2: Stephan J. Lorenz and Gerrit Lohmann. “On a critical reassessment of glacial snow lines with tropical sea surface temperatures”, revised version, to be resubmitted to *Geochemistry, Geophysics, Geosystems.*

Chapter 3: Stephan J. Lorenz and Gerrit Lohmann. “Acceleration technique for Milankovitch type forcing in a coupled atmosphere-ocean circulation model: method and application for the Holocene”, *Climate Dynamics, 23* (7-8), 727-743, doi:10.1007/s00382-004-0469-y, 2004.

Chapter 4: Stephan J. Lorenz, Jung-Hyun Kim, Norel Rimbu, Ralph R. Schneider, and Gerrit Lohmann. “Orbitally-driven insolation forcing on Holocene climate trends: evidence from alkenone data and climate modeling” *Paleoceanography, 21*, PA1002, doi:10.1029/2005PA001152, 2006.

Chapter 5: Thomas Felis, Gerrit Lohmann, Henning Kuhnert, Stephan J. Lorenz, Dennis Scholz, Jürgen Pätzold, Saber A. Al-Rousan, and Salim M. Al-Moghrabi. "Increased seasonality in Middle East temperatures during the last interglacial period", *Nature, 429,* S. 164-168, 2004.

Appendix A: Klaus Herterich, Stefan Determann, Björn Grieger, Imke Hansen, Philipp Helbig, Stephan J. Lorenz, Andreas Manschke, Michael Matthies, André Paul, Reiner Schlotte and Ulrike Wyputta. "Reconstructing and Modelling the Last Glacial Maximum: Beyond CLIMAP", in *"Use of Proxies in Paleoceanography: Examples from the South Atlantic"*, edited by Günther Fischer and Gerold Wefer, Springer-Verlag, Berlin, Heidelberg, 687-714, 1999.

1.4 References

Anderson, D. M., and R. S. Webb, Ice-age tropics revisited, *Nature*, *367*, 23–24, 1994.

Bard, E., Comparison of alkenone estimates with other paleotemperature proxies, *Geochemistry Geophysics Geosystems*, *2*, doi:2000GC000,050, 2001.

Bard, E., F. Rostek, and C. Sonzogni, Interhemispheric synchrony of the last deglaciation inferred from alkenone palaeothermometry, *Nature*, *385*, 707–710, 1997.

Baumann, K.-H., H. Andruleit, A. Schröder-Ritzrau, and C. Samtleben, Spatial and temporal dynamics of coccolithophore communites during non-production phases in the Norwegian-Greenland Sea, in *Contribution to the Micropaleontology and Paleoceanography of the northern North Atlantic*, edited by H. C. Hass and M. A. Kaminski, pp. 227–243, Grzybowski Found. Spec. Publ. 5, Krawów, 1997.

Berger, A. L., Long-term variations of daily insolation and Quaternary climatic changes, *Journal of the Atmospheric Sciences*, *35*, 2362–2367, 1978.

Berger, A. L., and M.-F. Loutre, Insolation values for the climate of the last 10 million years, *Quaternary Science Reviews*, *10*, 297–317, 1991.

Berger, A. L., M.-F. Loutre, and C. Tricot, Insolation and Earth's orbital periods, *Journal of Geophysical Research*, *98*, 10.341–10.362, 1993.

*Berger, A. L., M.-F. Loutre, F. Kaspar, and S. J. Lorenz, Insolation during interglacials, in *The climate of past interglacials*, edited by F. Sirocko, T. Litt, M. Claussen, and F. Sanchez-Goni, Development in Paleoenvironmental Research, Elsevier, accepted, Berlin, 2006.

Blunier, T., and E. J. Brook, Timing of millennial-scale climate change in Antarctica and Greenland during the last glacial period, *Science*, *291*, 109–112, 2001.

Brassell, S. C., G. Eglinton, I. T. Marlowe, U. Pflaumann, and M. Sarnthein, Molecular stratigraphy: a new tool for climatic assessment, *Nature*, *320*, 129–133, 1986.

Cane, M. A., A role for the tropical Pacific, *Science*, *282*, 59–61, 1998.

CLIMAP Project Members, The surface of the ice age Earth, *Science*, *191*, 1131–1137, 1976.

CLIMAP Project Members, Seasonal reconstructions of the Earth surface at the last glacial maximum, *GSA Map and Chart Ser. MC-36*, Geol. Soc. Am., Boulder, Colorado, 1981.

Cole, J. E., R. B. Dunbar, T. R. McClanahan, and N. A. Muthiga, Tropical Pacific forcing of decadal SST variability in the western Indian Ocean over the past two centuries, *Science*, *287*, 617–619, 2000.

Crowley, T. J., CLIMAP SSTs re-revisited, *Climate Dynamics*, *16*, 241–255, 2000.

*Publications with contributions of the author are marked with an asterisk

Crowley, T. J., and S. K. Baum, Effect of vegetation on an ice-age climate model simulation, *Journal of Geophysical Research*, *102*, 16.463–16.480, 1997.

Dansgaard, W., S. J. Johnsen, H. B. Clausen, D. Dahl-Jensen, N. S. Gundestrup, C. U. Hammer, C. S. Hvidberg, J. P. Steffensen, A. E. Sveinbjörnsdottir, J. Jouzel, and G. Bond, Evidence for general instability of past climate from a 250-kyr ice-core record, *Nature*, *364*, 218–220, 1993.

Emiliani, C., Pleistocene temperatures, *The Journal of Geology*, *63*, 538–578, 1955.

Fairbanks, R. G., A 17,000 year glacio-eustatic sea level record: Influence of glacial melting rates on the Younger Dryas event and deep ocean circulation, *Nature*, *342*, 637–642, 1989.

Farrera, I., S. Harrison, I. Prentice, G. Ramstein, J. Guiot, P. Bartlein, R. Bonnefille, M. Bush, U. von Grafenstein, K. Holmgren, H. Hooghiemstra, G. Hope, D. Jolly, S.-E. Lauritzen, Y. Ono, S. Pinot, M. Stute, and G. Yu, Tropical climates at the last glacial maximum: a new synthesis of terrestrial palaeoclimate data. 1. Vegetation, lake-levels and geochemistry, *Climate Dynamics*, *12*, 823–856, 1999.

Felis, T., and J. Pätzold, Climate records from corals, in *Marine Science Frontiers for Europe*, edited by G. Wefer, F. Lamy, and F. Mantoura, pp. 11–27, Springer-Verlag, Berlin, Heidelberg, 2003.

Felis, T., J. Pätzold, Y. Loya, M. Fine, A. H. Nawar, and G. Wefer, A coral oxygen isotope record from the northern Red Sea documenting NAO, ENSO, and North Pacific teleconnections on Middle East climate variability since the year 1750, *Paleoceanography*, *15*, 679–694, 2000.

*Felis, T., G. Lohmann, H. Kuhnert, S. J. Lorenz, D. Scholz, J. Pätzold, S. A. Al-Rousan, and S. M. Al-Moghrabi, Increased seasonality in Middle East temperatures during the last interglacial period, *Nature*, *429*, 164–168, 2004.

*François, L. M., Y. Goddéris, P. Warnant, G. Ramstein, N. de Noblet, and S. Lorenz, Carbon stocks and isotopic budgets of the terrestrial biosphere at mid-Holocene and last glacial maximum times, *Chemical Geology*, *159*, 163–189, 1999.

Franzke, C., K. Fraedrich, and F. Lunkeit, Teleconnection and low-frequency variability in idealized experiments with two storm tracks, *Q. J. Roy. Meteor. Soc.*, *127*, 1321–1340, 2001.

*Groll, N., M. Widmann, J. M. Jones, F. Kaspar, and S. J. Lorenz, Simulated differences in local to large-scale slimate relationships between the Eemian (125 ky BP) and the pre-industrial period, *Journal of Climate*, *18*, 4035–4048, 2005.

Grootes, P. M., M. Stuiver, J. W. C. White, S. J. Johnsen, and J. Jouzel, Comparison of oxygen isotope records from the GISP2 and GRIP Greenland ice cores, *Nature*, *366*, 552–554, 1993.

Guilderson, T. P., R. G. Fairbanks, and J. C. Rubenstone, Tropical temperature variations since 20,000 years ago: modulating interhemispheric climate change, *Science*, *263*, 663–665, 1994.

Hays, J. D., J. Imbrie, and N. J. Shackleton, Variations in the Earth's orbit: pacemaker of the ice ages, *Science*, *194*, 1121–1132, 1976.

Herterich, K., Modellierung eiszeitlicher Klimaschwankungen, *Habilitationsschrift*, Universität Hamburg, Fachbereich Geowissenschaften, Hamburg, Germany, 1990.

*Herterich, K., S. Determann, B. Grieger, I. Hansen, P. Helbig, S. Lorenz, A. Manschke, M. Matthies, A. Paul, R. Schlotte, and U. Wyputta, Reconstructing and modelling the last glacial maximum: Beyond CLIMAP, in *Use of Proxies in Paleoceanography: Examples from the South Atlantic*, edited by G. Fischer and G. Wefer, pp. 687–714, Springer-Verlag, Berlin, Heidelberg, 1999.

Imbrie, J., J. D. Hays, D. G. Martinson, A. McIntyre, A. C. Mix, J. J. Morley, N. G. Pisias, W. L. Prell, and N. J. Shackleton, The orbital theory of Pleistocene climate: Support from a revised chronology of the marine $\delta^{18}O$ record, in *Milankovič and Climate, Part I*, edited by A. Berger, J. Imbrie, J. Hays, G. Kukla, and B. Saltzman, pp. 269–306, D. Reidel Publishing Company, Dortrecht, Boston, Lancaster, 1984.

Imbrie, J., E. A. Boyle, S. C. Clemens, A. Duffy, W. R. Howard, G. Kukla, J. E. Kutzbach, D. G. Martinson, A. McIntyre, A. C. Mix, B. Molfino, J. J. Morley, L. C. Peterson, N. G. Pisias, W. L. Prell, M. E. Raymo, N. J. Shackleton, and J. R. Toggweiler, On the structure and origin of major glaciation cycles: 1. linear responses to Milankovitch forcing, *Paleoceanography*, *7*, 701–738, 1992.

Imbrie, J., A. Berger, E. A. Boyle, S. C. Clemens, A. Duffy, W. R. Howard, G. Kukla, J. E. Kutzbach, D. G. Martinson, A. McIntyre, A. C. Mix, B. Molfino, J. J. Morley, L. C. Peterson, N. G. Pisias, W. L. Prell, M. E. Raymo, N. J. Shackleton, and J. R. Toggweiler, On the structure and origin of major glaciation cycles: 2. the 100,000-year cycle, *Paleoceanography*, *8*, 699–735, 1993.

Jickells, T. D., P. P. Newton, P. King, R. S. Lampitt, and C. A. Boutle, Comparison of sediment trap records of particle fluxes from 19 to 48°N in the northeast Atlantic and their relation to surface water productivity, *Deep-Sea Research*, *48*, 971–986, 1996.

Joussaume, S., and K. E. Taylor, The Paleoclimate Modeling Intercomparison Project, in *Paleoclimate Modeling Intercomparison Project (PMIP): proceedings of the third PMIP workshop, Canada, 4-8 October 1999*, edited by P. Braconnot, WCRP-111, WMO/TD-1007, pp. 9–24, World Meteorological Organization, 2000.

Kiefer, T., M. Sarnthein, H. Erlenkeuser, P. M. Grootes, and A. P. Roberts, North Pacific response to millennial-scale changes in ocean circulation over the last 60 kyr, *Paleoceanography*, *16*, 179–189, 2001.

*Kiefer, T., S. J. Lorenz, M. Schulz, G. Lohmann, M. Sarnthein, and H. Elderfield, Response of precipitation over Greenland and the adjacent ocean to North-Pacific warm spells during Dansgaard-Oeschger stadials, *Terra Nova*, *14*, 295–300, 2002.

*Kim, J.-H., N. Rimbu, S. J. Lorenz, G. Lohmann, S. Schouten, S.-I. Nam, C. Rühlemann, and R. R. Schneider, North Pacific and North Atlantic sea-surface temperature variability during the Holocene, *Quaternary Science Reviews*, *23*, 2141–2154, 2004.

*Kleidon, A., and S. J. Lorenz, Deep roots sustain Amazonian rainforest in climate model simulations of the last ice age, *Geophysical Research Letters*, *28*, 2425–2428, 2001.

Kohfeld, K., and S. P. Harrison, How well can we simulate past climates? Evaluating the models using global palaeoenvironmental data sets, *Quaternary Science Reviews*, *19*, 321–346, 2000.

Laskar, J., P. Robutel, F. Joutel, M. Gastineau, A. C. M. Correia, and B. Levrard, A long-term numerical solution for the insolation quantities of the Earth, *Astronomy Astrophysics*, *428*, 261–285, 2004.

Lea, D. W., D. K. Pak, and H. J. Spero, Climate impact of late Quaternary equatorial Pacific sea surface temperature variations, *Science*, *289*, 1719–1724, 2000.

Lee, K. E., and N. C. Slowey, Cool surface waters of the subtropical North Pacic Ocean during the last glacial, *Nature*, *397*, 512–514, 1999.

Legutke, S., and R. Voss, The Hamburg atmosphere-ocean coupled circulation model ECHO-G, *Technical Report 18*, Deutsches Klimarechenzentrum, Hamburg, Germany, 1999.

Levitus, S., and T. P. Boyer, World Ocean Atlas 1994, Volume 4: Temperature, *NOAA Atlas NESDIS 4*, U.S. Gov. Printing Office, Washington D.C., 1994.

*Lohmann, G., and S. J. Lorenz, The hydrological cycle under paleoclimatic conditions as derived from AGCM simulations, *Journal of Geophysical Research*, *105*, 17,417–17,436, 2000.

*Lohmann, G., and S. J. Lorenz, Orbital forcing on atmospheric dynamics during the last interglacial and glacial inception, in *The climate of past interglacials*, edited by F. Sirocko, T. Litt, M. Claussen, and F. Sanchez-Goni, Development in Paleoenvironmental Research, Elsevier, accepted, Berlin, 2006.

*Lohmann, G., S. J. Lorenz, and M. Prange, Northern high-latitude climate changes during the Holocene as simulated by circulation models, in *The Nordic Seas: An Integrated Perspective*, edited by H. Drange, T. Dokken, T. Furevik, R. Gerdes, and W. Berger, no. 158 in Geophys. Monogr., pp. 273–288, American

Geophysical Union, Washington DC, 2005.

*Lorenz, S., B. Grieger, P. Helbig, and K. Herterich, Investigating the sensitivity of the atmospheric general circulation model ECHAM 3 to paleoclimatic boundary conditions, *International Journal of Earth Sciences*, *85*, 513–524, 1996.

*Lorenz, S. J., and G. Lohmann, Acceleration technique for Milankovitch type forcing in a coupled atmosphere-ocean circulation model: method and application for the Holocene, *Climate Dynamics*, *23*, 727–743, 2004.

*Lorenz, S. J., and G. Lohmann, On a critical reassessment of glacial snow lines with tropical sea surface temperatures, *Geochemistry Geophysics Geosystems*, *submitted, revised form*, 2006.

*Lorenz, S. J., D. Kasang, and G. Lohmann, Globaler Wasserkreislauf und Klimaänderung — eine Wechselbeziehung, in *Warnsignal Klima: Genug Wasser für alle?*, edited by J. Lozán, H. Graßl, P. Hupfer, L. Menzel, and C.-D. Schönwiese, Wissenschaftliche Auswertungen, Hamburg, 2004.

*Lorenz, S. J., J.-H. Kim, N. Rimbu, R. R. Schneider, and G. Lohmann, Orbitally driven insolation forcing on Holocene climate trends: evidence from alkenone records and climate modeling, *Paleoceanography*, *21*, PA1002, 2006.

Loutre, M. F., A. Berger, P. Bretagnon, and P.-L. Blanc, Astronomical frequencies for climate research at the decadal to century time scale, *Climate Dynamics*, *7*, 181–194, 1992.

Milankovič, M., *Kanon der Erdbestrahlung und seine Anwendung auf das Eiszeitenproblem*, 132, Königlich Serbische Akademie, Sektion der Naturwissenschaften und der Mathematik, Spezielle Ausgabe, Belgrad, 1941.

Mix, A. C., E. Bard, and R. Schneider, Environmental processes of the ice age: land, oceans, glaciers (EPILOG), *Quaternary Science Reviews*, *20*, 627–657, 2001.

Müller, P. J., and G. Fischer, A 4-year sediment trap record of alkenones from the filamentous upwelling region off Cape Blanc, NW Africa and a comparison with distributions in underlying sediments, *Deep-Sea Research*, *48*, 1877–1903, 2001.

Müller, P. J., G. Kirst, G. Ruhland, I. von Storch, and A. Rosell-Melé, Calibration of the alkenone palaeotemperature index (UK'37) based on core-tops from the eastern South Atlantic and the global ocean (60 °N-60°S), *Geochimica et Cosmochimica Acta*, *62*, 1757–1772, 1998.

Petit, J. R., J. Jouzel, D. Raynaud, N. I. Barkov, J.-M. Barnola, I. Basile, M. Bender, J. Chappellaz, M. Davis, G. Delaygue, M. Delmotte, V. M. Kotlyakov, M. Legrand, V. Y. Lipenkov, C. Lorius, L. Pépin, C. Ritz, E. Saltzman, and M. Stievenard, Climate and atmospheric history of the past 420,000 years from the Vostok ice core, Antarctica, *Nature*, *399*, 429–436, 1999.

Porter, S. C., Snowline depression in the tropics during the last glaciation, *Quaternary Science Reviews*, *20*, 1067–1091, 2001.

Prahl, F. G., and S. G. Wakeham, Calibration of unsaturation patterns in long-chain ketone compositions for paleotemperature assessment, *Nature*, *330*, 367–369, 1987.

Prahl, F. G., L. A. Muehlhausen, and D. L. Zahnle, Further evaluation of long-chain alkenones as indicators of paleoceanographic conditions, *Geochimica et Cosmochimica Acta*, *52*, 2303–2310, 1988.

Prell, W. L., The stability of low-latitude sea-surface temperatures: An evaluation of the CLIMAP reconstruction with emphasis on the positive SST anomalies, *Report TR025*, U.S. Department of Energy, Washington, D. C., 1985.

Rimbu, N., G. Lohmann, T. Felis, and J. Pätzold, Arctic Oscillation signature in a Red Sea coral, *Geophysical Research Letters*, *28*, 2959–2962, 2001.

Rimbu, N., G. Lohmann, T. Felis, and J. Pätzold, Shift in ENSO teleconnections recorded by a northern Red

Sea coral, *Journal of Climate*, *16*, 1414–1422, 2003a.

Rimbu, N., G. Lohmann, J.-H. Kim, H. W. Arz, and R. R. Schneider, Arctic/North Atlantic Oscillation signature in Holocene sea surface temperature trends as obtained from alkenone data, *Geophysical Research Letters*, *30*, 1280–1283, 2003b.

*Rimbu, N., G. Lohmann, S. J. Lorenz, J.-H. Kim, and R. R. Schneider, Holocene climate variability as derived from alkenone sea surface temperature and coupled ocean-atmosphere model experiments, *Climate Dynamics*, *23*, 215–227, 2004.

*Rodgers, K. B., G. Lohmann, S. J. Lorenz, R. Schneider, and G. M. Henderson, A tropical mechanism for northern hemisphere deglaciation, *Geochemistry Geophysics Geosystems*, *4*, doi:10.1029/2003GC000,508, 2003.

*Rodgers, K. B., S. Charbit, M. Kageyama, G. Ramstein, C. Ritz, J. Yin, G. Lohmann, S. J. Lorenz, and M. Khodri, Sensitivity of Northern Hemispheric continental ice sheets to tropical sst during deglaciation, *Geophysical Research Letters*, *31*, doi:10.1029/2003GL018,375, 2004.

Roeckner, E., K. Arpe, L. Bengtsson, S. Brinkop, L. Dümenil, M. Esch, E. Kirk, F. Lunkeit, M. Ponater, B. Rockel, R. Sausen, U. Schlese, S. Schubert, and M. Windelband, Simulation of the present-day climate with the ECHAM model: Impact of model physics and resolution, *Report 93*, Max-Planck-Institut für Meteorologie, 1992.

Roeckner, E., K. Arpe, L. Bengtsson, M. Christoph, M. Claussen, L. Dümenil, M. Esch, M. Giorgetta, U. Schlese, and U. Schulzweida, The atmospheric general circulation model ECHAM-4: Model description and simulation of the present-day climate, *Report 218*, Max-Planck-Institut für Meteorologie, 1996.

Rohling, E. J., M. Fenton, F. J. Jorissen, P. Bertrand, G. Ganssen, and J. P. Caulet, Magnitudes of sea-level lowstands of the past 500,000 years, *Nature*, *394*, 162–165, 1998.

Rosell-Melé, A., G. Eglinton, U. Pflaumann, and M. Sarnthein, Atlantic core-top calibration of the UK37 index as a sea-surface palaeotemperature indicator, *Geochimica et Cosmochimica Acta*, *59*, 3099–3107, 1995.

Rosell-Melé, A., E. Bard, K.-C. Emeis, J. O. Grimalt, P. J. Müller, R. R. Schneider, and 36 international participants, Precision of the current methods to measure the alkenone proxy UK'37 and absolute alkenone abundance in sediments: results of an interlaboratory comparision study, *Geochemistry Geophysics Geosystems*, *2*, 2000GC000,141, 1–28, 2001.

Rühlemann, C., S. Mulitza, P. J. Müller, G. Wefer, and R. Zahn, Warming of the tropical Atlantic Ocean and slowdown of thermohaline circulation during the last deglaciation, *Nature*, *399*, 452–455, 1999.

Sarnthein, M., R. Gersonde, H.-S. Niebler, U. Pflaumann, R. Spielhagen, J. Thiede, G. Wefer, and M. Weinelt, Overview of glacial Atlantic Ocean mapping (GLAMAP 2000), *Paleoceanography*, *18*, 2003.

Schlesinger, M. E., Discussion of "A global ocean-atmosphere model with seasonal variation for future studies of climate sensitivity", *Dynamics of Atmosphere and Oceans*, *3*, 427–432, 1979.

*Schneider, R. R., J.-H. Kim, N. Rimbu, S. J. Lorenz, G. Lohmann, U. Cubasch, J. Pätzold, and G. Wefer, Global Holocene Spatial and Temporal Climate Variability: combination of paleotemperature records, statistics and modeling, *Pages News*, *12*, 25–26, 2004.

Seltzer, G. O., Late Quaternary glaciation in the tropics: future research directions, *Quaternary Science Reviews*, *20*, 1063–1066, 2001.

Sikes, E. L., J. K. Volkman, L. G. Robertson, and J.-J. Pichon, Alkenones and alkenes in surface water and sediments of the Southern Ocean: implications for paleotemperature estimation in polar regions, *Geochimica et Cosmochimica Acta*, *61*, 1495–1505, 1997.

Stute, M., M. Forster, H. Frischkorn, A. Sereno, J. F. Clark, P. Schlosser, W. S. Broecker, and G. Bonani, Cooling of tropcal Brazil (5°C) during the Last Glacial Maximum, *Science*, *269*, 379–383, 1995.

Thompson, D. W. J., and J. M. Wallace, The Arctic oscillation signature in the wintertime geopotential height and temperature fields, *Geophysical Research Letters*, *25*, 1297–1300, 1998.

Thompson, D. W. J., and J. M. Wallace, Regional climate impacts of the Northern Hemisphere Annular Mode, *Science*, *293*, 85–89, 2001.

Thompson, L., E. Mosley-Thompson, M. E. Davis, P. N. Lin, K. A. Henderson, J. Cole-Dai, J. F. Bolzai, and K.-B. Liu, Late glacial stage and Holocene tropical ice core records from Huascaran, Peru, *Science*, *269*, 46–50, 1995.

Voss, R., R. Sausen, and U. Cubasch, Periodically synchronously coupled integrations with the atmosphere-ocean general circulation model ECHAM3/LSG, *Climate Dynamics*, *14*, 249–266, 1998.

Weyhenmeyer, C. E., S. J. Burns, H. N. Waber, W. Aeschbach-Hertig, R. Kipfer, H. H. Loosli, and A. Matter, Cool glacial temperatures and changes in moisture source recorded in Oman groundwaters, *Science*, *287*, 842–845, 2000.

Wolff, J.-O., E. Maier-Reimer, and S. Legutke, The Hamburg ocean primitive equation model HOPE, *Technical Report 13*, Deutsches Klimarechenzentrum, Hamburg, Germany, 1997.

Chapter 2

On a critical reassessment of glacial snowlines and tropical sea surface temperatures

Abstract.

Reconstructions of tropical snowlines during the last glacial maximum 21,000 years ago are incompatible with the sea surface temperature (SST) reconstructions of the Climate: Long-Range Investigation, Mapping, and Prediction (CLIMAP) project, when assuming present day atmospheric environmental lapse rates. Different reconstructions of the last glacial maximum and an interglacial climate are applied to an atmospheric general circulation model. The recent reconstructions of glacial Atlantic SST within the Glacial Atlantic Ocean Mapping Project (GLAMAP) as well as a cooling of tropical SSTs by 3 Kelvin relative to the ones suggested by CLIMAP are applied. The simulated glacial climate and the result of a vegetation model are compared with pollen based temperature proxy data. The experiments reveal that the moderate tropical cooling of SSTs relative to CLIMAP is consistent with much lower temperatures than today in the tropical mountains and reduced occurrence of tropical trees. The depression of tropical snowlines can be attributed to less moisture content affecting an increased lapse rate in the free atmosphere, and reduced surface temperature near tropical glaciers due to a longer duration of snow cover. Our model result provides a consistent view of the last glacial maximum climate with much lower temperatures than today in the tropical mountains in concordance with a moderate decrease of tropical SSTs.

2.1 Introduction

The global reconstruction of sea surface temperatures (SST) of the last glacial maximum (LGM) by the Climate: Long-Range Investigation, Mapping, and Prediction (CLIMAP) project in the late

Stephan Lorenz und Gerrit Lohmann, revised version, submitted to *Geochemistry, Geophysics, Geosystems.*

seventies [*CLIMAP Project Members*, 1976, 1981] has initiated an enduring dispute on its consistency with reconstructions of terrestrial tropical climate [*Webster and Streten*, 1978; *Rind and Peteet*, 1985; *Betts and Ridgway*, 1992; *Broccoli and Marciniak*, 1996; *Lee and Slowey*, 1999; *Hostetler and Clark*, 2000; *Crowley*, 2000a; *Mix et al.*, 2001; *Greene et al.*, 2002]. The CLIMAP-reconstruction of the tropical marine climate was based on transfer functions to connect assemblages of planktic foraminifera with near surface water temperature. Results show only moderate temperature decrease of SST in the tropical oceans. In the equatorial tropics (10°N to 10°S) SST was about 1–2 K lower than today, 1.4 K in the annual mean. In the subtropical gyres, especially in the Pacific Ocean, there are wide areas where surface waters were reconstructed to be even 1–3 K warmer during the LGM relative to the present day SST [*CLIMAP Project Members*, 1981; *Lohmann and Lorenz*, 2000].

A number of climate reconstructions are in conflict with these CLIMAP findings. From marine as well as from terrestrial sites colder glacial tropics have been detected [see *Anderson and Webb*, 1994; *Crowley*, 2000a]: analyses of noble gases from groundwater in tropical lowlands from Brasil and Florida [*Stute et al.*, 1995] as well as from Oman [*Weyhenmeyer et al.*, 2000] result in near surface temperature changes which are in agreement with those from isotopic measurements from tropical mountain glaciers [*Thompson et al.*, 1995]. More evidence exists from the analysis of oxygen isotopes and of strontium to calcium ratios in Caribbean corals [*Guilderson et al.*, 1994]. These three parameters indicate surface temperatures 4–6 K colder compared to today. This is about 2–4 K colder than the drop of SSTs suggested by CLIMAP. Newly calculated transfer functions for interpretation of assemblages of planctic foraminifera also suggest temperatures remarkably lower than CLIMAP in some tropical areas [*Lee and Slowey*, 1999; *Mix et al.*, 1999; *Mix et al.*, 2001]. Furthermore, SST-reconstructions from alkenones result in 3–4 K tropical temperature difference between LGM and today [*Bard et al.*, 1997; *Rühlemann et al.*, 1999]. This latter value is in between the reduction due to CLIMAP and the three former reconstructions of temperature change. In summary, different proxy methods (alkenones, magnesium and strontium to calcium ratios, oxygen isotopes, transfer functions) reveal discrepancies of some Kelvin in LGM temperature reconstructions [*Bard*, 2001; *Mix et al.*, 2001].

Recently, a new collection of glacial SST in the Atlantic Ocean has recently been completed by the Glacial Atlantic Ocean Mapping Project (GLAMAP-2000, GLAMAP in the following) [*Mix*, 2003; *Sarnthein et al.*, 2003; *Paul and Schäfer-Neth*, 2003]. This project has used 275 sediment cores between the North Pole and 60°S with carefully defined chronostratigraphies and has employed improved transfer-function techniques to reconstruct SSTs and sea ice boundaries for the LGM from census counts of microfossils, including radiolarians and diatoms [*Sarnthein et al.*, 2003; *Niebler et al.*, 2003]. While the GLAMAP SST patterns differ significantly in crucial regions of the Atlantic Ocean from the ones reconstructed by *CLIMAP Project Members* [1981], up to now there exist no such collections for the Indian and Pacific Oceans.

The height of the snowline of tropical mountain glaciers during LGM is another important indication for paleoclimate temperature changes. The snowline is the lowest elevation of perennial snow on a glacier and is equivalent with the minimal snow cover at the end of the ablation season [*Porter*, 2001]. The height above sea level of the equilibrium-line (the “equilibrium-line altitude”, ELA) of a glacier where the glacier mass balance equals zero divides the accumulation from the ablation zone.

The snowline of a glacier is often used as a synonym for the ELA. On a large scale average, both lines are very similar in height. On temperate and tropical glaciers they are in close vicinity with the zero-degree (0°C) isoline.

The ELA can be deduced from reconstructed extent and height of paleoclimatic moraines. Such moraines are built by deposit of detritus during periods of waxing glaciers and left over after their retreat. The reconstructed size of a tropical glacier during LGM can be translated into a glacial ELA using various methods. The "toe to head altitude ratio" (THAR) method assumes a constant ratio of $\sim 0.35 \pm 0.15$ for the the lowest and highest altitude of tropical glacier dimensions in the Central Andes [*Klein et al.*, 1999]. The "accumulation-area ratio" (AAR) method is based on a constant ratio of the accumulation area of such glaciers ($\sim 0.67 \pm 0.15$), which determines the altitude of the snowline in a given topography [*Klein et al.*, 1999; *Porter*, 2001].

Variations of the ELA of mountain glaciers have been interpreted in terms of their mean response to climatic fluctuations on time scales of 10^3 to 10^4 years, where glacier dynamics are not considered. Fluctuations in the height of the snowlines are controlled by various climate-related parameters, such as temperature, precipitation, radiation balance, wind speed, and humidity [*Seltzer*, 1994]. In most paleoclimate studies using snowline reconstructions, a change in ELA is translated into a temperature variation by assuming a constant vertical temperature gradient, the environmental lapse rate, typical for the large scale climate of the respective region. This approach does not consider the effect of changes in accumulation, radiation balance, and latent heat transfer on ELA.

Today, the snowline is at a height of more than 4.5 km in most of the tropical mountains [*Porter*, 2001]. During the last decades much research has been undertaken to reconstruct and precisely date the extent of tropical mountain glaciers and their ELA during glacial times [e. g. *Webster and Streten*, 1978; *Porter*, 1979; *Crowley and North*, 1990; *Seltzer*, 1994; *Mark et al.*, 2002]. Based on a review of the evidence from 12 tropical sites in Africa, America, and Pacific islands, *Porter* [2001] concluded that glacial snowlines were 800 to 1000 m lower than today (see also table 3 of *Greene et al.* [2002]). Taking into account the glacial change in sea level of 120 m [*Fairbanks*, 1989; *Rohling et al.*, 1998], the 900 ± 135 m change in ELA translates into a 780 m drop of the 0°C isoline. Using an appropriate constant environmental lapse rate, this corresponds to a ∼5–7 K mean annual temperature drop, which may at least provide a first-order approximation of regional and global tropical temperature reduction at the LGM [*Seltzer*, 2001]. This temperature drop is based on tropical lapse rates, which lie between the dry (10 K/km) and the moist (5 K/km) adiabatic lapse rate. In the tropics, lapse rates are more closely linked towards the moist adiabat [*Broecker*, 1997], which transforms a snowline depression of 1 km into a temperature reduction of some 6 K. Therefore an inconsistency of at least 4 K exists between tropical temperature reconstruction by CLIMAP at the surface (1 K colder than today) and the 5–7 K cooling during LGM at the height of the tropical snowline.

In this study, simulations with an atmospheric GCM for glacial conditions are analyzed. As lower boundary condition for the atmospheric GCM, three different glacial distributions of SST and sea ice are used: first, the older one by CLIMAP, second, the updated GLAMAP reconstruction for the Atlantic (and CLIMAP for the Indo-Pacific basins), and third the CLIMAP SST with an inserted tropical cooling of three Kelvin. Furthermore, the vegetation cover is evaluated to derive the fraction of tropical trees under the different glacial conditions. The models and their boundary conditions

are introduced in the next section. In section 3, the climatology of the GCM is shown, and we discuss distributions of tropical lapse rates as well as changes in tropical trees according to the various scenarios of tropical glacial ocean temperatures. With this study, we give evidence for increased tropical lapse rates during LGM, affected by moderately colder tropical SST than CLIMAP, which are discussed in section 4. Finally, conclusions are given in the last section.

2.2 Methodology

2.2.1 The GLAMAP Atlantic Ocean SST reconstruction

For the utilization of such sparsely and irregularly distributed core sampling data as validation and forcing data for various circulation models, an interpolation onto a regular longitude-latitude grid is necessary. The GLAMAP data set, consisting of proxy-derived SST data at various core sites, was gridded onto a regular $1^\circ \times 1^\circ$ grid using an objective mapping method [*Schäfer-Neth and Paul*, 2003]. The resulting gridded GLAMAP SST data set [*Paul and Schäfer-Neth*, 2003], suitable for validation as well as forcing of oceanic and atmospheric circulation models, has been provided as surface boundary condition for one of the simulations of this study.

Two regions of special emphasis arose from currently ongoing debates: the tropics and the northern North Atlantic. For example, in the Equatorial Current, especially along the eastern boundary upwelling system off Namibia, colder temperatures than CLIMAP (4–6 K colder than today) were reconstructed within GLAMAP using a recent transfer-function approach [*Mix et al.*, 1999]. Moreover, seasonally ice-free conditions in the northern North Atlantic during the LGM were proposed [*Weinelt et al.*, 1996; *Sarnthein et al.*, 2003b].

2.2.2 The atmospheric ciculation model ECHAM

For our numerical experiments, we apply the ECHAM3 atmospheric GCM [*Roeckner et al.*, 1992] in T42 horizontal resolution with 19 vertical layers. The model uses the primitive equations and includes calculation of radiation and a hydrological cycle with transport of water vapor and cloud water. The calculation of radiation occurs with respect to the glacial level of atmospheric greenhouse gases. In the model, this is represented by prescribing an equivalent portion of atmospheric carbon dioxide (CO_2). The equivalent greenhouse gas concentration includes the effects of other gases, such as methane and nitrous oxygene.

2.2.3 Glacial boundary conditions

For paleoclimate experiments, the model was adjusted to reflect changes in orbital parameters [*Berger*, 1978; *Lorenz et al.*, 1996]. For glacial conditions (experiment `LGM.0`), we provide SST and sea ice distribution (Figure 2.1) collected by *CLIMAP Project Members* [1981]. Furthermore, the lowering of the sea level by 120 m [*Fairbanks*, 1989; *Rohling et al.*, 1998] as well as the distribution of glacial ice sheets [*Peltier*, 1994] and changed continental distribution are taken into account.

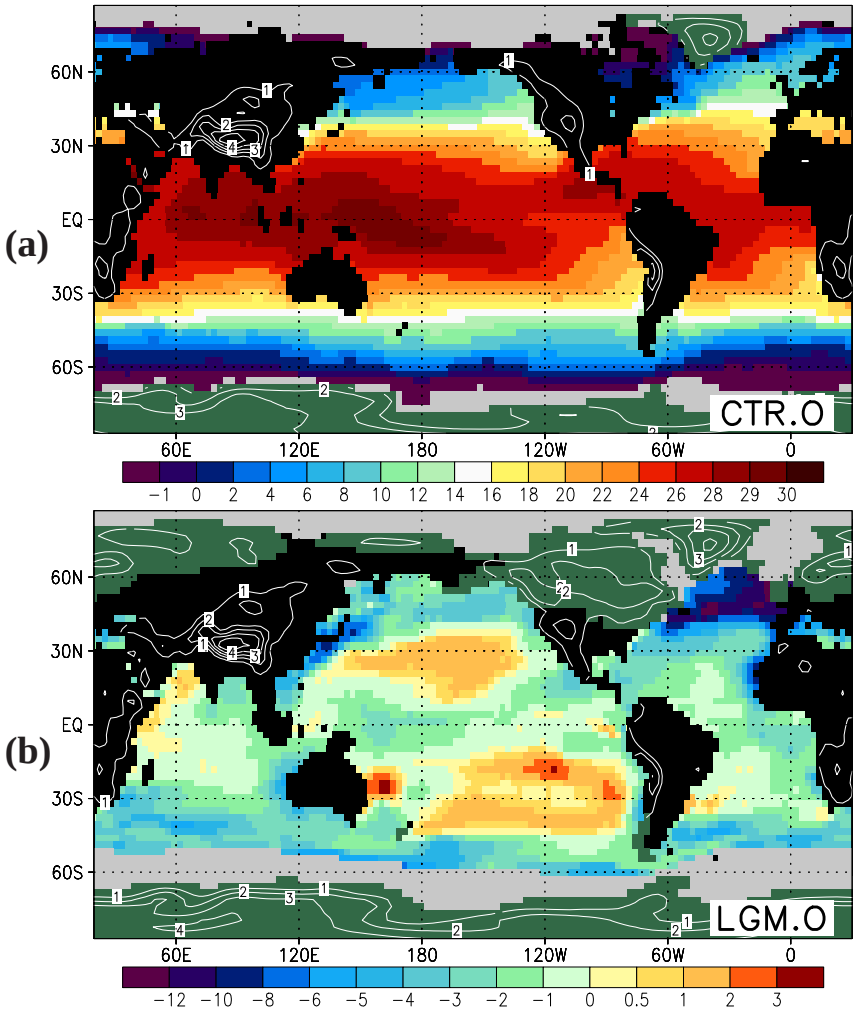

Figure 2.1: *Boundary conditions (annual mean) for (a) the control experiment (*CTR.O*) and the three LGM simulations, using different reconstructions of glacial SST and sea ice: (b) CLIMAP (exp.* LGM.O*), (c) GLAMAP in the Atlantic and CLIMAP elsewhere (exp.* LGM.G*, see continuation of this figure on next page), and (d) CLIMAP with applied cooling of 3 K between 30°N and 30°S (exp.* LGM.N*). The figure displays SST for the control experiment, anomalies from the control for the glacial experiments, sea ice cover (grey), land ice cover (green) and surface topography (isolines at 0.5, 1, 2, 3, and 4 km). SST and continents are shown in the horizontal resolution of the ECHAM (T42).*

The equivalent concentration of carbon dioxide, including the effect of other greenhouse gases like methane, used for the glacial experiments is 200 ppm.

A second glacial experiment was performed with the ECHAM model (experiment LGM.N) to test the influence of colder tropical ocean temperatures on climate [*Lohmann and Lorenz*, 2000]. In this experiment the tropical SST, as reconstructed by CLIMAP, is reduced by 3 K between 30° northern and southern latitude. A linear transition zone between 30° and 36° latitude is defined: one grid row with 2 K and one grid row with 1 K temperature reduction is used on the Northern and Southern Hemisphere, respectively. Additionally, all positive SST anomalies during glacial time are removed.

A new glacial experiment (LGM.G) is forced by the recently completed collection of glacial SST in the Atlantic Ocean (GLAMAP-2000) [*Sarnthein et al.*, 2003; *Schäfer-Neth and Paul*, 2003]. Due to the lack of similar new collections of SST for the Indian and Pacific Oceans, a combination of glacial SST is used for the GLAMAP experiment (LGM.G): the GLAMAP reconstruction is taken for the whole Atlantic Ocean down to 60°S, and that of CLIMAP for the rest of the global ocean surface (including the Mediterranean Sea). All other glacial boundary conditions for experiments LGM.N and LGM.G are the same as for LGM.O.

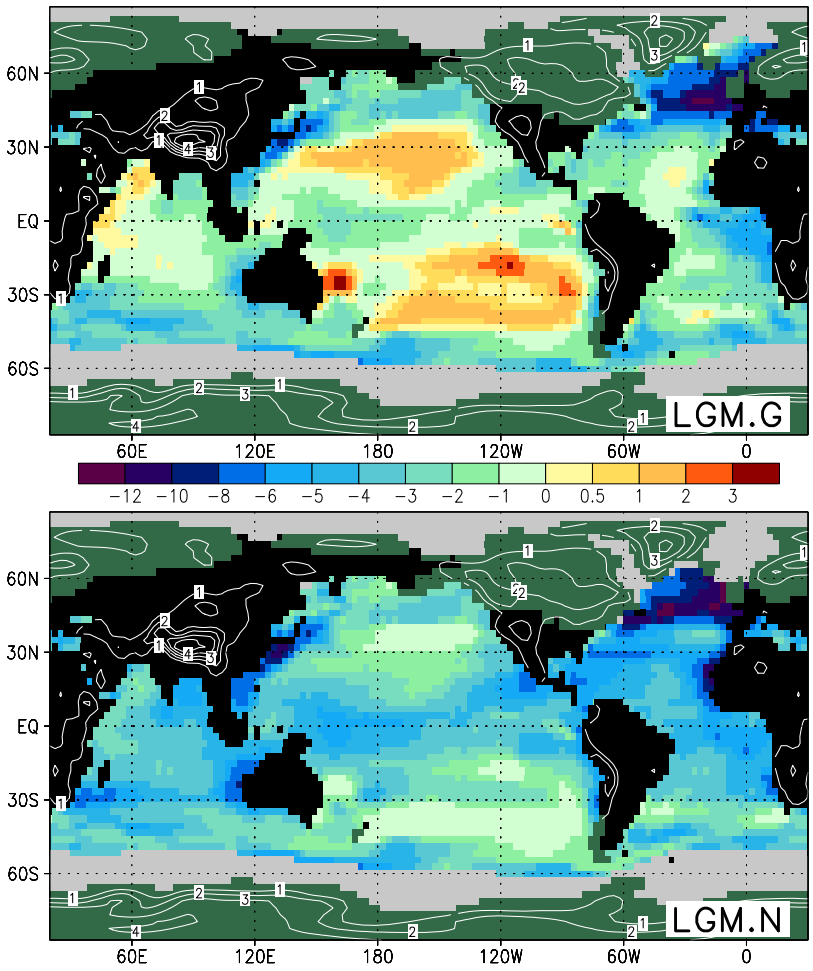

(c)

(d)

Figure 2.1 *(continued)*

The glacial experiments are compared to the control run (experiment `CTR.O`). This experiment used as lower boundary condition the distribution of SST and sea ice according to the AMIP project [*Gates*, 1992] Figure 2.1. In order to test the effect of reduced SST on modeled tropical lapse rates under interglacial conditions, a model simulation analogous to experiment `LGM.N` has been conducted (experiment `CTR.N`) using modern, interglacial SST. The SST data set according to AMIP has been reduced by 3 K in the same tropical latitude band and with the same transition zone as in experiment `LGM.N`. The boundary conditions for the control experiment as well as for the three glacial experiments are displayed in Figure 2.1.

All experiments utilizing the ECHAM3 atmospheric GCM have been integrated for 15 years in order to evaluate the climate state as the response of the model to the prescribed boundary conditions. For the analysis of these climates the first 5 years are regarded as the spin-up time of the model to adjust to the different boundary conditions. The last 10 years of each experiment are then disposed to evaluate the mean climatology of the respective simulation.

2.2.4 The global vegetation model

The Lund-Potsdam-Jena dynamic global vegetation model (LPJ) [*Sitch et al.*, 2003] combines process-based descriptions of terrestrial ecosystem structure (vegetation composition, biomass and height) and function (energy absorption, carbon cycling). Vegetation composition is described by

nine different plant functional types (PFT), which are distinguished according to their physiological, morphological (tree, grass) and phenological (deciduous, evergreen) attributes.

The model is run on a grid-cell basis with specified atmospheric CO_2–concentration and soil texture. Monthly fields of temperature, precipitation and radiation are taken from the output of the atmospheric GCM, the ECHAM3. Each grid-cell is divided into fractions covered by PFTs and bare ground. Both the presence and the covered fraction of PFTs within a grid-cell (T42) depend on their specific environmental limits and on resource competition among the PFTs.

The vegetation dynamics is calculated under four different climatic conditions for present (`CTR.O`) and glacial (`LGM.O`, `LGM.N`, and `LGM.G`) climates, respectively. The vegetation model is run for 3000 years of integration into equilibrium, using 15 years of monthly data from the ECHAM model repeatedly as input for the LPJ model. The last 10 years of each simulation have been used for the analysis of the equilibrium vegetation cover.

2.3 Results

2.3.1 Climatology of the LGM experiments

Near surface air temperature: In Figure 2.2 the global distribution of near surface temperature for the three LGM experiments are shown. Forced by CLIMAP SST anomalies (experiment `LGM.O`, Figure 2.1), moderate cooling takes place over the tropical latitude band, with stronger cooling located in northern and eastern Africa and eastern Asia. In contrast, large areas of higher temperature than today are evident in the subtropical Pacific and the western Indian Ocean, with continental warm peaks at the Amazonian mouth and northern Australia.

For the GLAMAP experiment (`LGM.G`), the patterns of surface temperature anomaly from control are very similar to those of experiment `LGM.O` over most parts of the globe. In contrast, the air temperature over the eastern equatorial Atlantic Ocean is lowered by 4–6 K in experiment `LGM.G` compared to the control experiment `CTR.O` and thus agrees more with experiment `LGM.N` than `LGM.O`. Here, the GLAMAP reconstruction of glacial SST takes effect on the simulated climate. Interestingly, the region with warm air over the Amazonian rain forest in experiment `LGM.O` is further increased up to 4 K warmer temperature than today in `LGM.G`.

The response patterns of temperature difference between the experiments `LGM.N` and `CTR.O` are very much like those of `LGM.O` minus `CTR.O`, except for the temperature drop of 3 K throughout the tropics (between 30°N and 30°S), impressed by the forcing. In the regions with warmer air than today in experiment `LGM.O` a marginal temperature decrease surrounded by regions with stronger cooling can be identified in experiment `LGM.N` (Figure 2.2). In this LGM simulation, no regions with glacial warming remain.

Precipitation: The changes in the climatological precipitation of the experiments are displayed in Figure 2.3. Vigorous changes in the global distribution of precipitation occur for the last glacial climate and are evident in the difference between the experiments `LGM.O` and `CTR.O` (upper panel of Figure 2.3). The strongest increase of precipitation takes place over the regions with glacial SST being warmer than today, like the western Indian and large parts of the subtropical Pacific Ocean. Due

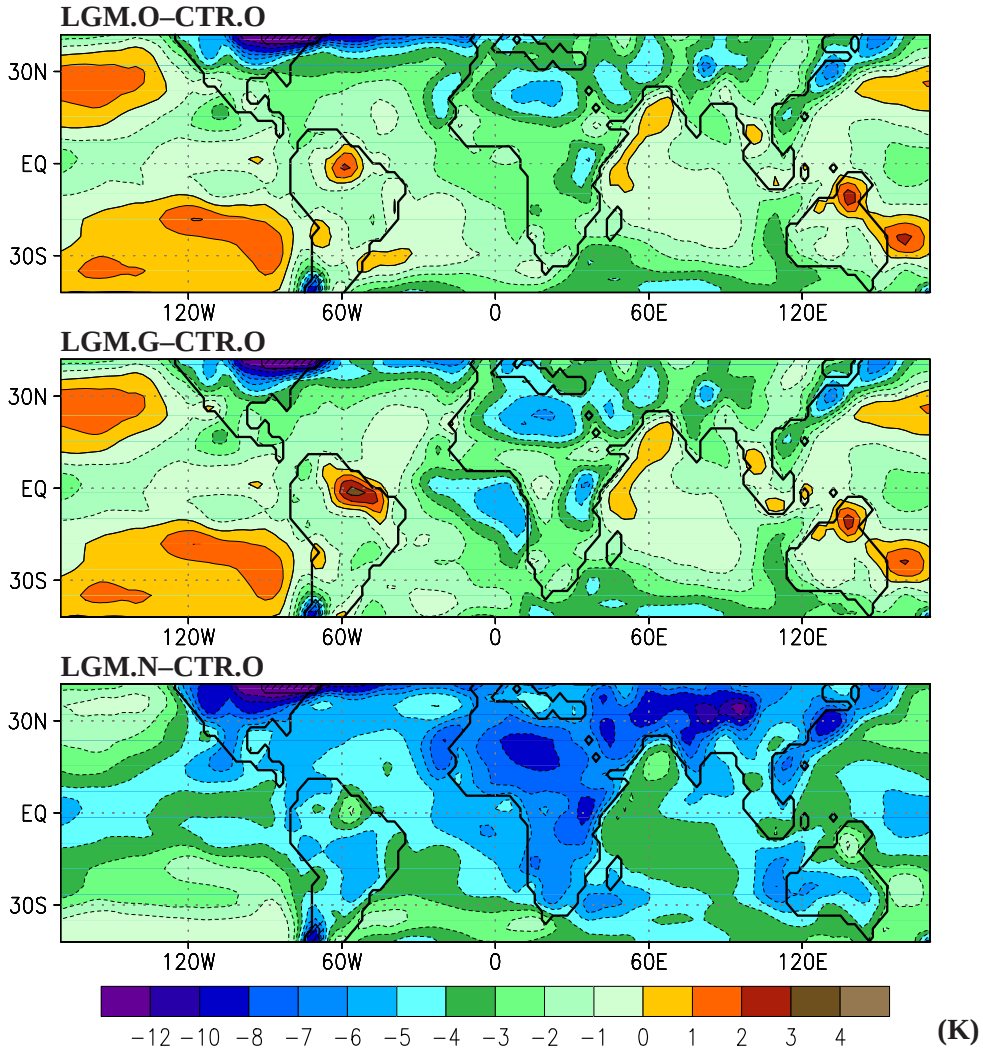

Figure 2.2: *Annual mean near surface temperature anomaly form the control experiment* `CTR.O` *(K) of three different LGM simulations as labelled in the upper left corner of each panel.*

to a strongly increased meridional temperature gradient in the subtropical Pacific, where higher SST is delimited poleward by much colder waters than today, severely changed precipitation patterns are evident. Over land, precipitation is generally reduced, moderately over the African and more vigorously over the Amazonian rainforests. Strong drying is found especially in southern and southeastern Asian summer monsoon regions.

The differences between the three LGM simulations are much less intense than between each of these experiments and the control run. Note, that in contrast to the upper panel, the other two panels in Figure 2.3 show anomalies of two experiments `LGM.G` and `LGM.N` with respect to experiment `LGM.O` (see the labels in the upper left of each panel).

Substantial changes in the experiment forced by the GLAMAP SST (`LGM.G`) relative to the CLIMAP experiment (`LGM.O`) take place in the Equatorial Atlantic and in the surrounding parts of Africa and South America. The precipitation in the Amazonian rainforest is further reduced. The experiment `LGM.N` exhibits very similar precipitation patterns (but with opposite sign) with respect to experiment `LGM.O` as does experiment `LGM.O` with respect to experiment `CTR.O`. Since the tropical

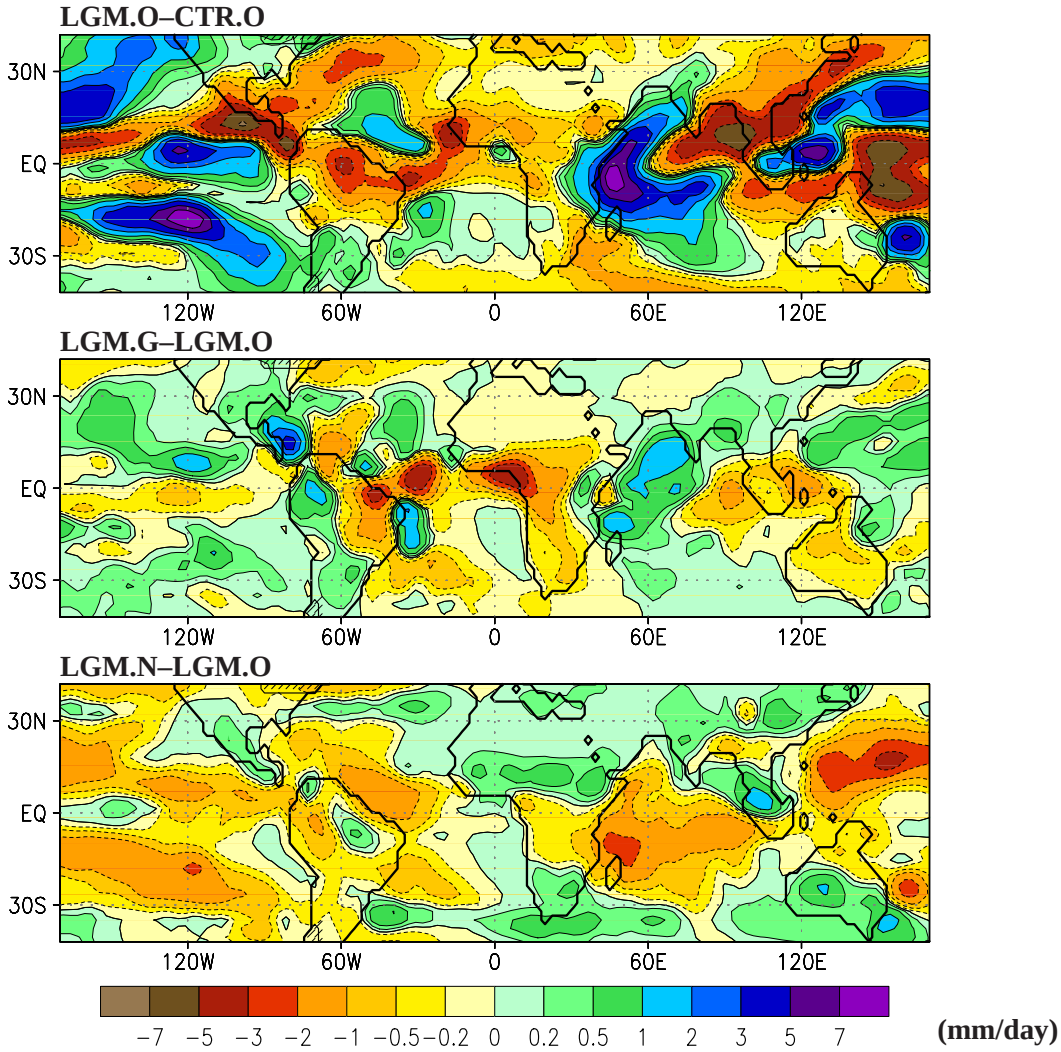

Figure 2.3: *Annual mean precipitation anomalies (mm/day) of three different LGM simulations. Note the different subtractor in the upper (experiment* `CTR.O`*), and the middle and lower (experiment* `LGM.O`*) panel, respectively.*

SST in `LGM.N` is reduced by 3 K, the meridional temperature gradient in the subtropical Pacific is also reduced. As a consequence, the differences `LGM.N` minus `CTR.O` are less extense than are those of `LGM.O` minus `CTR.O`.

Sea level pressure: The differences in sea level pressure between the glacial experiment `LGM.O` and the control experiment `CTR.O` (upper panel of Figure 2.4) indicate an enhancement of the subtropical northern and southern highs in the Atlantic but a weakening of the subtropical highs in the Pacific Ocean. Furthermore, over the southern part of the Eurasian continent the prevalent low pressure system is partly filled during glacial times. For the GLAMAP experiment `LGM.G`, the sea level pressure over the low latitude Atlantic Ocean is generally increased in comparison with experiment `LGM.O` (middle panel of Figure 2.4). The experiment `LGM.N` with colder tropical SST again opposes the changes between experiments `LGM.O` and `CTR.O`: reduced pressure in the Pacific in `LGM.O` is partly canceled in `LGM.N`, enhanced pressure in the North Atlantic in `LGM.O` is partly countervailed in `LGM.N` (lower panel of Figure 2.4).

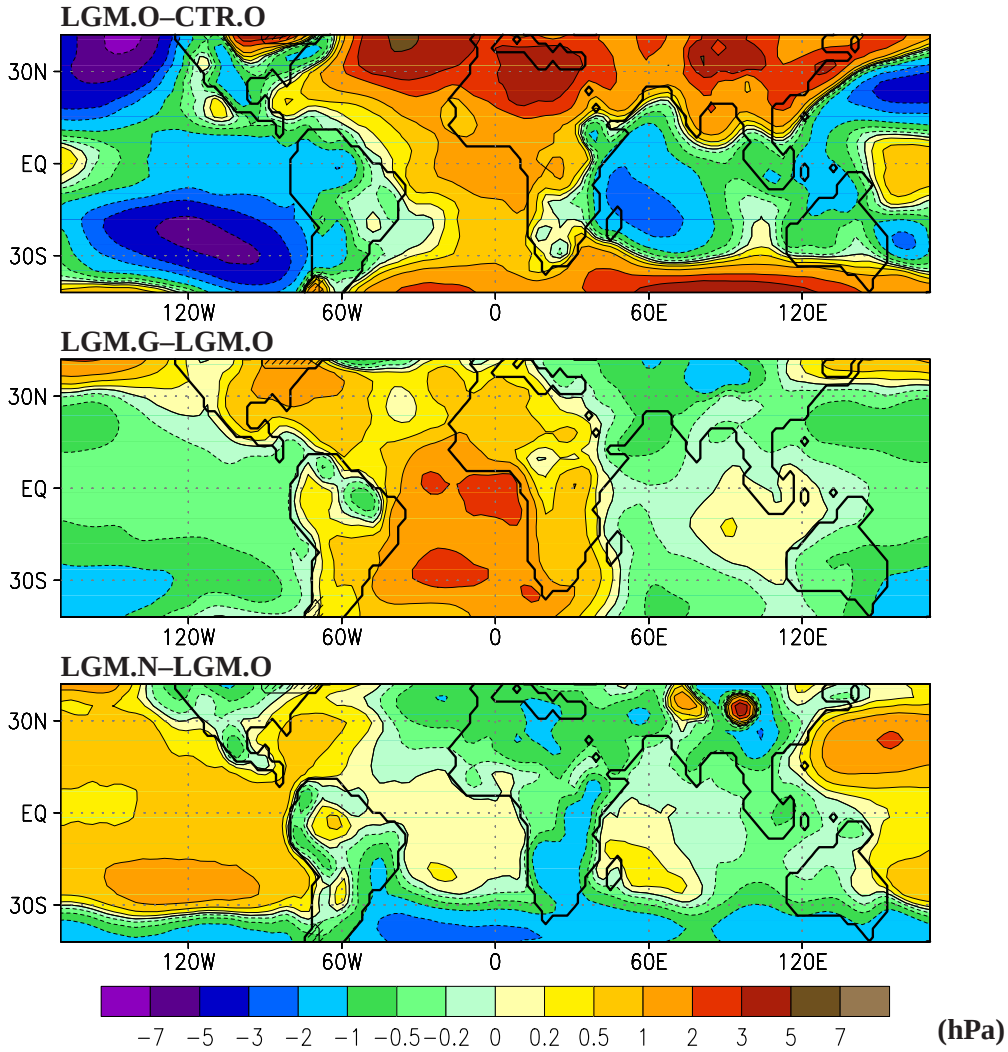

Figure 2.4: *Annual mean anomalies in sea level pressure (hPa) of three different LGM simulations. Note the different subtractor in the upper (experiment* `CTR.O`*), and the middle and lower (experiment* `LGM.O`*) panel, respectively. The difference in the global average of the mean sea level pressure (1011.2 hPa in the experiment* `CTR.O` *and 1023.4 hPa in* `LGM.O` *as well as in* `LGM.G` *and* `LGM.N`*) has been subtracted in the upper panel. This difference is caused by the displacement of air by the huge Northern Hemisphere ice caps during the last glacial.*

2.3.2 Temperature of the coldest month

For a validation of model results a comparison with terrestrial temperature proxy data is appropriate, since the ocean surface temperature is prescribed. In order to extract a comparable measure, we calculate the mean temperature of the coldest month (MTCO). The incidence of certain plants is more often connected to the minimum than to the annual mean temperature [*Farrera et al.*, 1999]. Therefore, MTCO can be linked to pollen data for which the data base is relatively large. Figure 2.5 shows MTCO for the glacial experiments `LGM.O`, `LGM.G`, and `LGM.N`, respectively.

In tropical and subtropical America and in western Africa, the `LGM.N` climate yields a better concordance with paleodata than the experiment `LGM.O` (Figure 2.5). In the western Pacific region, where

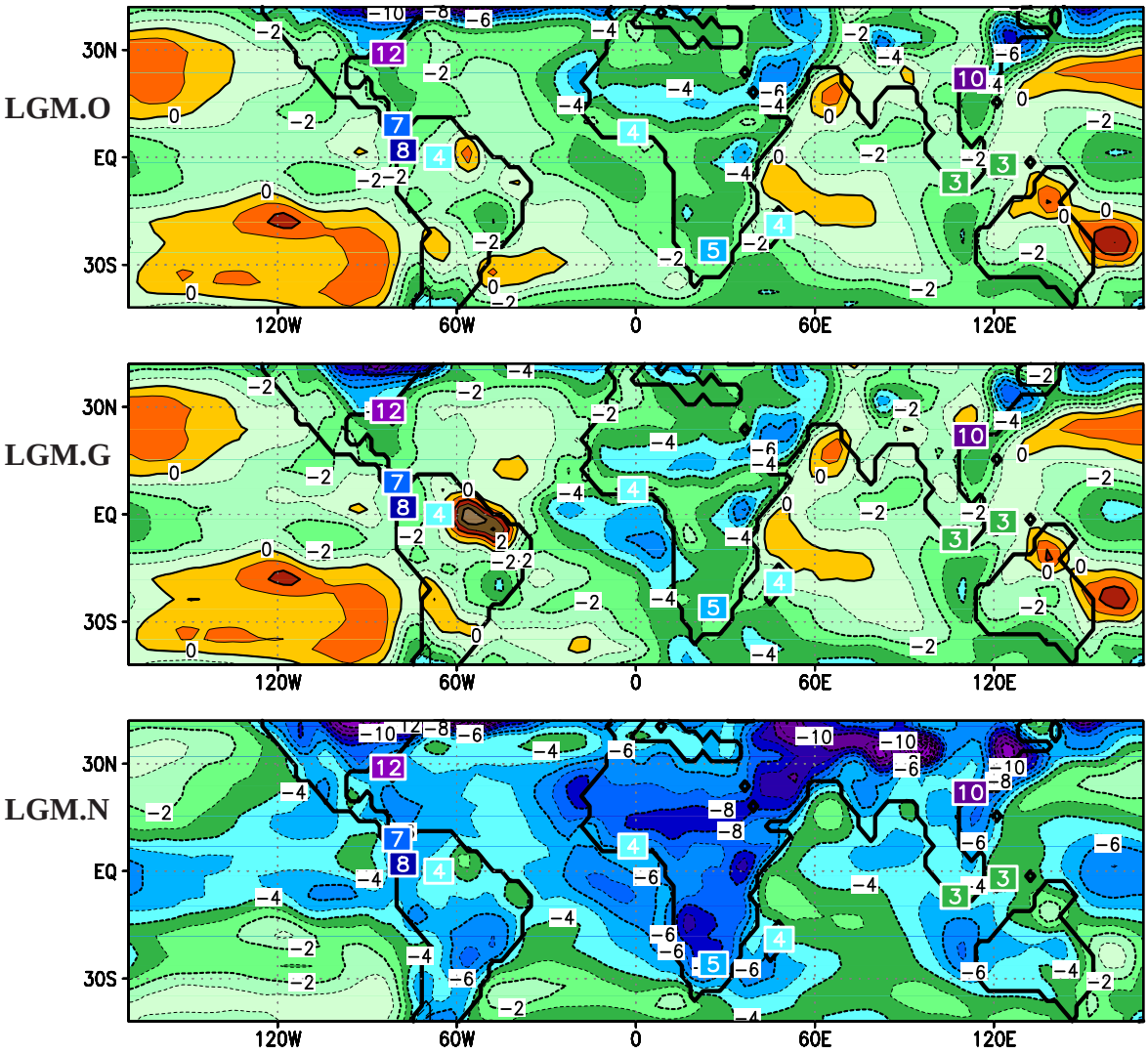

Figure 2.5: *Near surface air temperature anomalies (K) of the coldest month for the glacial experiments* `LGM.O`, `LGM.G`, *and* `LGM.N` *with reference to the control run* `CTR.O`. *The rectangles indicate reconstructions of glacial temperature decrease of MTCO (colour with respect to temperature drop, leading minus sign omitted), compiled by Farrera et al. [1999], cf. Table 2.1.*

the glacial cooling is significantly smaller than in the western Atlantic, the simulated cooling in `LGM.N` matches better with the *Farrera et al.* [1999] data than the warming in `LGM.O`. However, in southern Africa, in New Guinea, and some islands in the central Pacific Ocean the simulated glacial temperature drop in experiment `LGM.N` seems to be overestimated when compared with proxy data [*Farrera et al.*, 1999]. Similar results are listed in Table 2.1.

2.3.3 Vegetation

In order to test the sensitivity of the tropical vegetation cover with respect to the different climate conditions, the LPJ dynamical vegetation model is forced with the glacial and present climate conditions, as calculated by the atmospheric model ECHAM. The LPJ model calculates, beside other

Table 2.1: *Reconstructed and simulated air temperature anomalies (LGM minus present climate). Data: mean surface air temperature anomalies of the coldest month, compiled by Farrera et al. [1999]. Locations up to 1500 m above sea level are included only. Air temperatures are reduced to sea level. Some areas consist of several sites located in the same region. Simulated temperatures are not reduced, but the mean topographic height concerning to the model's resolution is near sea level. Model output are area averages of grid points over land.*

location	**sites**	**lat.**	**lon.**	**data**	LGM.N	LGM.0	LGM.G
			America				
Florida/USA	3	29°N	83°W	–12.0	–6.5	–4.5	–4.5
Panama	1	9°N	80°W	–7.0	–5.5	–2.5	–2.0
Ecuador	2	2°N	78°W	–7.5	–5.5	–2.0	–2.0
Rio Negro	2	0°N	66°W	–4.0	–4.5	–1.0	–1.5
			Africa				
Ghana	1	7°N	1°W	–4.0	–6.5	–2.5	–2.0
South Africa	2	26°S	26°E	–5.0	–7.5	–3.5	–3.0
Madagascar	1	19°S	47°E	–4.0	–6.5	–3.0	–3.5
			Pacific				
China	3	22°N	112°E	–10.0	–6.5	–1.0	0.0
Java	4	7°S	107°E	–2.5	–3.5	–0.5	0.0
Sulawesi	1	2°S	121°E	–3.0	–3.5	0.0	0.0

results, the fraction of the PFT with respect to the varying climate of the ECHAM experiments The analysis of the tropical trees shows that the fractional coverage is very different among the three LGM experiments (Figure 2.6). The control climate shows large areas of tropical evergreen and raingreen trees (Figure 2.6a). During glacial times, the fractional coverage is substantially reduced over central Africa and large parts of South America (Figure 2.6b-d), where temperate trees are expanding. The simulation using the coldest and dryest reconstruction (LGM.N) depicts only small areas of tropical trees over the African and South American continents (Figure 2.6c), where tropical rainforest is able to survive. The model simulations based on the CLIMAP (Figure 2.6b) and the GLAMAP (Figure 2.6d) reconstructions show an intermediate coverage over these tropical areas.

2.3.4 Environmental lapse rates

In Figure 2.7 the lapse rates in the tropical region are shown for the control run and the three glacial experiments. Lapse rates are calculated using the difference in the annual mean temperature of the free atmosphere at 500 hPa and the surface air temperature, divided by the respective height of the 500 hPa level.

In the control climate (CTR.0, Figure 2.7a), the lapse rate is steepest over tropical and subtropical

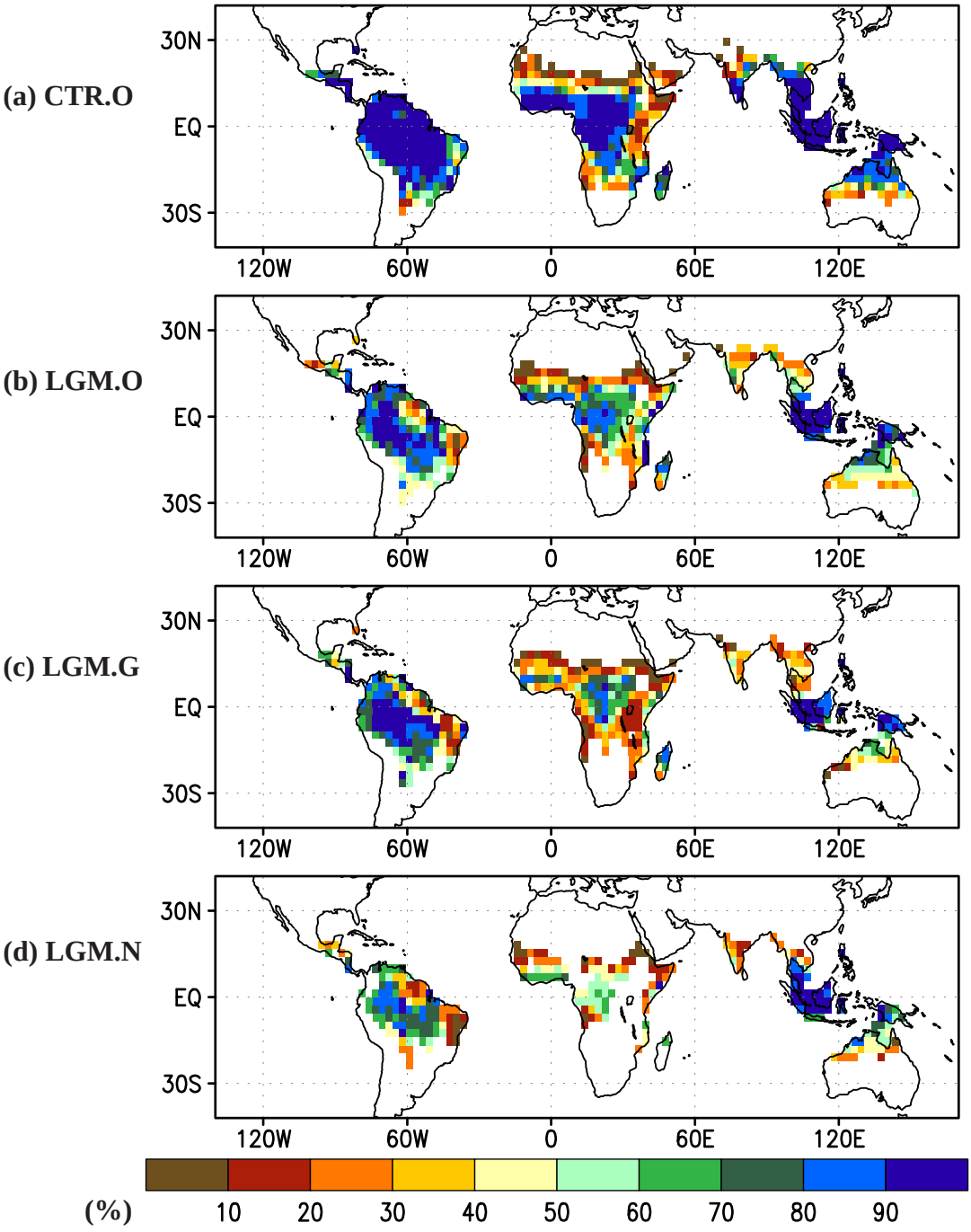

Figure 2.6: *Fractional coverage (in %) of tropical trees for the experiments (a)* `CTR.O`*, (b)* `LGM.O`*, (c)* `LGM.G`*, and (d)* `LGM.N`*.*

continents, where strong convection is driven by high surface temperature, leading to very cold temperature in the midtroposphere up to the tropopause. Over the oceans, convection is lower and lapse rates are reduced. The regions with lowest lapse rates mark notably the subtropical ocean areas off the western coasts of the North- and South American, the African, and the Australian continents, where upwelling is highest and SST is relatively cold.

For the glacial climate forced by CLIMAP SSTs (LGM.O, Figure 2.7b), the lapse rates are steeper over the tropical continents, in particular where the glacial temperature is higher than today (Amazon, Australia, cf. Figure 2.2). Also over the eastern Pacific, the western Indian and western Atlantic Ocean, the lapse rate is stronger with a steepened gradient by 0.3 to 0.5 $\mathrm{K\,km^{-1}}$. Only in the river Nile region, the vertical temperature gradient is slightly reduced.

For the glacial experiment forced by the GLAMAP SST (Figure 2.7c), we find steeper lapse rates over the western tropical Atlantic and a strongly increased vertical temperature gradient over the whole Amazonian rainforest. In contrast, in the eastern Atlantic off West Africa, the lapse rate over the upwelling region is further reduced.

The coldest LGM experiment (LGM.O, Figure 2.7d) exhibits an overall increase in the strength of the environmental lapse rate. The value of the gradient rises by 0.5 to 1.0 $\mathrm{K\,km^{-1}}$ with a maximum over large parts of the western Pacific as well as over the Amazon mouth and New Guinea. Only very limited areas over Africa and off China show a moderately flattaned lapse rate.

2.3.5 Temperature of the free atmosphere

Figure 2.8 shows the zonal mean temperature distributions for the glacial experiments. Apart from the high latitudes, the simulated glacial temperature drop in the experiment LGM.O amounts to 1–2 K in the lower and 3 K in the middle troposphere (500 hPa level, ca 5.8 km) compared to the control experiment CTR.O (Figure 2.8a). In contrast, the experiment LGM.N exhibits a glacial cooling of 4–6 K near the surface but 6–10 K in the tropical midtroposphere (Figure 2.8b). This implies that the vertical temperature gradient (environmental lapse rate) has changed in experiment LGM.N. The lapse rate steepened in the colder climate at low latitudes compared to the climate forced by the SST of the CLIMAP reconstruction. The temperature difference between both glacial runs (Figure 2.8c) indicates an enhanced cooling with height: the SST difference of 3 K at the surface level between the glacial runs increases by 2 K to 5 K at the 500 hPa level. A similar pattern is obtained for the two interglacial experiments CTR.N and CTR.O, where the anomaly increases from 3 K near the surface to 6 K in the midtroposphere (not shown).

The enhanced cooling of air temperature at higher elevation is due to the substantial water vapor content of tropical warm air. In the tropics the relative humidity of air is considerably high in comparison with extra-tropical climates. In the temperature range between 24°C and 30°C the water vapor content lies near 80% of the saturation value [*Broecker*, 1997]. In the LGM.N experiment, the absolute water vapor content in tropical warm water regions is reduced by more than 20% compared to the experiment LGM.O (Figure 2.9). This is in line with a study of *Seltzer* [2001], who stated that the water vapor content of the atmosphere is the ultimate control on temperature lapse rates.

Because less latent heat can be released by condensation in experiment LGM.N compared to LGM.O, the vertical temperature gradient is enhanced: comparing different air parcels with similar relative

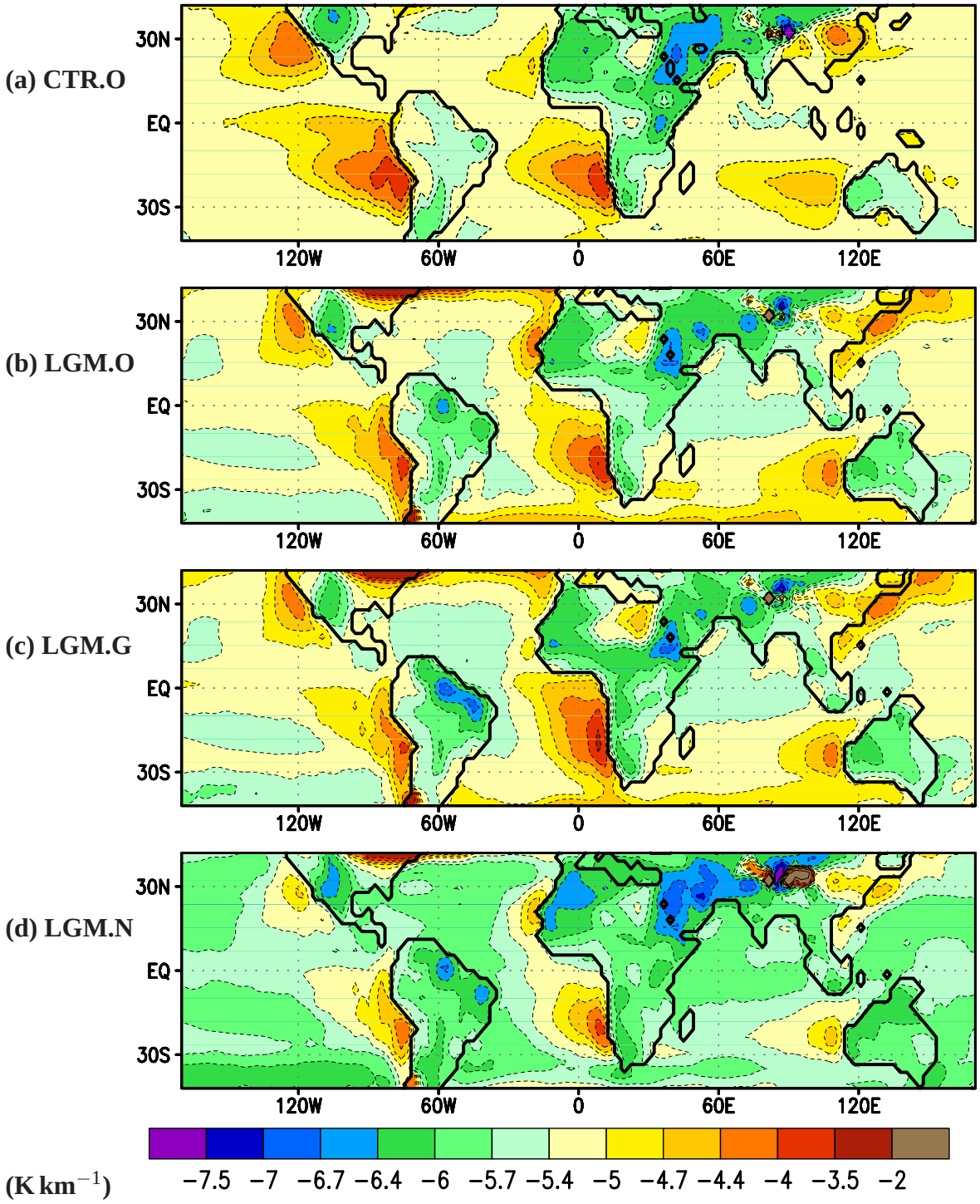

Figure 2.7: *Environmental lapse rate (K km^{-1}) in the free atmosphere between 500 hPa level and the surface of the control experiment* `CTR.O` *and the glacial experiments* `LGM.O`*,* `LGM.G`*, and* `LGM.N`*. Blue colors indicate a steeper lapse rate with colder temperatures in the midtroposphere.*

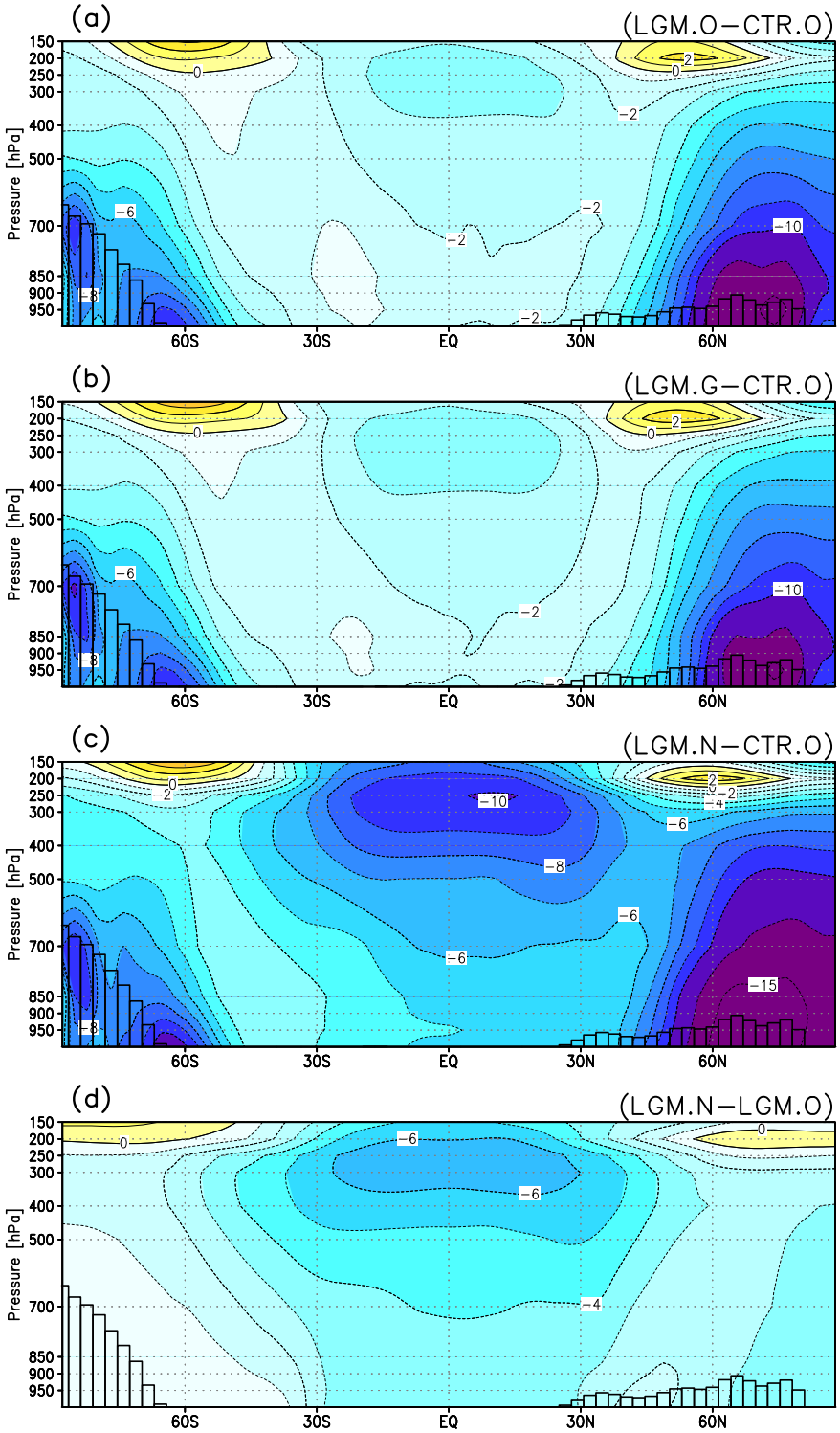

Figure 2.8: *Zonal and annual mean vertical distribution of temperature differences (K) of the experiments (a)* `LGM.O` − `CTR.O`*, (b)* `LGM.G` − `CTR.O`*, (c)* `LGM.N` − `CTR.O`*, and (d)* `LGM.N` − `LGM.O`*. The vertical bars indicate the zonal mean model topography for the LGM experiments.*

humidity during an adiabatic ascent, the magnitude of the lapse rate in colder air is larger (steeper) than in warmer air. This is due to the simple fact that warmer air can hold more water vapor, and therefore more latent heat is released during the ascent, when condensation occurs. On average the lapse rates of the free atmosphere in the tropics (30°N to 30°S, from the surface to 500 hPa) are –5.2, –5.3, –5.4, and –5.7 K km^{-1} for the experiments `CTR.O`, `LGM.O`, `LGM.G`, and `LGM.N`, respectively. In experiment `LGM.N` only, a substantially enhanced vertical temperature gradient is found.

2.3.6 Near surface temperature in tropical mountains

In order to understand the drop in glacial snowlines during the LGM, it is appropriate to examine the modeled decrease of surface air temperature with height in tropical mountains. Since the ECHAM3 T42 model cannot resolve the tropical high altitude region, the Himalayan mountains and the Tibetan highlands are taken as a surrogate for the calculation of tropical snowlines. Although the Himalaya is located outside the tropics the climate is rather similar to that of tropical mountains like the Andes or in central Africa, where the model topography does not exceed a height of 3 km. Only in Tibet a height of more than 4 km is reached (Figure 2.1).

A meridional section at 90°E includes the Tibetan plateau (Figure 2.10). The figure indicates a stronger temperature drop during glacial times at these mountains than elsewhere in the lower latitudes. At the 500 hPa level at 30°N, the glacial temperature is decreased by 9 K relative to the control climate, whereas at 30°S, where no mountains exist, the glacial drop amounts to 7 K only.

We analyze vertical temperature profiles in the free atmosphere along a zonal profile at 32°N from

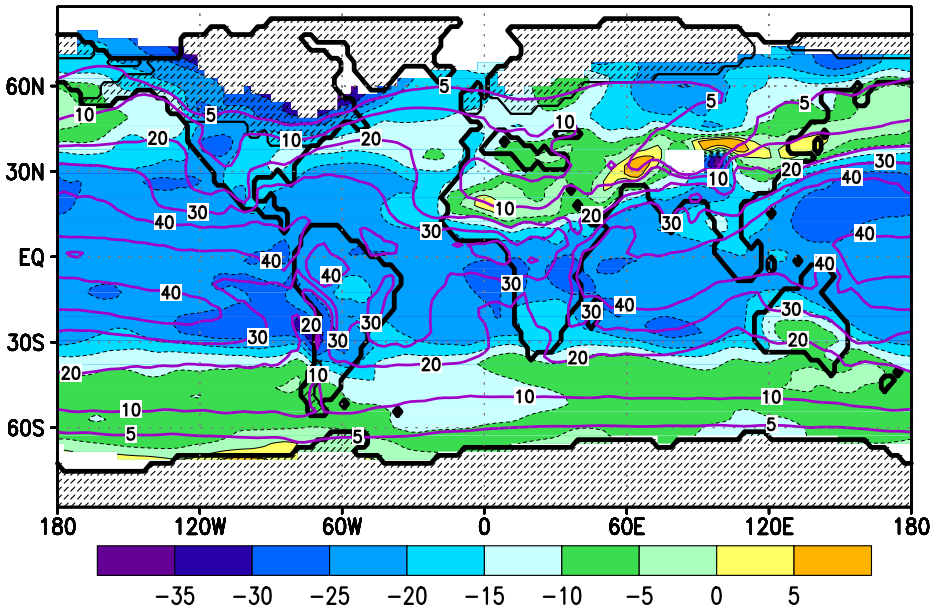

Figure 2.9: *Relative change (colour) of specific humidity of experiment* `LGM.N` *(q_n) relative to* `LGM.O` *(q_o) in percent: $(q_n - q_o) \cdot q_o^{-1} \cdot 100$. Areas where $q_o < 3$ kg m^{-2} are not coloured. The labelled isolines show the absolute values of vertically integrated specific humidity (kg m^{-2}) of experiment* `LGM.O`*. Values refer to water vapor, since the amount of cloud water is about two orders of magnitude smaller than that of water vapor and is neglected here.*

the western Pacific Ocean to the plateau of Tibet (Figure 2.11). The annual mean surface air temperature decreases along this profile with raising height above sea level (Figure 2.11a and c). Furthermore, in Figure 2.11b and c, the temperature difference from an idealized moist adiabatic lapse rate is plotted against surface pressure. The moist adiabatic lapse rate with saturated water vapor content (Pseudoadiabat) that is taken as reference has a potential temperature of 45°C at the pressure level of 1000 hPa and is marked in Figure 2.11a with a dashed line.

An enhanced vertical gradient is found in the surface air temperature of all experiments relative to the free atmosphere (Figure 2.11b). The resulting temperature difference between the glacial climate with reduced tropical SST and the control run (`LGM.N` minus `CTR.O`) is much larger in Tibet (13 K, Figure 2.11a) than in the free atmosphere (5 K, see arrows in Figure 2.11b), when comparing similar height levels ($\sim$ 570 hPa $\sim$ 5 km, Figure 2.11b). This is due to the snow-albedo feedback: the colder temperature of the glacial climate causes a longer duration of snow cover providing for a higher annual mean albedo, which in turn pronounces a further drop of the surface temperature.

2.4 Discussion

Analyzes of vertical temperature distribution in five climate simulations with the ECHAM model forced by glacial and present SST reveal two main results: First, a moderate cooling of tropical SST in both present and glacial climates induces a stronger vertical temperature gradient in the atmosphere. The midtroposphere is more vigorously cooled than the lower troposphere. Second, the near surface temperature at subtropical high elevation areas in the model is lower than in the free atmosphere. Both results contribute to a consistent view of the glacial climate, reconciling tropical glacial air temperature at peak elevation, reconstructed by snowlines, with those at sea level.

2.4.1 CLIMAP and glacial snowlines

Disagreement in reconstructions of glacial temperatures at sea level and at tropical mountains has been discussed extensively [*Webster and Streten*, 1978; *Rind and Peteet*, 1985; *Broccoli and*

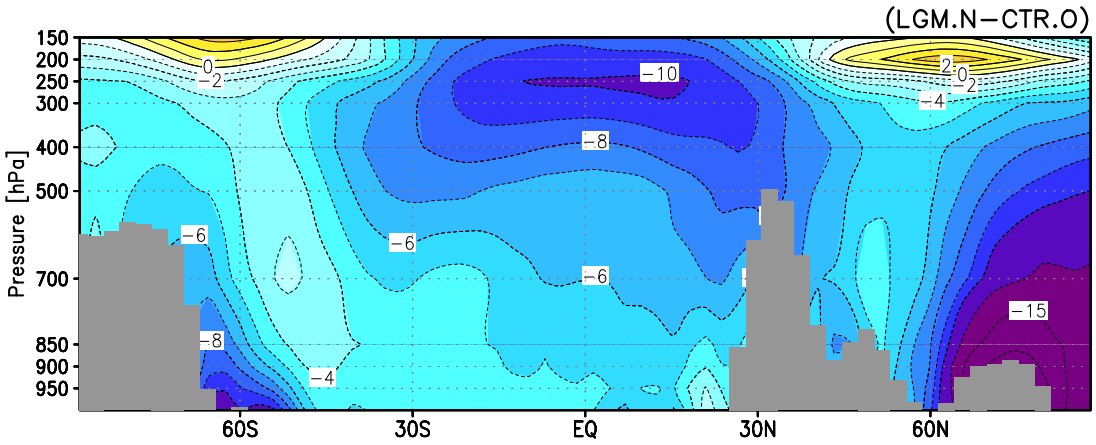

Figure 2.10: *Distribution of annual temperature anomaly of experiment* `LGM.N` *minus* `CTR.O` *along a meridional section at 90°E. The dark shaded bars indicate the local topography of the model.*

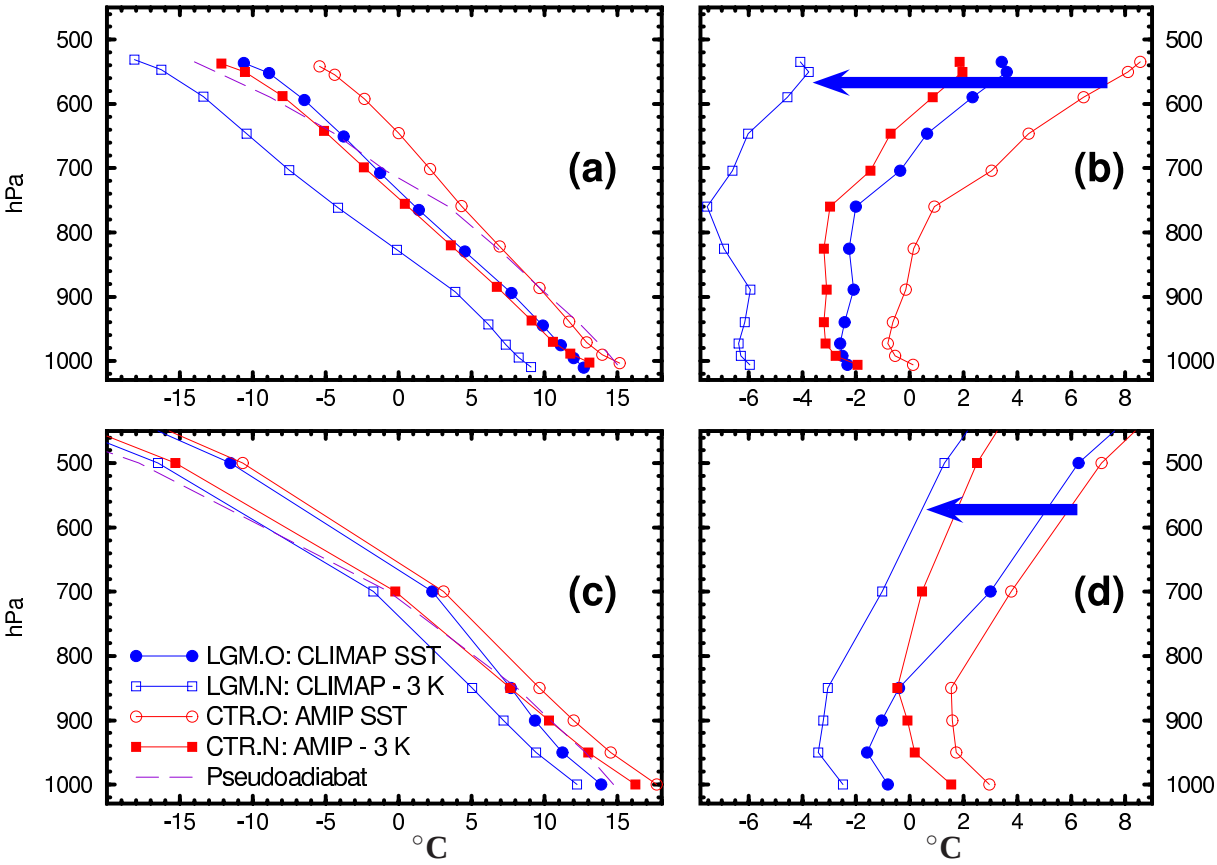

Figure 2.11: *Temperature profiles from the Pacific Ocean to Tibetan plateau: Profiles are plotted as differences from the saturated adiabat with the potential temperature of 45°C (at a pressure level of 1000 hPa, pseudoadiabat). (a) Near surface air temperature at a region of 2×7 grid points (ca. 6×20° latitude/longitude extension in the ECHAM3 T42 model) rising in zonal direction along 32°N from sea level at the western Pacific Ocean to the Tibetan plateau up to a height of more than 5 km. (b) Vertical profile of the free atmosphere taken from the same latitude over the western Pacific Ocean. In (b) and (d) profiles are plotted as differences from the saturated adiabat with the potential temperature of 45°C (at a pressure level of 1000 hPa), marked in (a) and (c). The blue arrows indicate the largest cooling between experiment* `LGM.N` *and the control run (*`CTR.O`*) at the snowline level. Due to the identical SST used as boundary conditions in the Pacific, results of experiment* `LGM.G` *are very similar to experiment* `LGM.O`*, compare Figure 2.2.*

Marciniak, 1996; *Farrera et al.*, 1999; *Crowley*, 2000a]. Initially, it has been argued that a remarkable increase of glacial lapse rates, necessary to reconcile CLIMAP SST with the extent of tropical glaciers, was unlikely to take place [*Webster and Streten*, 1978; *Rind and Peteet*, 1985]. *Webster and Streten* [1978] argued that either the temperature of the tropical oceans of the western Pacific were overestimated by CLIMAP or that cold air incursions from higher latitudes were frequent enough to allow snowlines to be 1000 to 1500 m lower than at present for the glacial period. This could match a 6 to 8 K fall of temperature in highland New Guinea.

In a comparison of a simulated LGM climate using an early version of the atmospheric GCM coupled to a mixed layer ocean model of *Manabe and Broccoli* [1985] with terrestrial paleodata, *Broccoli and Marciniak* [1996] did not found any evidence in the simulation for changes in the lapse

rate, which are able to reconcile the apparent disagreement in tropical temperature reconstructions. These authors stated that the correspondence between simulated and CLIMAP zonal mean anomalies is "excellent in the Atlantic, mediocre in the Indian, and poor in the Pacific" [*Broccoli and Marciniak*, 1996].

This result is in line with the conclusions of a multiproxy paleoclimate synthesis study of *Farrera et al.* [1999]. These authors discuss regionally varying glacial lapse rates in the tropics. Despite considerable regional variability they state generally steeper lapse rates in the glacial climate than present, consistent with our model results. Based on land surface reconstructions, *Farrera et al.* [1999] report about substantial cooling at tropical land sites with high elevation. They argue that surface temperature at tropical peaks lies generally close to that of the overlying air level. In contrast, ground temperature at low elevation is often a few degrees higher than that of surrounding air. These findings are in agreement with the simulated drop of surface air temperature over Tibet in experiment `LGM.N`.

2.4.2 Atmospheric model simulations and snowline depression

The modeling of the climate of the LGM using atmospheric general circulation models (GCMs) has a long tradition. The modeling study of *Rind and Peteet* [1985] was the first one which showed that colder tropical SSTs are able to reduce the discrepancy between tropical surface and mountainous paleotemperatures. They conducted a LGM experiment using an atmospheric GCM forced by SSTs uniformly lowered by 2 K with respect to CLIMAP. The result of this simulation was in better agreement with geological temperature reconstructions from tropical mountains than the result of the simulation forced by SST reconstruction of CLIMAP. Nevertheless, they detected regional differences in tropical lapse rates and a warm bias in the Pacific warm pool near Hawaii.

Webb et al. [1997] used an atmospheric GCM where they prescribed a poleward ocean heat transport similar to the present one. They argued that the ocean heat transport implied by the CLIMAP SST is unrealistically high in the Pacific and low in the Atlantic, leading to the controversially high subtropical SSTs, and relatively low ones in the mid-latitude Atlantic. They found southward heat transport in the South Atlantic, in contrast to the widely accepted reconstruction by *Duplessy et al.* [1988] indicating reduced but northward transport throughout the whole Atlantic Ocean. In their glacial model experiment, the tropical surface air temperature (between 16°N and 16°S) dropped by 5.7 K, compared to today. This result is in agreement with the coldest geological estimates of tropical sea level temperatures only, like fossil groundwater estimates from tropical lowlands [*Stute et al.*, 1995; *Weyhenmeyer et al.*, 2000], whereas most other estimates do not indicate such a strong tropical cooling.

In contrast, *Greene et al.* [2002] concluded that it proves difficult to reconcile the coldest estimates for tropical temperatures with the observed snowline depression. They used a single-cell tropical climate model adjusted for the Pacific warm pool [*Betts and Ridgway*, 1992; *Seager et al.*, 2000] and asserted that a tropical SST reduction of $\sim$3 K is found to be consistent with the geological evidence for glacial snowlines. *Seager et al.* [2000] used a modified version of this model and noted that a drying of the lower midtroposphere, for instance through atmospheric circulation changes, could induce the strong cooling necessary to cause the observed snowline depression.

A thorough comparison of various atmospheric GCMs, simulating the LGM climate, as well as LGM data-model comparisons have mainly been undertaken in the framework of the Paleoclimate Modeling Intercomparison Project (PMIP, [*Joussaume and Taylor*, 2000]). The experiment `LGM.O` was conducted confirming to the agreed boundary conditions within PMIP [*Lorenz et al.*, 1996] and the experiment results were part of the model synthesis study of *Pinot et al.* [1999]. This paper summarized eight model experiments using prescribed CLIMAP boundary conditions and nine model experiments, where SSTs are computed by a mixed layer ocean model with prescribed modern poleward ocean heat transport, following *Webb et al.* [1997]. *Pinot et al.* [1999] confirmed the conclusion of *Rind and Peteet* [1985] that SST reconstruction by CLIMAP and tropical terrestrial data are contradictory and showed that this result is not model dependent. Furthermore, none of the PMIP experiments with computed SST revealed any tropical ocean temperatures during the LGM as high as CLIMAP. Seven of nine simulations resulted in lower glacial ocean temperatures, than today.

An experiment with an atmospheric model, forced by a temperature drop of 1 K relative to the CLIMAP SST, exhibited a lowered snowline of 200 to 300 m only [*Crowley*, 2000a], indicating that a 1 K cooling of CLIMAP SST is not sufficient to explain the 800 m lowering of tropical snowlines during the LGM. The same physical phenomenon — surface temperatures affecting lapse rates — but with opposite sign, holds for the warmer climate during the Holocene optimum 6,000 years ago: the vertical temperature gradient was reconstructed to be by about one Kelvin per kilometer less (flatter) than today [*Cheddadi et al.*, 1997].

Apart from bottom temperature, the vegetation cover can have an additional effect on lapse rates [*Crowley and Baum*, 1997; *Crowley*, 2000a]. Similar to the snow-albedo effect, unvegetated bare highland with higher albedo can cool down and further enhance the local snowline depression. In an ECHAM3 simulation of the LGM including the effect of water storage of deep root vegetation, an enhanced altitudinal shift of vegetation zones was found [*Kleidon and Lorenz*, 2001]. For this simulation a degree-day methodology described by *Still et al.* [1998] was implemented. Due to enlarged soil moisture storage capacity, mainly in the tropics, these simulations reveal a downward vertical vegetation shift exceeding 229 m relative to experiments without deep roots [*Kleidon and Lorenz*, 2001].

In a LGM simulation *Hostetler and Mix* [1999] forced an atmospheric GCM with an updated faunal SST reconstruction [*Mix et al.*, 1999], where the ocean temperature of the equatorial current system in the eastern Pacific and tropical Atlantic oceans were reduced compared to CLIMAP. Due to the temperature reduction by about 2–4 K, the SST patterns in these regions are similar to those of experiment `LGM.N`. When atmospheric model results of *Hostetler and Mix* [1999] were used to force a high-resolution glacier mass-balance model [*Hostetler and Clark*, 2000], the resulting snowline depression for the highest peaks in tropical Africa and New Guinea were in reasonable agreement with proxy data. In contrast, at Hawaii, where the underlying glacial SST of CLIMAP in the Pacific warm pool was 1 K higher than today, huge discrepancies between SST and snowline depression remain. Both studies suggest a reassessment of glacial SST estimates in the Pacific Ocean, and imply for a minimum cooling of 3 K at least in the western Pacific warm pool [*Hostetler and Clark*, 2000].

2.4.3 GLAMAP modeling

The interpolation of proxy-derived SST estimates at sampling sites distributed over the Atlantic Ocean with varying area density was done with an inverse ocean model "SIMPLE" [*Grieger and Niebler*, 2003]. This model assimilates sparse data of past temperatures into a simple model of the upper ocean in an pioneering effort [*Mix*, 2003]. It serves as a type of intelligent interpolation method, which takes into account the wind driven surface ocean circulation. The main boundary condition to force this model is provided by wind stress data, where the data set of experiment `LGM.G` was used for the case of regridding the GLAMAP data. The limiting factor for this approach is the lack of simulation of changes in the deep ocean circulation [*Mix*, 2003].

A modeling study of the glacial water masses of the Atlantic Ocean [*Paul and Schäfer-Neth*, 2003] conducted simulations with the three-dimensional high resolution modular ocean model (MOM2), where the GLAMAP SST for the Atlantic as well as wind stress data of experiment `LGM.G` were prescribed as boundary conditions. The result was a detailed and consistent picture of the Atlantic Ocean circulation during the LGM, which is compatible with recent ocean proxy data: a relatively strong thermohaline circulation in the Atlantic due to deep convection and overturning in ice-free Nordic Seas, cooling of the Atlantic thermocline, and formation of very cold and salty bottom water stemming from the Weddell Sea was found [*Paul and Schäfer-Neth*, 2003; *Mix*, 2003].

In this study, apart from local temperature anomaly forced by SST changes, no substantial deviations in the simulated terrestrial climate could be detected when comparing the simulation forced by the GLAMAP SST with that forced by CLIMAP. Since the Indo-Pacific basins cover the major part of the world oceans, a change of the glacial Atlantic SST has only a minor effect on zonally averaged lapse rates Figure 2.8.

2.4.4 Coupled model simulations

Recent simulations of the LGM climate with fully coupled atmosphere-ocean GCMs [*Kitoh et al.*, 2001; *Hewitt et al.*, 2001; *Shin et al.*, 2003] provide SSTs independent from climate reconstructions. The resulting SSTs however, differ substantially between individual model simulations, even in the sign of change compared to present climate [*Mix*, 2003]: the HADCM3 [*Hewitt et al.*, 2001] and the NCAR-CCSM [*Shin et al.*, 2003] models calculated tropical SST patterns similar to our prescribed SST of experiment `LGM.N`, yielding relatively cold tropical surface water masses. In contrast, the SST of the MRI model [*Kitoh and Murakami*, 2002] bears resemblance with the CLIMAP reconstruction including water temperatures higher than today in the subtropical Pacific Ocean. Furthermore, *Kitoh and Murakami* [2002] found a steeper glacial lapse rate locally over anomalously warm surface waters near Hawaii. This is in contrast to our finding that the lapse rate steepens when the surface water is vigorously cooled.

The zonal mean temperature profile of the NCAR-CCSM [*Shin et al.*, 2003] model exhibits a glacial temperature drop of 5 K in the tropical upper troposphere (250 hPa level) compared to less than 2 K at the surface. Although this implies a slightly steeper lapse rate, the higher level cooling is considerably smaller than in our `LGM.N` experiment, where a 10 K temperature drop occurs at the same height (Figure 2.10). *Shin et al.* [2003] report a global steepening of the lapse rate of the free atmosphere

by 0.2 K km^{-1} in their LGM experiment, only. They state that this amount is only 25% of the glacial change relative to the present climate estimated by *Farrera et al.* [1999]. In our experiment `LGM.N`, the glacial lapse rate steepens by 0.5 K km^{-1} compared to the present day experiment, which fits reasonably with the estimates of *Farrera et al.* [1999]. *Pinot et al.* [1999] found regionally strongly varying lapse rates in different models, where most of the changes average out globally as well as in the mean over several models. Due to the ensemble model simulations, these authors confirm the conclusion of *Rind and Peteet* [1985] that tropical SST is overestimated by CLIMAP, especially in the Pacific warm pool.

2.4.5 The role of precipitation

An important factor determining large scale changes of the altitude of the equilibrium line is precipitation [*Seltzer*, 2001]. However, *Seltzer* [2001] also stated that relatively large changes in precipitation are needed during the LGM to affect ELA significantly. *Seltzer* [1994] estimated that a huge net increase in annual accumulation of 1000 kg/m^2 accounts for only about 300 m of ELA depression. This implies that a relatively strong increase in precipitation is needed during the LGM to depress snowlines significantly, as was recorded in tropical mountains. Similarly, a multiple regression analysis at tropical sites (from 30°N to 30°S) yielded a narrow relationship between precipitation and snowline [*Greene et al.*, 2002]. They used a single-cell tropical climate model [*Betts and Ridgway*, 1992; *Seager et al.*, 2000] and found that a 200 mm reduction in precipitation over tropical highlands would raise snowlines by not more than 100 m and that an increase in precipitation would have an effect of similar magnitude but of opposite sign.

In all three LGM simulations of this study the change in annual mean precipitation over land in tropical latitudes is generally small (less than 1 mm per day), except for equatorial eastern Africa and Asia (Java and Borneo), where an increase of 1–2 mm/day occurs (Figure 2.3). A precipitation anomaly of this magnitude can be translated into a net accumulation increase of 350 to 700 mm, as long as it falls as snow and is not compensated by increased melting. This relatively large amount can explain only a part of the reconstructed change in ELA. We believe that on a continental scale temperature change is the dominant quantity affecting ELA in tropical mountains.

A precipitation analysis of our experiments reveals a drastic increase of precipitation by more than 100 % during LGM near Hawaii, where no grid point with land characteristics exists in the ECHAM3 model. The annual mean precipitation in the region around Hawaii (165–155°W; 18–23°N) amounts to 2.9 mm/day for experiment `CTR.O`, whereas the glacial experiments exhibit 7.1, 7.8, and 5.8 mm/day for `LGM.O`, `LGM.G`, and `LGM.N`, respectively. This precipiation increase amounts to a maximum potential water accumulation of 1.5–2 m/y. This amount could be further increased by convective air ascent, due to the slope of the peaks on Hawaii. The simulated glacial precipitation increase supports a remarkable snowline depression in the vicinity of relatively high surface temperatures in the central North Pacific during LGM. This is valid as long as the heigth of the mountains exceed the zero degree isoline during LGM.

In contrast to evidence for severe decrease of ELA in Papua New Guinea, precipitation is reduced by 20% in the western and up to 70% in the eastern part of the island in all three LGM simulations

(slightly less in LGM.N). North of the equator, precipitation increases by 20% over Borneo and to more than 70% south of the Philippines in the LGM simulations.

The glacial simulations exhibit reduced precipitation in northern Africa, the Indian subcontinent and over eastern China. Furthermore, experiment LGM.O reveals a dipole structure in precipitation over tropical Africa with reduction in the west and increase in the east. These model results are in agreement with the PMIP model comparison study [*Pinot et al.*, 1999], where most of the models using prescribed CLIMAP boundary conditions exhibited similar results. This is related to a reasonable decrease in the strength of the Africa-Asian summer monsoon, which brings less summer rainfall over the Indian subcontinent, and less winter rainfall to tropical eastern Africa.

2.4.6 Limitations

This study is an attempt to assess large scale glacial changes of the vertical structure of the atmosphere, using simulations with a coarse-resolution ($\sim$ 250 km) circulation model. Due to the spectral formulation of the model equations, pattern changes on clusters of grid points (14 grid points, Figure 2.11) can be interpreted much better in terms of regional or large scale climate change, than differences at single grid points. In the model domain, tropical mountains cannot be resolved by the model grid, where the topographic height of a single grid point has to be the mean of the whole grid cell, for example averaging the heigth of the Andes with part of the Amazonian rain forest. Due to the lack of tropical mountains in the model, the vertical surface temperature profile of the subtropical Tibetan plateau was utilized as a surrogate for the influence of boundary layer processes at the height of the freezing level.

A large number of small scale processes — for example local wind direction, precipitation, exposition to the sun, dust loads and cloud cover — determines the local snowline. This can result in a varying lapse rate and temperature distribution during the LGM in different tropical mountains [*Porter*, 2001; *Mark et al.*, 2002; *Owen et al.*, 2002]. For the extent of low-latitude glaciers, the most important controls are accumulation-season precipitation and ablation-season temperature [*Porter*, 2001]. Therefore, it is argued that a unique value of past precipitation or temperature cannot be derived from the ΔELA alone.

More potential sources of error for estimating LGM snowlines lie in the uncertain dating of local moraines (e. g. relative age criteria based on the pattern of moraine sequences) as well as on deviations in ELA due to debris-covered glaciers, orographic details of small tropical mountain glaciers, and local wind changes. Since such processes go far beyond the scope of the model, this study is limited to first order changes of the glacial vertical temperature distribution. Due to the continental scale of the problem concerned with global average change in ELA during LGM, the major influence of temperature on ELA is evident. Other more local effects rather go beyond the scope of this paper where we focus on LGM temperature change in an atmospheric model, which results are interpreted on a global scale.

2.5 Concluding remarks

In this study, three different distributions of SST and sea ice were provided as an important glacial boundary condition in order to analyse differences in the glacial atmospheric circulation on different height levels. The simulation of the glacial climate driven by cooling of tropical SST relative to the CLIMAP reconstruction results in tropical land temperatures that are more consistent with reconstructed minimum temperatures by pollen assemblages (MTCO) [*Farrera et al.*, 1999], than the simulation based on the CLIMAP SST. The 3 K tropical cooling provides a consistent picture of the LGM climate, concerning the hydrological cycle and annual mean continental temperatures [*Lohmann and Lorenz*, 2000; *Kohfeld and Harrison*, 2000] as well as MTCO and tropical snowlines. Furthermore, when using results of the `LGM.N` experiment as boundary condition for an ocean model, *Prange et al.* [2002] found a consistent picture of the glacial circulation in the Atlantic Ocean with marine proxy data [*Sarnthein et al.*, 1994].

The free atmosphere in the experiment `LGM.N` with lower tropical SST exhibits a stronger lapse rate due to decreased water vapor content. In the tropical mountains a longer duration of snow cover raises the annual mean albedo, which induces a further reduction of surface temperature. Thus, the magnitude of the vertical temperature gradient along the continent from sea level to the midtropospheric level is increased in our experiment. The stronger lapse rate in near surface air temperature supports the coexistence of enhanced glacial cooling of tropical SST with reconstructed snowline reductions in tropical mountains of more than 800 m.

Acknowledgments. We like to thank D. Müller and U. Merkel for their help to improve the manuscript. The instructive comments of B. Mark and a second anonymous reviewer on an earlier version of this paper are very much appreciated. This work was supported by grants from the German Climate Research Program (DEKLIM).

2.6 References

Anderson, D. M., and R. S. Webb (1994), Ice-age tropics revisited, *Nature*, *367*, 23–24.

Bard, E. (2001), Comparison of alkenone estimates with other paleotemperature proxies, *Geochem. Geophys. Geosyst.*, *2*, doi:2000GC000,050.

Bard, E., F. Rostek, and C. Sonzogni (1997), Interhemispheric synchrony of the last deglaciation inferred from alkenone palaeothermometry, *Nature*, *385*, 707–710.

Berger, A. L. (1978), Long-term variations of daily insolation and Quaternary climatic changes, *J. Atmos. Sci.*, *35*, 2362–2367.

Betts, A. K., and W. Ridgway (1992), Tropical boundary layer equilibrium in the last ice age, *J. Geophys. Res.*, *97*, 2529–2534.

Broccoli, A. J. (2000), Tropical cooling at the last glacial maximum: an atmosphere-mixed layer ocean model simulation, *J. Clim.*, *13*, 951–976.

Broccoli, A. J., and E. P. Marciniak (1996), Comparing simulated glacial climate and paleodata: A reexamination, *Paleoceanography*, *11*, 3–14.

Broecker, W. S. (1997), Mountain glaciers: Recorders of atmospheric water vapor content?, *Glob. Biogeochem. Cyc.*, *11*, 589–597.

Cheddadi, R., G. Yu, J. Guiot, S. P. Harrison, and I. C. Prentice (1997), The climate of Europe 6000 years ago, *Climate Dyn.*, *13*, 1–9.

CLIMAP Project Members (1976), The surface of the ice age Earth, *Science*, *191*, 1131–1137.

CLIMAP Project Members (1981), Seasonal reconstructions of the Earth surface at the last glacial maximum, *GSA Map and Chart Ser. MC-36*, Geol. Soc. Am., Boulder, Colorado.

Crowley, T. J. (2000), CLIMAP SSTs re-revisited, *Climate Dyn.*, *16*, 241–255.

Crowley, T. J., and S. K. Baum (1997), Effect of vegetation on an ice-age climate model simulation, *J. Geophys. Res.*, *102*, 16,463–16,480.

Crowley, T. J., and G. R. North (1990), *Paleoclimatology*, Oxford University Press.

Diaz, H. F., and N. E. Graham (1996), Recent changes in tropical freezing heights and the role of sea surface temperature, *Nature*, *383*, 152–155.

Duplessy, J.-C., N. J. Shackleton, R. G. Fairbanks, L. D. Labeyrie, D. Oppo, and N. Kallel (1988), Deep water source variations during the last climatic cycle and their impact on the global deepwater circulation, *Paleoceanography*, *3*, 343–360.

Fairbanks, R. G. (1989), A 17,000 year glacio-eustatic sea level record: Influence of glacial melting rates on the Younger Dryas event and deep ocean circulation, *Nature*, *342*, 637–642.

Farrera, I., et al. (1999), Tropical climates at the last glacial maximum: a new synthesis of terrestrial palaeoclimate data. 1. Vegetation, lake-levels and geochemistry, *Climate Dyn.*, *12*, 823–856.

Gates, W. L. (1992), The atmospheric model intercomparison project, *Bull. Amer. Met. Soc.*, *73*, 1962–1970.

Greene, A. M., R. Seager, and W. S. Broecker (2002), Tropical snowline depression at the Last Glacial Maximum: Comparison with proxy records using a single-cell tropical climate model, *J. Geophys. Res.*, *107*, doi:10.1029/2001JD000,670.

Grieger, B., and H.-S. Niebler (2003), Glacial South Atlantic surface temperatures interpolated with a semi-inverse ocean model, *Paleoceanography*, *18*, 1056, doi:10.1029/2002PA000,773.

Guilderson, T. P., R. G. Fairbanks, and J. C. Rubenstone (1994), Tropical temperature variations since 20,000 years ago: modulating interhemispheric climate change, *Science*, *263*, 663–665.

Hewitt, C. D., A. J. Broccoli, J. F. B. Mitchell, and R. J. Stouffer (2001), A coupled model study of the last glacial maximum: Was part of the North Atlantic relatively warm?, *Geophys. Res. Lett.*, *28*, 1571–1574.

Hostetler, S. W., and P. U. Clark (2000), Tropical climate at the Last Glacial Maximum inferred from glacier mass-balance modeling, *Science*, *290*, 1747–1750.

Hostetler, S. W., and A. C. Mix (1999), Reassessment of ice-age cooling of the tropical ocean and atmosphere, *Nature*, *399*, 673–676.

Joussaume, S., and K. E. Taylor (2000), The Paleoclimate Modeling Intercomparison Project, in *Paleoclimate Modeling Intercomparison Project (PMIP): proceedings of the third PMIP workshop, Canada, 4-8 October 1999*, edited by P. Braconnot, WCRP-111, WMO/TD-1007, pp. 9–24, World Meteorological Organization.

Kitoh, A., and S. Murakami (2002), Tropical Pacific climate at the mid-Holocene and the Last Glacial Maximum simulated by a coupled atmosphere-ocean general circulation model, *Paleoceanography*, *17*, doi:10.1029/2001PA000,724.

Kitoh, A., S. Murakami, and H. Koide (2001), A simulation of the Last Glacial Maximum with a coupled atmosphere-ocean GCM, *Geophys. Res. Lett.*, *28*, 2221–2224.

Kleidon, A., and S. Lorenz (2001), Deep roots sustain Amazonian rainforest in climate model simulations of the last ice age, *Geophys. Res. Lett.*, *28*, 2425–2428.

Klein, A. G., G. O. Seltzer, and B. L. Isacks (1999), Modern and last local glacial maximum snowlines in the Central Andes of Peru, Bolivia, and Northern Chile, *Quat. Sci. Rev.*, *18*, 63–84.

Kohfeld, K., and S. P. Harrison (2000), How well can we simulate past climates? Evaluating the models using global palaeoenvironmental data sets, *Quat. Sci. Rev.*, *19*, 321–346.

Lee, K. E., and N. C. Slowey (1999), Cool surface waters of the subtropical North Pacic Ocean during the last glacial, *Nature*, *397*, 512–514.

Lohmann, G., and S. Lorenz (2000), The hydrological cycle under paleoclimatic conditions as derived from AGCM simulations, *J. Geophys. Res.*, *105*, 17,417–17,436.

Lorenz, S., B. Grieger, P. Helbig, and K. Herterich (1996), Investigating the sensitivity of the atmospheric general circulation model ECHAM 3 to paleoclimatic boundary conditions, *Int. J. Earth Sci.*, *85*, 513–524.

Manabe, S., and A. J. Broccoli (1985), A comparison of climate model sensitivity with data from the last glacial maximum, *J. Atmos. Sci.*, *42*, 2643–2651.

Mark, B. G., G. O. Seltzer, D. T. Rodbell, and A. Y. Goodman (2002), Rates of deglaciation during the last glaciation and holocene in the Cordillera Vilcanota-Quelccaya ice cap region, southeastern peru, *Quat. Res.*, *57*, 287–298.

Mix, A. C. (2003), Chilled out in the ice-age Atlantic, *Nature*, *425*, 32–33.

Mix, A. C., A. E. Morey, N. G. Pisias, and S. W. Hostetler (1999), Foraminiferal faunal estimates of paleotemperature: circumventing the no-analog problem yields cool ice age tropics, *Paleoceanography*, *14*, 350–359.

Mix, A. C., E. Bard, and R. Schneider (2001), Environmental processes of the ice age: land, oceans, glaciers (EPILOG), *Quat. Sci. Rev.*, *20*, 627–657.

Niebler, H.-S., S. Mulitza, B. Donner, H. Arz, J. Pätzold, and G. Wefer (2003), Sea surface temperatures in the equatorial and South Atlantic Ocean during the Last Glacial Maximum (23-19 ka), *Paleoceanography*, *18*, doi:10.1029/2002PA000,577.

Owen, L. A., R. C. Finkel, M. W. Caffee, and A. Y. Goodman (2002), A note on the extent of glaciation throughout the Himalaya during the global Last Glacial Maximum, *Quat. Sci. Rev.*, *21*, 147–157.

Paul, A., and C. Schäfer-Neth (2003), Modeling the water masses of the Atlantic Ocean at the Last Glacial Maximum, *Paleoceanography*, *18*, doi:10.1029/2002PA000,783.

Peltier, W. R. (1994), Ice age paleotopography, *Science*, *265*, 195–201.

Pinot, S., G. Ramstein, S. P. Harrison, I. C. Prentice, J. Guiot, S. Joussaume, M. Stute, and PMIP participating groups (1999), Tropical paleoclimates at the Last Glacial Maximum: comparison of paleoclimate modeling intercomparison project (PMIP) simulations and paleodata, *Climate Dyn.*, *15*, 857–874.

Porter, S. C. (1979), Hawaiian glacial ages, *Quat. Res.*, *12*, 161–187.

Porter, S. C. (2001), Snowline depression in the tropics during the last glaciation, *Quat. Sci. Rev.*, *20*, 1067–1091.

Prange, M., V. Romanova, and G. Lohmann (2002), The glacial thermohaline circulation: stable or unstable?, *Geophys. Res. Lett.*, *29*, 2028–2031.

Rind, D., and D. Peteet (1985), Terrestrial conditions at the last glacial maximum and CLIMAP sea-surface temperature estimates: are they consistent, *Quat. Res.*, *24*, 1–22.

Roeckner, E., et al. (1992), Simulation of the present-day climate with the ECHAM model: Impact of model physics and resolution, *Report 93*, Max-Planck-Institut für Meteorologie.

Rohling, E. J., M. Fenton, F. J. Jorissen, P. Bertrand, G. Ganssen, and J. P. Caulet (1998), Magnitudes of sea-level lowstands of the past 500,000 years, *Nature*, *394*, 162–165.

Rühlemann, C., S. Mulitza, P. J. Müller, G. Wefer, and R. Zahn (1999), Warming of the tropical Atlantic Ocean and slowdown of thermohaline circulation during the last deglaciation, *Nature*, *399*, 452–455.

Sarnthein, M., K. Winn, S. J. A. Jung, J.-C. Duplessy, L. Labeyrie, H. Erlenkeuser, and G. Ganssen (1994), Changes in East Atlantic deepwater circulation over the last 30,000 years: eight time slice reconstructions,

Paleoceanography, *9*, 209–268.

Sarnthein, M., R. Gersonde, H.-S. Niebler, U. Pflaumann, R. Spielhagen, J. Thiede, G. Wefer, and M. Weinelt (2003a), Overview of glacial Atlantic Ocean mapping (GLAMAP 2000), *Paleoceanography*, *18*, doi:10.1029/2002PA000,769.

Sarnthein, M., U. Pflaumann, and M. Weinelt (2003b), Past extent of sea ice in the northern North Atlantic inferred from foraminiferal paleotemperature estimates, *Paleoceanography*, *18*, doi:10.1029/2002PA000,771.

Schäfer-Neth, C., and A. Paul (2003), The Atlantic Ocean at the Last Glacial Maximum, 1: Objective mapping of the GLAMAP sea-surface conditions, in *The South Atlantic in the late Quaternary: material budget and current system*, edited by G. W. et al., pp. 531–548.

Seager, R., A. C. Clement, and M. A. Cane (2000), Glacial cooling in the tropics: exploring the roles of tropospheric water vapor, surface wind speed and boundary layer processes, *J. Atmos. Sci.*, *57*, 2144–2157.

Seltzer, G. O. (1994), Climatic interpretation of alpine snowline variations on millennial time scales, *Quat. Res.*, *41*, 154–159.

Seltzer, G. O. (2001), Late Quaternary glaciation in the tropics: future research directions, *Quat. Sci. Rev.*, *20*, 1063–1066.

Shin, S.-I., Z. Liu, B. Otto-Bliesner, E. C. Brady, J. E. Kutzbach, and S. P. Harrison (2003), A simulation of the Last Glacial Maximum climate using the NCAR-CCSM, *Climate Dyn.*, *20*, 127–151.

Sitch, S., et al. (2003), Evaluation of ecosystem dynamics, plant geography and terrestrial carbon cycling in the LPJ dynamic global vegetation model, *Glob. Change Biol.*, *9*, 161–185.

Still, C. J., P. N. Foster, and S. H. Schneider (1998), Simulating the effects of climate change on tropical montane cloud forests, *Nature*, *398*, 608–610.

Stute, M., M. Forster, H. Frischkorn, A. Sereno, J. F. Clark, P. Schlosser, W. S. Broecker, and G. Bonani (1995), Cooling of tropcal Brazil (5°C) during the Last Glacial Maximum, *Science*, *269*, 379–383.

Thompson, L., E. Mosley-Thompson, M. E. Davis, P. N. Lin, K. A. Henderson, J. Cole-Dai, J. F. Bolzai, and K.-B. Liu (1995), Late glacial stage and Holocene tropical ice core records from Huascaran, Peru, *Science*, *269*, 46–50.

Webb, R. S., D. H. Rind, S. J. Lehman, R. J. Healy, and D. Sigman (1997), Influence of ocean heat transport on the climate of the Last Glacial Maximum, *Nature*, *385*, 695–699.

Webster, P. J., and N. A. Streten (1978), Late Quaternary ice age climate of tropical Australasia: interpretations and reconstructions, *Quat. Res.*, *10*, 279–309.

Weinelt, M., M. Sarnthein, U. Pflaumann, H. Schulz, S. Jung, and H. Erlenkeuser (1996), Ice-free nordic seas during the last glacial maximum? Potential sites of deepwater formation, *Palaeoclimates*, *1*, 283–309.

Weyhenmeyer, C. E., S. J. Burns, H. N. Waber, W. Aeschbach-Hertig, R. Kipfer, H. H. Loosli, and A. Matter (2000), Cool glacial temperatures and changes in moisture source recorded in Oman groundwaters, *Science*, *287*, 842–845.

Chapter 3

Acceleration technique for Milankovitch type forcing in a coupled atmosphere-ocean circulation model: method and application for the Holocene

Abstract.

A method is introduced which allows the calculation of long-term climate trends within the framework of a coupled atmosphere-ocean circulation model. The change in the seasonal cycle of incident solar radiation induced by varying orbital parameters has been accelerated by factors of 10 and 100 in order to allow transient simulations over the period from the mid-Holocene until today, covering the last 7,000 years. In contrast to conventional time-slice experiments, this approach is not restricted to equilibrium simulations and is capable to utilise all available data for validation. We find that opposing Holocene climate trends in tropics and extra-tropics are a robust feature in our experiments. Results from the transient simulations of the mid-Holocene climate at 6,000 years before present show considerable differences to atmosphere-alone model simulations, in particular at high latitudes, attributed to atmosphere-ocean-sea ice effects. The simulations were extended for the time period 1800 to 2000 AD, where, in contrast to the Holocene climate, increased concentrations of greenhouse gases in the atmosphere provide for the strongest driving mechanism. The experiments reveal that a Northern Hemisphere cooling trend over the Holocene is completely cancelled by the warming trend during the last century, which brings the recent global warming into a long-term context.

Stephan J. Lorenz and Gerrit Lohmann (2004), *Climate Dynamics 23(7-8)*, 727-743, doi:10.1007/s00382-004-0469-y,

3.1 Introduction

Palaeoclimatic modelling studies, aiming at reconstruction of past climate states, are usually performed either on the basis of time slices or time dependent (transient) simulations. Restricted by computer resources, atmospheric and oceanic general circulation models (AOGCMs) have at first been used to simulate Palaeoclimate time slices allowing for acceptable amounts of computing time [*Gates*, 1976; *Manabe and Broccoli*, 1985; *Fichefet et al.*, 1994]. In these types of experiments with component models, boundary conditions have to be prescribed, especially at the surface boundary between atmosphere and ocean (e. g. sea surface temperatures of the last glacial maximum by *CLIMAP Project Members* [1976]). More recent work is based on coupled models of different complexity, predicting physical quantities such as sea surface temperatures (SSTs) internally [e. g. *Ganopolski et al.*, 1998b; *Weaver et al.*, 1998; *Hewitt et al.*, 2001; *Shin et al.*, 2003]. These studies show that the additional feedbacks included are essential for a sound comparison and hence also interpretation of reconstructed data.

However, modelling of time slices cannot provide insights into the temporal evolution of the climate system. The time slices approach implies that the climate is in equilibrium and it cannot shed light on the transient behavior of the climate system. Furthermore, it refers to only a small fraction of the available data. When stepping forward to transient simulations, models of intermediate complexity have been used [e. g., *Stocker et al.*, 1992; *Ganopolski and Rahmstorf*, 2001; *Bertrand et al.*, 2002b; *Crucifix et al.*, 2002; *Prange et al.*, 2003, for a review: *Claussen et al.* 2002], where the complexity of sub-models is reduced. For example, a statistical and parameterised prescription instead of explicitly resolved internal atmospheric variability is used, which enables longer simulation times and the analyses of feedback processes by switching on and off the effect of different climatic components.

Recent studies [*Keigwin and Pickart*, 1999; *Rimbu et al.*, 2003] indicated that reconstructed Holocene climate in the North Atlantic realm reflects circulation changes. In order to investigate the dynamic evolution of the atmosphere-ocean system, transient modelling of the Holocene climate with AOGCMs becomes essential for the interpretation of long-term climate change and variability. Motivated by the finding that the atmospheric dynamics [*Rimbu et al.*, 2003] as well as the feedback processes at the atmosphere-ocean interface may play an active part for climate trends, we use a comprehensive coupled circulation model to simulate long-term temperature trends.

Complementary to previous studies dealing with the climate evolution linked to solar irradiance and volcano forcing [*Shindell et al.*, 1999; *Crowley*, 2000b; *Shindell et al.*, 2003], we concentrate on Holocene climate trends induced by the long-term astronomical forcing associated with the varying parameters of the Earth's orbital parameters [*Berger*, 1978]. On multi-millennial time scales, the astronomical forcing provides for large imbalances in the seasonal distribution of sun light. Variations of the orbital parameters with higher frequencies are at least two orders of magnitude smaller [cf. *Bertrand et al.*, 2002], which we do not take into account in this study.

The time scales of the astronomical or "Milankovitch type" forcing are separated from the much shorter time scales of the atmosphere, including the mixed layer of the ocean, by several orders of magnitude. This motivated our idea to accelerate the astronomical forcing, which enables multi-millennial integrations with a fully coupled AOGCM and relatively low computational costs. This method is used to investigate long-term effects of the atmosphere-sea ice-ocean system induced by

the astronomical forcing. Excluded are only those processes that vary on time scales longer than the actual length of the model experiments (decades to centennials). Long-term variations of the ocean circulation on millennial time scales, changes in the land ice distribution, as well as long-term sea level variations are not considered in our simulations. Our survey is concerned with the middle to late Holocene, which can be considered as a relatively stable period, wherein rapid climate events were absent [*Grootes et al.*, 1993; *Clark et al.*, 2002].

The temperature evolution of the Holocene is also important in light of recent climate change. The new third assessment report of the *Intergovernmental Panel on Climate Change* [2001] (IPCC) stated a global surface air temperature increase during the past century by 0.6 ± 0.2 Kelvin (K). On the longer perspective, the 20th century warming is likely to be the largest during any century over the past 1,000 years for the Northern Hemisphere, with the 1990s being the warmest decade and 1998 the warmest year of the millennium [*Mann et al.*, 1998, 1999]. With our modelling study, we aim to relate the Holocene temperature trends prior to the industrialisation period to the more recent temperature trend over the last century.

Our approach is aimed to simulate the response of the coupled system of atmosphere, ocean and sea ice to astronomical forcing, which sheds light into the transient behavior of the Holocene dynamics. With the continuation of our Holocene experiments into the industrial era, by simulating the recent climate change with increasing greenhouse gas concentration, starting from the background Holocene climate, we want to bring the 20th century warming trend into the context of the temperature trend over the last 7,000 years. This allows a comparison of astronomically and greenhouse gas induced temperature trends within one AOGCM integration.

The paper is organised as follows: the simulation methods are described in section 3.2. Here, the coupled model is introduced, and we elucidate our acceleration technique for the Milankovitch type forcing. Furthermore, we explain the model setup used for the ensemble experiments and describe the main forcing by the orbital parameters. In section 3.3, we present the model results for the Holocene climate trends with different acceleration factors and show the northern high latitude climate in our transient simulations. Additionally, we evaluate and compare the Holocene and recent global warming trends in our simulations. Finally, discussion (section 3.4) and conclusions (section 3.5) of our main results are given.

3.2 Methodology

3.2.1 The Atmosphere-ocean circulation model

For the simulation of the Holocene climate, we use the coupled atmosphere-ocean general circulation model ECHO–G [*Legutke and Voss*, 1999]. The atmospheric part of this model is the 4^h generation of the European Centre atmospheric model of Hamburg [ECHAM4, *Roeckner et al.*, 1996]. The prognostic variables are calculated in the spectral domain with a triangular truncation at wave number 30 (T30), which corresponds to a Gaussian longitude-latitude grid of approximately $3.8^\circ \times 3.8^\circ$. The vertical domain is represented by 19 hybrid sigma-pressure (terrain following) levels with the highest level at 10 hPa. The time step of the atmospheric model is depending on the resolution. Its value is

30 minutes when using T30 resolution. The ECHAM model has been modified with respect to the standard version in order to account for sub-grid scale partial ice cover [*Grötzner et al.*, 1996] that is also considered in the ocean model.

The ECHAM4 model is coupled through the OASIS program [Ocean Atmosphere Sea Ice Soil, *Terray et al.*, 1998] to the HOPE ocean circulation model [Hamburg Ocean Primitive Equation model, *Wolff et al.*, 1997]. The ocean model includes a dynamic-thermodynamic sea-ice model with snow cover. It is discretised on an Arakawa-E grid with a resolution of approximately $2.8^\circ \times 2.8^\circ$. In the tropics, its meridional resolution is increased to 0.5°. The model consists of 20 irregularly spaced vertical levels with 10 levels covering the upper 300 m. The time step of the ocean model amounts to two hours.

The model uses annual mean flux corrections for heat and freshwater, applied to the ocean model component. These fluxes are diagnosed from sea surface temperature and salinity restoring terms in a coupled spin-up integration for the current climate [*Legutke and Voss*, 1999], using present boundary conditions (e. g., 353 ppm CO_2 concentration in the atmosphere) and climatologies. The fluxes are constant in time and their global integral over the ocean has no sources or sinks of energy and mass. Although the use of flux corrections is not ideal for climate simulations strongly deviating from the present climate, they are utilised even in model simulations of a glacial climate [e. g. *Kitoh and Murakami*, 2002; *Kim et al.*, 2002]. Due to the similiarity of the Holocene and present climate, the use of flux corrections in our simulations is less problematic. The coupled model has been used in a number of climate variability studies on various time scales [e. g., *Raible et al.*, 2001; *Zorita et al.*, 2003; *Rodgers et al.*, 2004].

3.2.2 Orbital forcing

The ECHO-G model has been adapted to account for the influence of variations in the annual distribution of solar radiation due to the slowly varying orbital parameters: the eccentricity of the Earth's orbit, the angle between the vernal equinox and the perihelion on the orbit, as well as the obliquity, i. e. the angle of the Earth's rotation axis with the normal on the orbit. These parameters cause the astronomical or Milankovitch-forcing [*Milanković*, 1941; *Imbrie et al.*, 1992] of the climate system. Here, it should be noted that the seasonal distribution of insolation at the outer boundary of the atmosphere is independent from the variability of the solar constant, which is linked to the Sun's output of radiation [e. g. *Hoyt and Schatten*, 1993; *Lean and Rind*, 1998]. Such variations in the solar output as well as shortened insolation due to volcanic eruptions are not taken into account, since no continuous data apart from the last millennium [*Crowley*, 2000b] exist. The calculation of the orbital parameters follows *Berger* [1978]. They are used in the ECHAM model to evaluate the seasonal cycle of incoming solar radiation.

Figure 3.1 shows the changing solar irradiance due to the slowly evolving orbital parameters during the last 15,000 years at the (boreal) summer solstice (Figure 3.1a) and the winter solstice (Figure 3.1b), respectively. While the insolation is very similar to today during the last glacial maximum at 21,000 years before present (abbreviated as kyr BP in the following), it achieves its maximum deviation from today between 13 and 9 kyr BP at Northern Hemisphere summer solstice. This is due to both, a larger tilt of the Earth's rotation axis and the precession cycle, moving the passage of the

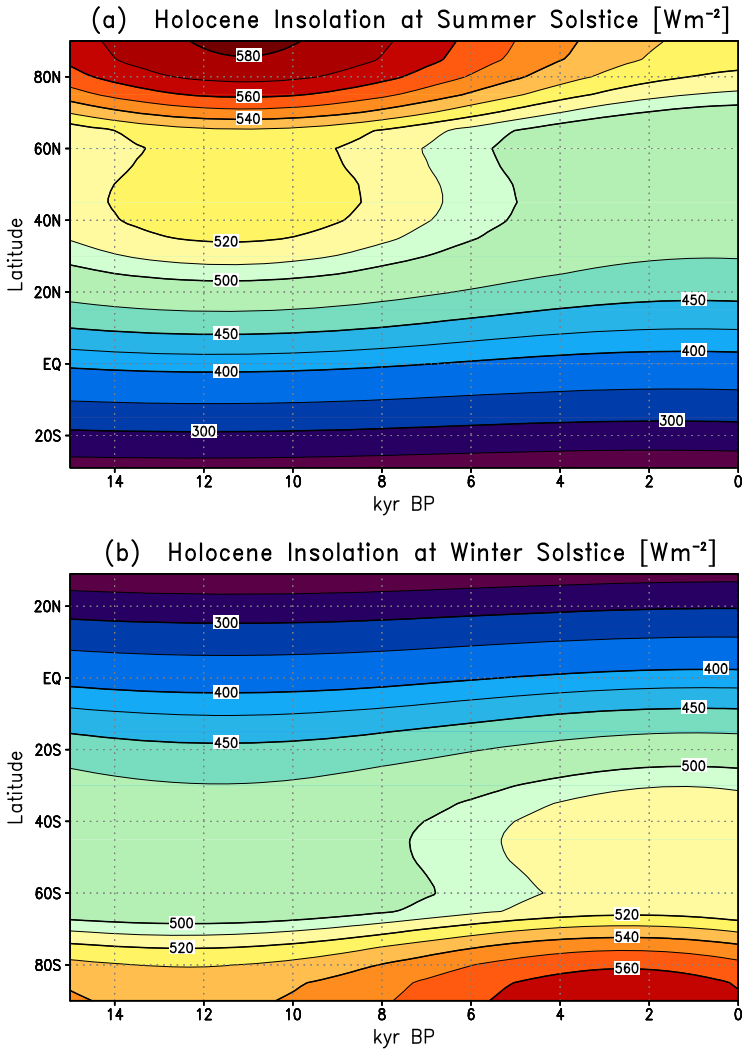

Figure 3.1: *Evolution of the latitudinal distribution of solar radiation for the last 15 kyr, following [Berger, 1978]. Shown is the zonal average of insolation at the time of (a) the boreal summer solstice and (b) the boreal winter solstice in Wm^{-2}. Note the different range of latitudes: regions poleward of 20° of the respective hemisphere with polar night are omitted, where the radiation keeps less than 200 Wm^{-2} and no significant change occurs.*

Earth through its perihelion from boreal summer in early Holocene to begin of January today. At the winter solstice (Figure 3.1b), a lack of insolation during early to mid-Holocene compared to today is centred around the equator. This is mainly affected by the precession cycle, since the distance to the sun was at maximum in boreal winter at middle Holocene. At 3 kyr BP, the insolation reaches nearly the present energy level.

3.2.3 Acceleration technique

Computer resources to run a complex model like the ECHO-G over the time period of the Holocene are very demanding: For example, the ECHO-G model consumes around 3 CPU-hours computing time for one simulation year on the present NEC SX-6 machine using a single CPU at the German Climate Computing Centre (DKRZ), where the calculations have been conducted. In order to save computational costs, the time scale of the astronomical forcing has been shortened in different experiments. For the simulation of the Holocene climate we perform two sets of experiments, where we use two different acceleration factors of 10 and 100 for the orbital forcing: For each simulated year we calculate stepwise the respective orbital parameters, which are the basis for the calculation of the

Table 3.1: *Names and characteristics of simulations with the ECHO-G model:*

Experiment-name	PRE–CTR	HOL–INS100	HOL–INS10	GHG–INS1
acceleration factor	1	100	10	1
number of exp.	1	6	2	2
integration length	3000	90	700	200
insolation (kyr BP)	0	9–0	7–0	0.2–0
greenh. gases (AD)	1800	1800	1800	1800–2000
CO_2 (ppm)	280	280	280	280– 370
CH_4 (ppb)	700	700	700	700–1715
N_2O (ppb)	265	265	265	265– 315

seasonal cycle of insolation. The subsequently simulated year is then forced by orbital parameters calculated from the next decade (century) of the Holocene, when utilising a factor of 10 (100) for the accelerated Milankovitch forcing. The stepwise change in seasonal insolation is small (less than 1 Wm^{-2} at maximum equatorwards of 65 degrees with the acceleration factor 100) compared to the seasonal cycle.

The underlying assumptions of our procedure are twofold: (1) the astronomical Milankovitch type forcing operates on much longer time scales (millennia) than those inherent in the atmosphere including the mixed layer of the ocean (months to a few years), and (2) climatic changes related to long-term variability of the thermohaline circulation during the considered time period are small in comparison with surface temperature trends. With this method the simulations with the fully coupled AOGCM capture feedbacks and variabilities of the atmosphere-ocean system with time scales up to decades or centennials, depending on the actual length of the model experiment. The insolation trends of the last 7,000 years are represented in 70 and 700 simulation years, respectively.

3.2.4 Model experiments

a) Pre-industrial control experiment

We perform an experiment for pre-industrial climate conditions that serves as a basic state for our Holocene and greenhouse gas scenario experiments. Control experiments usually prescribe values of atmospheric greenhouse gases valid for the last decade, including a CO_2 concentration between 350 and 370 ppm [e. g. *Boville and Gent*, 1998; *Hewitt et al.*, 2001]. Here, we utilise concentrations of the main three greenhouse gases (carbon dioxide, methane, and nitrous oxide) typical for the pre-industrial era of the latest Holocene (end of 18th century): 280 ppm CO_2, 700 ppb CH_4, and 265 ppb N_2O. Other boundary conditions are the vegetation ratio, surface background albedo, and the distribution of continents and oceans. These quantities are derived from modern worldwide measurements and kept constant throughout the simulation [*Roeckner et al.*, 1996]. Modern solar radiation has been prescribed for the control experiment, abbreviated as `PRE-CTR` (Table 3.1).

This control experiment has been integrated over 3,000 years of model simulation into a climate state that is regarded as the quasi-equilibrium response of the model to pre-industrial boundary conditions prior to the perturbation by the anthropogenic emissions of greenhouse gases. The transient simulations of the Holocene climate use the quasi-equilibrium state after 1250 simulation years of this experiment for their initial conditions. In the subsequent 600 years, the control integration exhibits a global surface temperature reduction of 0.018 K per century, which is mainly due to an artificial increase of the Southern Hemisphere sea ice (see section 3.3.1). North of 40°S, the cooling trend is less than 0.008 K per century.

b) Transient Holocene experiments

In order to isolate the Milankovitch-effect on the Holocene climate we neglect small changes in greenhouse gases in our Holocene experiments and prescribe constantly the same pre-industrial concentrations as for the control experiment `PRE-CTR`. The variability of the three gases during the Holocene is relatively small compared to that of the last ice age or compared to the increase during the 20th century. For example, the fluctuation of CO_2 during the last 7,000 years has a maximal range between 265 and 285 ppm [*Indermühle et al.*, 1999]. All other boundary conditions (vegetation, distribution of land and oceans, etc.) remain unchanged compared to the control experiment (`PRE-CTR`) and for the Holocene experiments.

We perform two sets of transient experiments to simulate the Holocene climate evolution. The first set of ensemble experiments consists of six model runs over 90 simulation years, representing the last 9,000 years, using an acceleration factor of 100 (experiments `HOL-INS100`). In this ensemble, all experiments are set up with different initial conditions in the atmosphere-ocean system, given by subsequent years of the control integration (`PRE-CTR`), the end of the years 1249 to 1254, respectively. The experiments start after 1250 simulation years of the control experiment, when the coupled system including the deep ocean is regarded to be in a quasi-equilibrium with the pre-industrial boundary conditions and modern insolation. The experiments `HOL-INS100` are then instantaneously forced with the varying insolation beginning with 9 kyr BP. The first 20 years of the simulations are taken as spin-up time for the atmospheric model coupled with the mixed layer of the ocean model but excluding the deep ocean to adapt to the changed insolation distribution. The following 70 years of model integration are analysed, reflecting the time evolution of the mid-to-late Holocene, the last 7,000 years.

In order to test the effect of the acceleration technique we perform a second set of simulations of the Holocene. It consists of two experiments using the acceleration factor of 10, instead of 100 (experiments `HOL-INS10`). These two model simulations are associated to 700 model years which simulate the orbitally forced climate change during the last 7,000 years. The experiments start after the 20 year spin-up time of the first set of Holocene experiments (`HOL-INS100`, Table 3.1). In the initial year after this spin-up time, orbitally defined at 7 kyr BP, the new experiments `HOL-INS10` are forced with an annual cycle of insolation identical to that of experiments `HOL-INS100`.

c) Greenhouse gas experiments

For a comparison of the orbital forced temperature with the effect by the anthropogenically induced increase of greenhouse gases we perform another set of experiments. The two experiments HOL-INS10 are continued to simulate the period from the year 1800 to 2000 AD, without using the acceleration technique (factor 1, GHG-INS1). They initialise at 0.2 kyr BP of experiments HOL-INS10 and are forced with both, transient orbital forcing and the historical records of greenhouse gases for the last two centuries. The concentration of the three main greenhouse gases (CO_2, CH_4 and N_2O; the most prominent CFCs and their increase are taken into account) during the last two centuries have been compiled [a compendium: *Boden et al.*, 1994] from ice core and instrumental records [e. g. *Etheridge et al.*, 1996, 1998; *Sowers et al.*, 2003]. Direct and indirect aerosol effects are not included in the depicted experiments with the ECHO-G model.

3.3 Results

For our analysis of the experiments HOL-INS100 we use the ensemble mean of the six experiments in order to evaluate the trend and the standard deviation over the last 70 simulation years after the spin-up time. Due to the inherent noise of the system, all experiments exhibit independent realisations of the orbitally forced Holocene climate evolution. The ensemble mean for this period is damped by averaging over the six experiments. For the experiments HOL-INS10 we used the complete 700 simulation years long period of the two experiments to evaluate the Holocene climate trend. Since the average of the simulated climate evolution consists of two realisations only, the mean variability of this time series is higher than the ensemble mean of HOL-INS100.

3.3.1 Surface temperature trends

In Figure 3.2, we present the evolution of regional surface temperature indices for the two sets of experiments HOL-INS100 (Figure 3.2a, d) and HOL-INS10 (Figure 3.2b, e), respectively. The experiments represent the time span from the mid-Holocene to the pre-industrial climate (lower axis labelling) with their integration time of 90 and 700 model years, respectively (upper axis labelling). Shown are regional averages over surface temperatures, where SST over ice free water is taken. Elsewhere, ground, ice and snow temperatures are considered.

The ensemble simulations performed with the ECHO-G model exhibit significant surface temperature trends during the middle to late Holocene. The orbital induced signal of decreased boreal summer insolation in northern mid and high latitudes (Figure 3.1a) is represented by a surface temperature drop of 1.4 K between 30°N and 50°N during the last 7,000 years (Figure 3.2a–c). In the tropics, a rise in simulated surface temperature of 0.4 K is found in boreal winter season (Figure 3.2d–f) in accordance with the observed increasing tropical solar radiation during the Holocene (Figure 3.1b).

The shape of the temperature trends is similar in the two different sets of experiments (Figure 3.2c, f): there is a strong decrease in northern mid-latitudes (Figure 3.2c) and an increase in low latitudes (Figure 3.2d) between 7 and 4 kyr BP. After 4 kyr BP, the trends are weaker due to relatively small variations in solar radiation relative to the mid-Holocene period (Figure 3.1). Within

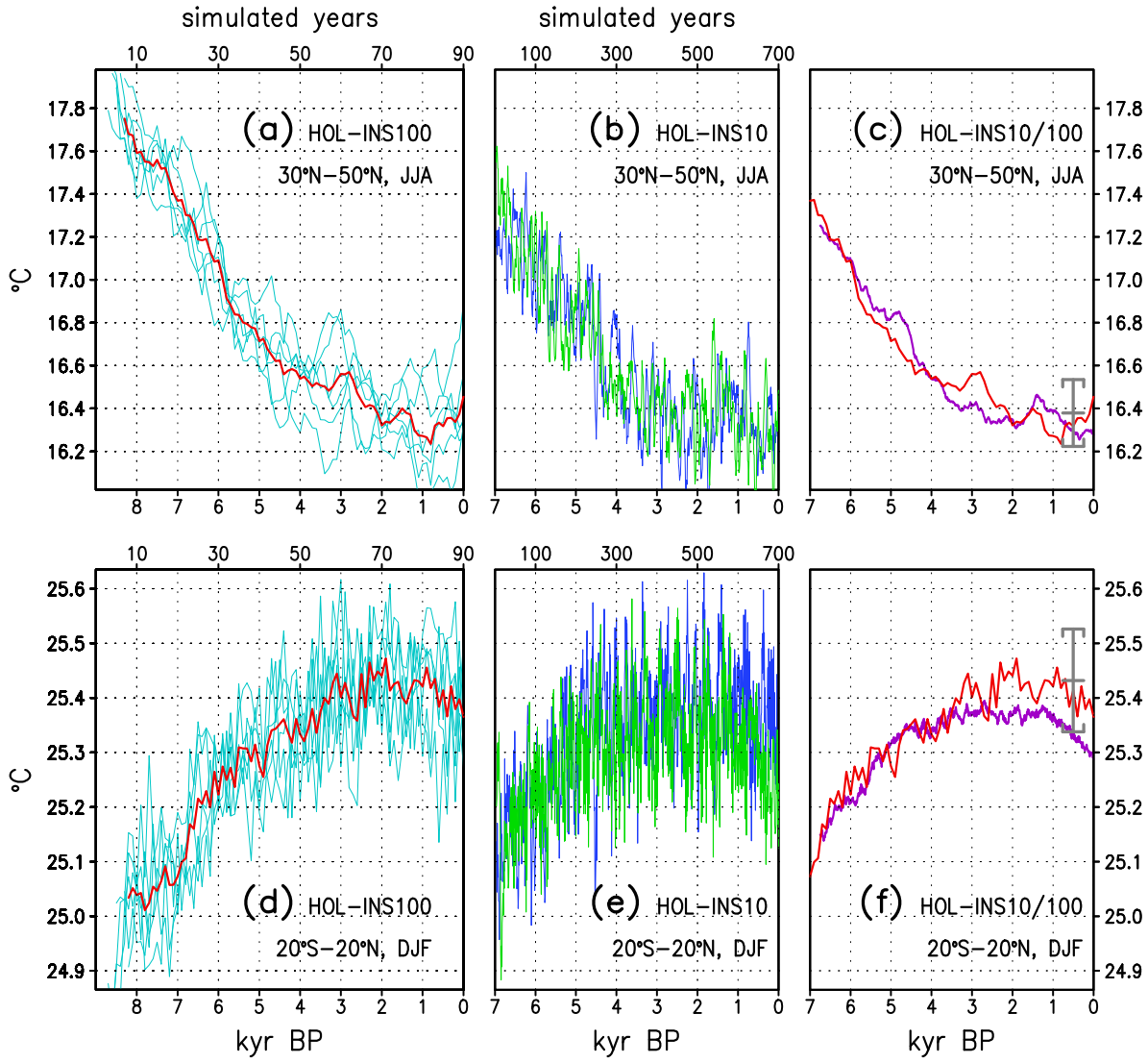

Figure 3.2: *Holocene surface temperature at (a–c) northern mid-latitudes during boreal summer season, and (d–f) in the tropics during boreal winter, simulated with the ECHO-G model. The red lines display the ensemble mean of the six individual experiments (*`HOL-INS100`*, thin blue lines) using an acceleration factor of 100 for the orbital forcing: 70 years of model integration (from modelled year 20 to 90, upper axis labels) comprise the time span of the last 7,000 years (lower axis labels). The blue and green line in (b) and (e) are two realisations of Holocene experiments using an acceleration factor of 10 (*`HOL-INS10`*), i. e. 700 simulation years. For comparison the ensemble means of both sets of experiments are shown together (red:* `HOL-INS100`*, purple:* `HOL-INS10`*) in (c) and (f). A 5-year running mean is used as a low-pass filter for all experiments, except for the purple line in (c) and (f) where a 50-year filter is used. The error bars indicate* 2σ *standard deviations of the control experiment* `PRE-CTR` *(years 1000-1500), calculated using a 5-year running mean. The real time axes on all panels utilise the same scaling for one kyr.*

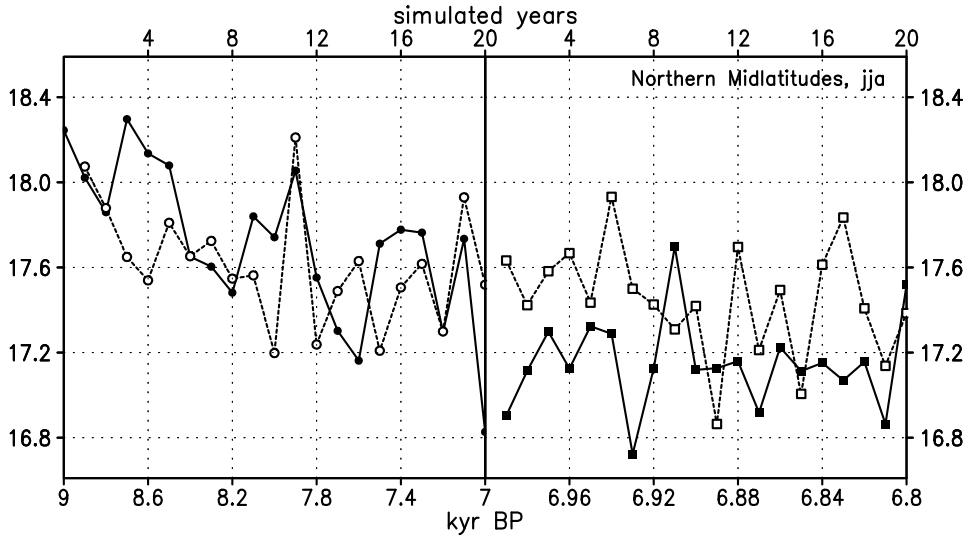

Figure 3.3: *Summer surface temperature (in °C) of northern mid-latitudes (cf. Figure 3.2a) of two experiments of* HOL-INS100 *and the continuation of these experiments with* HOL-INS10 *at 7 kyr BP where the acceleration factor for the orbital forcing changes from 100 to 10. Shown are 3-monthly means of single model years, no running mean filter is applied. Note the change in the scaling of the real time axis belonging to the change in the acceleration factor.*

the last 1,000 to 2,000 years, the trends indicate a moderate cooling in the tropics or nearly vanish at mid-latitudes. These characteristics are analogue in the ensemble mean curves of experiments HOL-INS100 (red line in Figure 3.2c, f), and in experiments HOL-INS10 (purple line in Figure 3.2c, f).

We examine the transition at 7 kyr BP between our different experiments when changing the acceleration factor from 100 to 10 (Figure 3.3). Apart from the inter-annual variability, there is no remarkable change in the temperature evolution. A comparison with Figure 3.2a-c indicates that the temperature trend, induced by the insolation change due to the orbital forcing, remains unchanged.

For our two sets of Holocene simulations, we evaluate the spatial distribution of the annual mean temperature trend (Figure 3.4). A general agreement in the spatial distribution of the surface temperature trends is detected between HOL-INS100 and HOL-INS10 (the spatial correlation coefficient amounts to 0.64, cf. Figure 3.4). The SST in the tropical region shows an increase from the middle to the late Holocene.

The most pronounced temperature trends occur over the continents. The smaller heat capacity compared to the ocean induces an amplification of the temperature trends. Enhanced warming during the Holocene occurs in the arid subtropical continents from northern Africa via western Asia to the Indian subcontinent. The most distinct cooling takes place over continental and sea ice covered northern high latitudes, exceeding 2 K temperature drop in both sets of experiments. We find that the trend is robust against the choice of ensemble members, showing that the difference in the inter-annual variability of both sets of experiments has no significant effect on the amplitude and distribution of the regional trends.

The temperature trends in the North Atlantic realm indicate both positive and negative values: a continuous cooling in the northeastern Atlantic is accompanied by a continuous warming in large

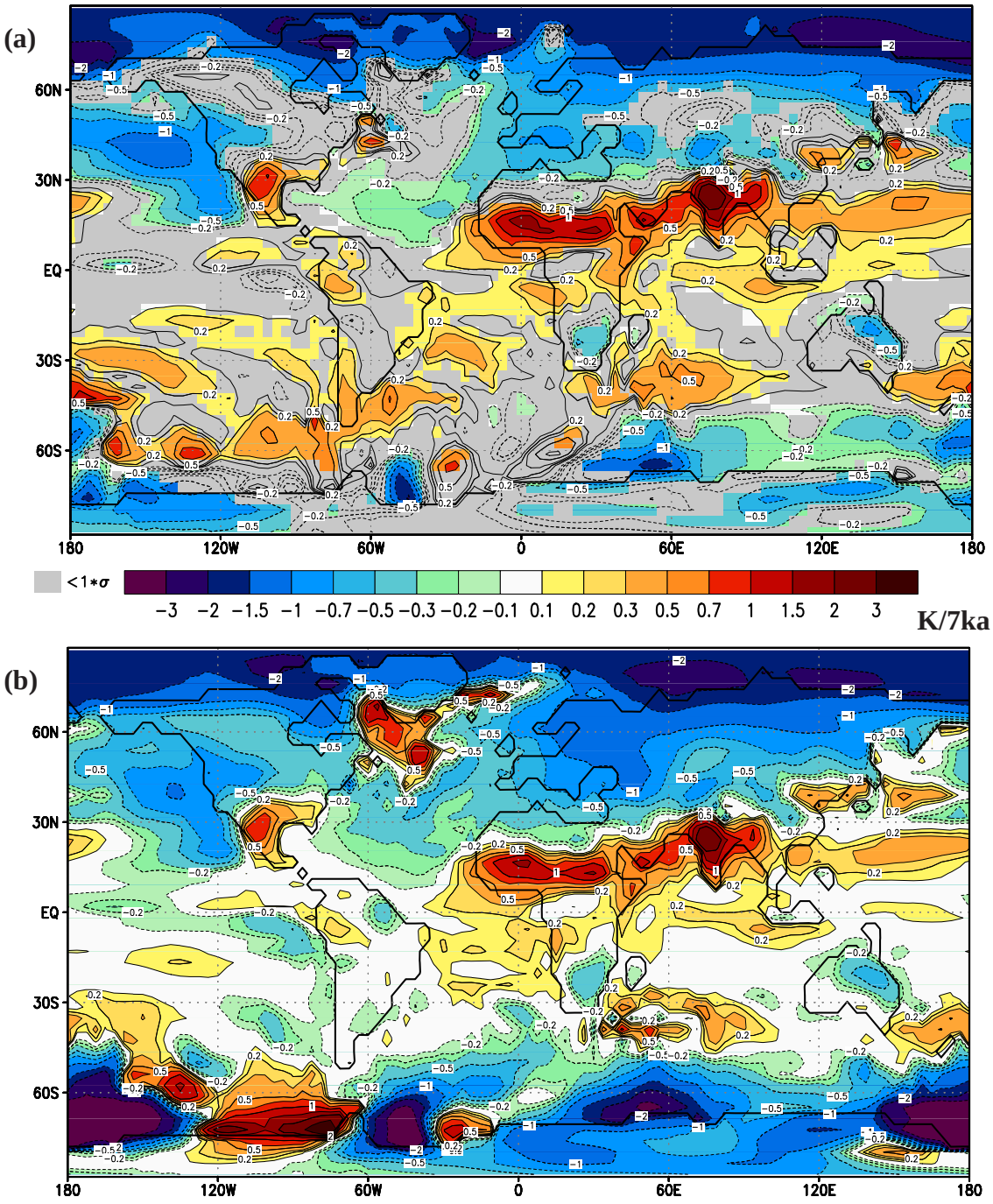

Figure 3.4: *Mean surface temperature trend from the mid-Holocene into the pre-industrial era (from 7 kyr BP to 0 kyr BP) of (a)* `HOL-INS100` *(70 simulation years) and (b)* `HOL-INS10` *(700 simulation years). Values depict the trend over the whole period (Kelvin per 7 kyr) statistically evaluated from the averaged set of experiments. Regions where the trend does not exceed one standard deviation are grey shaded in (a). Due to two realisations only, shading is omitted in (b). The pattern correlation coefficient between both data sets, calculated on grid points where the trend exceeds one standard deviation in (a), amounts to 0.64.*

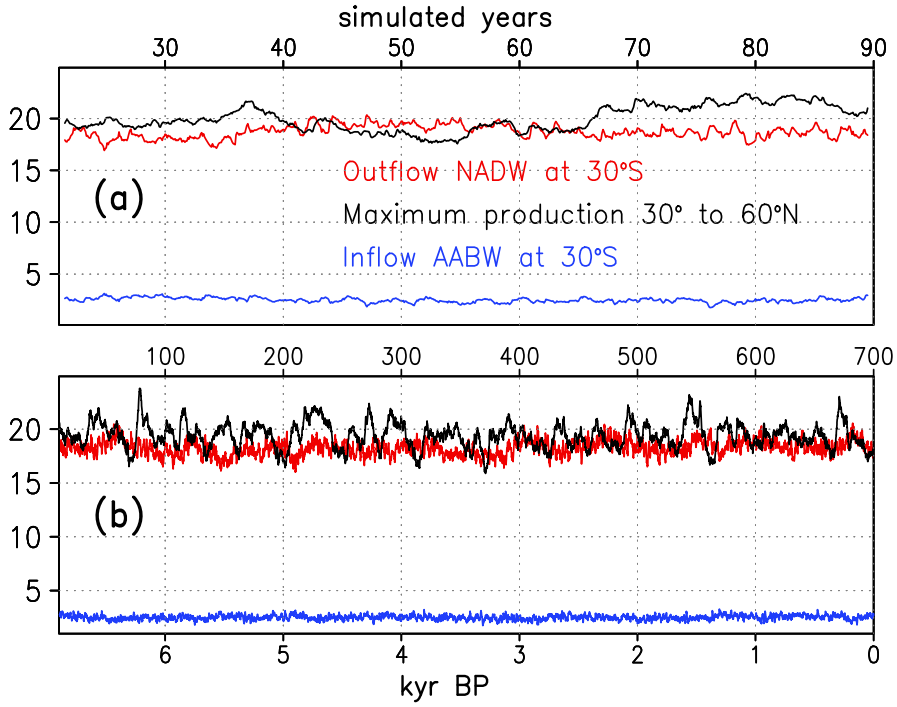

Figure 3.5: *Measure of the meridional overturning circulation in the Atlantic Ocean during the Holocene from one of the experiments (a)* `HOL-INS100` *with 70 years integration time, and (b) one of* `HOL-INS10` *with 700 years integration time, respectively. Note the different scaling in the integration time axis (upper axis) in (a) and (b). Maximum production rate of North Atlantic deep water (NADW) and its export rate into the Southern Ocean. Also shown is the inflow (positive) of Antarctic bottom water (AABW) into the North Atlantic Ocean. Values are in Sverdrup (1 Sv =* $1 \cdot 10^6\ m^3\ s^{-1}$*).*

areas of the subtropical Atlantic Ocean, as well as in the northwestern Atlantic off Newfoundland (Figure 3.4a), the Labrador Sea and south of Greenland (Figure 3.4b). Moreover, the Labrador realm shows a strong positive trend (Figure 3.4b), but is also a region of high variability, due to varying convection sites on multi-decadal time scales (note the shading in Figure 3.4a, indicating a high noise level in `HOL-INS100`). These stochastic convective events are the main reason for differences between the two 700 simulation years long realisations of the Holocene climate in the Labrador Sea (not shown).

The largest mismatches between experiments `HOL-INS100` and `HOL-INS10` are located near the sea ice margins north of the Antarctic and in small regions in the northern North Atlantic. There are matching and mismatching dipole structures in the Antarctic Circumpolar Current. Here, the model results are less reliable than on the Northern Hemisphere: the sea ice thickness is much smaller than observed, which is a prevalent drawback in coupled climate models [*Marsland et al.*, 2003, Legutke, pers. comm.]. We note that this model deficiency is also responsible for the spurious trend south of 40°S in the control experiment.

In order to estimate the orbital irradiation effect on the thermohaline circulation, the meridional mass transport in the Atlantic Ocean is evaluated for the two sets of experiments. For this purpose, we show indices of the meridional stream function (Figure 3.5): the maximal overturning in the

North Atlantic Ocean (between 30°N and 60°N, below 1,000 m depth), the export of deep water into the Southern Ocean at 30°S, and the import of Antarctic Bottom Water into the Atlantic Ocean at the same latitude. From Figure 3.5, it can be deduced that the meridional overturning circulation is nearly unchanged throughout the Holocene experiments. This is, a posteriori, an indication for the valid assumption of a relatively stable thermohaline circulation during the middle to late Holocene.

The evolution of the zonal mean surface temperature in the boreal winter season during the Holocene is displayed in Figure 3.6, where the deviation of each of the two sets of Holocene experiments from its respective zonal average of the entire time series are taken. Except for the region south of 40°S, the similarities between the two sets are evident: a moderate warming in low latitudes (cf. Figure 3.2f) and the strongest cooling of more than 1.5 K in the Arctic. Between 4 kyr BP and 2 kyr BP we find a warm phase widespread into the northern mid to high latitudes, which is especially located over the North American and Eurasian continents [*Lohmann et al.*, 2004]. Interestingly, in experiments `HOL-INS100` as well as in `HOL-INS10`, the tropical warming is compensated by the cooling signal coming from the high latitudes during the last two millennia. This feature is evident in both sets of simulations indicating that it is not linked to internal multi-decadal variability of the atmosphere-ocean-sea ice system.

3.3.2 Mid-Holocene climate

Motivated by the Palaeoclimate Modeling Intercomparison Project [PMIP, *Joussaume and Taylor*, 2000], we evaluate the climate of the time slice at the mid-Holocene optimum (6 kyr BP) in comparison to the pre-industrial climate. The PMIP project has fostered a systematic evaluation of climate models, besides others, under conditions during the mid-Holocene. This time slice was chosen to test the near-equilibrium response of climate models to orbital forcing at the so-called Holocene Climate Optimum with CO_2 concentration and ice sheets at pre-industrial conditions. The dating of this time slice was selected to 6 kyr BP because at this time no remaining melting ice caps were present, which may have survived the deglaciation phase at the early Holocene period.

We analyse averages of 60 simulation years out of 700 years of experiments `HOL-INS10`, centred at 6 kyr BP and 0 kyr BP, respectively. The latter time slice in our transient simulation characterises the pre-industrial climate. We find that the largest Northern Hemisphere temperature difference between the two time slices occurs in October (not shown). For October, we display the simulated surface temperature of the mid-Holocene climate and its deviation from the pre-industrial climate (Figure 3.7a, b), as well as sea ice thickness and its anomaly (Figure 3.7c, d). Note that in this section we present differences of the mid-Holocene climate from the latest Holocene and that a positve anomaly in Figure 3.7b indicates warmer temperatures at 6 kyr BP, which is concordant with a cooling trend during the last 6,000 years (Figure 3.4).

A region of warmer temperature during the mid-Holocene compared to the latest Holocene (3 to 6 K) is located over the entire Arctic Ocean (Figure 3.7b), accompanied by a decrease of the Arctic sea ice thickness of 40 to 80 cm (Figure 3.7d). The maximum anomalies are located in the Laptev Sea, in the Labrador Sea and near Svalbard. In these regions the temperature anomaly exceeds 6 K and the sea ice reduction amounts to more than 80 cm in the same areas. Note also a reduction in sea ice extent in the mid-Holocene simulation in Hudson Bay, Greenland Sea, Barents and Bering Sea,

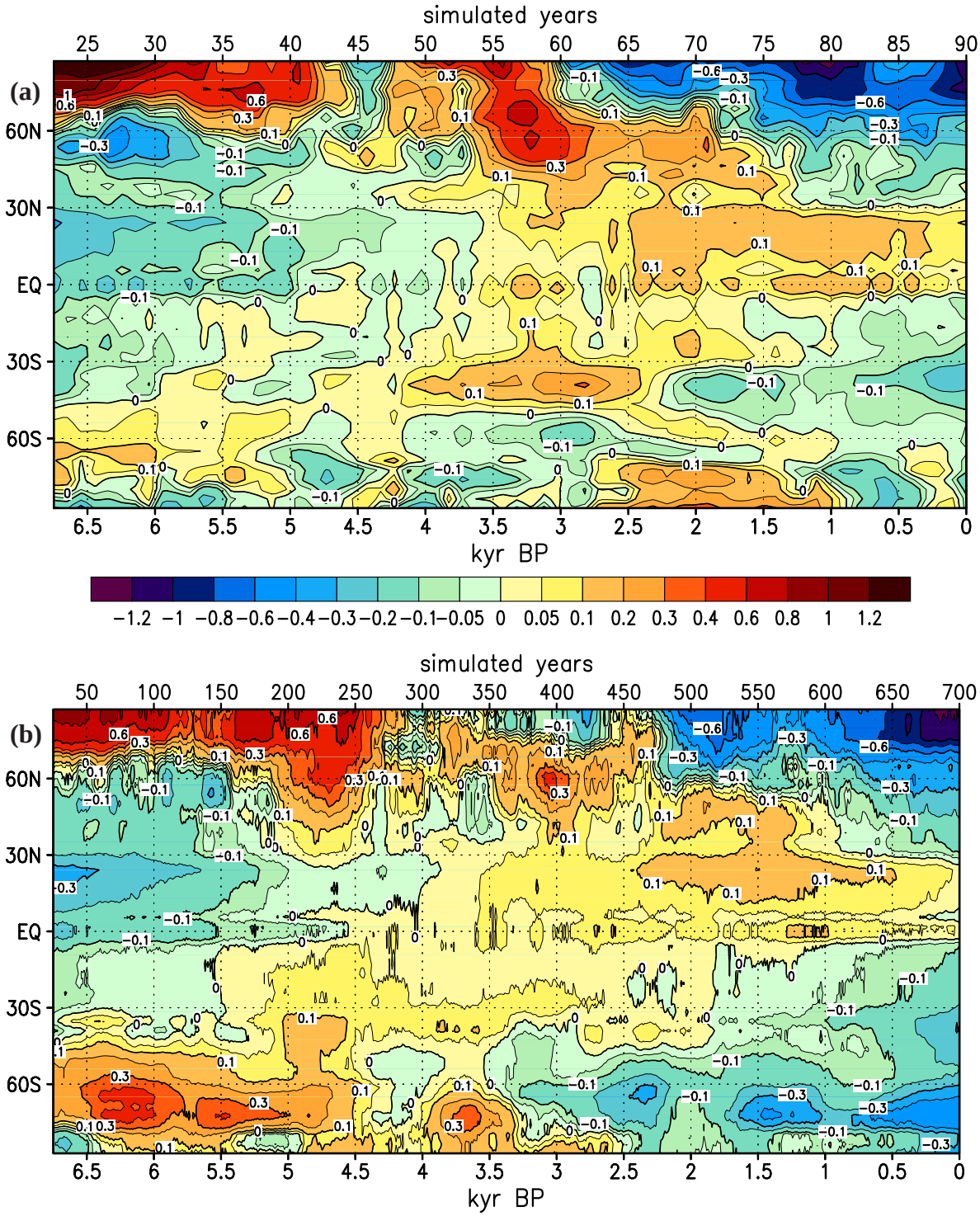

Figure 3.6: *Temporal evolution of zonal mean surface temperature anomaly (in K) during boreal winter from the mid-Holocene into the pre-industrial era of experiments* `HOL-INS100` *(a) and* `HOL-INS10` *(b). The respective long-term zonal mean is subtracted and a running mean filter of 4 years (a) and 50 years (b) is applied, respectively. For the axes scaling cf. Figure 3.2 and Figure 3.5.*

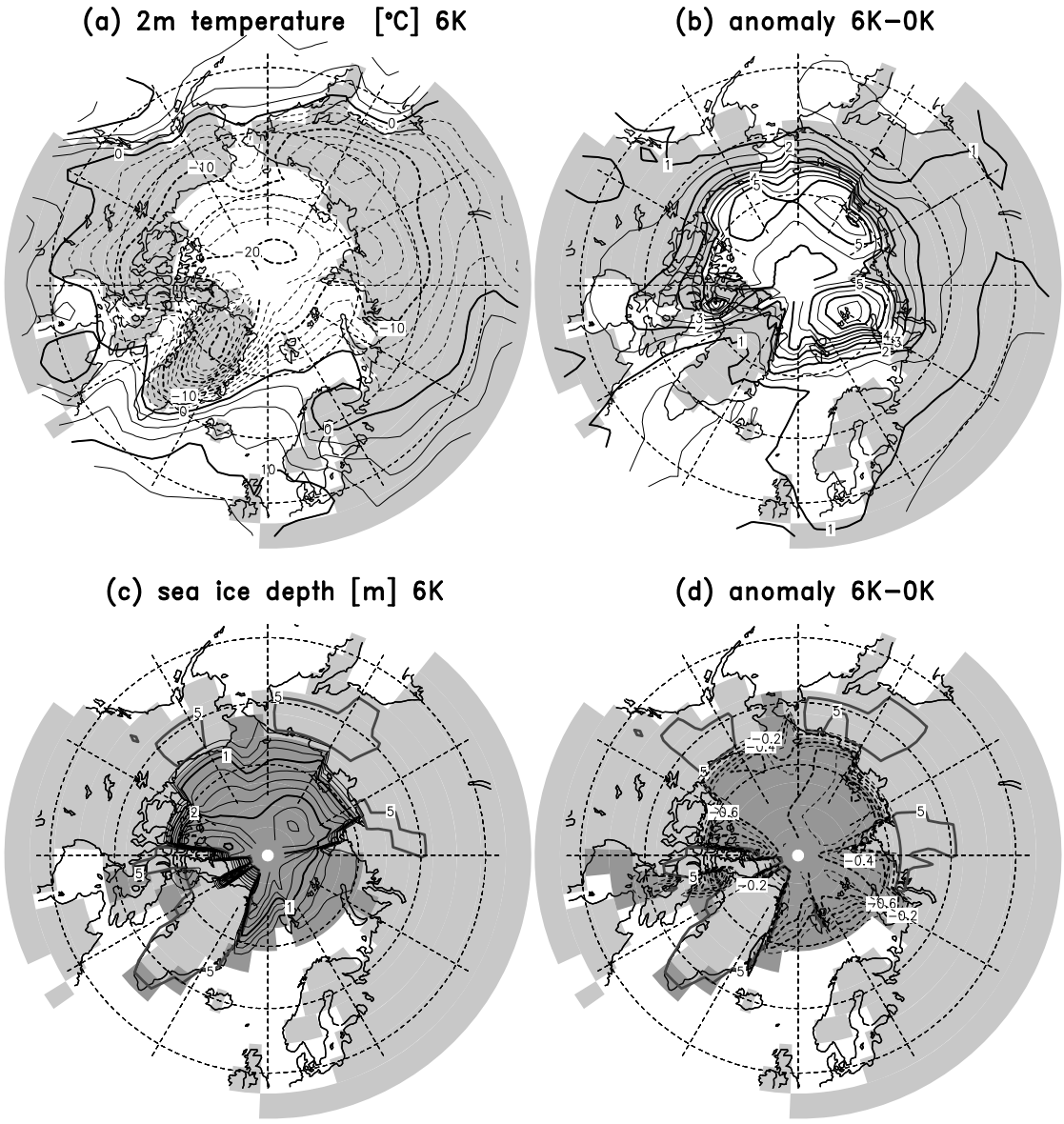

Figure 3.7: *Near surface air temperature (a), sea ice thickness and compactness (c) in October for the mid-Holocene climate at 6 kyr BP; surface air temperature (b) and sea ice thickness (d) difference between the mid-Holocene and the pre-industrial climate. Areas where sea ice compactness exceeds 20 % are darkly shaded for 6 kyr BP in (c) and for 0 kyr BP in (d) (no difference). Additionally, the 5 cm contour line for snow depth is indicated with a thick grey line for 6 kyr BP in (c) and 0 kyr BP in (d) (no difference). Light shading indicates continents in the T30 resolution of the atmospheric sub-model ECHAM. Displayed is experiment* `HOL-INS10` *for October, where 6 kyr BP is a mean of 60 years between 5.7 and 6.3 kyr BP, and 0 kyr BP is a similar average around the pre-industrial climate (1800 AD). The contour intervals for temperature (sea ice thickness) are 2.5 K (0.25 m) and 0.5 K (0.1 m) for anomalies, respectively.*

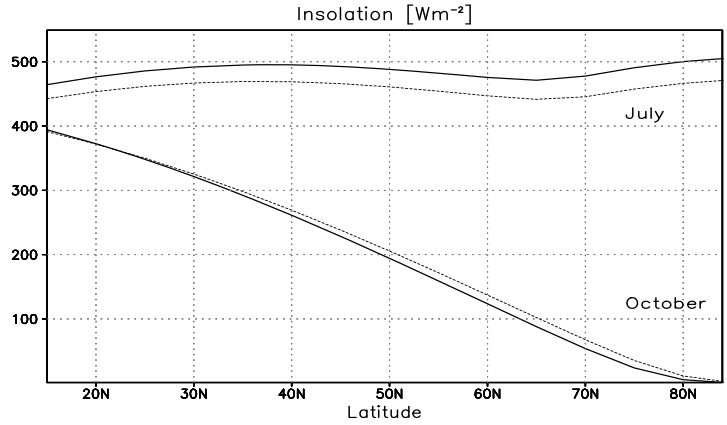

Figure 3.8: *Latitudinal distribution of solar radiation during the mid-Holocene (6 kyr BP, solid line) compared to the present radiation (dashed line) in July and October [Berger, 1978].*

compared to 0 kyr BP (dark shaded area with sea ice compactness of more than 20 % for 6 kyr BP in Figure 3.7c, and for 0 kyr BP in Figure 3.7d). Similarly, a reduction in the snow covered area in central Siberia, eastern Siberia, and Alaska can be detected from the 5 cm snow depth contour line in Figure 3.7c and Figure 3.7d.

The temperature change indicates a strong nonlinear signal in the model response to the radiative forcing: the solar radiation at 6 kyr BP during October, when the most intense warming takes place, has an energy deficit of 15 Wm^{-2} at 60°N compared to today (Figure 3.8). The heat capacity of the upper ocean stores the warming of the boreal summer insolation, i. e. 30 Wm^{-2} more energy input than today in the Arctic from mid of June to end of July (Figure 3.8). The warmer SST during the summer season with high level energy input lengthens the ice free season, reduces average sea ice thickness as well as snow depth in the neighbouring northern continents in October. This occurs despite the fact that the seasonal radiation anomaly has already turned its sign. Therefore, the sea ice and snow cover indicate a delayed response of the climate to the Milankovitch forcing.

The model simulates also modified surface winds during mid-Holocene boreal winter in the Arctic region (Figure 3.9). We find enhanced southward winds in the western part of the Greenland Sea and the region south of Greenland and Iceland. Furthermore, there is intensified cyclonic circulation in the Norwegian Sea. This is consistent with an increased eastward wind pattern during 6 kyr BP relative to the pre-industrial climate. The wind affects the sea ice dynamics in these regions and, in particular, enhance southward sea ice transport along the eastern coast of Greenland. This causes increased sea ice concentration and a temperature drop southeast of Greenland.

We acknowledge the critical use of a modern calender in our mid-Holocene comparison, instead of a calendar of angular months, defined by 12 times 30° sectors on the Earth's orbit [*Joussaume and Braconnot*, 1997]. This is in particular crucial when comparing results for October, because the calendar is fixed at the vernal equinox and due to Kepler's laws, the length of the season varies with the precession cycle. Nonetheless, *Joussaume and Braconnot* [1997] stated that a relevant part of their 1-2 K difference of September air temperature difference caused by the different calendar methods is connected with the prescribed modern cycle of SST. Since our AOGCM calculates the seasonal cycle of SST dependent of the changing insolation signal, we do not expect significant inconsistency of our results due to the use of a modern calendar. Moreover, since the begin of the astronomically defined Öctoberïs shifted by 4 days into September [*Joussaume and Braconnot*, 1997, their Table A1], the

temperature difference in Figure 3.7b is even larger, when underlying the astronomical calendar.

3.3.3 Holocene and 20th century global warming trends

In order to relate the Holocene climate evolution to the temperature trends of the last century we performed integrations with historical evolution of greenhouse gases for the period year 1800 until 2000 AD. These simulations are continued from the two realisations of Holocene experiments `HOL-INS10` without acceleration, since the greenhouse gas forcing provides a strong forcing on the time scale of the atmosphere-ocean-sea ice system. Figure 3.10 shows a smooth transition between the surface temperature of the `HOL-INS10` and `GHG-INS1` experiments, when changing the acceleration factor for the orbital forcing from 10 to no acceleration.

Figure 3.11 displays the temperature evolution of the Northern Hemisphere from 7 kyr BP until today. For the boreal summer, a long-term cooling trend during the Holocene until the begin of the anthropogenic area is detected. This cooling trend is of the same order of magnitude as the warming from the period 1800 to approximately 1950 AD in the model. We note, however, that the recent warming trend is overestimated in the experiment, which is probably linked to the missing cooling effect of aerosols in the utilised version of the ECHAM4 model. For boreal winter, Figure 3.11b indicates a small Northern Hemisphere cooling trend after 3 kyr BP, linked to the forcing by the precessional cycle in tropical latitudes (cf. Figure 3.2d–f). Due to the spatial heterogeneity in the annual mean surface temperature trends, as seen in Figure 3.4, the Northern Hemisphere surface

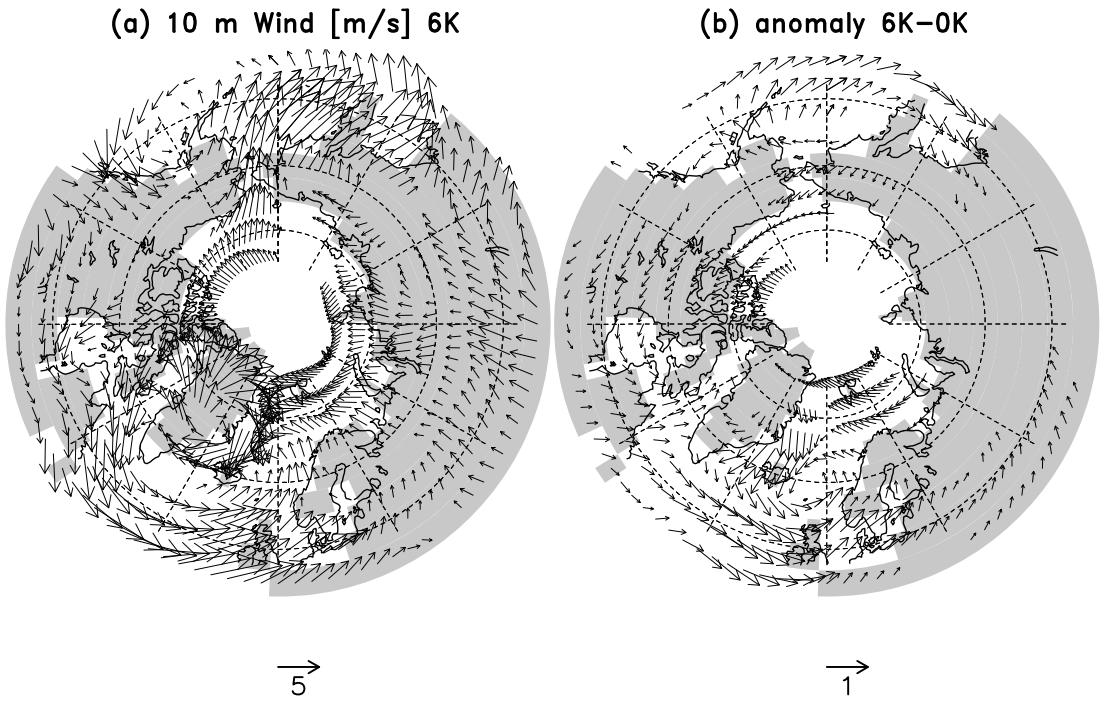

Figure 3.9: *Surface wind (a) during boreal winter season (January to March) for the mid-Holocene climate at 6 kyr BP and wind anomaly (b) of the mid-Holocene from the pre-industrial climate (for details see Figure 3.7). The arrows below indicate the strength of the respective wind speed (in m/s). Vectors with a magnitude less than 1 m/s and 0.2 m/s are omitted in (a) and (b), respectively.*

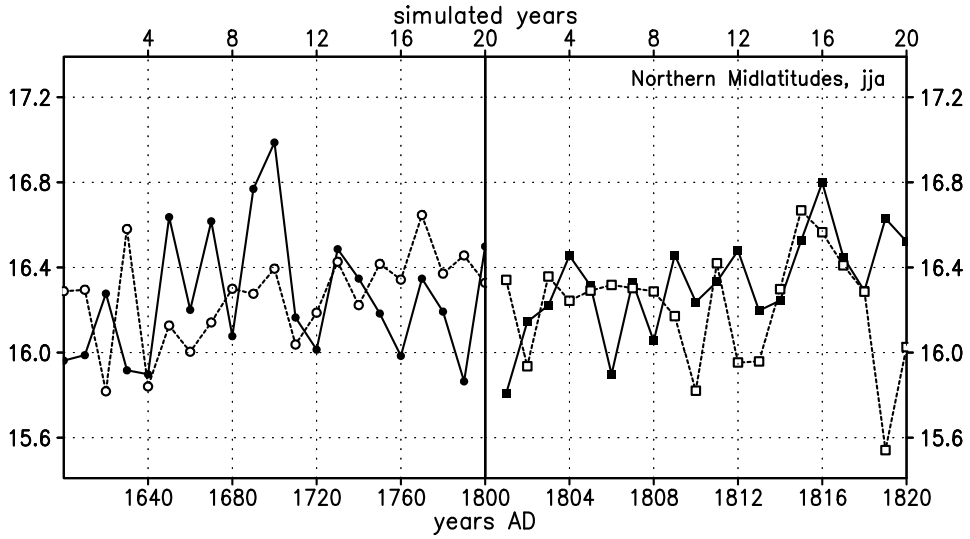

Figure 3.10: *Summer surface temperature (in °C) of northern mid-latitudes (cf. Figure 3.2a) of two experiments of* `HOL-INS10` *and the continuation of these experiments with* `GHG-INS1` *at the year 1800 AD where the acceleration factor for the orbital forcing varies from 10 to 1 (no acceleration). See text and Figure 3.3 for details.*

temperature cooling trend during the Holocene is small when comparing it with the recent global warming trend (Figure 3.11c).

When passing over to spatial signatures at northern high latitudes for October, differences between the climates at 6 kyr BP and present day (1950-1999 AD, including the anthropogenic warming) are displayed in Figure 3.12. The deviation of the mid-Holocene temperature from the present day climate (Figure 3.12a) shows warming over the Arctic Ocean but little change or weak cooling over the high latitude continents. The warmer temperature over the Arctic Ocean at 6 kyr BP corresponds with thinner sea ice, in comparison with both the pre-industrial climate (0 kyr BP, Figure 3.7c, d) as well as with present day climate (Figure 3.12b). Over the northern continents, the warming induced by the anthropogenic increase of greenhouse gases exceeds the orbitally forced cooling during the last 6,000 years until 1800 AD, which can be detected from a positive anomaly in Figure 3.7b (6 kyr BP minus 0 kyr BP). This results in lower temperatures at 6 kyr BP than today in Figure 3.12a.

3.3.4 Comparison with PMIP results

In order to understand the physical mechanisms related to the precessional and obliquity cycles during the Holocene, we compare our transient mid-Holocene experiments with previous PMIP studies. At 6 kyr BP the precessional forcing was nearly in an opposite phase (the passage through the perihelion occurred in September compared to January today) of the 21,000 year period, which is the dominant period for tropical insolation changes. Within PMIP, simulations of the present day and the 6 kyr BP climate were done with the former ECHAM3 atmospheric general circulation model [*Roeckner et al.*, 1992]. We show results of this model Figure 3.13, applying fixed vegetation distribution [*Lorenz et al.*, 1996], and including an interactive vegetation model [*Claussen*, 1997; *Claussen and Gayler*, 1997]. *Claussen and Gayler* [1997] coupled asynchronously a vegetation model with the ECHAM3

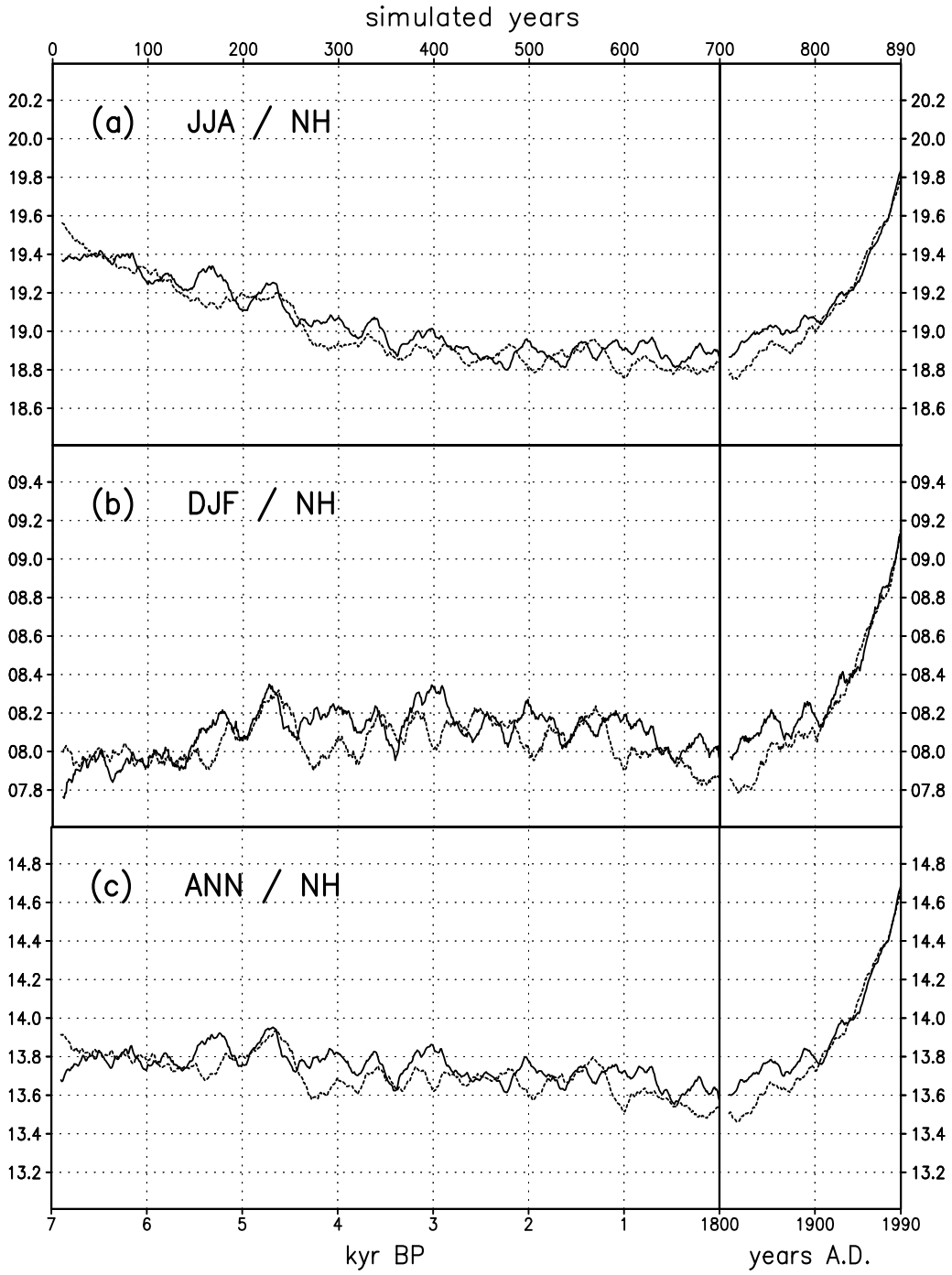

Figure 3.11: *Temporal evolution of surface temperature (in °C) of the Northern Hemisphere in (a) summer, (b) winter, and the (c) annual mean. The left part indicates two experiments (acceleration factor 10,* `HOL-INS10`*) from 7 kyr BP to the latest Holocene (1800 AD), the right part displays the continuation of these experiments into the anthropogenic era until today (2000 AD), without using the acceleration technique for the Milankovitch forcing (experiment* `GHG-INS1`*, note the simulation time on the upper axis). The gap in the data is due to the application of a centred running mean filter of 21 simulation years that suppresses the appearance of the first 10 years of the experiments. A range of 2 K is used for all three ordinates.*

model. The model generates a climate in equilibrium with potential vegetation distribution and the boundary conditions for the middle Holocene. Prescribed sea surface temperature, orography, ice sheet distribution, insolation, and CO_2 concentration were employed identically for both sets of simulations. The precessional forcing caused intensified precipitation and a shift of vegetation mostly in the southwestern part of the Sahara in this simulation. At high latitudes, the taiga extended northward at the expense of tundra during the mid-Holocen, when using the ECHAM3 including the vegetation model [*Claussen and Gayler*, 1997; *Claussen*, 1997].

The distribution of temperature difference for October, simulated with fixed SST (Figure 3.13a), displays strong regional discrepancy with our study (Figure 3.12a) using a coupled AOGCM. We note that the atmospheric temperature change induced by interactive vegetation (Figure 3.13b) is in the same order of magnitude as the effect of the coupling to the ocean-sea ice system (compare Figs. 3.12a and 3.13a).

3.4 Discussion

Using our acceleration technique, we evaluated the temperature evolution of the Holocene and the last 200 years, a period of strong anthropogenic impact. The acceleration technique, the temperature trends, and the simulated mid-Holocene climate is discussed in the following.

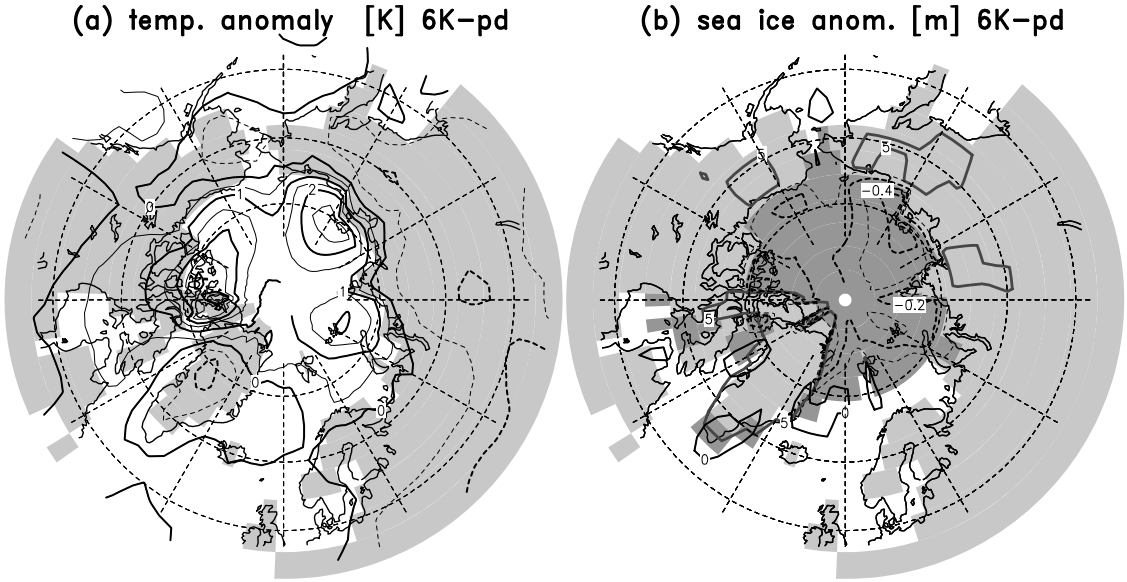

Figure 3.12: *Difference of October near surface air temperature (a) and sea ice thickness (b) between the mid-Holocene climate at 6 kyr BP and the present day climate. Analogue to Figure 3.7b, d, areas where sea ice compactness in the present day climate exceeds 20 % are darkly shaded, and the 5 cm contour line for snow depth in the present day climate is indicated with a thick grey line (no difference, cf. Figure 3.7). Displayed is the average of 1950-1999 AD (50 years) of experiments* `GHG-INS1` *for October.*

3.4.1 Acceleration technique

The similarity in the results of the two sets of experiments when changing the acceleration factor places emphasis on the validity of the method. Therefore, our method of accelerating the orbital forcing in a complex AOGCM turns out to be a valuable tool to perform transient simulations of the Holocene climate.

The method is similar to distorted physics approach that is commonly applied for computer time reduction in ocean circulation models [*Bryan,* 1984]. In these ocean models the asynchrony lies in the separation of distinct ocean waves, which act on time scales of different orders of magnitude [*Pacanowski et al.,* 1993]. Another technique was introduced by *Voss et al.* [1998], using the ECHAM3 model coupled to the coarse resolution ocean circulation model LSG [*Maier-Reimer et al.*, 1993]. They based their asynchronous coupling on separated time scales of the atmosphere-oceanic mixed layer and the deep ocean circulation. In their periodically-synchronous coupling technique the synchronously coupled model is integrated subsequently for 15 months, followed by an asynchronous phase of four years length, where the oceanic sub-model is calculated without the atmospheric sub-model [*Voss and Sausen,* 1996; *Voss et al.,* 1998].

We find no significant changes in the thermohaline circulation in our multi-decadal as well as in our centennial simulations (Figure 3.5), which is consistent with the relatively stable climate during the middle to late Holocene period. For example, melting inland ice caps caused meltwater pulses including sea level rise. This may have provoked severe shifts of the thermohaline circulation during the early Holocene (e. g. during the Younger Dryas event). Although the astronomical forcing might be vigorous enough to effect changes in the location and strength of convection sites, there is no evidence in the marine geological record that the thermohaline circulation was subject to abrupt changes during the last 7,000 years [*Grootes et al.*, 1993; *Clark et al.*, 2002]. Smaller rearrangements in the deep ocean circulation can modify regional trend patterns in particular near the Antarctic sea ice border and around Greenland (Figure 3.4b).

3.4.2 Temperature trends

The subtropical warming trend from the middle to late Holocene is also consistent with SST reconstructions based on the alkenone method [*Emeis et al.*, 2000; *Marchal et al.*, 2002; *Rohling et al.*, 2002]. The spatial heterogeneity of the temperature trend in the North Atlantic realm (Figure 3.4) is furthermore consistent with the SST signature of the Arctic Oscillation/North Atlantic Oscillation (AO/NAO) [*Thompson and Wallace,* 1998; *Hurrell,* 1995], indicating a trend from a positive phase of the AO/NAO to a negative one during the Holocene. The AO/NAO phenomenon is the dominant mode of North Atlantic SST variability on inter-annual to decadal time scales. This surface temperature signature is consistent with proxy data [*Rimbu et al.*, 2003]. Along with the positive phase of the NAO, a temperature rise in Europe in the 6 kyr BP climate are seen in the model results (Figure 3.4b).

The trend in the AO/NAO from a more positive to a more negative phase, is possibly triggered by the boreal winter insolation. Since the precessional forcing is dominant in the tropics (Figure 3.1), we speculate that the tropical Pacific provides for a rectification effect to the varying seasonal distribution of the solar radiation. The rectification is associated with an asymmetric response of the climate

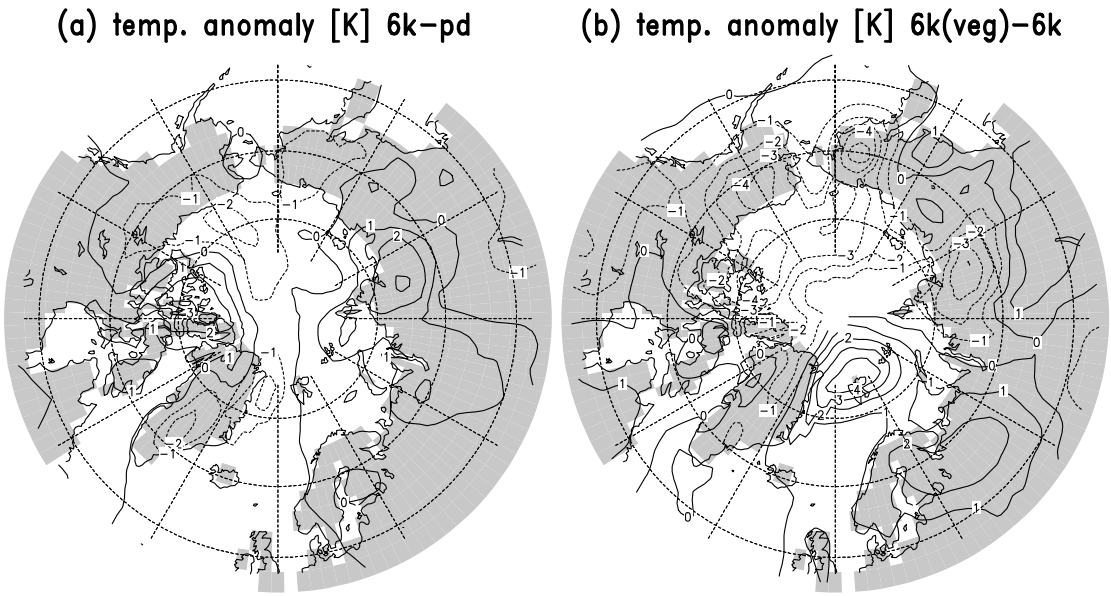

Figure 3.13: *Near surface temperature of the simulation of the Holocene climate at 6 kyr BP with the ECHAM3 atmosphere model, participating in PMIP. Shown is the mean temperature difference for October from simulations of the mid-Holocene climate applying fixed present day vegetation distribution [Lorenz et al., 1996], with respect to the present day climate (a), and the difference temperature calculating interactively the equilibrium potential vegetation distribution [Claussen and Gayler, 1997], with respect to fixed vegetation (b) SST and sea ice distribution are fixed in these simulations (cf. Figure 3.7).*

system to external forcing, such as e. g. the faster retreat than buildup of ice caps in the case of glacial-interglacial cycles [*Imbrie et al.*, 1993], and a nonlinear response of a circulation model for the tropical Pacific Ocean to insolation forcing [*Clement et al.*, 1999]. In our case, the asymmetry is via the modes of atmospheric circulation: the insolation during the boreal winter season affects the atmospheric circulation on the Northern Hemisphere, thereby imprinting the typical AO/NAO temperature pattern [*Thompson and Wallace*, 1998; *Hurrell*, 1995; *Rimbu et al.*, 2003].

In our experiments we find a continuous cooling trend during the last two millenia in the boreal winter season, which is less obvious in the annual mean (0.4 K in the last 2,000 years mainly in the Northern Hemisphere). This cooling trend may also attribute to a millennial cooling trend as detected in Northern Hemisphere temperature reconstructions based on high resolution proxy data [*Mann et al.*, 1999; *Mann and Jones*, 2003]. We note, however, that multi-decadal to millennial climate variability could be strongly effected by other forcing mechanisms like solar radiation changes linked to sunspot variability and volcano activity affecting the atmospheric circulation [e. g. *Crowley*, 2000b; *Shindell et al.*, 1999, 2001].

We extended our Holocene climate simulations into the period 1800-2000 AD, by including the forcing by the observed increase of atmospheric greenhouse gases. With this forcing we are able to relate the effect of the astronomical forcing to the temperature change influenced by anthropogenic emissions of greenhouse gases. We recognise the annual mean temperature trend during the last 200 years to be much larger than the trends induced by the Milankovitch forcing during the middle to latest Holocene.

3.4.3 Mid-Holocene climate

To avoid the use of prescribed SST, coupled atmosphere-ocean simulations of the mid-Holocene climate [*Hewitt and Mitchell*, 1998; *Voss and Mikolajewicz*, 2001; *Kitoh and Murakami*, 2002] have recently been performed. These experiments simulate near-equilibrium states of the mid-Holocene climate (6 kyr BP), or perform a series of time slices stepping through the Holocene [*Liu et al.*, 2003]. *Liu et al.* [2003] using the time slice concept find also a cooling at low latitudes and a warming at higher latitudes during the Holocene and attribute this to direct radiation changes. Our method has been used to obtain the evolution of the Holocene climate related to modes of variability.

The pronounced warming in the Arctic Ocean at the mid-Holocene climate optimum, which is evident in our experiments, is supported by pollen and macrofossil proxy data [*Texier et al.*, 1997] as well as by a northward shift of the Arctic tree-line [*Tarasov et al.*, 1998]. In the annual mean, we find a 1–2 K warming of the mid-Holocene temperature relative to today, which is smaller than for the June to October season (not shown). The annual mean high-latitude warming is a prominent feature in modelling experiments [*Voss and Mikolajewicz*, 2001; *Crucifix et al.*, 2002; *Liu et al.*, 2003; *Claussen et al.*, 1999, Kubatzki, pers. comm.]. It can be attributed to the asymmetric response to the seasonal cycle of insolation forcing.

3.5 Concluding remarks

We investigate the impact of the slowly evolving change in the Earth's boundary condition during the Holocene, the annual distribution of incident solar radiation, on the climate of the coupled atmosphere-ocean-sea ice system. Justified by the much longer time scale of this astronomical forcing than that of the dynamical feedback processes in the atmosphere-ocean system we accelerate the time scale of the orbitally varying solar radiation [*Berger*, 1978] by a factor of up to 100. This enables the simulation of the middle to late Holocene period with a complex AOGCM. Furthermore, our approach allows for ensemble simulations of the Holocene climate in order to obtain the deterministic climate model response to external forcing. The advantage of our technique is that we included the feedbacks inherent in the AOGCM without changing the model code and the control climate.

The transient simulation of the Holocene climate renders a possibility to validate complex climate models with palaeoclimate proxy data, and furthermore, to separate between different forcing factors affecting Holocene climate trends. In a companion paper [*Rimbu et al.*, 2004], we use our technique to compare the results with a new global set of collected marine proxy temperature data, based on the alkenone method. We obtain a coherent picture of neo-glaciation since 7 kyr BP in the model and proxy data. We find opposite trends of warming and cooling occurring in the tropics and mid-latitudes. Performing new model experiments including other forcing mechanisms, model components, and feedbacks, such as the climate feedback induced by vegetation changes [e. g., *Ganopolski et al.*, 1998] could significantly extend our findings of a dominant orbital mechanism for Holocene surface temperature variations. Our acceleration technique has already been applied to the climate of the last interglacial (Eem, at 130–120 kyr BP) showing that the changes in the circulation and seasonal cycle are in accordance with high resolution proxy data [*Felis et al.*, 2004].

In order to properly address the question, how increasing human population and industrialisation will induce a significant climate change, requires intimate knowledge on amplitude and rapidness in the natural variations of temperature or other temperature-related environmental properties. Unfortunately, historical records of direct temperature measurements that would allow consideration of changing climate on a global scale are too short and fall already within the period of strong human impact on natural conditions. The time period of the Holocene, which is prior to strong human impact, could be used as a basis for assessment of natural climate variability.

The models used in the IPCC process are clearly unrivaled in their ability to simulate a broad suite of variables across the entire world [*Intergovernmental Panel on Climate Change*, 2001], but their reliability on longer time scales requires additional evaluation. We argue that the paleoclimate record of the Holocene provides an excellent test of these models on a quantitative basis. As a logical next step, we propose to continue simulations, which are validated with proxy data for the Holocene period, into the recent period of anthropogenic greenhouse warming with subsequent scenario integrations to simulate future climate change. This can enhance confidence into numerical projections of future climate change, and provide a better comparison of climate variability under natural and anthropogenic forcing.

Acknowledgments We like to thank C. Heinze and J. Jungclaus and two anonymous reviewers for their helpful comments which improved the manuscript considerably. M. Claussen is acknowledged for providing us with part of the ECHAM3 data and S. Schubert for help with preparing Figure 3.13. The model simulations have been done at the Deutsches Klimarechenzentrum (DKRZ), Hamburg, Germany. We thank S. Legutke for her support concerning the ECHO-G model experiments as well as the staff of the Max-Planck-Institut für Meteorologie and the DKRZ for technical support. This study was funded by grants from the German Ministry of Research and Education (BMBF) through the program DEKLIM.

3.6 References

Berger, A. L., Long-term variations of daily insolation and Quaternary climatic changes, *Journal of the Atmospheric Sciences*, *35*, 2362–2367, 1978.

Bertrand, C., M.-F. Loutre, and A. Berger, High frequency variations of the Earth's orbital parameters and climate change, *Geophysical Research Letters*, *29*, doi:10.1029/2002GL015,622, 2002a.

Bertrand, C., M.-F. Loutre, M. Crucifix, and A. Berger, Climate of the last millennium: a sensitivity study., *Tellus*, *54A*, 221–224, 2002b.

Boden, T. A., D. P. Kaiser, R. J. Sepanski, and F. W. Stoss, Trends '93: A compendium of data on global change, *Carbon Dioxide Information Analysis Center ORNL/CDIAC-65*, Oak Ridge National Laboratory, Oak Ridge, Tenn., U.S.A., 1994.

Boville, A. B., and P. R. Gent, The NCAR climate system model, version one, *Journal of Climate*, *11*, 1115–1130, 1998.

Bryan, K., Accelerating the convergence to equilibrium of ocean-climate models, *Journal of Physical Oceanography*, *14*, 666–673, 1984.

Clark, P. U., N. G. Pisias, T. F. Stocker, and A. J. Weaver, The role of thermohaline circulation in abrupt climate change, *Nature*, *415*, 863–869, 2002.

Claussen, M., Modeling bio-geophysical feedback in the African and Indian monsoon region, *Climate Dynamics*, *13*, 247–257, 1997.

Claussen, M., and V. Gayler, The greening of Sahara during the mid-Holocene: results of an interactive atmosphere-biome model, *Global Ecol. and Biogeogr. Letters*, *6*, 369–377, 1997.

Claussen, M., C. Kubatzki, V. Brovkin, A. Ganopolski, P. Hoelzmann, and H. J. Pachur, Simulation of an abrupt change in Saharan vegetation in the mid-Holocene, *Geophysical Research Letters*, *24*, 2037–2040, 1999.

Claussen, M., et al., Earth system models of intermediate complexity: Closing the gap in the spectrum of climate system models, *Climate Dynamics*, *18*, 579–586, 2002.

Clement, A. C., R. Seager, and M. A. Cane, Orbital controls on the el nino/southern oscillation and the tropical climate, *Paleoceanography*, *14*, 441–456, 1999.

CLIMAP Project Members, The surface of the ice age Earth, *Science*, *191*, 1131–1137, 1976.

Crowley, T. J., Causes of climate change over the past 1000 years, *Science*, *289*, 270–277, 2000.

Crucifix, M., M.-F. Loutre, P. Tulkens, T. Fichefet, and A. Berger, Climate evolution during the Holocene: a study with an Earth system model of intermediate complexity, *Climate Dynamics*, *19*, 43–60, 2002.

Emeis, K.-C., U. Struck, H.-M. Schulz, R. Rosenberg, S. Bernasconi, H. Erlenkeuser, T. Sakamoto, and F. Martinez-Ruiz, Temperature and salinity variations of Mediterranean Sea surface waters over the last 16,000 years from records of planktonic stable oxygen isotopes and alkenone unsaturation ratios, *Palaeogeography Palaeoclimatology Palaeoecology*, *158*, 259–280, 2000.

Etheridge, D. M., L. Steele, R. Langenfelds, R. Francey, J. Barnola, and V. Morgan, Natural and anthropogenic changes in atmospheric CO_2 over the last 1000 years from air in Antarctic ice and firn, *Journal of Geophysical Research*, *101*, 4115–4128, 1996.

Etheridge, D. M., L. Steele, R. Francey, and R. Langenfelds, Atmospheric methane between 1000 a.d. and present: evidence of anthropogenic emissions and climatic variability, *Journal of Geophysical Research*, *103*, 15,979–15,993, 1998.

Felis, T., G. Lohmann, H. Kuhnert, S. J. Lorenz, D. Scholz, J. Pätzold, S. A. Al-Rousan, and S. M. Al-Moghrabi, Increased seasonality in Middle East temperatures during the last interglacial period, *Nature*, *429*, 164–168, 2004.

Fichefet, T., S. Hovine, and J.-C. Duplessy, A model study of the Atlantic thermohaline circulation during the last glacial maximum, *Nature*, *372*, 252–255, 1994.

Ganopolski, A., and S. Rahmstorf, Rapid changes of glacial climate simulated in a coupled climate model, *Nature*, *409*, 153–158, 2001.

Ganopolski, A., C. Kubatzki, M. Claussen, V. Brovkin, and V. Petoukhov, The influence of vegetation-atmosphere-ocean interaction on climate during the mid-Holocene, *Science*, *280*, 1916–1919, 1998a.

Ganopolski, A., S. Rahmstorf, V. Petoukhov, and M. Claussen, Simulation of modern and glacial climates with a coupled global model of intermediate complexity, *Nature*, *391*, 351–356, 1998b.

Gates, W. L., The numerical simulation of ice-age climate with a global general circulation model, *Journal of the Atmospheric Sciences*, *33*, 1844–1873, 1976.

Grootes, P. M., M. Stuiver, J. W. C. White, S. J. Johnsen, and J. Jouzel, Comparison of oxygen isotope records from the GISP2 and GRIP Greenland ice cores, *Nature*, *366*, 552–554, 1993.

Grötzner, A., R. Sausen, and M. Claussen, The impact of sub-grid scale sea-ice inhomogeneities on the performance of the atmospheric general circulation model ECHAM3, *Climate Dynamics*, *12*, 477–496, 1996.

Hewitt, C. D., and J. F. B. Mitchell, A fully coupled GCM simulation of the climate of the mid-Holocene, *Geophysical Research Letters*, *25*, 361–364, 1998.

Hewitt, C. D., A. J. Broccoli, J. F. B. Mitchell, and R. J. Stouffer, A coupled model study of the last glacial

maximum: Was part of the North Atlantic relatively warm?, *Geophysical Research Letters*, *28*, 1571–1574, 2001.

Hoyt, D. V., and K. H. Schatten, A discussion of plausible solar irradiance variations, *Journal of Geophysical Research*, *98*, 18,895–18,906, 1993.

Hurrell, J. W., Decadal trends in the North Atlantic oscillation: regional temperatures and precipitation, *Science*, *269*, 676–679, 1995.

Imbrie, J., E. A. Boyle, S. C. Clemens, A. Duffy, and W. R. Howard et al., On the structure and origin of major glaciation cycles: 1. linear responses to Milankovitch forcing, *Paleoceanography*, *7*, 701–738, 1992.

Imbrie, J., et al., On the structure and origin of major glaciation cycles: 2. the 100,000-year cycle, *Paleoceanography*, *8*, 699–735, 1993.

Indermühle, A., et al., Holocene carbon-cycle dynamics based on CO_2 trapped in ice at Taylor Dome, Antarctica, *Nature*, *398*, 121–126, 1999.

IPCC, *Climate Change 2001: The scientific basis. Contribution of the Working Group I to the Third Assessment Report of the Intergovernmental Panel on Climate Change*, Houghton, J. T. et al. (Eds.), Cambridge University Press, Cambridge, United Kingdom, 2001.

Joussaume, S., and P. Braconnot, Sensitivity of paleoclimate simulation results to season definitions, *Journal of Geophysical Research*, *102*, 1943–1956, 1997.

Joussaume, S., and K. E. Taylor, The Paleoclimate Modeling Intercomparison Project, in *Paleoclimate Modeling Intercomparison Project (PMIP): proceedings of the third PMIP workshop, Canada, 4-8 October 1999*, edited by P. Braconnot, WCRP-111, WMO/TD-1007, pp. 9–24, World Meteorological Organization, 2000.

Keigwin, L. D., and R. S. Pickart, Slope water current over the Laurentian Fan on interannual to millennial time scales, *Science*, *286*, 520–523, 1999.

Kim, S.-J., G. M. Flato, G. J. Boer, and N. McFarlane, A coupled climate model simulation of the Last Glacial Maximum, Part 1: transient multi-decadal response, *Climate Dynamics*, *19*, 515–537, 2002.

Kitoh, A., and S. Murakami, Tropical Pacific climate at the mid-Holocene and the Last Glacial Maximum simulated by a coupled atmosphere-ocean general circulation model, *Paleoceanography*, *17*, doi:10.1029/2001PA000,724, 2002.

Lean, J., and D. Rind, Climate forcing by changing solar radiation, *Journal of Climate*, *11*, 3069–3094, 1998.

Legutke, S., and R. Voss, The Hamburg atmosphere-ocean coupled circulation model ECHO-G, *Technical Report 18*, Deutsches Klimarechenzentrum, Hamburg, Germany, 1999.

Liu, Z., E. Brady, and J. Lynch-Stieglitz, Global ocean response to orbital forcing in the Holocene, *Paleoceanography*, *18*, doi:10.1029/2002PA000,819, 2003.

Lohmann, G., S. J. Lorenz, and M. Prange, Northern high-latitude climate changes during the Holocene as simulated by circulation models, *Agu monograph series, accepted*, American Geophysical Union, 2004.

Lorenz, S., B. Grieger, P. Helbig, and K. Herterich, Investigating the sensitivity of the atmospheric general circulation model ECHAM 3 to paleoclimatic boundary conditions, *International Journal of Earth Sciences*, *85*, 513–524, 1996.

Maier-Reimer, E., U. Mikolajewicz, and K. Hasselmann, Mean circulation of the Hamburg LSG OGCM and its sensitivity to the thermohaline surface forcing, *Journal of Physical Oceanography*, *23*, 731–757, 1993.

Manabe, S., and A. J. Broccoli, A comparison of climate model sensitivity with data from the last glacial maximum, *Journal of the Atmospheric Sciences*, *42*, 2643–2651, 1985.

Mann, M. E., and P. D. Jones, Global surface temperatures over the past two millennia, *Geophysical Research Letters*, *30*, doi:10.1029/2003GL017,814, 2003.

Mann, M. E., R. S. Bradley, and M. K. Hughes, Global-scale temperature patterns and climate forcing over the

past six centuries, *Nature*, *392*, 779–787, 1998.

Mann, M. E., R. S. Bradley, and M. K. Hughes, Northern Hemisphere temperature during the past millennium: inferences, uncertainties, and limitations, *Geophysical Research Letters*, *26*, 759–762, 1999.

Marchal, O., et al., Apparent long-term cooling of the sea surface in the northeast Atlantic and Mediterranean during the Holocene, *Quaternary Science Reviews*, *21*, 455–483, 2002.

Marsland, S. J., M. Latif, and S. Legutke, Variability of the Antarctic circumpolar wave in a coupled ocean-atmosphere model, *Ocean Dynamics*, *53*, 323–331, 2003.

Milankovitch, M., *Kanon der Erdbestrahlung und seine Anwendung auf das Eiszeitenproblem*, 132, Royal Serb. Acad. Spec. Publ., Belgrad, 1941.

Pacanowski, R. C., K. D. Dixon, and A. Rosati, The G.F.D.L. Modular Ocean Model users guide, *GFDL Ocean Group, Technical Report 2*, NOAA/Geophysical Fluid Dynamics Laboratory, Princeton, NJ, 1993.

Prange, M., G. Lohmann, and A. Paul, Influence of vertical mixing on the thermohaline hysteresis: Analyses of an OGCM, *Journal of Physical Oceanography*, *33*, 1707–1721, 2003.

Raible, C., U. Luksch, K. Fraedrich, and R. Voss, North Atlantic decadal regimes in a coupled GCM simulation, *Climate Dynamics*, *18*, 321–330, 2001.

Rimbu, N., G. Lohmann, J.-H. Kim, H. W. Arz, and R. R. Schneider, Arctic/North Atlantic Oscillation signature in Holocene sea surface temperature trends as obtained from alkenone data, *Geophysical Research Letters*, *30*, 1280–1283, 2003.

Rimbu, N., G. Lohmann, S. Lorenz, J.-H. Kim, and R. R. Schneider, Holocene climate variability as derived from alkenone sea surface temperature and coupled ocean-atmosphere model experiments, *Climate Dynamics*, *in press*, 2004.

Rodgers, K., P. Friedrichs, and M. Latif, Decadal enso amplitude modulations and their effect on the mean state, *Journal of Climate*, *in press*, 2004.

Roeckner, E., et al., Simulation of the present-day climate with the ECHAM model: Impact of model physics and resolution, *Report 93*, Max-Planck-Institut für Meteorologie, 1992.

Roeckner, E., et al., The atmospheric general circulation model ECHAM-4: Model description and simulation of the present-day climate, *Report 218*, Max-Planck-Institut für Meteorologie, 1996.

Rohling, E., P. Mayewski, R. Abu-Zied, J. Casford, and A. Hayes, Holocene atmosphere-ocean interactions: records from Greenland and the Aegean Sea, *Climate Dynamics*, *18*, 587–593, 2002.

Shin, S.-I., Z. Liu, B. Otto-Bliesner, E. C. Brady, J. E. Kutzbach, and S. P. Harrison, A simulation of the Last Glacial Maximum climate using the NCAR-CCSM, *Climate Dynamics*, *20*, 127–151, 2003.

Shindell, D., D. Rind, N. Balachandran, J. Lean, and P. Lonergan, Solar cycle variability, ozone, and climate, *Science*, *284*, 305–308, 1999.

Shindell, D. T., G. A. Schmidt, M. E. Mann, D. Rind, and A. Waple, Solar forcing of regional climate change during the Maunder Minimum, *Science*, *294*, 2149–2152, 2001.

Shindell, D. T., G. A. Schmidt, R. L. Miller, and M. E. Mann, Volcanic and solar forcing of climate change during the preindustrial era, *Journal of Climate*, *16*, 4094–4107, 2003.

Sowers, T., R. B. Alley, and J. Jubenville, Ice core records of atmospheric N_2O covering the last 106,000 years, *Science*, *301*, 945–948, 2003.

Stocker, T. F., D. Wright, and L. Mysak, A zonally averaged, coupled ocean-atmosphere model for paleoclimate studies, *Journal of Climate*, *5*, 773–797, 1992.

Tarasov, P., et al., Present-day and mid-holocene biomes reconstructed from pollen and plant macrofossil data from the former soviet union and mongolia, *Journal of Biogeography*, *25*, 1029–1053, 1998.

Terray, L., S. Valcke, and A. Piacentini, The OASIS coupler user guide, version 2.2, *Technical Report*

TR/CMGC/98-05, CERFACS, 1998.

Texier, D., N. de Noblet, S. P. Harrison, A. Haxeltine, D. Jolly, S. Joussaume, F. Laarif, I. C. Prentice, and P. Tarasov, Quantifying the role of biosphere-atmosphere feedbacks in climate change: coupled model simulations for 6000 years BP and comparison with palaeodata for northern Eurasia and northern Africa, *Climate Dynamics*, *13*, 865–882, 1997.

Thompson, D. W. J., and J. M. Wallace, The Arctic oscillation signature in the wintertime geopotential height and temperature fields, *Geophysical Research Letters*, *25*, 1297–1300, 1998.

Voss, R., and U. Mikolajewicz, The climate of 6000 years BP in near-equilibrium simulations with a coupled AOGCM, *Geophysical Research Letters*, *28*, 2213–2216, 2001.

Voss, R., and R. Sausen, Techniques for asynchronous and periodically synchronous coupling of atmosphere and ocean models. Part II: impact of variability, *Climate Dynamics*, *12*, 605–614, 1996.

Voss, R., R. Sausen, and U. Cubasch, Periodically synchronously coupled integrations with the atmosphere-ocean general circulation model ECHAM3/LSG, *Climate Dynamics*, *14*, 249–266, 1998.

Weaver, A. L., M. Eby, A. F. Fanning, and E. C. Wiebe, Simulated influence of carbon dioxide, orbital forcing and ice sheets on the climate of the Last Glacial Maximum, *Nature*, *394*, 847–853, 1998.

Wolff, J.-O., E. Maier-Reimer, and S. Legutke, The Hamburg ocean primitive equation model HOPE, *Technical Report 13*, Deutsches Klimarechenzentrum, Hamburg, Germany, 1997.

Zorita, E., F. González-Rouco, and S. Legutke, Testing the Mann et al. (1998) approach to paleoclimate reconstructions in the context of a 1000-Yr control simulation with the ECHO-G coupled climate model, *Journal of Climate*, *16*, 1378–1390, 2003.

Chapter 4

Orbitally driven insolation forcing on Holocene climate trends: evidence from alkenone data and climate modeling

Abstract.

A global spatial pattern of long-term sea-surface temperature (SST) trends over the last 7000 years is explored using a comparison of alkenone-derived SST records to transient ensemble climate simulations with a coupled atmosphere-ocean circulation model under orbitally driven insolation forcing. The spatial trend pattern both in paleo-SST data and in model results shows pronounced global heterogeneity. Generally, the extra-tropics cooled while the tropics experienced a warming during the middle to late Holocene. We attribute these divergent Holocene climate trends to seasonally opposing insolation changes. Furthermore, climate mode changes similar to the Arctic/North Atlantic Oscillation are superimposed on the prevalent pattern. It is concluded that nonlinear changes in the entire seasonal cycle of insolation played a dominant role for the temporal evolution of Holocene surface temperatures. For understanding of marine proxy data, apart from the dominance of summer insolation in high latitudes, a notable shift in the maximum insolation of the year in low latitudes has to be taken into account, which may influence timing of phytoplankton production and thus alters the seasonal origin of temperature signals recorded in the proxies.

4.1 Introduction

The changes in the seasonal cycle of solar irradiance at the outer boundary of the atmosphere, caused by the varying parameters of the Earth's orbit around the Sun (astronomical forcing or orbitally driven insolation forcing), is one of the most prominent forcing mechanisms for long-term climate

Stephan J. Lorenz, Jung-Hyun Kim, Norel Rimbu, Ralph R. Schneider, and Gerrit Lohmann, *Paleoceanography, 21,* PA1002, doi:10.1029/2005PA001152, 2006,

change. The insolation changes at northern high latitudes during boreal summer have been regarded as the dominant external forcing for glacial-interglacial climate changes during the Quaternary ("Milankovitch forcing") [*Milankovič*, 1941; *Hays et al.*, 1976; *Imbrie et al.*, 1992].

The relative role of the effect of orbital forcing on Holocene climate change is, however, not well known. The climate of the last glacial, preceding the Holocene, was periodically punctuated by a series of abrupt climate changes, known as Dansgaard-Oeschger events [*Broecker*, 1998; *McManus et al.*, 1999]. In contrast, the Holocene trends in sea level [*Fairbanks*, 1989] as well as in the oxygen isotope composition of polar ice sheets [*Grootes et al.*, 1993] imply that the Holocene climate was relatively stable when compared to the last glacial. *Broecker* [1998] stated that neither the sea level nor the Greenland ice $\delta^{18}O$ record show a tendency toward the cooling expected in response to the Holocene decrease in boreal summer insolation in high northern latitudes. To challenge this view, we here show spatially varying patterns of long-term surface temperature trends for the Holocene. We address the role of orbital forcing during the Holocene based on globally distributed alkenone-derived sea-surface temperature (SST) records in comparison with transient climate simulations using a coupled atmosphere-ocean general circulation model (AOGCM).

The majority of AOGCMs has been utilized to quantitatively evaluate the magnitude of future climate change. Their results served as a scientific basis for the third assessment report of the *Intergovernmental Panel on Climate Change* [2001] (IPCC). Validation of these models by simulating different climate states is essential for understanding the sensitivity of the climate system to both natural and anthropogenic forcing.

Up to now, the validation of AOGCMs has primarily been based on the comparison of results reproducing the instrumental climate record of the last 150 years. However, the instrumental period coincides with that of strong anthropogenic impacts. Therefore it is necessary to test the results of AOGCMs beyond this period (at least the Holocene) in order to identify coherent natural climate variations and their underlying mechanisms and hence to properly address the question of anthropogenic influence on climate.

Recent modeling efforts to simulate Holocene climate changes using coupled AOGCMs [*Hewitt and Mitchell*, 1998; *Liu et al.*, 1999; *Voss and Mikolajewicz*, 2001; *Kitoh and Murakami*, 2002; *Liu et al.*, 2003] assume that the atmosphere-ocean system is in equilibrium with the external forcing. Modeling studies based on simulations with a single model [*Hewitt and Mitchell*, 1998; *Lohmann and Lorenz*, 2000], and model–model comparisons [*Guiot et al.*, 1999; *Braconnot et al.*, 2002], as well as data–model syntheses [*Kohfeld and Harrison*, 2000; *Texier et al.*, 2000] have mainly been undertaken in the framework of the Paleoclimate Modeling Intercomparison Project (PMIP, [*Joussaume and Taylor*, 2000]). Transient simulations of the Holocene without the assumption of an equilibrium climate and including orbital forcing were predominantly performed utilizing models of intermediate complexity [a summary: *Claussen et al.*, 2002]. Some of the simulations with these models [*Bertrand et al.*, 2002; *Weber et al.*, 2004; *Renssen et al.*, 2005] confirmed the influence of insolation changes as well as the importance of including ocean feedbacks.

In this study, the ensemble simulations were conducted with a state-of-the-art fully coupled AOGCM, the ECHO-G [*Legutke and Voss*, 1999], where an acceleration technique for the orbital forcing has been employed [*Lorenz and Lohmann*, 2004]. The ECHO-G model has participated in

the “Coupled Model Intercomparison Project” (CMIP) and will participate with other AOGCMs in the next set of IPCC experiments for the Fourth Assessment Report of the IPCC, planned for 2007.

Recently, based on the control run of the ECHO-G model in comparison with alkenone-derived SST records, internal processes which underlay teleconnections between the North Atlantic and the North Pacific [*Kim et al.*, 2004] as well as between the North Atlantic and tropical oceans [*Rimbu et al.*, 2004] were investigated on centennial to millennial time scales. Here we focus on the effect of the seasonal insolation changes on heterogeneous Holocene surface temperature trends as observed in both globally distributed alkenone-derived SST records and transient ensemble simulations with the ECHO-G model.

Conforming with the PMIP definition of the middle Holocene time slice, which was chosen to be 6000 years before present (kyr BP in the following), this data-model comparison study concentrates on the middle to late Holocene. The last 7000 years can be regarded as relatively stable compared to former eras, because these were probably excluded from severe shifts in the atmosphere-ocean system [*Grootes et al.*, 1993; *McManus et al.*, 2004].

Since the development of the unsaturated alkenone index as a temperature proxy in the late 1980s, the seasonal origin of alkenone-derived temperature signals in different latitudes has been questioned. In high latitudes, maximum phytoplankton coccolithophorid production is observed in summer [*Baumann et al.*, 1997] suggesting that alkenone-derived SSTs should reflect summer temperatures [*Rosell-Melé et al.*, 1995; *Sikes et al.*, 1997]. In contrast, seasonality in phytoplankton production is generally less pronounced in tropical to subtropical regions [*Jickells et al.*, 1996] and alkenone-derived SSTs are more likely to show temperatures close to the annual mean values [*Müller and Fischer*, 2001]. For comparison, our AOGCM results show Holocene climate changes in the seasonal cycle of surface temperatures and can thus provide hints to the seasonal origin of alkenone-derived SST in different latitudes.

The paper is organized as follows. In the next section we start with a discussion of the orbitally driven changes in the seasonal cycle of insolation during the Holocene. Next (Section 4.3) an introduction to the methods is given: the reconstruction of SST records from alkenones, and the AOGCM, including its orbital forcing, the acceleration technique for this forcing, and the model experiments. The long-term Holocene trends in surface temperature of reconstructed data and model results, including analysis of seasonal trends, are then shown (Section 4.4). The dependence of these trends on orbitally driven insolation change and its impact in relation to other forcing and feedback mechanisms is discussed (Section 4.5). Finally, concluding remarks (Section 4.6) are given.

4.2 Orbitally driven insolation changes during the Holocene

Three main parameters of the Earth’s orbit around the Sun control the seasonal distribution of solar radiation at the top of the atmosphere: the eccentricity of the orbit with the Sun in one of the two foci, the time of the Earth’s passage through its perihelion, and the tilt of its rotation axis. Long-term variation in these parameters cause the astronomical or “Milankovitch-forcing” of the climate system [*Milanković*, 1941; *Imbrie et al.*, 1992]. The variation can easily be calculated with sufficient accuracy using the algorithm of *Berger* [1978]. Newer calculations span much longer time scales,

beyond millions of years [*Laskar et al.*, 2004], or take into account short-term variability [*Loutre et al.*, 1992], which is far beyond the requirements of our model experiments.

The eccentricity (ε) has cycles with periods near 100,000 years and affects the annual mean top-of-atmosphere insolation on the entire Earth by much less than 0.1% during the Holocene. The amplitude of the precession parameter e, where $e = \varepsilon \sin(\lambda)$ with λ the longitude of the perihelion measured from the vernal equinox ($\approx 282^\circ$ today, with perihelion at the beginning of January) is modulated by the eccentricity and has cycles with periods near 20,000 years. It determines the time of the year when the insolation of the whole Earth is at maximum. The third parameter, the Earth's axis tilt (obliquity) has a main long-term cycle with a period near 40,000 years and governs the amplitude of the seasonal cycle of both hemispheres.

During the Holocene, the seasonal distribution of Earth's top-of-atmosphere insolation varied considerably due to precession and obliquity cycles. During the last 7000 years, these cycles caused a shift of perihelion from September ($\lambda = 164^\circ$) to January ($\lambda = 282^\circ$) and a decrease in the tilt of the Earth's axis from 24.2° to 23.4°. The resulting radiative changes over the last 7000 years are displayed in Figure 4.1. It shows the latitudinal distribution through the year of the today minus 7 kyr BP difference in top-of-atmosphere insolation. The most pronounced radiative changes were a decrease in the boreal summer insolation (June-July-August, JJA) of more than 30 Wm^{-2} in the northern middle to high latitudes accompanied by an increase in the boreal winter insolation (December-January-February, DJF) of about 25 Wm^{-2} in the low latitudes (Figure 4.1).

Along with the seasonal changes, the dominant orbital parameter in the tropics — the precession parameter — is able to cause a shift in the occurrence of the maximum insolation throughout the

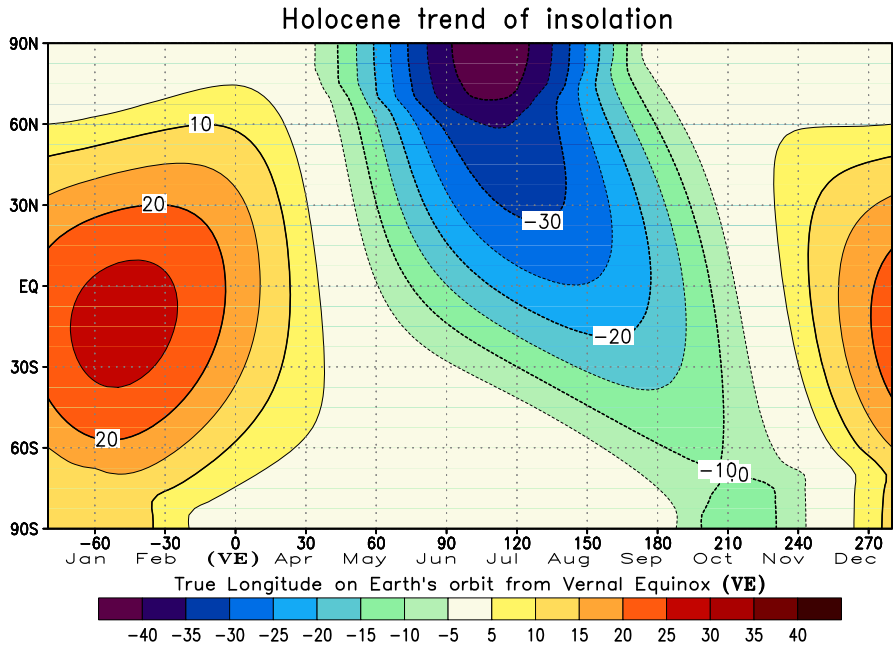

Figure 4.1: *Latitudinal distribution through the year, with respect to the Earth's orbital longitude measured from vernal equinox (marked as "true longitude" and "VE"), of the today minus 7 kyr BP difference in top-of-atmosphere insolation (Wm^{-2}), calculated after Berger [1978]. Note that, for comparison with SST trends, this is equivalent to the linear trend in insolation over the last 7000 years.*

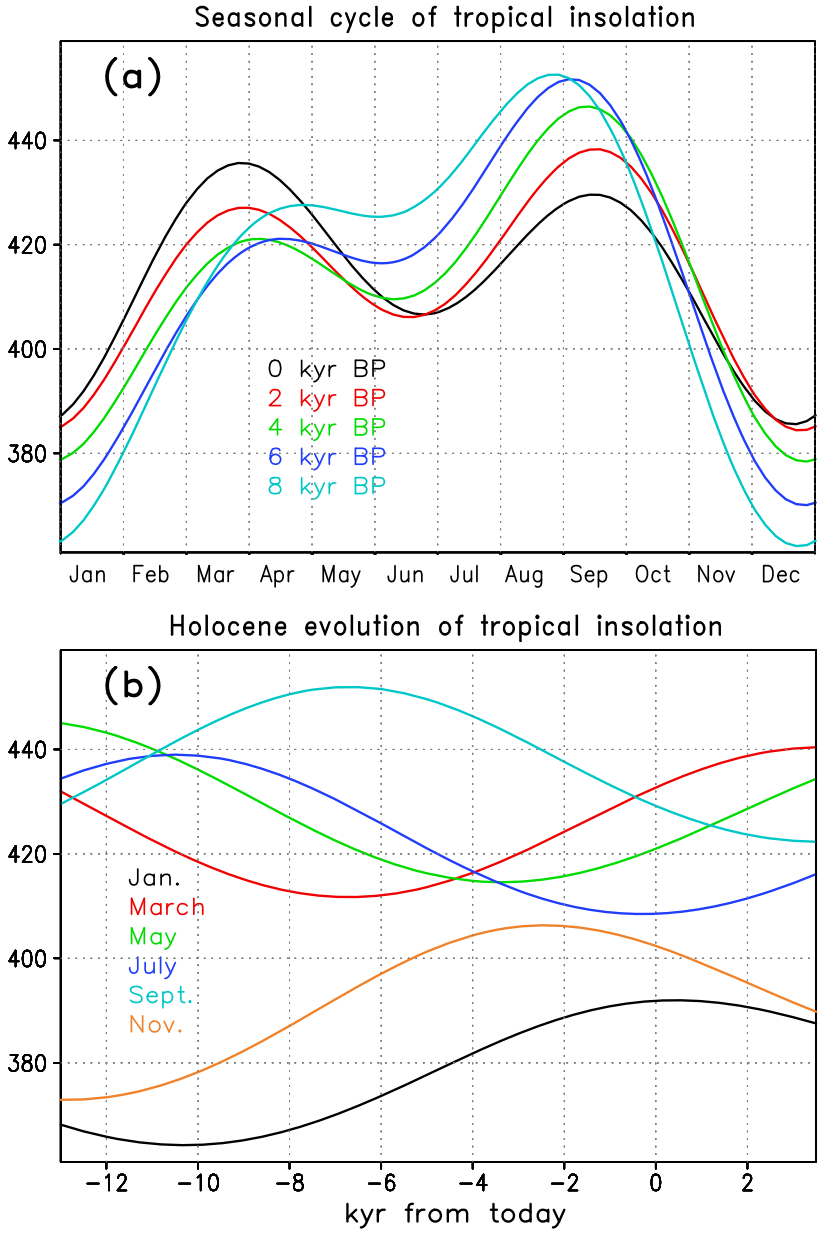

Figure 4.2: *Changes in the seasonal cycle of insolation (Wm^{-2}) in the tropics (0–10°N) during the Holocene (calculated after [Berger, 1978]): (a) seasonal cycle of insolation for five time slices in the Holocene; and (b) evolution from the early Holocene into the next millenia of insolation for the tenth day of selected months.*

year. Equatorial insolation is generally highest during passage through the equinoxes, when the Sun is at the zenith. Equatorward of the two tropics the Sun reaches the zenith two times a year resulting in a characteristic semi-annual cycle of tropical insolation. The precession cycles can vigorously modulate this seasonal cycle. For example, in the zonal band between 10°N and the equator, insolation at present has nearly equal maxima in March and September (Figure 4.2a). In contrast, during the middle Holocene insolation was at its maximum in September, when the distance to the Sun was at its minimum and insolation reached 30 Wm^{-2} more than during March (Figure 4.2a,b). Therefore, comparing the seasonal cycle of present and middle Holocene insolation, the time when its maximum is reached shifts from middle of March to the beginning of September (Figure 4.2a).

4.3 Data and methods

4.3.1 Alkenone-derived SST data

For this study, a marine Holocene paleotemperature data set covering all major ocean basins [*Kim and Schneider*, 2004] has been compiled. The data set has been derived from a temperature proxy (alkenones) that is internationally calibrated and standardized among 24 laboratories worldwide [*Rosell-Melé et al.*, 2001]. We consider 46 SST records solely based on the alkenone method as paleothermometry in order to avoid potential biases due to using different SST proxies. The paleotemperature estimates are based on the abundance ratios of long-chain unsaturated alkenones with two to four double bonds [*Brassell et al.*, 1986; *Prahl and Wakeham*, 1987]. Alkenones are synthesized by the class Prymnesiophyceae of which the coccolithophorids *Emiliania huxleyi* and *Gephyrocapsa oceanica* are the two most common sources of alkenones in contemporary oceans and sediments [*Volkman et al.*, 1980; *Conte et al.*, 1995].

Different alkenone unsaturation indices (U^{K}_{37} or $U^{K'}_{37}$) and calibrations were applied for each alkenone-derived SST record. The errors in alkenone-derived temperature reported for the culture calibration and for a global core-top calibration reach ± 0.5°C [*Prahl and Wakeham*, 1987] and ± 1.5°C [*Müller et al.*, 1998], respectively. Analytical accuracy for each record considered here, however, was better than ± 0.3°C [see *Kim and Schneider*, 2004]. The age models of the alkenone-derived SST time series were established mainly by accelerator mass spectrometry (AMS) ^{14}C determinations on planktic foraminifera and by oxygen isotope chronologies. All SST records were from ocean margin sites with sedimentation rates sufficiently high to provide SST records with at least one value per 1000 years. Detailed information on each SST record are given by *Kim and Schneider* [2004], including the original data references. Figure 4.3 shows 20 examples of alkenone-derived SST records along with their linear regressions and their locations in the map.

4.3.2 General circulation model and experimental setup

Coupled atmosphere-ocean general circulation model

The transient climate simulations were performed with the coupled general circulation model ECHO-G [*Legutke and Voss*, 1999]. The atmospheric part of this model is ECHAM4 [*Roeckner et al.*, 1996], whose prognostic variables are calculated in the spectral domain using a medium resolution (T30), corresponding to a longitude-latitude grid of approximately $3.8° \times 3.8°$ with 19 levels in the vertical. The time step of the atmospheric model is 30 minutes. The ECHAM4 model is coupled to the HOPE ocean general circulation model [*Wolff et al.*, 1997], which includes a dynamic-thermodynamic sea ice model with snow cover. It is discretized with a horizontal resolution of approximately $2.8° \times 2.8°$ ($0.5°$ resolution in the tropics, 20 vertical levels) and has a time step of two hours. The model utilizes annual mean flux corrections for heat and freshwater. These fluxes are constant in time and have no sources or sinks of energy or mass.

In the ECHO-G model, the calculation of the orbital parameters follows *Berger* [1978]. The atmospheric part of the ECHO-G model, the ECHAM4, has been adapted to account for the different insolation during paleoclimatic time slices [*Lorenz et al.*, 1996]. Moreover, to evaluate the dynamical

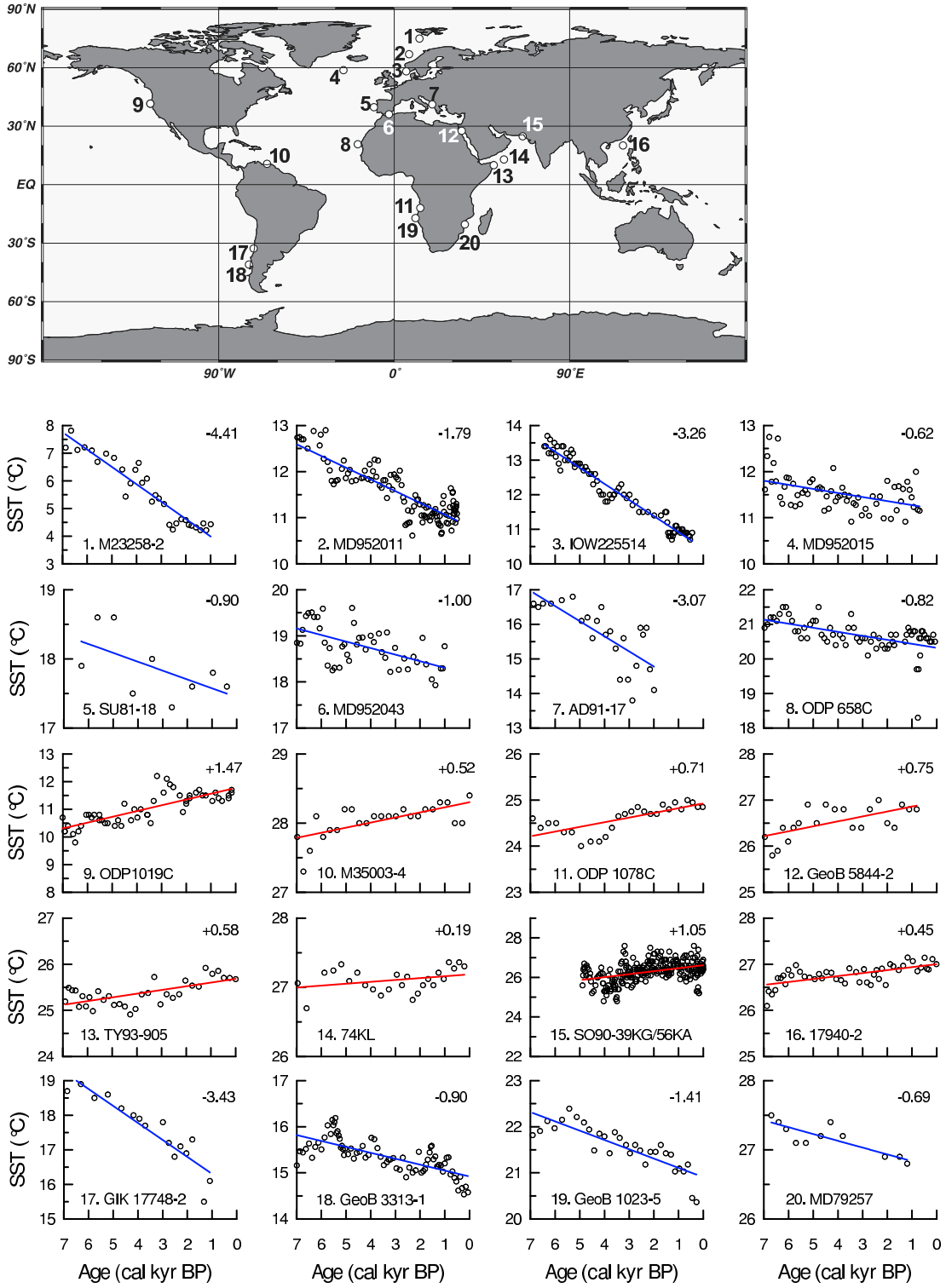

Figure 4.3: *Examples of alkenone-derived SST records (circles) and their linear trends (solid lines) evaluated from 20 cores, whose positions are shown on the map ([Kim and Schneider, 2004]; see also Table 1 in [Kim et al., 2004]). The magnitude of SST change over the last 7000 years (calendar age) is indicated in the upper right corner of each panel.*

variation of insolation during the Holocene, the calculation of the orbital parameters is done individually for each simulation year.

Acceleration technique

We use an acceleration technique implemented into the ECHO-G model to conduct transient simulations over millennia [*Lorenz and Lohmann*, 2004]. To be able to simulate a period of 7000 years with this model, the time scale of the orbital forcing is shortened by an acceleration factor of 100. The underlying assumptions are that the orbital forcing operates on much longer time scales (millennia) than those inherent in the atmosphere including the surface mixed layer of the ocean (months to years), and that climatic changes related to long-term variability of the thermohaline circulation during the time period considered are negligible in comparison with orbitally driven surface temperature variation. With this method, climate trends and feedbacks of the last 7000 years, imposed by the external orbitally driven insolation changes, are represented in the experiments with only 70 simulation years. The experiments with the coupled AOGCM capture the internal variability of the atmosphere-ocean–sea ice system with time scales up to decades.

In line with Holocene reconstructions, additional experiments using an acceleration factor of 10 (700 simulation years) exhibit no change in the simulated meridional overturning circulation during the last 7000 years. Moreover, these experiments demonstrate that the magnitude of orbitally-forced Holocene trends is independent of the chosen factor [*Lorenz and Lohmann*, 2004].

Experimental setup

We performed one simulation of pre-industrial climate. Constant greenhouse gas concentrations typical for the pre-industrial era at the very end of the Holocene (ca. 1800 AD) were prescribed. These have been compiled mainly from ice core records [*Etheridge et al.*, 1996, 1998; *Indermühle et al.*, 1999; *Sowers et al.*, 2003]: 280 ppm CO_2, 700 ppb CH_4, and 265 ppb N_2O. Other boundary conditions (surface background albedo, vegetation ratio, leaf area index, distribution of continents and oceans) were kept constant at their present values throughout the simulation and modern insolation was used. This control experiment was integrated over a total of 3000 model years The climate state, which becomes relatively stable after 1250 model years [*Lorenz and Lohmann*, 2004], is regarded as the quasi-equilibrium response of the model to pre-industrial boundary conditions.

The set of ensemble simulations of the Holocene comprises six model runs, each going through the entire last 9000 years, using an acceleration factor of 100. In order to isolate the orbitally driven insolation effect on the simulated Holocene climate evolution, small changes in greenhouse gases during the Holocene [*Indermühle et al.*, 1999] are ignored and the model is forced only with orbitally-varying insolation. Similarly, variations in the Sun's output of radiation (solar constant) as well as reduced insolation due to atmospheric dust loads after volcanic eruptions are not taken into account, since no continuous data apart from the last millennium exist [*Crowley*, 2000b].

The Holocene simulations start after year 1250 of the control experiment when the coupled system including the deep ocean is regarded to be in a quasi-equilibrium with the pre-industrial boundary conditions and modern insolation. The simulation of the early Holocene (9–7 kyr BP) at the beginning

of the Holocene experiments is taken as spin-up time for the model to adapt to the non-modern insolation distribution. The simulation of the subsequent period from the middle Holocene into the pre-industrial era (7 kyr BP to 1800 AD) is used for the trend analysis.

4.4 Long-term surface temperature trends

In this section the temporal and spatial patterns of long-term surface temperature trends, evaluated from alkenone-derived SST reconstructions and transient general circulation experiments, are compared. We explore the Holocene trends of annual mean temperature, as well as seasonal trends evaluated from the ensemble of model experiments.

4.4.1 Annual mean trends

The alkenone-derived SST records show diverging linear trends over the last 7000 years (Figure 4.3, Figure 4.4a). In general, the extra-tropics cooled while the tropics experienced a warming or no substantial temperature changes from 7 kyr BP to the present. The magnitude varied between -0.62°C and -4.41°C/7kyr for the cooling and between +0.19°C and +1.47°C/7kyr for the warming (Fig. 3). However, the zonal distribution of SST trends is inhomogeneous, showing east-west variations for the same latitudes and abrupt changes in trends across oceanic frontal systems, e. g., the Angola-Benguela Front in the southeast Atlantic. The leading EOF of SST variability (not shown) describes 58% of the field variance and indicates a spatial pattern similar to the pattern of linear temperature trend as derived from alkenone-data for the last 7000 years (Figure 4.4a).

The described coupled AOGCM experiments reveal pronounced annual surface temperature trends over the last 7000 years. The temperature trend pattern is evaluated from the uppermost surface temperature in the model: SST over ice-free water, and ground- (bare or vegetated land), ice- (sea ice or land ice), or snow-temperature (snow-covered areas) wherever appropriate (Figure 4.4b). A continuous cooling in the northern middle to high latitudes and in the southern high latitudes was accompanied by a warming in the tropics as well as in the southern midlatitudes. The simulated cooling exceeds 2°C in the Arctic and 1°C over the Pacific and northern Europe. A transient warming is most pronounced in the northern low latitudes, especially over the continents, where the low heat capacity of soil compared to ocean amplifies the surface temperature trend. It exceeds 1°C over North Africa, the Arabian Peninsula and the Indian subcontinent. Off the continents, the warming reaches 0.5°C over the eastern tropical Atlantic, the northern Indian Ocean, and the western tropical Pacific. The surface temperature trends are not zonally homogeneous over a whole basin: for example, in the northern midlatitudes, there is a warming in the western Atlantic and Pacific, while their eastern counterparts experienced a cooling (Figure 4.4b).

The simulated surface temperature trends are similar to the linear trends in the alkenone-derived SSTs in the northern extra-tropics as well as in the tropics. In general, the amplitudes of SST trends from the simulations are smaller compared to those of alkenone-derived SSTs. A significant discrepancy between alkenone-derived SST data and model results occurs off Chile and Namibia. Generally, in the coastal regions around South America and southern Africa, reconstructed SST trends are negative whereas simulated trends are positive (South America) or uncertain in sign (southern Africa).

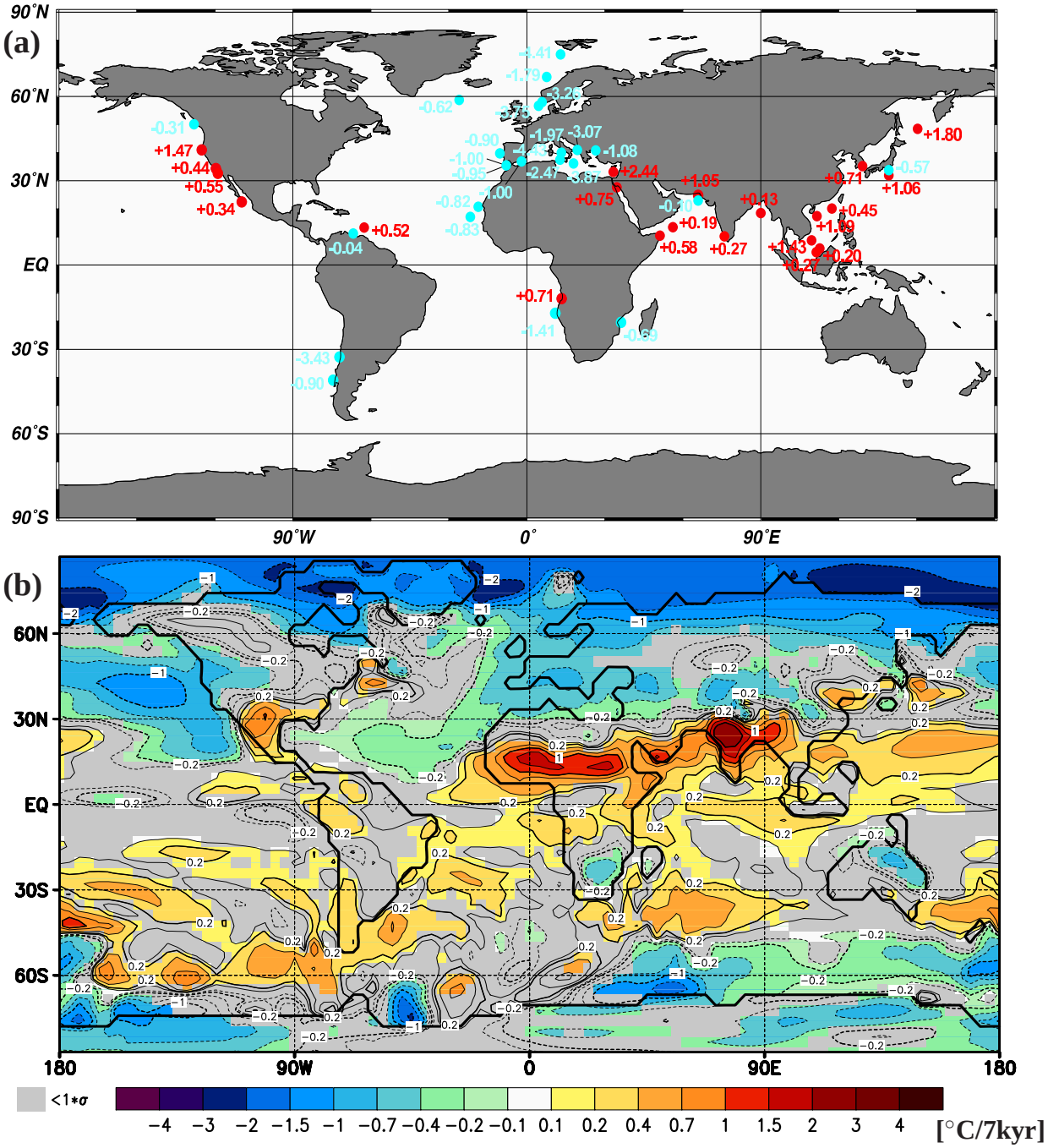

Figure 4.4: *Holocene surface temperature trends derived from alkenone proxies and coupled AOGCM simulations in °C/7kyr: (a) marine sediment core positions and corresponding magnitudes of alkenone-derived SST change over the last 7000 years; and (b) spatial distribution of annual mean surface temperature trends from six ensemble simulations, each covering the last 7000 years. Values are sea-surface temperature changes over ice-free water and ground-, ice- or snow temperatures over continents and ice-covered oceans. Shaded areas represent the regions where the trend does not exceed one standard deviation. The continents are shown in the resolution of the atmospheric model.*

4.4.2 Seasonal trends

Since seasonality cannot be resolved by the alkenone method, we concentrate on the model results and examine the trends over the last 7000 years for the boreal summer (JJA) and winter (DJF) seasons, respectively (Figure 4.5). In the boreal summer (Figure 4.5a), there is a Holocene cooling mainly over the continents of the Northern Hemisphere (1°C–3°C), which is in line with the reduction of insolation by 15 to 30 Wm^{-2} north of 30°N. The cooling is less pronounced in the North Atlantic and the North Pacific and large parts of the Southern Hemisphere continents.

In the boreal winter (Figure 4.5b), the continents generally exhibit a pronounced warming of 1°C–2°C. This signal is not only significant in the tropics, where it follows the increase in insolation (Figure 4.1), but also in the midlatitudes. Over the oceans, the trend patterns are much less significant, although they do show a warming over the central and northwest Pacific Oceans as well as off West Africa. Over the North Atlantic a dipole structure is found with a warming in the eastern and a cooling in the western part and over Europe. Over the whole ocean, cooling is located mainly in the Arctic, the northeast Atlantic and Pacific, and parts of the Southern Oceans.

Furthermore, we look now at the trends of the simulated maximum and minimum monthly temperature: from the ensemble mean of the six Holocene experiments we extract the coldest and warmest months of each simulated year. Then the trend at each of the grid points is evaluated. Thus the temperature trend from the warmest or coldest month in each year is computed locally, no matter which month this is. With this method, the trends reflect the characteristic change of the local summer or local winter at each grid point in Figures 4.6a and 4.6b, respectively. For example, in high latitudes, Figure 4.6a shows the local summer of both hemispheres combined. In the tropics, with its semi-annual cycle of insolation, the extremes of surface temperature trends also include the precession effect of a Holocene shift in the seasonal cycle of insolation.

The most significant trends are found for local summer (Figure 4.6a). Both hemispheres show opposite signals with a strong temperature decrease (1°C–4°C) in the Northern Hemisphere and an increase in the Southern Hemisphere. This can be attributed to the precessional shift of perihelion from September in the middle Holocene to January today: over the last 7000 years, the reduction in insolation during the JJA season exceeded 20 Wm^{-2} in the Northern Hemisphere, while simultaneously almost the whole Earth experienced an insolation increase during the DJF season (Figure 4.1). For this reason today the maximum daily mean insolation anywhere on Earth is at the South Pole (560 Wm^{-2}) at the winter solstice (austral summer), when the distance to the Sun is near its minimum. In the Northern Hemisphere, the trend pattern of the local winter (Figure 4.6b) is very close to the pattern of the DJF season (Figure 4.5b).

4.5 Discussion

4.5.1 Orbital forcing of surface temperature trends

The global spatial pattern of alkenone-derived and modeled SST trends during the last 7000 years can be summarized by an overall decrease in the extra-tropics accompanied by a slight increase in the tropics. The cooling trends observed in the northern middle to high latitudes concur with a previous

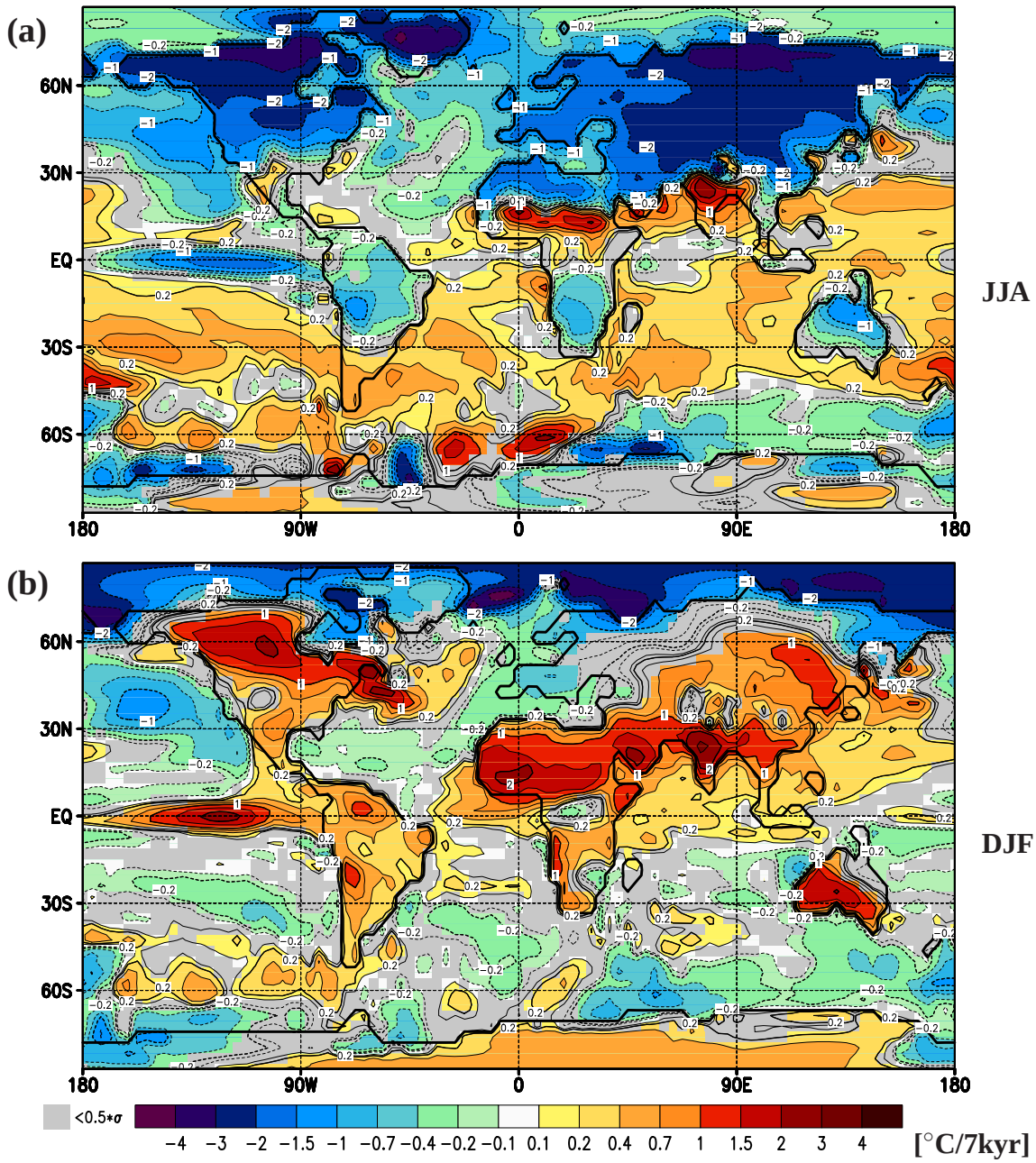

Figure 4.5: *Simulated seasonal mean surface temperature trends during the Holocene (in °C/7kyr): (a) boreal summer, June-July-August (JJA), and (b) boreal winter, December-January-February (DJF). Shaded areas represent the regions where the trend does not exceed one half standard deviation. See Figure 4.4 for further details.*

study [*Marchal et al.*, 2002], which showed a long-term cooling in the northeastern Atlantic Ocean and the western Mediterranean Sea during the Holocene. However, small-scale changes of sign in alkenone-derived SST trends occur off the coasts of Caribbean South America, southwest Africa, and Japan. These changes may be related to regional patterns across oceanic frontal systems. Such relatively small-scale patterns are difficult to reproduce accurately using a medium-resolution global climate model under generalized forcing.

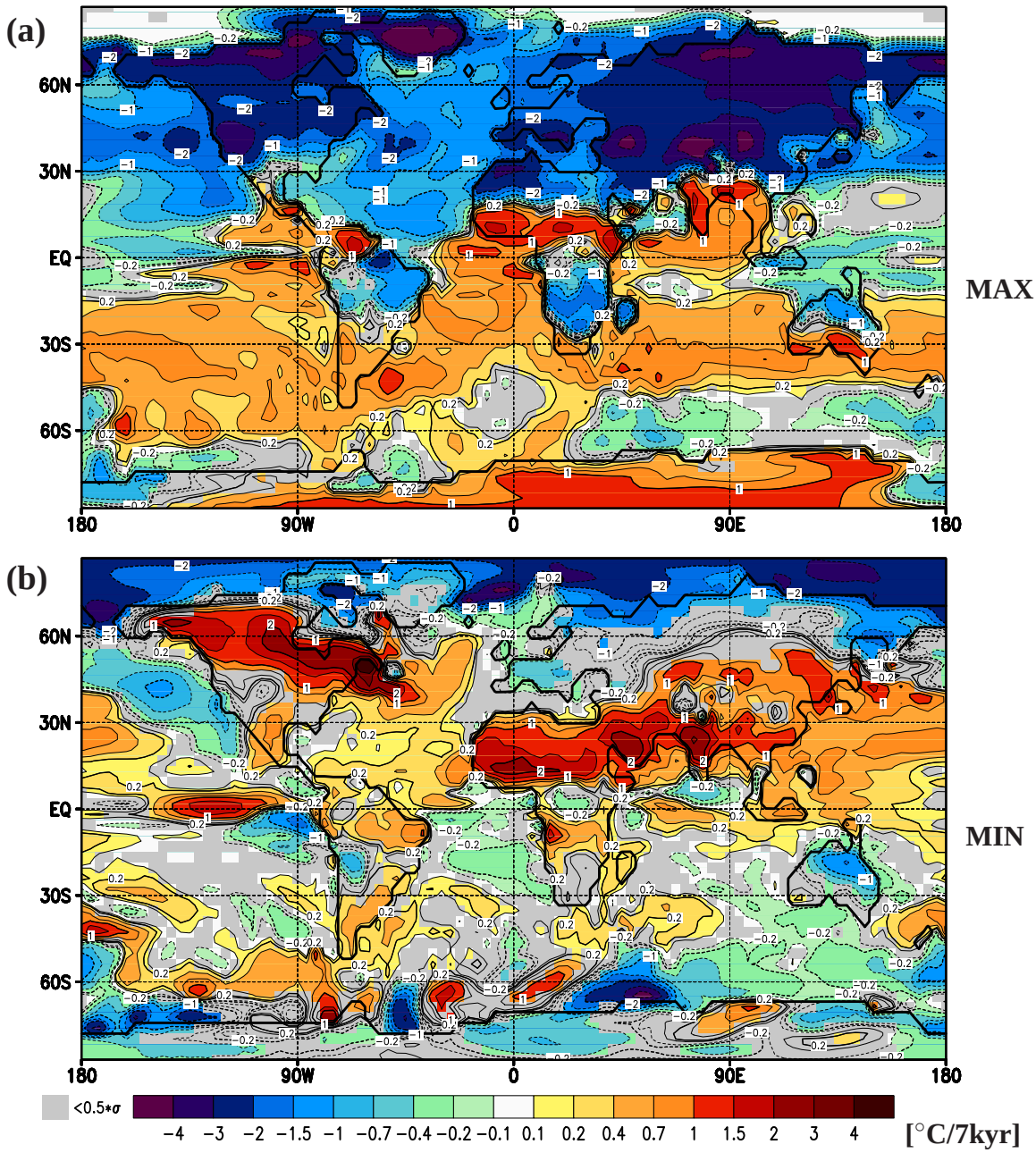

Figure 4.6: *Simulated surface temperature trends (in °C/7kyr) of the (a) warmest (local summer) and (b) coldest (local winter) month of the year, during the Holocene. See Figure 4.4 and text for further details.*

The zonally-averaged model results suggest that the strongly decreasing boreal summer insolation induced a progressive surface temperature cooling of 1.4°C in the northern middle to high latitudes (north of 30°N; Figure 4.5a) [see *Lorenz and Lohmann*, 2004]. During boreal winter (DJF) in low latitudes (30°N to 30°S), a rise in simulated surface temperature (Figure 4.5b) amounts to 0.4°C in the zonal mean (not shown) and is in concordance with the increasing tropical insolation in that season (Figure 4.1).

The seasonally-averaged model results imply that the DJF warming slightly exceeded the JJA cooling in the tropics, resulting in a moderate warming. This suggests that surface temperatures responded

non-linearly to the seasonal signal of orbitally driven insolation over the last 7000 years. The main result of colder tropics and warmer extra-tropics for the middle Holocene climate compared to the present is in overall agreement with previous modeling studies based on the time slice approach [*Hewitt and Mitchell*, 1998; *Voss and Mikolajewicz*, 2001; *Kitoh and Murakami*, 2002; *Liu et al.*, 2003]. However, besides the transient simulations performed here, we analyzed the temperature trends for different seasons: the boreal summer and boreal winter as well as the warmest (local summer) and coldest (local winter) months, respectively.

The larger amplitudes of the simulated trends during the boreal summer (Figure 4.5a), in particular for the North Atlantic and Mediterranean, are in better agreement with the alkenone-derived SSTs (Figure 4.4a) than the simulated relatively-weak annual mean trends (Figure 4.4b). Off the west coast of the North Pacific, larger positive trends are found, whereas in the eastern part the mismatches between data and model results remain for the boreal winter.

Analyzing the trends of the maximum and minimum monthly surface temperature, we note a striking agreement in sign and amplitude of the simulated trends of the local summer (Figure 4.6a) with the alkenone-derived SST trends in the whole North Atlantic (around 1°C cooling) and Mediterranean (2°C–3°C cooling). This may be taken as evidence that alkenone-derived temperature signals in the northern extra-tropics are more likely to stem from summer conditions, when the phytoplankton blooming occurs, than to reflect annual mean temperature. It is likely that coccolithophorid blooming during the early to middle Holocene took place in late summer (September), when high latitude insolation was at its maximum.

Interestingly, even in the tropics, there is a match of the alkenone-derived SST trend pattern with that of local summer, with a decrease of 1°C in the tropical Atlantic and an increase of around 0.5°C–1°C in the northern Indian Ocean and the China Sea. For these regions, this pattern match is better than with any other of the simulated seasonal and annual mean surface temperature trends.

Although the seasonal cycle of SST in the tropics is small, phytoplankton production is not constant throughout the year. It is reasonable that a change of seasonal insolation on the order of 10% is able to impact marine biological productivity. If the alkenone production is thought to be highest during the month with the warmest water temperature in the mixed layer, then the resemblance of reconstructed trends with the simulated trends of local summer can be taken as an indication that the time of maximum production may have changed with the insolation signal.

4.5.2 The Arctic/North Atlantic Oscillation

The Holocene tropical warming and extra-tropical cooling observed in both the alkenone-derived SST records and in the model results was accompanied by a weakening of the Atlantic midlatitude zonal surface temperature contrast, mainly in boreal winter (Figure 4.5b): a cooling over the eastern North Atlantic opposes a warming over the western North Atlantic and eastern part of North America.

Also in boreal winter in the North Atlantic, we find a notable Holocene decrease in sea level pressure difference between the high latitude (Icelandic) low and the subtropical (Azores) high by more than 3 hPa (Figure 4.7). We relate the decrease in east-west surface temperature difference in the North Atlantic with a Holocene weakening of the midlatitude atmospheric circulation pattern that

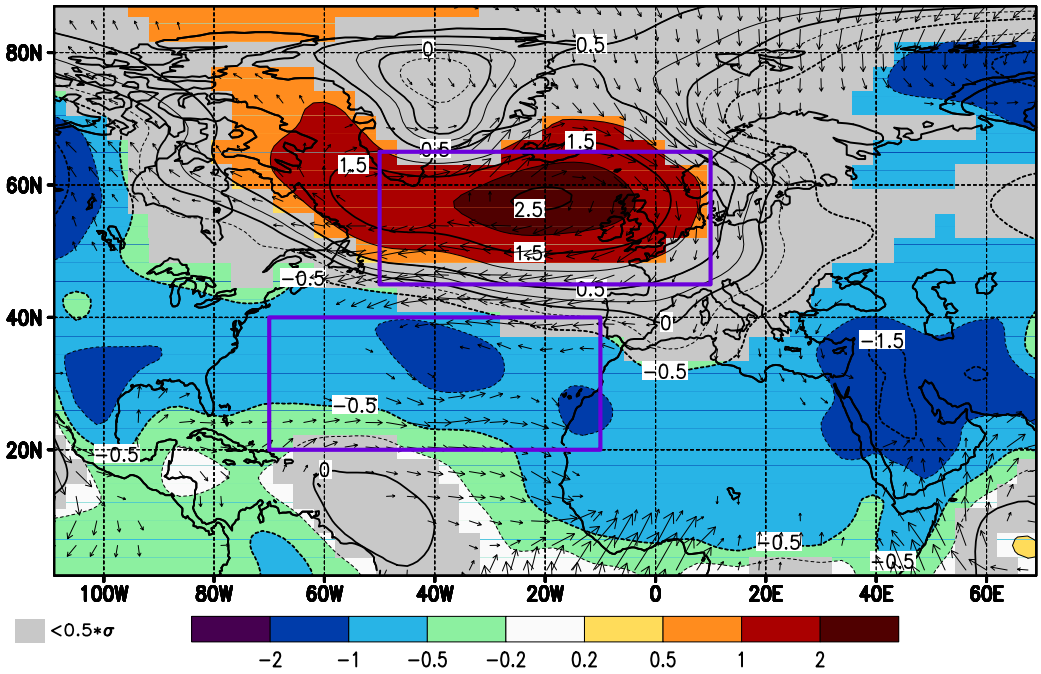

Figure 4.7: *Simulated trend of boreal winter (DJF) sea level pressure from the six ensemble Holocene (7 kyr BP to present) simulations. Shaded areas represent the regions where the trend does not exceed one half standard deviation. The rectangles indicate two regions in the North Atlantic, between which the meridional pressure difference for Figure 4.8 is calculated. Additionally, 10 m wind vectors of the 7000 years trend are shown, but only where their magnitude exceeds 0.3 m/s.*

resembles the modern Arctic/North Atlantic Oscillation (AO/NAO) [*Hurrell*, 1995; *Thompson and Wallace*, 1998]. This pattern, also known as the northern annular mode, is the dominant winter circulation mode in the extra-tropics of the Northern Hemisphere, in particular in the North Atlantic realm [*Thompson and Wallace*, 2001]. The time series of the pressure difference (Figure 4.8) between the two large-scale areas outlined in Figure 4.7 indicates a decrease of the Atlantic meridional pressure gradient by 2 hPa over the last 7000 years. This led to considerable changes in surface winds, exceeding 1 $\mathrm{m\,s^{-1}}$ (see Holocene wind change vectors in Figure 4.7) and including reduced westerly winds in the Atlantic at 45°N (less advection of warm air into Europe), southerly wind components in central Europe (advection of cold air), and northerly anomalous winds into Africa and the Red Sea (advection of warm air). These changes are typical of a decrease in AO/NAO. The reduction of this mode leads to a characteristic dipole structure, with cooling over Europe and warming in the subtropics, mainly in the eastern Mediterranean Sea and the Red Sea [e. g., *Felis et al.*, 2000]. A Holocene temperature decrease over Europe in winter is contrary to enhanced insolation from the orbital changes (Figure 4.1). The simulated European winter cooling is in line with a recent study analyzing alkenone-derived Holocene SST records and instrumental data from the North Atlantic and Mediterranean [*Rimbu et al.*, 2003] as well as a study analyzing the circulation pattern in the Nordic Seas [*Lohmann et al.*, 2005].

The net annual mean cooling in the northern extra-tropics (Figure 4.4) is related to the strong SST response to a decrease in JJA insolation, even while there was an increase in DJF insolation. It is likely that rectification processes in the tropical Pacific lead to a more pronounced boreal winter signal than

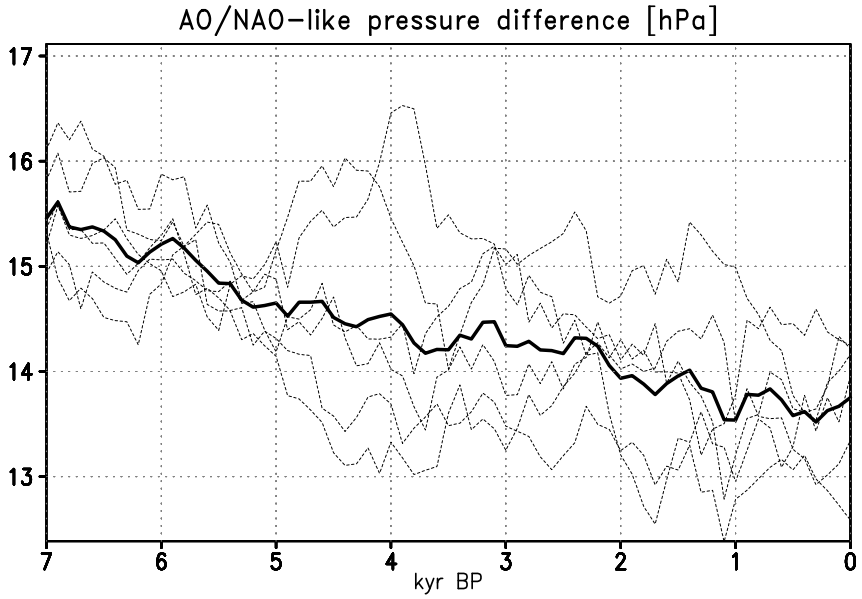

Figure 4.8: *Meridional pressure gradient between the two regions shown in Figure 4.7. It is interpreted as the evolution of the AO/NAO index over the last 7000 years: the difference in mean sea level pressure during boreal winter (DJF) between a low latitude/high pressure box (longitude: 50°W to 10°E, latitude: 45°N to 65°N) minus a high latitude/low pressure box (longitude: 70°W to 10°W, latitude: 20°N to 40°N) in the North Atlantic. The thick line depicts the ensemble mean of the six Holocene experiments, which are shown individually as thin dashed lines. A 21-year running mean is used as a low-pass filter for all experiments.*

for boreal summer [*Clement et al.*, 1999]. In a similar way, the annual mean Holocene cooling in the eastern North Atlantic and Europe, contrary to the insolation signal, is related to a boreal winter phenomenon, the AO/NAO circulation pattern. The Holocene weakening of the AO/NAO is possibly driven by the tropical warming during the DJF season.

Our main findings disagree with the study of *Liu et al.* [2003], which suggested that the annual mean SST changes during the early to middle Holocene were mainly caused by the annual mean insolation changes. For example, in the Arctic, the greater tilt of the Earth's axis at 7 kyr BP probably contributed to higher temperatures there relative to the present (pre-industrial): poleward of 60°N, an increase of more than 2.5 Wm^{-2} in annual mean insolation occurs. In the tropics, the net annual mean insolation decrease is less than 1 Wm^{-2}, which is negligible compared to the seasonal change of more than 20 Wm^{-2}.

The boreal winter signal dominates the temperature response over the North Atlantic through atmospheric circulation changes. We associate the Holocene weakening of the AO/NAO pattern with the tropical warming caused by the precession-related increasing boreal winter insolation. Indeed, seasonally-resolved coral data from the Northern Red Sea and modeling experiments covering the last interglacial and the Holocene suggest a strong modulation of the AO/NAO by orbitally driven insolation changes [*Felis et al.*, 2004]. During the last interglacial-glacial transition (125 to 115 kyr BP), when eccentricity was larger and precession had a more pronounced influence on the subtropics than during the Holocene, the AO/NAO-like climate mode was dominant and its change occurred with significantly-enhanced amplitude [*Felis et al.*, 2004].

4.5.3 Limitations

For simulation by various climate models, PMIP defined the Holocene Maximum time slice to be at 6 kyr BP. This is about a thousand years later than the northern high latitude summer insolation maximum. The reason for this definition was simply that the Laurentide and Fennoscandian continental glaciers had disappeared by then. During the last deglaciation (after the late Pleniglacial until the early Holocene, ≈15–7 kyr BP) the melting ice caps with their input of huge freshwater pulses into the North Atlantic caused abrupt climate changes and severe shifts in the Atlantic ocean circulation system, with global impact [*Clark et al.*, 2002]. Examples are the end of the Younger Dryas cold event at 11.5 kyr BP and the 8.2 kyr climate shift event [*Grootes et al.*, 1993]. In order to exclude these periods, we confined this study to the middle to late Holocene. The last 7000 years can be regarded as a relatively stable climate period compared to earlier eras and were probably free of abrupt climate shifts and rearrangements in the atmosphere-ocean system [*Fairbanks*, 1989; *Grootes et al.*, 1993; *Clark et al.*, 2002; *McManus et al.*, 2004].

Accordingly, in the ensemble of Holocene simulations no noteworthy changes in the thermohaline circulation were found [*Lorenz and Lohmann*, 2004]. This mitigates the limitation that the model cannot adequately simulate fast climate transitions using the acceleration technique for the orbital forcing. Moreover, we find no indication in modeled and reconstructed data that global scale circulation changes are responsible for the observed surface temperature trends.

The mismatch between the alkenone-derived SST data and the model results around South America (and partly southern Africa) can be taken as an indication that mechanisms other than the orbitally driven insolation changes are primarily responsible for variations in Southern Hemisphere SST, in contrast to the Northern Hemisphere. In the Southern Ocean, it is plausible that sea ice dynamics and changes in the thermohaline circulation may have significant influence on large-scale SST distribution possibly via the hemispheric seesaw effect [*Crowley*, 1992; *Stocker*, 1998; *Knorr and Lohmann*, 2003]. Due to the acceleration technique used, these Holocene experiments could not simulate millennial-scale climate variability seen in the alkenone-derived SST records [*Rimbu et al.*, 2004]. Hence, we speculate that deep ocean adjustments involving atmosphere and sea ice dynamics played a more dominant role in the Southern Hemisphere than in the Northern Hemisphere for Holocene surface temperature trends.

One important component that is lacking in the ECHO-G model is a module for adaptive vegetation, since the terrestrial biosphere with its vegetation ratio, background albedo, leaf area index, etc. is prescribed. The vegetation-climate feedback almost certainly has a significant impact on climate, regionally exceeding that of the atmosphere-ocean interaction, for example, in the case of African and Asian monsoon amplification [*Texier et al.*, 2000; *Braconnot et al.*, 2002]. Therefore, one of the important steps to improve the model results is to consider vegetation-climate interaction in transient climate change simulations with the ECHO-G.

A large number of paleoclimate simulations have been performed utilizing so-called “Earth system models of intermediate complexity” (EMICs). For the sake of simulating feedbacks between as many climate components as feasible, the number of processes and the detail of description in these models are reduced [*Claussen et al.*, 2002]. For example, the atmospheric circulation may be partly parameterized [*Petoukhov et al.*, 2000; *Weber et al.*, 2004; *Renssen et al.*, 2005] or the oceanic component

zonally-averaged [*Petoukhov et al.*, 2000; *Crucifix et al.*, 2002]. The advantage of these models is that they include more of the components and their interactions that have a significant effect on long-term natural climate change.

In the zonal mean, the magnitude of Holocene surface temperature changes of our model are in general agreement with studies using EMICs [*Crucifix et al.*, 2002; *Weber et al.*, 2004]. Notably, the experiments confirm much earlier findings [e. g., *Berger et al.*, 1990] that a considerable fraction of the climate variance is caused by orbitally driven insolation changes. However, coarse resolution or simplifications, inherent in fast-running EMICs, can partly impede the simulation of important interactions like the AO/NAO climate mode. The transient simulations provided by AOGCMs account in more detail for the dynamics that are necessary to interpret the response of the climate system to the orbital forcing during the Holocene. We find that the dominant signal of orbitally-induced temperature change has more regional patterns superimposed on it. Beyond the global scale, the weakening of the AO/NAO climate mode is the most important phenomenon affecting Holocene climate change.

4.6 Concluding remarks

The approach in this study was to compare a global Holocene proxy SST data set to results from climate model simulations with respect to changes in seasonality and global distribution patterns. We use a novel method for model acceleration regarding the orbitally driven insolation forcing in a complex circulation model [*Lorenz and Lohmann*, 2004]. With this method, a coupled atmosphere-ocean general circulation model, the ECHO-G model [*Legutke and Voss*, 1999], is able to simulate orbitally driven long-term transient climate changes.

The main finding of this study is that changes in the seasonal insolation cycle during the last 7000 years of the Holocene, forced by variations in the Earth's orbital parameters, are a significant cause for the observed opposing trends of cooling and warming in the extra-tropics and the tropics, respectively. The spatial and seasonal heterogeneity of the simulated climate is a detailed non-linear response of the atmosphere-ocean system to the external forcing, the seasonal and latitudinal distribution of insolation. Moreover, the similarities of the alkenone-derived and simulated SST trends strongly suggest that Holocene SST changes in the extra-tropics and the tropics (mainly in the Northern Hemisphere) are controlled by nonlinear changes in the entire seasonal cycle of insolation. This finding supplements the theory [*Milanković*, 1941; *Hays et al.*, 1976; *Imbrie et al.*, 1992] that the predominant pacemaker of long-term climate changes is primarily the orbitally driven boreal summer insolation at high northern latitudes.

There has been an ongoing debate about the seasonal origin of the alkenone-derived SST signal in tropical, subtropical and high latitude regions [*Rosell-Melé et al.*, 1995; *Baumann et al.*, 1997; *Müller and Fischer*, 2001]. Our model simulations provide the possibility to compare surface temperature trends of any season to alkenone-derived SST records. In the northern high latitudes, there is better agreement of the alkenone-derived SST data with our model results during the JJA season. This suggests that high latitude alkenone-derived SST records probably reflect boreal summer conditions more than the annual mean signal. Note that the Holocene shift of the time of year of the maximum tropical insolation may have influenced the timing of coccolithophorid production and thus the trend

pattern in the alkenone-derived SST data.

The imprint of orbitally driven insolation forcing on Holocene surface temperature trends is dominant on a global scale but regional trend patterns are superimposed on this. In the Northern Hemisphere, changes in the AO/NAO pattern during the Holocene are detected in the simulated, as well as alkenone-derived, surface temperature patterns. The prevalent mechanisms in the Southern Hemisphere are less clear. Since long-term deep ocean adjustments could have greater influence here, orbitally driven insolation signals may not be able to dominate regional scale changes in ocean surface waters.

Our study provides a consistent interpretation of reconstructed and simulated temporal and spatial patterns of surface temperature during the middle to late Holocene. We show that temporal and spatial distribution patterns are important for the interpretation of proxy temperature trends. This study could be advantageously extended by compiling a larger global alkenone-derived SST data set, as well as adding a comprehensive compilation of other marine and land proxy data. Performing new model experiments with atmosphere-ocean-vegetation feedbacks added in the model [*Ganopolski et al.*, 1998; *Renssen et al.*, 2005] would also be an improvement.

We have extended the Holocene climate simulations into the last two centuries taking into account the increase in greenhouse gases in the atmosphere [*Lorenz and Lohmann*, 2004]. The results indicate that the Northern Hemisphere summer cooling during the Holocene is of the same order of magnitude as the warming trend over the last 100 years. The extension of the model experiments into the coming centuries, so that they span the Holocene and the era of anthropogenic greenhouse gas increases, would enable the comparison of climate variability under natural and anthropogenic conditions and the investigation of differences in their characteristic temporal and spatial patterns. Such an approach could render a better assessment of future climate change.

Acknowledgments. We would sincerely like to thank the contributors to the project GHOST (Global Holocene Spatial and Temporal Variability) as well as S. Legutke for her support concerning the ECHO-G model. Instructive comments by D. Thresher helped to improve the manuscript substantially and discussion with and comments by A. Berger are also acknowledged. The numerical experiments have been carried out with the NEC supercomputer at the German climate computing center (DKRZ). This study was funded by grants from the German Ministry of Research and Education (BMBF) through the GHOST project of the German Climate Research Program (DEKLIM). S. J. Lorenz and J.-H. Kim contributed equally to this paper.

4.7 References

Baumann, K.-H., H. Andruleit, A. Schröder-Ritzrau, and C. Samtleben (1997), Spatial and temporal dynamics of coccolithophore communites during non-production phases in the Norwegian-Greenland Sea, in *Contribution to the Micropaleontology and Paleoceanography of the northern North Atlantic*, edited by H. C. Hass and M. A. Kaminski, pp. 227–243, Grzybowski Found. Spec. Publ. 5, Krawów.

Berger, A. L. (1978), Long-term variations of daily insolation and Quaternary climatic changes, *J. Atmos. Sci.*, *35*, 2362–2367.

Berger, A. L., H. Gallée, T. Fichefet, I. Marsiat, and C. Tricot (1990), Testing the astronomical theory with a coupled climate-ice-sheet model, *Palaeogeogr. Palaeoclimatol. Palaeoecol.*, *89*, 125–141.

Bertrand, C., M.-F. Loutre, and A. Berger (2002), High frequency variations of the Earth's orbital parameters and climate change, *Geophys. Res. Lett.*, *29*, doi:10.1029/2002GL015,622.

Braconnot, P., M.-F. Loutre, B. Dong, S. Joussaume, P. Valdes, and PMIP participating groups (2002), How the simulated change in monsoon at 6 ka bp is related to the simulation of the modern climate: results from the Paleoclimate Modeling Intercomparison Project, *Climate Dyn.*, *19*, 107–121, doi: 10.1007/s00382-001-0217-5.

Brassell, S. C., G. Eglinton, I. T. Marlowe, U. Pflaumann, and M. Sarnthein (1986), Molecular stratigraphy: a new tool for climatic assessment, *Nature*, *320*, 129–133.

Broecker, W. S. (1998), The end of the present interglacial: how and when?, *Quat. Sci. Rev.*, *17*, 689–694.

Clark, P. U., N. G. Pisias, T. F. Stocker, and A. J. Weaver (2002), The role of thermohaline circulation in abrupt climate change, *Nature*, *415*, 863–869.

Claussen, M., et al. (2002), Earth system models of intermediate complexity: Closing the gap in the spectrum of climate system models, *Climate Dyn.*, *18*, 579–586.

Clement, A. C., R. Seager, and M. A. Cane (1999), Orbital controls on the El Nino/Southern Oscillation and the tropical climate, *Paleoceanography*, *14*, 441–456.

Conte, M. H., A. Thompson, G. Eglinton, and J. C. Green (1995), Lipid biomarker diversity in the coccolithophorid Emiliania huxleyi (Prymnesiophyceae) and the related species Gephyrocapsa oceanica, *J. Phycol.*, *31*, 272–282.

Crowley, T. J. (1992), North Atlantic deep water cools the southern hemisphere, *Paleoceanography*, *7*, 489–497.

Crowley, T. J. (2000), Causes of climate change over the past 1000 years, *Science*, *289*, 270–277.

Crucifix, M., M.-F. Loutre, P. Tulkens, T. Fichefet, and A. Berger (2002), Climate evolution during the Holocene: a study with an Earth system model of intermediate complexity, *Climate Dyn.*, *19*, 43–60.

Etheridge, D. M., L. Steele, R. Langenfelds, R. Francey, J. Barnola, and V. Morgan (1996), Natural and anthropogenic changes in atmospheric CO_2 over the last 1000 years from air in Antarctic ice and firn, *J. Geophys. Res.*, *101*, 4115–4128.

Etheridge, D. M., L. Steele, R. Francey, and R. Langenfelds (1998), Atmospheric methane between 1000 A.D. and present: evidence of anthropogenic emissions and climatic variability, *J. Geophys. Res.*, *103*, 15,979–15,993.

Fairbanks, R. G. (1989), A 17,000 year glacio-eustatic sea level record: Influence of glacial melting rates on the Younger Dryas event and deep ocean circulation, *Nature*, *342*, 637–642.

Felis, T., J. Pätzold, Y. Loya, M. Fine, A. H. Nawar, and G. Wefer (2000), A coral oxygen isotope record from the northern Red Sea documenting NAO, ENSO, and North Pacific teleconnections on Middle East climate variability since the year 1750, *Paleoceanography*, *15*, 679–694.

Felis, T., G. Lohmann, H. Kuhnert, S. J. Lorenz, D. Scholz, J. Pätzold, S. A. Al-Rousan, and S. M. Al-Moghrabi (2004), Increased seasonality in Middle East temperatures during the last interglacial period, *Nature*, *429*, 164–168, doi:10.1038/nature02546.

Ganopolski, A., C. Kubatzki, M. Claussen, V. Brovkin, and V. Petoukhov (1998), The influence of vegetation-atmosphere-ocean interaction on climate during the mid-Holocene, *Science*, *280*, 1916–1919.

Grootes, P. M., M. Stuiver, J. W. C. White, S. J. Johnsen, and J. Jouzel (1993), Comparison of oxygen isotope records from the GISP2 and GRIP Greenland ice cores, *Nature*, *366*, 552–554.

Guiot, J., J. Boreux, P. Braconnot, F. Torre, and PMIP participating groups (1999), Data-models comparison using fuzzy logic in palaeoclimatology, *Climate Dyn.*, *15*, 569–581.

Hays, J. D., J. Imbrie, and N. J. Shackleton (1976), Variations in the Earth's orbit: pacemaker of the ice ages, *Science*, *194*, 1121–1132.

Hewitt, C. D., and J. F. B. Mitchell (1998), A fully coupled GCM simulation of the climate of the mid-Holocene, *Geophys. Res. Lett.*, *25*, 361–364.

Hurrell, J. W. (1995), Decadal trends in the North Atlantic oscillation: regional temperatures and precipitation, *Science*, *269*, 676–679.

Imbrie, J., et al. (1992), On the structure and origin of major glaciation cycles: 1. linear responses to Milankovitch forcing, *Paleoceanography*, *7*, 701–738.

Indermühle, A., et al. (1999), Holocene carbon-cycle dynamics based on CO_2 trapped in ice at Taylor Dome, Antarctica, *Nature*, *398*, 121–126.

Intergovernmental Panel on Climate Change (2001), *Climate Change 2001: The Scientific Basis: Contribution of Working Group I to the Third Assessment Report of the IPCC*, 881 pp., edited by J. T. Houghton et al., Cambridge University Press, Cambridge, UK.

Jickells, T. D., P. P. Newton, P. King, R. S. Lampitt, and C. A. Boutle (1996), Comparison of sediment trap records of particle fluxes from 19 to 48°N in the northeast Atlantic and their relation to surface water productivity, *Deep-Sea Res.*, *48*, 971–986.

Joussaume, S., and K. E. Taylor (2000), The Paleoclimate Modeling Intercomparison Project, in *Paleoclimate Modeling Intercomparison Project (PMIP): proceedings of the third PMIP workshop, Canada, 4-8 October 1999*, edited by P. Braconnot, WCRP-111, WMO/TD-1007, pp. 9–24, World Meteorological Organization.

Kim, J.-H., and R. R. Schneider (2004), GHOST global database for alkenone-derived Holocene sea-surface temperature records, http://www.pangaea.de/Projects/GHOST/, PANGAEA Network for Geol. and Environ. Data, Bremerhaven, Germany.

Kim, J.-H., N. Rimbu, S. J. Lorenz, G. Lohmann, S. Schouten, S.-I. Nam, C. Rühlemann, and R. R. Schneider (2004), North Pacific and North Atlantic sea-surface temperature variability during the Holocene, *Quat. Sci. Rev.*, *23*, 2141–2154, doi:10.1016/j.quascirev.2004.08.010.

Kitoh, A., and S. Murakami (2002), Tropical Pacific climate at the mid-Holocene and the Last Glacial Maximum simulated by a coupled atmosphere-ocean general circulation model, *Paleoceanography*, *17*, doi:10.1029/2001PA000,724.

Knorr, G., and G. Lohmann (2003), Southern Ocean origin for resumption of Atlantic thermohaline circulation during deglaciation, *Nature*, *424*, 532–536.

Kohfeld, K., and S. P. Harrison (2000), How well can we simulate past climates? Evaluating the

models using global palaeoenvironmental data sets, *Quat. Sci. Rev.*, *19*, 321–346.

Laskar, J., P. Robutel, F. Joutel, M. Gastineau, A. C. M. Correia, and B. Levrard (2004), A long-term numerical solution for the insolation quantities of the Earth, *Astron. Astrophys.*, *428*, 261–285, doi:10.1051/0004-6361:20041335.

Legutke, S., and R. Voss (1999), The Hamburg atmosphere-ocean coupled circulation model ECHO-G, *Technical Report 18*, Deutsches Klimarechenzentrum, Hamburg, Germany.

Liu, Z., R. G. Gallimore, J. E. Kutzbach, W. Xu, Y. Golubev, P. Behling, and R. Selin (1999), Modeling long-term climate changes with equilibrium asynchronous coupling, *Climate Dyn.*, *15*, 325–340.

Liu, Z., E. Brady, and J. Lynch-Stieglitz (2003), Global ocean response to orbital forcing in the Holocene, *Paleoceanography*, *18*, doi:10.1029/2002PA000,819.

Lohmann, G., and S. Lorenz (2000), The hydrological cycle under paleoclimatic conditions as derived from AGCM simulations, *J. Geophys. Res.*, *105*, 17,417–17,436.

Lohmann, G., S. J. Lorenz, and M. Prange (2005), Northern high-latitude climate changes during the Holocene as simulated by circulation models, in *The Nordic Seas: An Integrated Perspective*, edited by H. Drange et al., no. 158 in Geophys. Monogr., pp. 273–288, American Geophysical Union, Washington DC, doi:10.1029/158GM18.

Lorenz, S., and G. Lohmann (2004), Acceleration technique for Milankovitch type forcing in a coupled atmosphere-ocean circulation model: method and application for the Holocene, *Climate Dyn.*, *23*, 727–743, doi:10.1007/s00382-004-0469-y.

Lorenz, S., B. Grieger, P. Helbig, and K. Herterich (1996), Investigating the sensitivity of the atmospheric general circulation model ECHAM 3 to paleoclimatic boundary conditions, *Int. J. Earth Sci.*, *85*, 513–524.

Loutre, M. F., A. Berger, P. Bretagnon, and P.-L. Blanc (1992), Astronomical frequencies for climate research at the decadal to century time scale, *Climate Dyn.*, *7*, 181–194.

Marchal, O., et al. (2002), Apparent long-term cooling of the sea surface in the northeast Atlantic and Mediterranean during the Holocene, *Quat. Sci. Rev.*, *21*, 455–483.

McManus, J. F., D. W. Oppo, and J. L. Cullen (1999), A 0.5-million-year record of millennial-scale climate variability in the North Atlantic, *Science*, *283*, 971–975.

McManus, J. F., R. Francois, J.-M. Gherardi, L. D. Keigwin, and S. Brown-Leger (2004), Collapse and rapid resumption of Atlantic meridional circulation linked to deglacial climate changes, *Nature*, *428*, 834–837.

Milankovitch, M. (1941), *Kanon der Erdbestrahlung und seine Anwendung auf das Eiszeitenproblem*, 132, 633 pp., Royal Serb. Acad. Spec. Publ., Belgrad.

Müller, P. J., and G. Fischer (2001), A 4-year sediment trap record of alkenones from the filamentous upwelling region off Cape Blanc, NW Africa and a comparison with distributions in underlying sediments, *Deep-Sea Res.*, *48*, 1877–1903.

Müller, P. J., G. Kirst, G. Ruhland, I. von Storch, and A. Rosell-Melé (1998), Calibration of the alkenone palaeotemperature index (UK'37) based on core-tops from the eastern South Atlantic and

the global ocean (60°N-60°S), *Geochim. Cosmochim. Acta, 62*, 1757–1772.

Petoukhov, V., A. Ganopolski, V. Brovkin, M. Claussen, A. Eliseev, C. Kubatzki, and S. Rahmstorf (2000), CLIMBER-2: a climate system model of intermediate complexity. Part I: model description and performance for present climate, *Climate Dyn., 16*, 1–17.

Prahl, F. G., and S. G. Wakeham (1987), Calibration of unsaturation patterns in long-chain ketone compositions for paleotemperature assessment, *Nature, 330*, 367–369.

Renssen, H., H. Goosse, T. Fichefet, V. Brovkin, E. Driesschaert, and F. Wolk (2005), Simulating the holocene climate evolution at northern high latitudes using a coupled atmosphere-sea ice-ocean-vegetation model, *Climate Dyn., 24*, 23–43, doi:10.1007/s00382-004-0485-y.

Rimbu, N., G. Lohmann, J.-H. Kim, H. W. Arz, and R. R. Schneider (2003), Arctic/North Atlantic Oscillation signature in Holocene sea surface temperature trends as obtained from alkenone data, *Geophys. Res. Lett., 30*, 1280–1283, doi:10.1029/2002/GL016570.

Rimbu, N., G. Lohmann, S. J. Lorenz, J.-H. Kim, and R. R. Schneider (2004), Holocene climate variability as derived from alkenone sea surface temperature and coupled ocean-atmosphere model experiments, *Climate Dyn., 23*, 215–227, doi:10.1007/s00382-004-0435-8.

Roeckner, E., et al. (1996), The atmospheric general circulation model ECHAM-4: Model description and simulation of the present-day climate, *Report 218*, Max-Planck-Institut für Meteorologie.

Rosell-Melé, A., G. Eglinton, U. Pflaumann, and M. Sarnthein (1995), Atlantic core-top calibration of the UK37 index as a sea-surface palaeotemperature indicator, *Geochim. Cosmochim. Acta*, *59*, 3099–3107.

Rosell-Melé, A., E. Bard, K.-C. Emeis, J. O. Grimalt, P. J. Müller, R. R. Schneider, and 36 international participants (2001), Precision of the current methods to measure the alkenone proxy UK'37 and absolute alkenone abundance in sediments: results of an interlaboratory comparision study, *Geochem. Geophys. Geosyst., 2*, 2000GC000,141, 1–28.

Sikes, E. L., J. K. Volkman, L. G. Robertson, and J.-J. Pichon (1997), Alkenones and alkenes in surface water and sediments of the Southern Ocean: implications for paleotemperature estimation in polar regions, *Geochim. Cosmochim. Acta*, *61*, 1495–1505.

Sowers, T., R. B. Alley, and J. Jubenville (2003), Ice core records of atmospheric N_2O covering the last 106,000 years, *Science*, *301*, 945–948.

Stocker, T. F. (1998), The seesaw effect, *Science*, *282*, 61–62.

Texier, D., N. de Noblet, and P. Braconnot (2000), Sensitivity of the African and Asian monsoons to mid-Holocene insolation and data-inferred surface changes, *J. Clim., 13*, 164–181.

Thompson, D. W. J., and J. M. Wallace (1998), The Arctic oscillation signature in the wintertime geopotential height and temperature fields, *Geophys. Res. Lett., 25*, 1297–1300.

Thompson, D. W. J., and J. M. Wallace (2001), Regional climate impacts of the Northern Hemisphere Annular Mode, *Science*, *293*, 85–89.

Volkman, J. K., G. Eglinton, E. D. S. Corner, and J. R. Sargent (1980), Novel unsaturated straight-chain methyl and ethyl ketones in marine sedimens and a coccolithophore Emiliania huxleyi, *Phytochemistry*, *19*, 2619–2622.

Voss, R., and U. Mikolajewicz (2001), The climate of 6000 years BP in near-equilibrium simulations with a coupled AOGCM, *Geophys. Res. Lett.*, *28*, 2213–2216.

Weber, S. L., T. Crowley, and G. van der Schrier (2004), Solar irradiance forcing of centennial climate variability during the Holocene, *Climate Dyn.*, *22*, 539–553, doi:10.1007/s00382-004-0396-y.

Wolff, J.-O., E. Maier-Reimer, and S. Legutke (1997), The Hamburg ocean primitive equation model HOPE, *Technical Report 13*, Deutsches Klimarechenzentrum, Hamburg, Germany.

Chapter 5

Increased seasonality in Middle East temperatures during the last interglacial period

5.1 Introduction

The last interglacial period (about 125,000 years ago) is thought to have been at least as warm as the present climate [*Kukla et al.*, 2002]. Owing to changes in the Earth's orbit around the Sun, it is thought that insolation in the Northern Hemisphere varied more strongly than today on seasonal timescales [*Berger*, 1978], which would have led to corresponding changes in the seasonal temperature cycle [*Montoya et al.*, 2000]. Here we present seasonally resolved proxy records using corals from the northernmost Red Sea, which record climate during the last interglacial period, the late Holocene epoch and the present. We find an increased seasonality in the temperature recorded in the last interglacial coral. Today, climate in the northern Red Sea is sensitive to the North Atlantic Oscillation [*Felis et al.*, 2000; *Rimbu et al.*, 2001], a climate oscillation that strongly influences winter temperatures and precipitation in the North Atlantic region. From our coral records and simulations with a coupled atmosphere-ocean circulation model, we conclude that a tendency towards the high-index state of the North Atlantic Oscillation during the last interglacial period, which is consistent with European proxy records [*Zagwijn*, 1996; *Aalbersberg and Litt*, 1998; *Klotz et al.*, 2003], contributed to the larger amplitude of the seasonal cycle in the Middle East.

The Arctic Oscillation/North Atlantic Oscillation (AO/NAO), the Northern Hemisphere's dominant mode of atmospheric variability, exerts a strong influence on mid- and high-latitude continental climate by modulating the strength of the subpolar westerlies at interannual to interdecadal timescales [*Hurrell*, 1995; *Thompson and Wallace*, 2001]. Previous work has shown that the northernmost Red Sea represents a location to study past AO/NAO-related atmospheric variability over the Northern Hemisphere, and that annually banded corals from this subtropical site provide proxy records of this variability over the past centuries [*Felis et al.*, 2000; *Rimbu et al.*, 2001]. This narrow, desert-enclosed

Thomas Felis, Gerrit Lohmann, Henning Kuhnert, Stephan J. Lorenz, Dennis Scholz, Jürgen Pätzold, Saber A. Al-Rousan, and Salim M. Al-Moghrabi, *Nature, 429*, S. 164-168, doi:10.1038/nature02546, ©2004 Nature Publishing Group

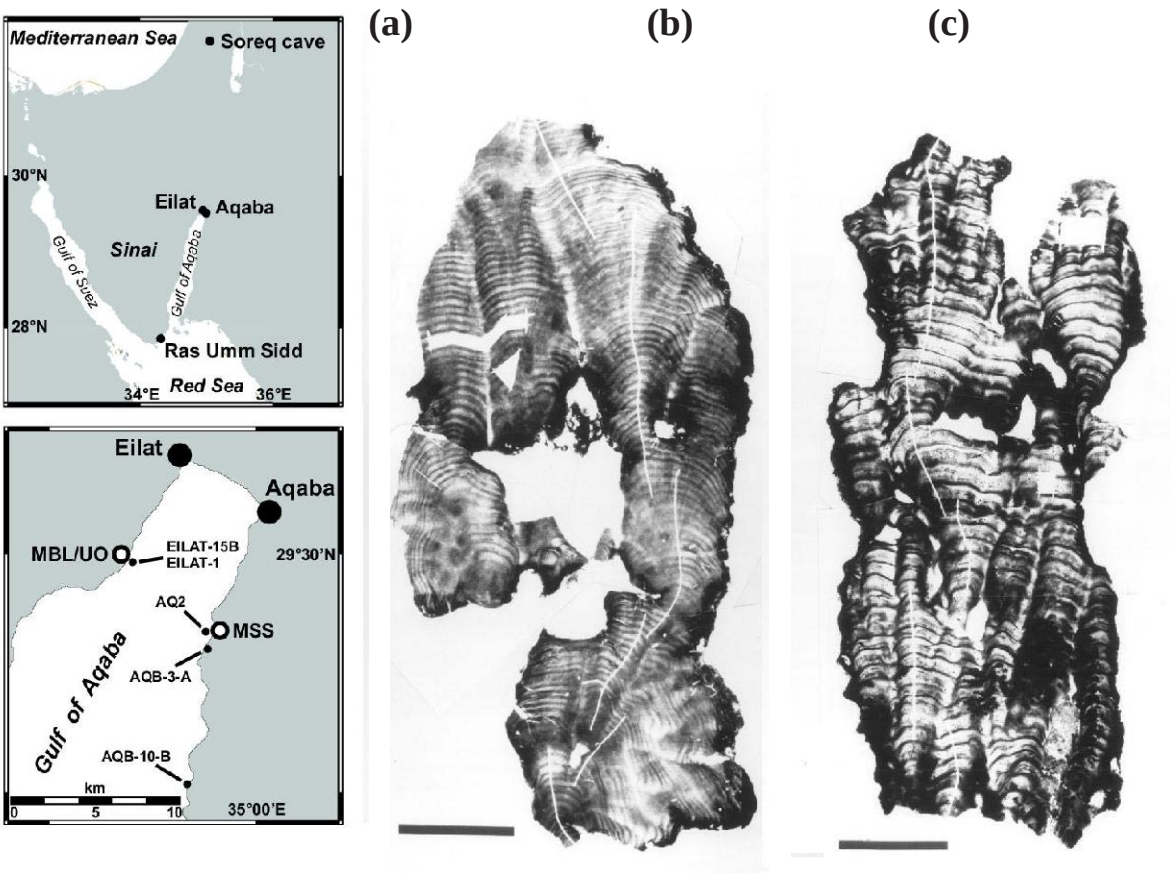

Figure 5.1: *Maps of the northernmost Red Sea, and X-radiographs of the two fossil Porites corals. (a) The sites of coral collection in the northern Gulf of Aqaba. Coral AQB-10-B was collected at 34°57.84′E, 29°22.91′N; coral AQB-3-A was collected at 34°58.28′E, 29°27.12′N. MBL/UO, H. Steinitz Marine Biology Laboratory/Underwater Observatory, Eilat; MSS, Marine Science Station, Aqaba; sea surface temperature was measured at UO*[25]*. (b, c), X-radiograph positive prints of 5-mm-thick slabs sliced parallel to the growth axis of coral AQB-10-B (b; 2.9 kyr) and coral AQB-3-A (c; 122 kyr). Alternating bands of high (dark colour) and low skeletal density (light colour) are visible. One year is represented by a high-density/low-density band pair. The sampling transect appears as a white line. The corals are about 60 cm high and 25-30 cm in diameter. Scale bars, 10 cm.*

ocean basin is influenced by mid-latitude continental climate [*Rimbu et al.*, 2001, 2003] and is sensitive to atmospheric processes owing to a weak water column stratification [*Eshel et al.*, 2000].

5.2 Late Holocene and last interglacial corals

Two fossil coral colonies (Porites) were collected near Aqaba on the Jordanian coast of the Gulf of Aqaba, the northeastern extension of the northernmost Red Sea (Figure 5.1a). Colony AQB-10-B was recovered from a canal cut into the modern reef flat, whereas colony AQB-3-A was collected from a complex of raised reef terraces. X-radiographs revealed annual density bands and were used to identify areas within the colonies that appear to be unaffected by diagenetic alteration (Figure 5.1b, c). X-ray diffraction analyses of these areas indicate an aragonite content of 98-99%, and petrographic

thin sections show only traces of secondary aragonite. The bimonthly resolution time series of both coral $\delta^{18}O$ and $\delta^{13}C$ (not shown) generated from these areas show clear annual cycles, suggesting that the sampled sections were not subject to major diagenetic alterations with respect to stable isotopes (see Methods and Supplementary Information).

Radiocarbon dating indicates that coral AQB-10-B grew 2.9 kyr ago during the late Holocene. The age of coral AQB-3-A is 121.9 (+7.0/6.3) kyr, based on U-series dating including a correction for open-system behaviour. Additional uncertainty due to model assumptions is reflected in the larger age error compared to usual U-series dating of corals [*Scholz et al.*, 2004] (see Methods). The latter coral grew during the last interglacial period, which, in the Middle East, is documented between 124 and 119 kyr ago based on a U-series dated speleothem record of eastern Mediterranean climate [*Bar-Matthews et al.*, 2000], with the main peak at 122 kyr coinciding with the coral's age.

The late Holocene and last interglacial corals provide bimonthly resolution $\delta^{18}O$ time series for time windows of 98 and 44 yr, respectively. Multitaper method spectral analysis reveals significant variance at interannual periods of 5-6 yr in both records (Figure 5.2c, d), which can be interpreted as an indication of AO/NAO-like atmospheric variability over the Northern Hemisphere at 2.9 and 122 kyr ago. Similar variability is evident in the time series of a modern coral from the northernmost Red Sea (Figure 5.2a), where it is strongly linked with regional sea surface temperature (SST) and the AO/NAO4. Cross-spectral analysis reveals that this interannual variability is highly coherent and in phase with the AO index (Figure 5.2b), although a minor fraction is associated with weaker and non-stationary tropical Pacific teleconnections modulated by higher-latitude atmospheric circulation [*Felis et al.*, 2000; *Rimbu et al.*, 2003]. Although the AO/NAO is most pronounced during winter, it is present throughout the year [*Barnston and Livezey*, 1987; *Rogers and McHugh*, 2002]. Consequently, spectral analyses were performed with bimonthly resolution time series, reflecting variability throughout the year. This procedure is supported by the finding that the physical mechanism that provides a link between the AO/NAO and Middle East climate during winter [*Rimbu et al.*, 2001] is similar to that for interannual variability throughout the year (see Supplementary Fig. S1): a high-pressure anomaly over the Mediterranean Sea associated with the AO/NAO favours an anticyclonic flow of surface winds in the eastern Mediterranean, which results in advection of colder air from southeastern Europe, controlling SST and coral $\delta^{18}O$ variability in the northern Red Sea [*Rimbu et al.*, 2003].

5.3 Methods

5.3.1 Microsampling, oxygen isotope and Sr/Ca analyses, age model

Microsampling, $\delta^{18}O$ analyses, age model construction, and interpolation to a bimonthly resolution were performed as recently described for a modern coral from the northernmost Red Sea4. The microdrill bit diameter was adapted to a coral's mean growth rate as estimated from X-radiographs in order to obtain at least six samples per year on average by continuous spot-sampling. For Sr/Ca analyses, inductively coupled plasma mass spectrometry was used (see Supplementary Information).

5.3.2 Radiocarbon and U-series dating

An accelerator mass spectrometry (AMS) ^{14}C date of 3,290±35 yr before present (BP) was determined on coral AQB-10-B (KIA13708) at the Leibniz-Labor for Radiometric Dating and Isotope Research (Kiel, Germany). The 14C age was converted to calendar age using the CALIB 4.3 calibration program [*Stuiver and Reimer*, 1993], yielding an age of 2,910 calibrated yr BP (2σ range: 3,0022,807 cal. yr BP). A ΔR value of 154 yr was used to correct for regional differences in reservoir age, based on six AMS ^{14}C dates determined on two modern coral cores with established age models and data from the Marine Reservoir Correction Database (see Supplementary Table S1). Six thermal ionization mass spectrometry (TIMS) U-series dates were determined on coral AQB-3-A at the Forschungsstelle für Radiometrische Altersbestimmungen of the Heidelberger Akademie der Wissenschaften (Heidelberg, Germany).

The U-series ages range from 137.3 to 126.4 kyr ago and the initial δ^{234}U values are elevated, ranging from 21.5% to 38.5% and suggesting open-system behaviour of U-series isotopes. In order to solve this problem, a model approach was applied that yields an isochron age of 121.9 (+7.0/6.3) kyr (2σ range) [*Scholz et al.*, 2004]. The larger age error compared to usual U-series dating of corals arises from additional uncertainty due to the model assumptions. The age is consistent with peak sea-level conditions during the last interglacial, based on dated coral reef terraces from the Red Sea [*Walter et al.*, 2000] (136 to 118 kyr ago) and elsewhere [*Stirling et al.*, 1998] (128 to 121 kyr ago), as well as with the last interglacial period in the Middle East [*Bar-Matthews et al.*, 2000] (124 to 119 kyr ago). Moreover, coral AQB-3-A was collected from a complex of raised reef terraces with an elevation in the range of other last interglacial reef terraces along the Red Sea coast [*Walter et al.*, 2000].

5.3.3 Calibration of the proxies

The seasonal maxima and minima in the Sr/Ca record of a modern coral (EILAT-15B) were tied to the corresponding extreme values in a monthly record of in situ SST [*Genin et al.*, 1995]. A linear least-squares regression was then carried out for bimonthly interpolated Sr/Ca and SST data (with SST defined as the independent variable), giving a relationship of: $\mathrm{Sr/Ca}\times 10^3 = 10.781(\pm 0.1181) - 0.0597(\pm 0.00501)\times \mathrm{SST}$ (r2=0.78). The slope of this regression equation is similar to that of calibrations at other locations [*Marshall and McCulloch*, 2002]. The same procedure was applied to the coral δ^{18}O record of EILAT-15B, giving a relationship of: $\delta^{18}\mathrm{O} = 0.801(\pm 0.2773) - 0.1514(\pm 0.01176)\times \mathrm{SST}$ (r^2=0.81). The slope is similar to that of a calibration from the region [*Felis et al.*, 2000].

Using these equations to convert coral Sr/Ca and δ^{18}O to SST reveals large offsets in the coral-based mean SST between coral EILAT-15B and two other modern corals (AQ2, EILAT-1) for both proxies, most probably due to so-called vital effects. We therefore do not interpret coral Sr/Ca and δ^{18}O in terms of absolute SST, but quantitative estimates of the range of the seasonal SST cycle are possible, as the slope of the proxy-SST calibrations remains unaffected. Modern coral δ^{18}O data are from *Felis et al.* [2003], age models were constructed according to *Felis et al.* [2000].

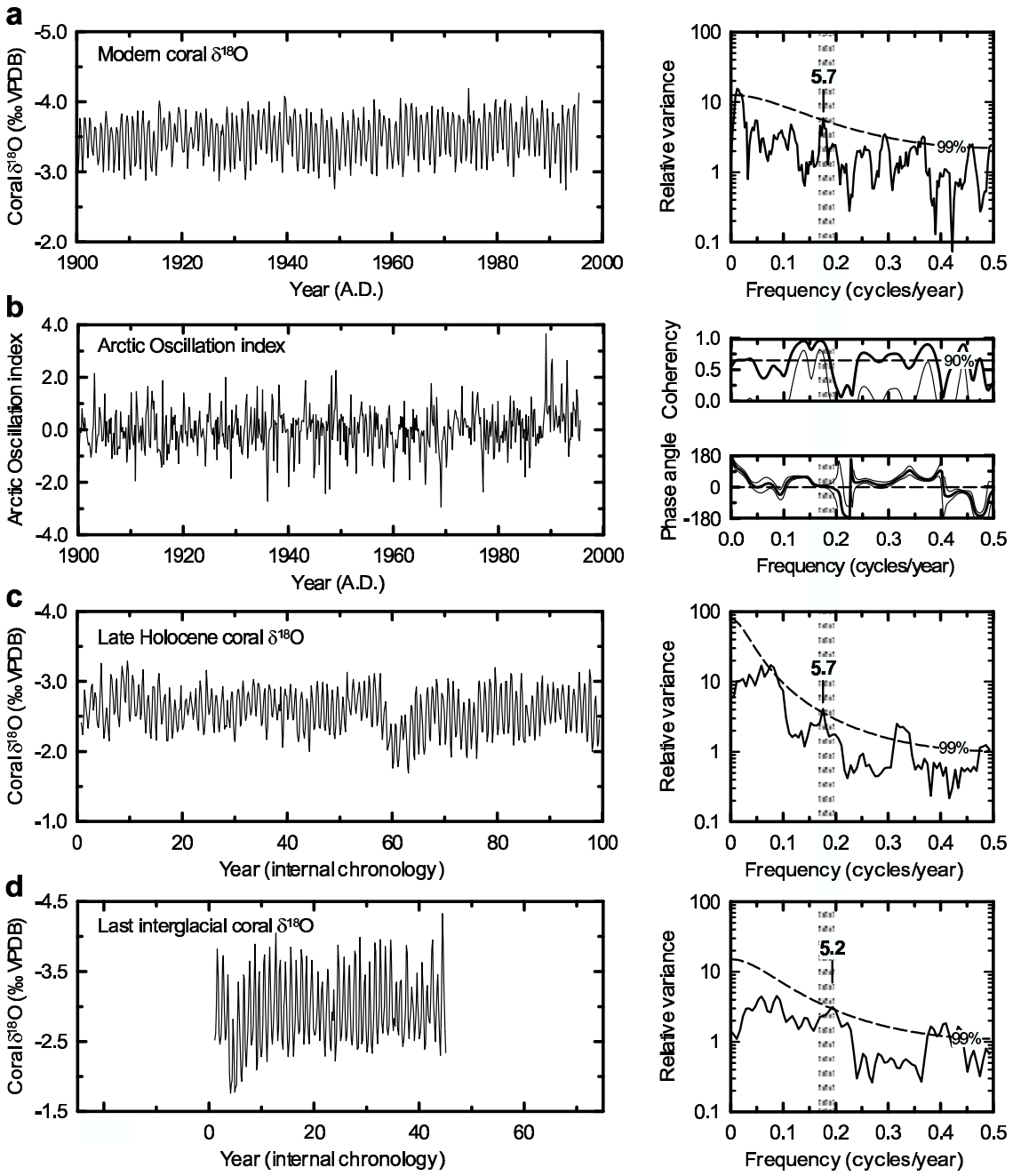

Figure 5.2: *Time series of coral $\delta^{18}O$ based on modern, late Holocene, and last interglacial Porites colonies from the northernmost Red Sea and their spectral properties. Bimonthly coral $\delta^{18}O$ time series (left panel) and results of multitaper method spectral analysis with red noise null hypothesis [Ghil et al., 2002] (number of tapers, 3; bandwidth parameter, 2; 99% significance level is indicated) (right panel) for (a), a modern coral from Ras Umm Sidd [Felis et al., 2000] (RUS-95, AD 1750-1995), (c), a late Holocene coral (AQB-10-B, 2.9 kyr) and (d), a last interglacial coral (AQB-3-A, 122 kyr) from Aqaba. (b), Bimonthly time series of the Arctic Oscillation (AO) index10 (left panel). Cross-spectral analysis between the time series of the modern coral and the AO index (right panel). The 90% confidence level for coherency is indicated. Spectral analyses were performed for bimonthly, detrended and normalized time series with the average seasonal cycle removed.*

5.3.4 Global circulation model and experimental set-up

The coupled atmosphere-ocean general circulation model ECHO-G is applied [*Legutke and Voss*, 1999]. The atmospheric part of ECHO-G is the general circulation model ECHAM4 with its T30 resolution, which corresponds to a gaussian longitude-latitude grid of approximately $3.8^{\circ} times 3.8^{\circ}$. ECHAM4 is coupled to the HOPE ocean model including a dynamic-thermodynamic sea-ice model. ECHO-G was adapted to account for the influence of variations in the annual distribution of solar radiation resulting from the varying orbital parameters [*Lorenz and Lohmann*, 2004], which were calculated after *Berger* [1978]. The timescale of the astronomical forcing was shortened by an acceleration factor of 100 to enable simulations of a $>$100 kyr period with ECHO-G [*Lorenz and Lohmann*, 2004]. The insolation trends of the last 140 kyr are represented in 1,400 simulation years. Three ensemble experiments for the period 140 kyr ago to AD 1800 were performed with orbital forcing [*Berger*, 1978] only. Throughout the experiments, the greenhouse gas concentrations were fixed (latest Holocene values: 280 p.p.m. CO_2, 700 p.p.b. CH_4, 265 p.p.b. N_2O) and modern values for vegetation, sea level, and distribution of land, ocean and continental ice were used. The experiments were continued from AD 1800 onward with increasing greenhouse gas concentrations, reaching 370 p.p.m. CO_2 in AD 2000. The temperature anomalies induced by anthropogenic greenhouse gases are shown in Supplementary Fig. S10.

5.4 Results

The most striking feature of the coral $\delta^{18}O$ time series is increased seasonality in the last interglacial record compared to the modern and late Holocene records (Figure 5.2). Because coral $\delta^{18}O$ is influenced by both temperature and $\delta^{18}O$ of sea water, we applied the coral Sr/Ca palaeothermometer to the fossil corals and to three modern reference corals. Combined Sr/Ca and $\delta^{18}O$ analyses on modern corals show that both proxies satisfactorily document the seasonal SST cycle of 5.4°C, indicating a seasonal cycle between 4.5 and 5.6°C (Figure 5.3a), in agreement with earlier findings that $\delta^{18}O$ seasonality in northern Red Sea corals is mainly controlled by temperature [*Felis et al.*, 2000]. Both Sr/Ca and $\delta^{18}O$ of the late Holocene coral indicate a seasonal SST cycle of 5.2°C at 2.9 kyr ago (Figure 5.3b), similar to today. In contrast, in the last interglacial coral both proxies indicate increased SST seasonality of 8.4°C at 122 kyr ago (Figure 5.3d) (see Methods and Supplementary Information).

In order to understand the physical mechanisms responsible for increased SST seasonality in the northernmost Red Sea during the last interglacial, and seasonality similar to today at 2.9 kyr ago, we performed coupled atmosphere-ocean general circulation model simulations (ECHO-G) for last interglacial, late Holocene, pre-industrial, and modern conditions (see Methods). Consistent with coral-based results, the corresponding modelled SST indicates increased seasonality during the last interglacial, and seasonality similar to modern and pre-industrial conditions at 3 kyr ago (Figure 5.3c, e). Consistent with model-based SST, the modelled Middle East surface air temperature (SAT) anomalies indicate warmer summers and colder winters relative to modern conditions during the last interglacial (Figure 5.4a, b). This increased seasonality would usually be explained by an amplified seasonal insolation cycle at that time (Figure 1.8).

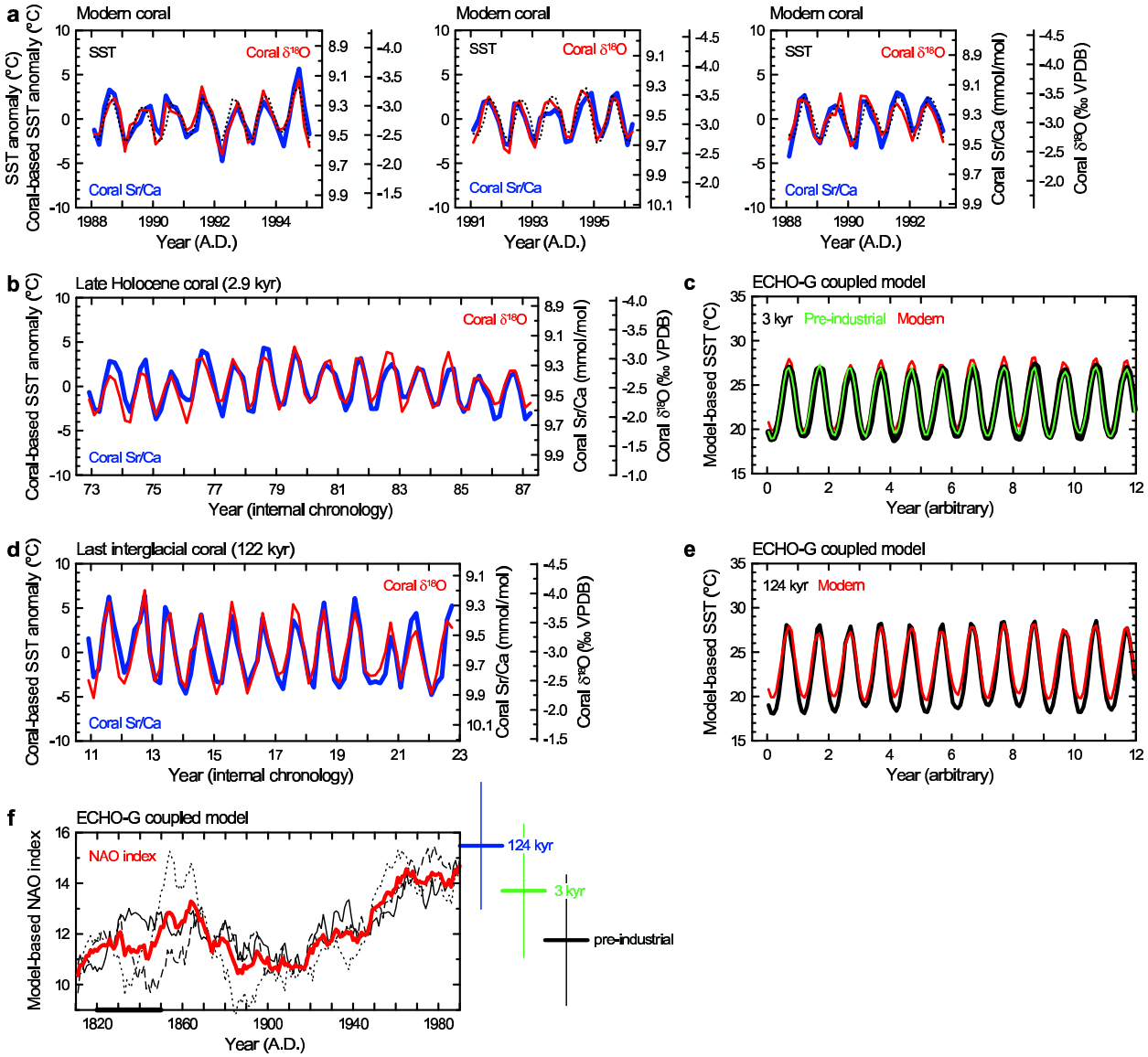

Figure 5.3: *Coral-based sea surface temperature (SST) anomalies for the northernmost Red Sea and ECHO-G model-based SST and AO/NAO indices. Bimonthly Porites coral $\delta^{18}O$ (red) and Sr/Ca (blue) time series and coral-based SST anomalies (respective mean was subtracted). (a), Modern corals EILAT-15B (left), AQ2 (centre), EILAT-1 (right), in situ SST [Genin et al., 1995] (dotted line); (b), late Holocene (AQB-10-B; 2.9 kyr) and (d), last interglacial coral (AQB-3-A; 122 kyr). (c), (e), Modelled monthly SST index of the coral region for 3 kyr (c, red), 123 kyr (e, red), pre-industrial (around AD 1830; c, black) and modern conditions (around AD 1980; e, black). f, Modelled AO/NAO index (December-February). Three greenhouse gas scenarios (black lines) and the ensemble mean (red line) for the period AD 1800-2000 (centred 41-yr running means). Mean standard deviations for 41 winters centred at 122 kyr, 3 kyr and the pre-industrial period (thick horizontal bar) are shown on the right. See Figure 5.6 for index definitions and Figure 6.1 for a comparison of the index during the Eemian period in chapter 6.*

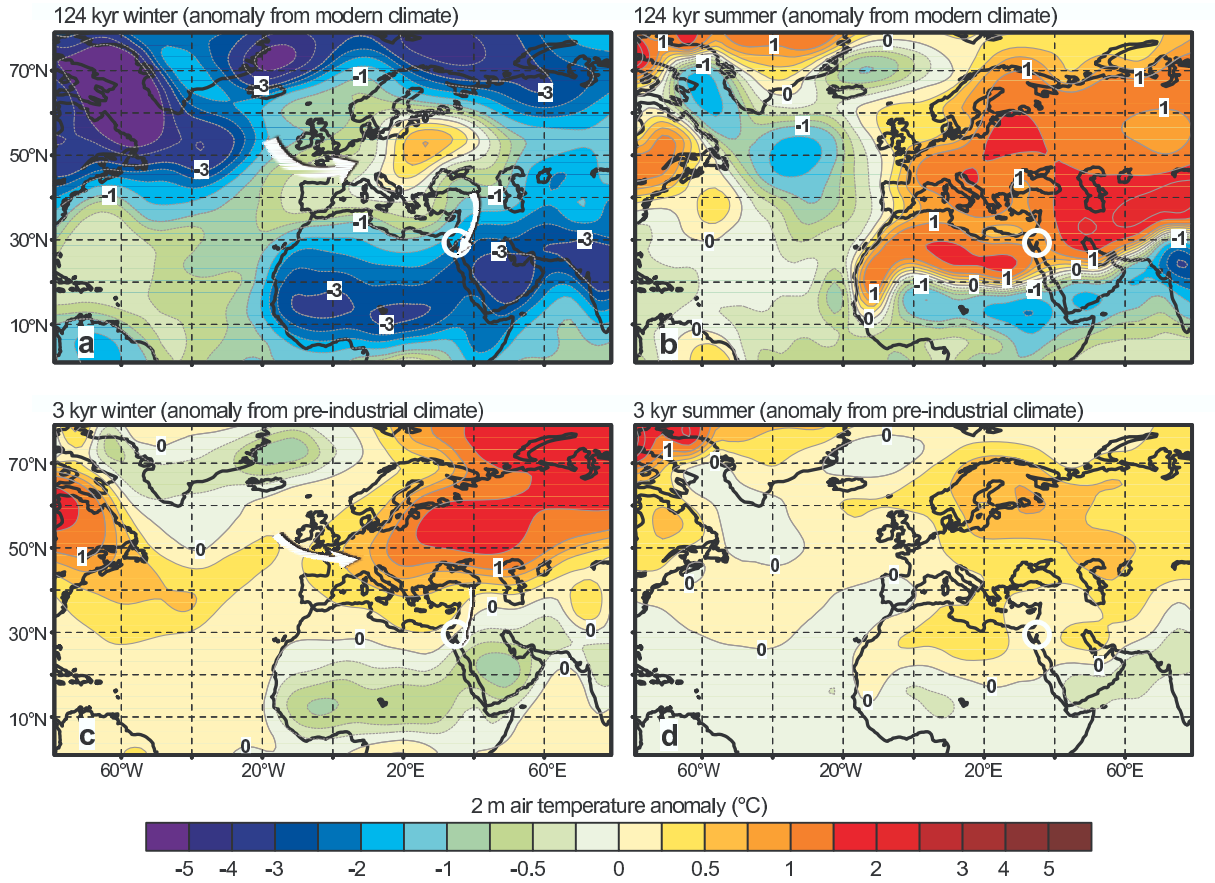

Figure 5.4: *Near-surface air temperature anomalies for the last interglacial and the late Holocene based on the coupled atmosphere-ocean general circulation model ECHO-G. Difference between last interglacial (124 kyr) and modern climate (AD 1975-85) for (a), winter (December, January, February; DJF) and (b), summer (June, July, August; JJA). The corresponding anomalies from pre-industrial climate are shown in Supplementary Fig. S8. Difference between late Holocene (3 kyr) and pre-industrial climate (AD 1820-50) for (c), winter (DJF) and (d), summer (JJA). The corresponding anomalies from modern climate are shown in Supplementary Fig. S9. Near surface wind anomaly is schematically represented as white arrows. An average of 11 simulation years has been applied to the last interglacial and late Holocene climate centred at the respective time period. The region of coral collection in the northernmost Red Sea is marked by a white circle.*

Indeed, our model suggests that warmer Middle East summers during the last interglacial result from increased summer insolation, as they are part of a spatially homogenous warming pattern over mid-latitude continental areas where insolation was enhanced (Figure 5.4b). However, the model suggests that colder Middle East winters at that time did not solely result from reduced winter insolation at these latitudes, but are associated with the AO/NAO. The modelled winter SAT difference between last interglacial and modern climate reveals a warming and cooling pattern over the North Atlantic and adjacent continental areas that cannot be explained by differences in direct insolation forcing, but that resembles the spatial signature of the AO/NAO [*Hurrell*, 1995; *Thompson and Wallace*, 2001]. This winter SAT anomaly indicates a tendency towards the AO/NAO high-index state during the last interglacial, with warmer winters in central Europe owing to increased advection of

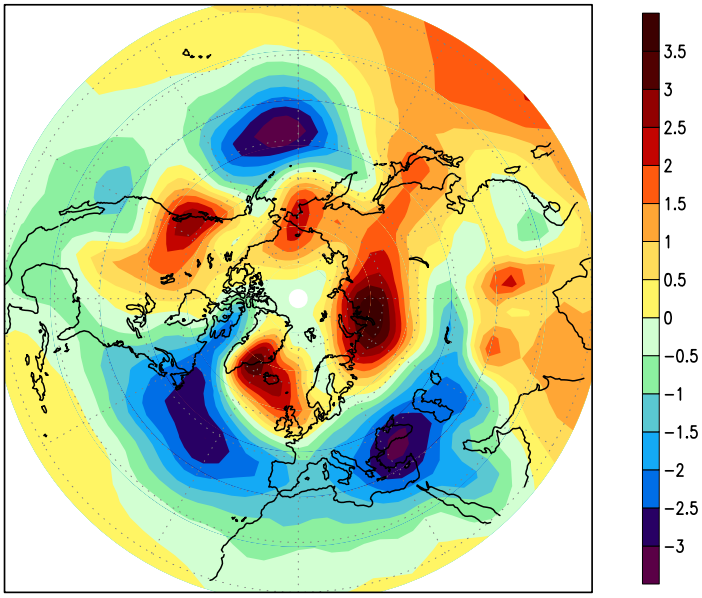

Figure 5.5: *Relationship between the modelled SST index of the coral region and the modelled sea level pressure (SLP) field of the Northern Hemisphere, based on the coupled atmosphere-ocean general circulation model ECHO-G. Regression of the modelled SST index covering the eastern Mediterranean and the Red Sea (see Figure 5.6 for definition) against the modelled Northern Hemisphere SLP field for the period 1820-1920 A.D. (December, January, February). Prior to the calculation the trends have been eliminated.*

warm oceanic air from the west, and colder winters in the Middle East owing to increased advection of cold continental air from the north (Figure 5.4a). This implies that the AO/NAO contributed to increased SST seasonality in the northernmost Red Sea during the last interglacial through winter cooling. This is consistent with (1) coral-based results of AO/NAO-like interannual variability during the last interglacial, (2) observations during recent decades where a shift towards the high-index AO/NAO is accompanied by colder winters in the northernmost Red Sea leading to increased seasonality, and (3) a strong relationship between interannual variability of modelled regional winter SST and the AO/NAO (Figure 5.5, see Supplementary Figs S5, S6). Furthermore, a tendency towards the high-index AO/NAO provides an explanation for warmer winters in central Europe during the last interglacial, as indicated by terrestrial proxy climate records [*Zagwijn*, 1996; *Aalbersberg and Litt*, 1998; *Klotz et al.*, 2003], a finding in conflict with an explanation via reduced winter insolation at these latitudes.

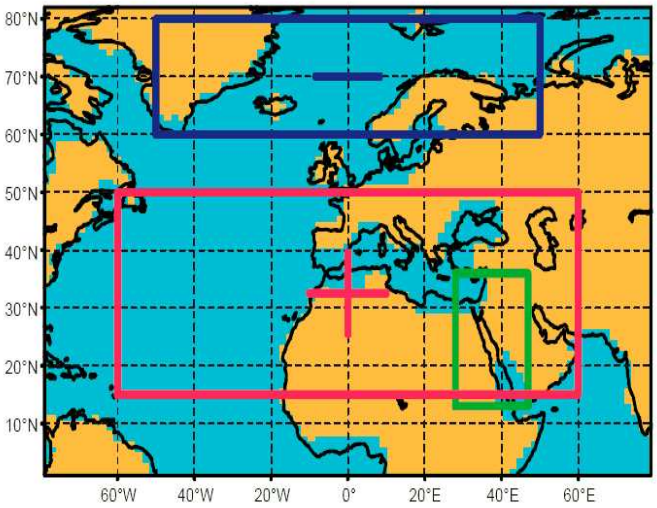

Figure 5.6: *Definition of modelled indices used in this study. The SST index of the coral region (Figure 5.3c, e) has been obtained from the averaged modelled SST over the eastern Mediterranean and the Red Sea (green box). This index is used for the calculation of the regression depicted in Figure 5.5. The modelled AO/NAO index (Figure 5.3f and Figure 6.1) is calculated from the sea level pressure (SLP) difference between a southerly high pressure region (red box) and a northerly low pressure region (blue box). The brown rectangles mark the sea-landmask of the atmospheric submodel ECHAM4 in its T30 resolution.*

5.5 Discussion and conclusions

Consistent with coral- and model-based SST, the modelled northernmost Red Sea SAT anomalies indicate seasonality similar to modern and pre-industrial conditions at 3 kyr ago (Figure 5.4c, d). The winter SAT anomaly indicates a tendency towards the high-index AO/NAO at 3 kyr ago relative to pre-industrial conditions, which is less pronounced compared to the last interglacial. Compared to the latter, the amplified seasonal insolation cycle at 3 kyr ago is also less pronounced (see Figure 1.8). For the last interglacial, the winter SAT anomaly from pre-industrial climate indicates a more pronounced tendency towards the high-index AO/NAO compared to that from modern conditions (see Supplementary Fig. S8).

The modelled SAT anomalies, as well as the modelled AO/NAO indices, suggest a combined response of the AO/NAO to seasonal insolation changes on orbital timescales and to atmospheric greenhouse gases (Figure 5.3f). Consistent with other model-based studies [*Fyfe et al.*, 1999; *Shindell et al.*, 1999], a greenhouse gas increase from pre-industrial to modern values results in a slight tendency towards the high-index AO/NAO. The pronounced last interglacial high-index AO/NAO relative to 3 kyr ago and pre-industrial climate, however, can only be explained by differences in insolation forcing, as greenhouse gas concentrations were similar. Interestingly, the interannual AO/NAO variability is nearly unaffected by the orbital forcing, consistent with coral-based results. The physical mechanism linking orbital forcing and the last interglacial high-index AO/NAO most probably involves reduced boreal winter insolation in the tropics (Figure 1.8). In the model, this leads to a reduced pole-to-equator temperature gradient, and a subsequent weakening of the Hadley cell accompanied by planetary wave activity, with increased Icelandic low and subtropical North Atlantic/eastern Mediterranean highs. The anomalous circulation pattern represents a quasi-equilibrium response to thermal forcing linked to land-sea temperature contrasts and orography [*Held et al.*, 2002]. Furthermore, a northward shift of the North American and Atlantic jet stream by downward propagating stratospheric anomalies is consistent with the high-index AO/NAO10.

The AO/NAO, the dominant mode of Northern Hemisphere climate variability on interannual to interdecadal timescales [*Hurrell*, 1995; *Thompson and Wallace*, 2001], has also been suggested to be important on millennial timescales [*Keigwin and Pickart*, 1999; *Noren et al.*, 2002]. In addition, our approach (of combining seasonal resolution coral proxy records from a climatically sensitive, exceptionally northern, subtropical reef site with coupled atmosphere-ocean circulation model simulations) suggests an important role of the AO/NAO in modulating regional Northern Hemisphere climate patterns and seasonality on orbital timescales. The cross-validation of well-dated, high-resolution palaeoclimatic records and state-of-the-art climate models provides a strong tool for evaluating the sensitivity of different modes of climate variability to natural and anthropogenic forcing factors. This provides a crucial step in understanding and predicting pronounced changes in past, present and future climate.

Acknowledgments. We thank M. Segl and her team for stable isotope analyses, A. Abu-Hilal and the Aqaba Marine Science Station for support within the Red Sea Programme, N. Rimbu for discussions, M. Zuther for X-ray diffraction analyses, N. Zatloukal for thin sections, J. Zinke for material, W. Hale for comments, and S. Legutke for support with the ECHO-G model. This work was supported by Bundesministerium für Bildung und Forschung through KIHZ and DEKLIM, and by Deutsche Forschungsgemeinschaft through DFG Research

Centre Ocean Margins at Bremen University.

5.6 References

Aalbersberg, G., and T. Litt, Multiproxy climate reconstructions for the Eemian and early Weichselian, *J. Quat. Sci.*, *13*, 367–390, 1998.

Bar-Matthews, M., A. Ayalon, and A. Kaufman, Timing and hydrological conditions of sapropel events in the Eastern Mediterranean, as evident from speleothems, Soreq cave, Israel, *Chem. Geol.*, *169*, 145–156, 2000.

Barnston, A. G., and R. E. Livezey, Classification, seasonality and persistence of low-frequency atmospheric circulation patterns, *Mon. Weather Rev.*, *115*, 1083–1126, 1987.

Berger, A. L., Long-term variations of daily insolation and Quaternary climatic changes, *J. Atmos. Sci.*, *35*, 2362–2367, 1978.

Eshel, G., D. P. Schrag, and B. F. Farrell, Troposphere-planetary boundary layer interaction and the evolution of ocean surface density: Lessons from Red Sea corals, *J. Clim.*, *13*, 339–351, 2000.

Felis, T., J. Pätzold, Y. Loya, M. Fine, A. H. Nawar, and G. Wefer, A coral oxygen isotope record from the northern Red Sea documenting NAO, ENSO, and North Pacific teleconnections on Middle East climate variability since the year 1750, *Paleoceanography*, *15*, 679–694, 2000.

Felis, T., Jürgen Pätzold, and Y. Loya, Mean oxygen-isotope signatures in Porites spp. corals: Inter-colony variability and correction for extension-rate effects, *Coral Reefs*, *22*, 328–336, 2003.

Fyfe, J. C., G. J. Boer, and G. M. Flato, The Arctic and Antarctic Oscillations and their projected changes under global warming, *Geophys. Res. Lett.*, *26*, 1601–1604, 1999.

Genin, A., B. Lazar, and S. Brenner, Vertical mixing and coral death in the Red Sea following the eruption of Mount Pinatubo, *Nature*, *377*, 507–510, 1995.

Ghil, M., M. R. Allen, M. D. Dettinger, K. Ide, D. Kondrashov, M. E. Mann, A. W. Robertson, A. Saunders, and Y. Tian et al., Advanced spectral methods for climatic time series, *Rev. Geophys.*, *40*, 2002.

Held, I. M., M. Ting, and H. Wang, Northern winter stationary waves: theory and modeling, *J. Clim.*, *15*, 2125–2144, 2002.

Hurrell, J. W., Decadal trends in the North Atlantic oscillation: regional temperatures and precipitation, *Science*, *269*, 676–679, 1995.

Keigwin, L. D., and R. S. Pickart, Slope water current over the Laurentian Fan on interannual to millennial time scales, *Science*, *286*, 520–523, 1999.

Klotz, S., J. Guiot, and V. Mosbrugger, Continental European Eemian and early Würmian climate evolution: comparing signals using different quantitative reconstruction approaches based on pollen, *Glob. Planet. Change*, *36*, 277–294, 2003.

Kukla, G. J., M. L. Bende, J.-L. de Beaulie, G. Bon, W. S. Broecke, P. Clevering, J. E. Gavi, T. D. Herber, and J. Imbri and J. Jouzel et al., Last interglacial climates, *Quat. Res.*, *58*, 2–13, 2002.

Legutke, S., and R. Voss, The Hamburg atmosphere-ocean coupled circulation model ECHO-G, *Technical Report 18*, Deutsches Klimarechenzentrum, Hamburg, Germany, 1999.

Lorenz, S. J., and G. Lohmann, Acceleration technique for Milankovitch type forcing in a coupled atmosphere-ocean circulation model: method and application for the Holocene, *Climate Dyn.*, *23*, 727–743, 2004.

Marshall, J. F., and M. T. McCulloch, An assessment of the Sr/Ca ratio in shallow water hermatypic corals as a proxy for sea surface temperature, *Geochim. Cosmochim. Acta*, *66*, 3263–3280, 2002.

Montoya, M., H. von Storch, and T. J. Crowley, Climate simulation for 125 kyr BP with a coupled ocean-atmosphere general circulation model, *J. Clim.*, *15*, 1057–1072, 2000.

Noren, A. J., P. R. Bierman, E. J. Steig, A. Lini, and J. Southon, Millennial-scale storminess variability in the northeastern United States during the Holocene epoch, *Nature, 419*, 821–824, 2002.

Rimbu, N., G. Lohmann, T. Felis, and J. Pätzold, Arctic Oscillation signature in a Red Sea coral, *Geophys. Res. Lett.*, *28*, 2959–2962, 2001.

Rimbu, N., G. Lohmann, T. Felis, and J. Pätzold, Shift in ENSO teleconnections recorded by a northern Red Sea coral, *J. Clim.*, *16*, 1414–1422, 2003.

Rogers, J. C., and M. J. McHugh, On the separability of the North Atlantic oscillation and Arctic oscillation, *Climate Dyn.*, *19*, 599–608, 2002.

Scholz, D., A. Mangini, and T. Felis, U-series dating of diagenetically altered fossil reef corals, *Earth Planet. Sci. Lett.*, *218*, 163–178, 2004.

Shindell, D. T., R. L. Miller, G. A. Schmidt, and L. Pandolfo, Simulation of recent northern winter climate trends by greenhouse-gas forcing, *Nature, 399*, 452–455, 1999.

Stirling, C. H., T. M. Esat, K. Lambeck, and M. T. McCulloch, Timing and duration of the Last Interglacial: evidence for a restricted interval of widespread coral reef growth, *Earth Planet. Sci. Lett.*, *160*, 745–762, 1998.

Stuiver, M., and P. J. Reimer, Extended ^{14}C database and revised CALIB radiocarbon calibration program, *Radiocarbon*, *35*, 215–230, 1993.

Thompson, D. W. J., and J. M. Wallace, Regional climate impacts of the Northern Hemisphere Annular Mode, *Science*, *293*, 85–89, 2001.

Walter, R. C., et al., Early human occupation of the Red Sea coast of Eritrea during the last interglacial, *Nature*, *405*, 65–69, 2000.

Zagwijn, W. H., An analysis of Eemian climate in western and central Europe, *Quat. Sci. Rev.*, *15*, 451–469, 1996.

Chapter 6

Synthesis

6.1 Summary

The aim of the present study was to render an integrated approach through a combined model-data investigation. For the understanding of processes that have caused long-term natural climate variability a concomitant analysis of general circulation model (GCM) results and recent geological palaeoclimatic data have been performed, with a special focus on the Eemian (125 kyr ago), the last glacial maximum (21 kyr ago, LGM), and the Holocene (here, the last 7 kyr) periods. Here, the questions raised in the introduction (Chapter 1) are summarised together with the findings of this thesis.

The tropical climate of the LGM has been investigated with a series of atmospheric GCM simulations using the ECHAM model. By varying the main lower boundary condition for ECHAM (sea surface temperatures, SST), the vertical structure of the simulated atmosphere has been analysed in detail to decide which simulation provides for the best match in terms of a consistent picture of the LGM climate, and to explain the apparent mismatch between tropical SST and temperature at the snowline level derived from tropical glacier moraines during the LGM.

(1) *What is the most probable scenario for tropical air temperatures at sea level in coexistence with those at the level of the tropical snowline? How can the inconsistency between tropical SST and air temperature at the snowline be explained?*

One of the ECHAM simulations of the LGM climate utilised as boundary condition the SST reconstruction by CLIMAP (Climate: Long-Range Investigation, Mapping, and Prediction) [*CLIMAP Project Members*, 1981] with an additional cooling of 3 K (Kelvin) in the tropical oceans, corroborated by recent findings of colder tropical LGM temperatures (for a summary see [*Crowley*, 2000a; *Mix et al.*, 2001]). The simulation with imposed tropical cooling provides for the most consistent picture of the LGM climate with respect to (1) reconstructed minimum temperatures by pollen assemblages [*Farrera et al.*, 1999], (2) hydrological cycle and annual mean continental temperatures [*Lohmann and Lorenz*, 2000; *Kohfeld and Harrison*, 2000], and tropical snowlines [*Lorenz and Lohmann*, 2006]. This experiment leads to the best match of surface temperatures with the anticipated cooling of more than 6 K at the zero-degree level due to the lowering of the snowline of about 900 m. Moreover, the simulated air temperature near

the ground at the height of the tropical snowline ($\sim$ 5,000 m) is particularly colder (12 K colder than today, Figure 2.11b, p. 43) than for the experiment using the CLIMAP SST (4.5 K colder than today).

This result can be explained by two characteristics detected from the model: (1) The free atmosphere in the experiment with lower tropical SST exhibits a stronger lapse rate due to decreased water vapour content; (2) in the tropical mountains, a longer duration of snow cover raises the annual mean albedo, which induces a further reduction of surface temperature. The simulations exhibit an image of the atmospheric circulation during LGM where a tropical snowline lowering by 900 m [*Porter*, 2001] and isotopic measurements from tropical mountain glaciers [*Thompson et al.*, 1995] are in sound concordance with glacial SSTs that are comparable with recent updates of the CLIMAP reconstruction [e. g., *Lee and Slowey*, 1999; *Hostetler and Mix*, 1999].

For an assessment of the impact of the Earth's orbital parameters on the evolution of long-term climate trends in the late Quaternary, millennial-scale palaeoclimate simulations are necessary. A novel method for accelerating the orbitally driven insolation forcing [*Lorenz and Lohmann*, 2004] has been applied to an atmosphere-ocean GCM (AOGCM), the ECHAM4 atmospheric GCM coupled to the global ocean model HOPE-G (ECHO-G) [*Legutke and Voss*, 1999]. Thus, surface ocean and air temperatures can be simulated independently from proxy-derived SST. In an integrated approach, surface temperature trends over the last 7 kyr have been evaluated on the one hand from ensemble transient simulations (six members) using the ECHO-G model and on the other hand from alkenone-derived SST estimates [*Lorenz et al.*, 2006]. Furthermore, an ensemble integration with three members has been conducted spanning the time period from 140 kyr to 110 kyr ago, including the Eemian interglacial and the transition into the onset of the last glaciation ($\sim$115 kyr).

(2) *How does the orbitally driven insolation forcing affect the long-term climate trends from the middle to the late Holocene? Are changes in the seasonal cycle of insolation reflected in Holocene and Eemian proxy data?*

The comparison of the Holocene simulation results with reconstructed SST trends, derived from the alkenone-method, exhibits general concordance with a cooling of up to 3 K, predominantly in northern high latitudes, and minor warming in low latitudes during the last 7 kyr. These surface temperature trends are driven to a large extent by the astronomical insolation signal. The northern high-latitude cooling trend is directly linked to the decreasing boreal summer insolation, whereas the tropical warming is associated with the boreal winter warming during the middle to late Holocene. On an annual mean basis, however, the magnitude of simulated trends is generally smaller compared to that of alkenone-derived SSTs.

When analysing the simulated Holocene trends of the warmest month during the year (local summer, Figure 4.6a, p. 93), there is a much better agreement in sign and amplitude with the alkenone-derived SST trends in the North Atlantic and Mediterranean area (1–3 K cooling). This can be taken as an important argument that alkenone-derived temperature signals in the northern extra-tropics are more likely to stem from summer conditions than to reflect annual

mean temperature. Furthermore, the Holocene shift of the maximum tropical insolation could have influenced the timing of coccolithophorid production, and thus the trend pattern in the alkenone-derived SST data.

Enhanced seasonality was recorded in the Red Sea coral stemming from the Eemian period and is confirmed by the seasonal cycle of SST of the respective region, as simulated by the ECHO-G model (Figure 5.3d, e, p. 111). In contrast, the late Holocene coral (2.9 kyr ago) revealed a similar seasonality as was found in a modern coral from this area, which is in line with the simulated temperature cycle by ECHO-G (Figure 5.3a-c) [*Felis et al.*, 2004]. This result can be directly linked to the enhanced seasonal cycle of insolation during the Eemian period, while the insolation in the late Holocene is comparable to today (Figure 1.1.5).

(3) *In what way are regional temperatures of the Eemian and Holocene periods governed by changes in atmospheric circulation patterns?*

During the middle to late Holocene, an orbitally driven decrease in the boreal winter sea level pressure difference between the Icelandic low and the subtropical high by 2-3 hPa (Figure 4.8, p. 96) is detected. This is attributed to a continuous weakening of the AO/NAO circulation mode. The weakening of this mode is associated with reduced westerly winter winds over Europe that are replaced by more southward cold winds from the Arctic and more northward flowing warm air in the eastern Mediterranean region (Figure 4.7). This results in a characteristic dipole temperature structure, with cooling over Europe and warming in the subtropics, mainly in the eastern Mediterranean Sea and the Red Sea, that is reflected in the distribution of alkenone-derived SST.

In turn, during the Eemian period, when eccentricity was high and the precessional cycle caused reduced subtropical winter insolation, a prevalent circulation with a related high index AO/NAO-like pattern is found: strong westerly winds advect marine air and lead to warm European winters as recorded in proxy data [e. g., *Aalbersberg and Litt*, 1998; *Klotz et al.*, 2003]. Furthermore, the simulated AO/NAO-index follows the precessional signal with the characteristic $\sim$20 kyr period (Figure 6.1), a strong indication for the orbital influence on atmospheric circulation in the coupled GCM.

In the southeast of Europe, enhanced winter cooling in the Eemian period as well as moderate cooling in the middle Holocene, as detected in the simulations (Figure 5.4a, c), is validated by the two fossil corals from the Northern Red Sea [*Felis et al.*, 2004]. In the north of Europe, reduced Arctic sea ice extent is evident during the high index phase of the AO/NAO circulation mode, but less pronounced during the middle Holocene (6 kyr ago). This is corroborated by results from a comparison study using a regional North Atlantic ocean model [*Lohmann et al.*, 2005].

6.2 Perspectives

When using an atmospheric GCM for simulating palaeoclimates, modellers have to rely on reconstructed palaeoclimate distribution of SST as a lower boundary condition for these models, such as

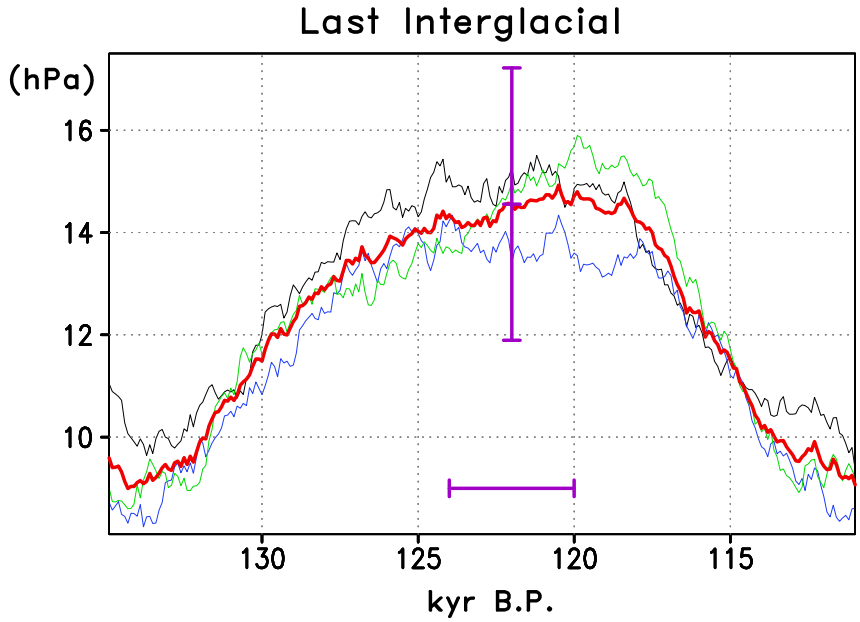

Figure 6.1: *Evolution of the pressure index as a measure for the AO/NAO-like circulation pattern in the ECHO-G model for the last interglacial period to the onset of the last glaciation (135 to 110 kyr BP) using accelerated orbital parameters. The AO/NAO index is defined as the sea level pressure difference (December, January, February; DJF) between a southerly high pressure region and a northerly low pressure region (see Figure 5.6 for definition of index regions). A centred 41 year running mean for each of the three individual ensemble members has been applied (thin lines). The thick red line displays the ensemble mean. The average and mean standard deviation for 41 winters are marked by the horizontal and vertical bars (see Section 5.3).*

the CLIMAP reconstruction. Modelling results can then be considered as a consistency test between marine and terrestrial geological data, because the terrestrial climate is generated independently by the model. In the case of simulating the LGM climate, atmospheric model results strongly depend on the CLIMAP reconstruction, at least for the Pacific and Indian Oceans, since no updated data set for these basins exist. The recently derived new collection of glacial SST by the Glacial Atlantic Ocean Mapping Project (GLAMAP) [*Mix*, 2003; *Sarnthein et al.*, 2003] is limited to the Atlantic Ocean. Apart from polar latitudes where the sea ice margin is significantly altered, the differences to CLIMAP are on average relatively small and affect more local gradients than basin-wide temperatures. In the tropical Atlantic between 30°N and 30°S, the LGM temperature difference to today was –1.7 K according to CLIMAP and –2.2 K according to GLAMAP (see Figure 2.1), which is only a minor cooling compared to the imposed cooling of 3 K that was used in the experiment `LGM.N` (Chapter 2). Since the tropical Indo-Pacific basins cover more than two thirds of the world's tropical oceans, a moderate change of the Atlantic SST according to GLAMAP has only a minor effect on zonally averaged tropical lapse rates (Figure 2.8).

A simulation using the GLAMAP SSTs for the Atlantic and the imposed 3 K cooling for the Indo-Pacific basin is missing. This combination of modified reconstructions could be expected to reveal a more suitable worldwide distribution of SST for the LGM in concordance with updated tropical Pacific temperatures [*Lee and Slowey*, 1999; *Hostetler and Mix*, 1999] than the combined GLAMAP/CLIMAP with the large areas of subtropical warming in the Pacific (see Figure 1.2). Nev-

ertheless, the up-to-date GLAMAP reconstruction of SST and sea ice distribution in the whole Atlantic Ocean is an important step in understanding the LGM climate in this area. Moreover, it is a new basis for modelling the glacial climate in particular in the Atlantic-European sector using atmospheric and oceanic GCMs.

When investigating the LGM climate (Chapter 2), no ocean model was involved and the ocean influence was mimicked by varying the lower boundary condition for the model, the SST. Other studies have used the combined GLAMAP/CLIMAP SST reconstruction as well as wind stress and freshwater fields as boundary conditions for ocean models, calculated by the discussed experiments. Using the large scale geostrophic (LSG) oceanic GCM, *Romanova et al.* [2004] as well as *Butzin et al.* [2005] prescribed SST, wind stress and freshwater fields according to the different ECHAM simulations that were subject to Chapter 2. These authors found reduced meridional overturning circulation (MOC) in the Atlantic when using boundary conditions of experiment `LGM.N` (CLIMAP, imposed tropical cooling) and enhanced MOC when using those of experiment `LGM.G` (GLAMAP/CLIMAP SST distribution). A regional modelling study of the glacial water masses of the Atlantic Ocean using the MOM2 ocean model [*Paul and Schäfer-Neth*, 2003], revealed a similar result in terms of enhanced Atlantic MOC compared to the control experiment when using GLAMAP SST and wind forcing of experiment `LGM.G` as boundary condition. Increased northward heat transport in the Atlantic is also reported for these model studies forced by GLAMAP. This is consistent with the northward displacement of the summer and winter North Atlantic sea ice margins in the GLAMAP reconstruction compared to CLIMAP. Moreover, it was stated that ocean simulations are strongly dependent on other relatively uncertain glacial boundary conditions for ocean models, in particular surface salinity and wind stress [*Winguth et al.*, 1999; *Paul and Schäfer-Neth*, 2003; *Mix*, 2003; *Wunsch*, 2003; *Romanova et al.*, 2004; *Butzin et al.*, 2005]. In a study by *Winguth et al.* [1999], a series of sensitivity experiments using the LSG model including an ocean carbon cycle model corroborated the strong sensitivity of the MOC on wind and freshwater forcing. These authors concluded that the circulation strength remains an open question, because palaeonutrient tracer distributions could be consistent with a much stronger, as well as a near-shutdown of the Atlantic deep ocean circulation.

In order to overcome the strong dependency of atmospheric and oceanic GCMs on surface boundary conditions at the atmosphere-ocean interface, coupled GCMs have been used for simulating glacial climates [e. g., *Weaver et al.*, 1998; *Bush and Philander*, 1998; *Kim et al.*, 2002]. This renders possible a comparison of independently modelled SST distributions with the recent reconstructions. However, the modelling results for the LGM have been critically challenged due to contradictory temperature as well as ocean circulation characteristics. The results show strongly differing SST in large parts of the major ocean basins: For example, in the subtropical Pacific, warmer [*Kitoh and Murakami*, 2002], moderately cooler [*Bush and Philander*, 1998; *Hewitt et al.*, 2003; *Shin et al.*, 2003], and much colder [*Kim et al.*, 2002, 2003] temperatures than today have been simulated. When summarising results of the Paleoclimate Modeling Intercomparison Project (PMIP) [*Joussaume and Taylor*, 2000], it was concluded that none of the AOGCM experiments with computed SST revealed tropical ocean temperatures during the LGM as high as suggested by CLIMAP. Seven of nine simulations resulted in lower glacial ocean temperatures than today [*Pinot et al.*, 1999]. Distribution of glacial SST, in particular in the subtropical Pacific, is still an interesting open issue that could not yet be reasonably

answered [e. g., *Crowley*, 2000a; *Timmermann et al.*, 2004]. Neither proxy data from different sources [*Lee and Slowey*, 1999; *Hostetler and Mix*, 1999; *Mix et al.*, 2001; *Henderson*, 2002] nor summarising independent simulations have led to a general consensus so far [e. g., *Liu et al.*, 2000; *Timmermann et al.*, 2004].

Palaeoclimatic modelling studies, aimed at reconstructing past climate states such as the LGM and the last interglacial, are usually performed on the basis of time slices. However, the modelling of time slices cannot provide insights into the temporal evolution of the climate system. Since complex GCMs are restricted by computer resources, models of intermediate complexity have been used for transient simulations of glacial and Holocene periods [*Berger et al.*, 1990; *Stocker et al.*, 1992; *Ganopolski and Rahmstorf*, 2001; *Schmittner et al.*, 2002; *Crucifix et al.*, 2002; *Weber et al.*, 2004; *Renssen et al.*, 2005], where the complexity of sub-models is reduced. For example, internal atmospheric variability is statistically prescribed or parameterised instead of resolving it explicitly [*Claussen et al.*, 2002]. This strategy allows for longer simulation times as well as a detailed analysis of several feedback processes by switching on and off the effect of different climatic components [*Ganopolski et al.*, 1998]. In this thesis another approach is followed: applying the acceleration technique for the orbitally driven insolation changes into the ECHO-G model enabled ensemble integrations of the long-term evolution of the Eemian and the Holocene interglacials with this complex model.

However, using this technique does not provide for adequate consideration of the long-term evolution or abrupt shifts of the MOC, because its timescale is too long (about 1,000 years) to be in equilibrium with the artificially accelerated orbital forcing. In the marine geological record no evidence for strong changes in the deep ocean circulation during interglacial periods can be found, when glacial ice caps were absent, such as the middle to late Holocene [*Grootes et al.*, 1993; *Clark et al.*, 2002] and the Eemian interglacial [*Hillaire-Marcel et al.*, 2001; *Kukla et al.*, 2002]. The astronomical forcing could effect changes in the location and strength of convection sites. During interglacials though, ocean circulation changes might be of minor importance, without global impact. The Holocene experiments, using different acceleration factors, exhibit no significant changes in the MOC in the multi-decadal as well as in the centennial simulations (Figure 3.5). This confirms the prerequisite that the ocean circulation was relatively stable during the respective period and thus the orbital insolation forcing is responsible for the major part of the global-scale alkenone-derived Holocene SST trends. Consistently, the changes in the deep ocean circulation during the Eemian were only minor when simulating a quasi-equilibrium response of the coupled ECHAM1/LSG model to adjusted orbital and CO_2 boundary conditions [*Montoya et al.*, 2000].

The modelling studies discussed in this thesis lack important components of the climate system: modules for the dynamic evolution of (1) vegetation and (2) continental ice caps under changing boundary conditions as well as their related feedback on the climate. For the glacial simulations with the ECHAM3 as well as for the transient simulations with the ECHO-G model, the parameters for the terrestrial biosphere (albedo, vegetation ratio, leaf area index, etc.) were prescribed to modern values, apart from the LGM ice caps. The vegetation-climate feedback can significantly alter the response to external forcing via nonlinear mechanisms: (1) the taiga–tundra feedback, controlled via the winter albedo [*Brovkin et al.*, 2003], and similarly, the sea ice–snow cover–albedo feedback [*Lohmann et al.*, 2005]; (2) the desertification through a weakening of the hydrological cycle [*Zeng et al.*, 1999]; (3)

sustainment or extinction of tropical rainforest controlled by moisture availability (partly via deep root vegetation [*Kleidon and Lorenz*, 2001]); and (4) continental-scale amplification via influencing subtropical monsoon variability [*Braconnot et al.*, 2002]. *Ganopolski et al.* [1998] have demonstrated that responses of atmosphere, ocean, and vegetation components to changing boundary conditions do not sum up to a combined response, but result in a strong nonlinear behaviour.

Furthermore, the transient simulations around the Eemian period (140 to 110 kyr ago) should not be regarded as a detailed simulation of the last interglacial period, because the dynamic evolution of the continental ice caps is not accounted for. A dynamic land-ice module would be essential for the sound modelling of climate transitions such as a deglaciation as well as the onset of the last glaciation at about 115 kyr ago. Moreover, an additional change in the greenhouse gas concentrations, as recorded in the Vostok ice core [*Petit et al.*, 1999] (see Figure 1.1), could help to initiate ice accumulation on the continents of the Northern Hemisphere. The interglacial simulations with the ECHO-G model are considered as a sensitivity study to test the effect of a changing insolation cycle on the coupled atmosphere-ocean system.

For the first time, an AOGCM could be launched for the investigation of the multi-millennial effect of orbital forcing on climate by applying the acceleration technique to the ECHO-G model. This provides for effects of changes in the entire seasonal cycle on the atmosphere-ocean system. The orbital insolation change in the order of 100 Wm^{-2} is a dominant factor in triggering climate change during the Quaternary [*Imbrie et al.*, 1992]. The insolation anomaly during the LGM, which was also regarded in the LGM experiments of Chapter 2, is only minor (Figure 1.8). But this is important, because it is unlikely that the maximum glaciation occurs during a period with enhanced boreal summer insolation, therewith favouring ice melting. The influence of orbitally driven insolation changes was formerly often related to boreal summer insolation. Mid-June insolation at high latitudes was regarded to be the predominant pacemaker of long-term climate changes by affecting the Northern Hemisphere continents and their ice caps [*Milankovič*, 1941; *Hays et al.*, 1976; *Imbrie et al.*, 1992, 1993]. In the transient ECHO-G simulations, summer insolation directly drives surface temperature trends in the high northern latitudes. Specifically in the tropics, the winter insolation is important for climate change, presumably by affecting tropical-extratropical teleconnection patterns. These results could supplement the previous findings of the effect of boreal summer insolation on palaeoclimate change: the comparison of the GCM experiments with coral and alkenone data suggests that the climate transitions during the last glacial cycle are to a large part affected by nonlinear changes in the entire seasonal cycle of insolation.

The strong impact of the orbital insolation forcing on the AO/NAO index during the period with enhanced eccentricity (see Figure 1.6) is depicted in Figure 6.1: The subtropical minus high-latitude Atlantic pressure difference (index areas are marked in Figure 5.6) is varied by more than 6 hPa. A high AO/NAO index (warm European and cold Middle Eastern winters) occurred during the Eemian. The lowest index values are found after 115 kyr ago, which could probably influence the build-up of a European continental ice cap. A possible link between tropical insolation and the AO/NAO via atmospheric circulation changes needs further evaluation. The long-term model simulations depict a strong correlation between a positive phase of the AO/NAO-index and decreased atmospheric convection in the central tropical Pacific corresponding with the winter insolation at the equator [*Lohmann*

and Lorenz, 2006]. This is complementary to recent studies: *Kucharski et al.* [2006] evaluated the observed correlation between the NAO-index and the N-S temperature gradient in the western Pacific tropical warm pool. The mechanisms behind this link are in debate and no consensus has yet been found [*Kucharski et al.*, 2006; *Hoerling et al.*, 2001].

Apart from the astronomical forcing, the variation of the Sun's output into space and severe volcanic eruptions represent other external driving mechanisms for the Quaternary climate, which are not taken into account in the model simulations of this thesis. The insolation forcing due to solar variability is several orders of magnitude smaller than the differences in the seasonal cycle due to the orbital parameters. Satellite-based measurements over the last two decades indicate solar irradiance cycles with 11 years length and 0.1% amplitude [*Beer et al.*, 2000]. Estimates of the strength of the solar output forcing [*Lean and Rind*, 1998; *Beer et al.*, 2000; *Crowley*, 2000b] and model simulations investigating this effect on the historical climate are available [e. g., *Cubasch et al.*, 1997; *Shindell et al.*, 2003]. Changes in the radiation balance in the atmosphere due to atmospheric dust loads and chemical processes induced by severe volcanic eruptions have influenced the Holocene climate. However, estimates of the amount of erupted debris as well as the load of chemically active gases reaching the stratosphere are not well known. Apart from recent estimates [e. g., *Solanki et al.*, 2004], assessment of both solar output variations and volcanic eruptions are more or less restricted to the last millennium [*Crowley*, 2000b].

6.3 Outlook

For the investigation of the multi-millennial effect of orbitally driven insolation changes on climate, transient ensemble simulations of palaeoclimates have been performed utilising a coupled AOGCM, the ECHO-G model. Surface temperature trends, in the annual mean as well as for the different seasons, could be calculated and compared with proxy data. As an extension of this physical approach, a next step could be the direct simulation of the biogeophysical generation of proxy data, such as simulation of sedimentation rates [*Heinze et al.*, 1999] in a changing palaeoclimate. For this purpose, AOGCM results are essential for providing the necessary palaeoenvironmental boundary conditions. The production of coccolithophorids and therewith the alkenone flux to sediments varies during the annual cycle. The seasonal timing of production could have changed under extreme climate conditions. *Müller et al.* [1998] estimated that regional variations in the seasonality of primary production have only a minor effect on the alkenone-derived temperature. However, other studies [*Sachs et al.*, 2000; *Bard*, 2001] summarise arguments that could possibly bias an SST time series, e. g. by a shift in the growing of the main alkenone producers from late spring to early summer under extreme cold conditions [*Bard*, 2001]. The biogeophysical simulation of organic rain to the deep sea floor and seasonal production changes according to palaeoclimate transitions could help to assess how such a climate transition in the upper ocean is recorded in the alkenone unsaturation index.

To properly address the question of anthropogenic influence on climate, it is necessary to test the results of AOGCMs beyond the industrial period when the anthropogenic influence is absent. During the last years the discussion of a potential long-term cooling trend of the last millennium was initiated by the statistical evaluation of mainly tree-ring records in comparison with the instrumental tempera-

ture record by *Mann et al.* [1998, 1999], recently extended to cover the last two millennia [*Mann and Jones*, 2003; *Moberg et al.*, 2005]. Interpretation of ECHO-G model results, driven by solar output changes and solar radiation decrease due to volcanic dust loads in the atmosphere [*González-Rouco et al.*, 2003; *von Storch et al.*, 2004] according to the collection of forcing data by *Crowley* [2000b], suggests that a large part of the reconstructed variability of the last millennium is the result of a response to these radiative changes [*Moberg et al.*, 2005].

A comparison of the simulated temperature trends driven by the changing Earth's orbit during the last 7 kyr with the ones forced by increasing greenhouse gases (CO_2, CH_4, N_2O, and the most prominent CFCs) during the last 200 years reveals that a Northern Hemisphere cooling trend over the last 7 kyr during summer ($\sim$0.6 K, Figure 3.11) is exceeded by the simulated warming trend during the last century ($\sim$0.9 K). The annual mean cooling trend is even smaller (0.2-0.4 K over the last 7 kyr). In comparison with the estimated millennium trend by *Mann et al.* [1999] (0.4 K during 1 kyr), the ECHO-G experiments [*Lorenz and Lohmann*, 2004] exhibit an orbitally driven long-term Holocene background cooling of the Northern Hemisphere that is about one order of magnitude weaker However, when such studies are extended back to several millennia, the orbitally driven insolation forcing should be considered in estimating natural climate variability, in particular when investigating seasonal temperature changes.

For the simulation of the next centuries, existing data sets have to be collected to determine the expected natural and anthropogenic forcing. Emissions of greenhouse gases and aerosols can be applied according to the Special Report on Emissions Scenarios [*SRES*, 2000]. As far as possible, such simulations should include future projections of natural forcing, i. e. probability of volcanic eruptions [*Hyde and Crowley*, 2000] as well as periodic continuation of solar cycles [*Beer et al.*, 2000]. These experiments could quantitatively examine the climate change for the last 6,000 years before, and the next 1,000 years beyond the present. This approach would lead GCM-based research into investigation of long-term (after 2100 AD, which is beyond the near future as envisaged by the *Intergovernmental Panel on Climate Change* [2001]) impacts on climate, influenced by the anthropogenic increase of greenhouse gases. The analysis of a model experiment covering the Holocene, including the recent period of anthropogenic greenhouse warming and the simulation of the future millennium, enables the comparison of climate variability under natural and anthropogenic conditions. Such an approach has never been accomplished before. This could help to understand the mechanisms of natural climate variability and man-made climate change and, furthermore, can help to improve the predictability of the climate in the mid-term future.

6.4 References

Aalbersberg, G., and T. Litt, Multiproxy climate reconstructions for the Eemian and early Weichselian, *J. Quat. Sci.*, *13*, 367–390, 1998.

Bard, E., Comparison of alkenone estimates with other paleotemperature proxies, *Geochemistry Geophysics Geosystems*, *2*, doi:2000GC000,050, 2001.

Beer, J., W. Mende, and R. Stellmacher, The role of the sun in climate forcing, *Quaternary Science Reviews*, *19*, 403–415, 2000.

Berger, A. L., H. Gallée, T. Fichefet, I. Marsiat, and C. Tricot, Testing the astronomical theory with a coupled climate-ice-sheet model, *Palaeogeography Palaeoclimatology Palaeoecology*, *89*, 125–141, 1990.

Braconnot, P., M.-F. Loutre, B. Dong, S. Joussaume, P. Valdes, and PMIP participating groups, How the simulated change in monsoon at 6 ka BP is related to the simulation of the modern climate: results from the Paleoclimate Modeling Intercomparison Project, *Climate Dynamics*, *19*, 107–121, 2002.

Brovkin, V., S. Levis, M.-F. Loutre, M. C. M. C. A. Ganopolski, C. Kubatzki, and V. Petoukhov, Stability analysis of the climate-vegetation system in the northern high latitudes, *Climatic Change*, *57*, 119–138, 2003.

Bush, A. B. G., and S. G. H. Philander, The role of ocean-atmosphere interactions in tropical cooling during the Last Glacial Maximum, *Science*, *279*, 1341–1344, 1998.

Butzin, M., M. Prange, and G. Lohmann, Radiocarbon simulations for the glacial ocean: the effects of wind stress, Southern Ocean sea ice and Heinrich events, *Earth and Planetary Science Letters*, *235*, 45–61, 2005.

Clark, P. U., N. G. Pisias, T. F. Stocker, and A. J. Weaver, The role of thermohaline circulation in abrupt climate change, *Nature*, *415*, 863–869, 2002.

Claussen, M., L. A. Mysak, A. J. Weaver, M. Crucifix, T. Fichefet, M.-F. Loutre, S. L. Weber, J. Alcamo, V. A. Alexeev, A. Berger, R. Calov, A. Ganopolski, H. Goosse, G. Lohmann, F. Lunkeit, I. I. Mokhov, V. Petoukhov, P. Stone, and Z. Wang, Earth system models of intermediate complexity: Closing the gap in the spectrum of climate system models, *Climate Dynamics*, *18*, 579–586, 2002.

CLIMAP Project Members, Seasonal reconstructions of the Earth surface at the last glacial maximum, *GSA Map and Chart Ser. MC-36*, Geol. Soc. Am., Boulder, Colorado, 1981.

Crowley, T. J., CLIMAP SSTs re-revisited, *Climate Dynamics*, *16*, 241–255, 2000a.

Crowley, T. J., Causes of climate change over the past 1000 years, *Science*, *289*, 270–277, 2000b.

Crucifix, M., M.-F. Loutre, P. Tulkens, T. Fichefet, and A. Berger, Climate evolution during the Holocene: a study with an Earth system model of intermediate complexity, *Climate Dynamics*, *19*, 43–60, 2002.

Cubasch, U., R. Voss, G. C. Hegerl, and J. W. und Thomas J. Crowley, Simulation of the influence of solar radiation variations on the global climate with an ocean-atmosphere general circulation model, *Climate Dynamics*, *13*, 757–767, 1997.

Farrera, I., S. Harrison, I. Prentice, G. Ramstein, J. Guiot, P. Bartlein, R. Bonnefille, M. Bush, U. von Grafenstein, K. Holmgren, H. Hooghiemstra, G. Hope, D. Jolly, S.-E. Lauritzen, Y. Ono, S. Pinot, M. Stute, and G. Yu, Tropical climates at the last glacial maximum: a new synthesis of terrestrial palaeoclimate data. 1. Vegetation, lake-levels and geochemistry, *Climate Dynamics*, *12*, 823–856, 1999.

Felis, T., G. Lohmann, H. Kuhnert, S. J. Lorenz, D. Scholz, J. Pätzold, S. A. Al-Rousan, and S. M. Al-Moghrabi, Increased seasonality in Middle East temperatures during the last interglacial period, *Nature*, *429*, 164–168, 2004.

Ganopolski, A., and S. Rahmstorf, Rapid changes of glacial climate simulated in a coupled climate model, *Nature*, *409*, 153–158, 2001.

Ganopolski, A., C. Kubatzki, M. Claussen, V. Brovkin, and V. Petoukhov, The influence of vegetation-atmosphere-ocean interaction on climate during the mid-Holocene, *Science*, *280*, 1916–1919, 1998.

González-Rouco, J. F., H. von Storch, and E. Zorita, Deep soil temperature as a proxy for surface air-temperature in a coupled model simulation of the last thousand years, *Geophysical Research Letters*, *30*, 2116, 2003.

Grootes, P. M., M. Stuiver, J. W. C. White, S. J. Johnsen, and J. Jouzel, Comparison of oxygen isotope records from the GISP2 and GRIP Greenland ice cores, *Nature*, *366*, 552–554, 1993.

Hays, J. D., J. Imbrie, and N. J. Shackleton, Variations in the Earth's orbit: pacemaker of the ice ages, *Science*,

194, 1121–1132, 1976.

Heinze, C., E. Maier-Reimer, A. M. E. Winguth, and D. Archer, A global oceanic sediment model for long-term climate studies, *Global Biogeochemical Cycles*, *13*, 221–250, 1999.

Henderson, G. M., New oceanic proxies for paleoclimate, *Earth and Planetary Science Letters*, *203*, 1–13, 2002.

Hewitt, C. D., R. J. Stouffer, A. J. Broccoli, J. F. B. Mitchell, and P. J. Valdes, The effect of ocean dynamics in a coupled GCM simulation of the last glacial maximum, *Climate Dynamics*, *20*, 203–218, 2003.

Hillaire-Marcel, C., A. de Vernal, G. Bilodeau, and A. J. Weaver, Absence of deep-water formation in the Labrador Sea during the last interglacial period, *Nature*, *410*, 1073–1077, 2001.

Hoerling, M. P., J. W. Hurrell, and T. Xu, Tropical origins for recent North Atlantic climate change, *Science*, *292*, 90–92, 2001.

Hostetler, S. W., and A. C. Mix, Reassessment of ice-age cooling of the tropical ocean and atmosphere, *Nature*, *399*, 673–676, 1999.

Hyde, W. T., and T. J. Crowley, Probability of future climatically significant volcanic eruptions, *Journal of Climate*, *14*, 1445–1450, 2000.

Imbrie, J., E. A. Boyle, S. C. Clemens, A. Duffy, W. R. Howard, G. Kukla, J. E. Kutzbach, D. G. Martinson, A. McIntyre, A. C. Mix, B. Molfino, J. J. Morley, L. C. Peterson, N. G. Pisias, W. L. Prell, M. E. Raymo, N. J. Shackleton, and J. R. Toggweiler, On the structure and origin of major glaciation cycles: 1. linear responses to Milankovitch forcing, *Paleoceanography*, *7*, 701–738, 1992.

Imbrie, J., A. Berger, E. A. Boyle, S. C. Clemens, A. Duffy, W. R. Howard, G. Kukla, J. E. Kutzbach, D. G. Martinson, A. McIntyre, A. C. Mix, B. Molfino, J. J. Morley, L. C. Peterson, N. G. Pisias, W. L. Prell, M. E. Raymo, N. J. Shackleton, and J. R. Toggweiler, On the structure and origin of major glaciation cycles: 2. the 100,000-year cycle, *Paleoceanography*, *8*, 699–735, 1993.

Intergovernmental Panel on Climate Change, *Climate Change 2001: The Scientific Basis: Contribution of Working Group I to the Third Assessment Report of the IPCC*, edited by J. T. Houghton et al., Cambridge University Press, Cambridge, UK, 2001.

Joussaume, S., and K. E. Taylor, The Paleoclimate Modeling Intercomparison Project, in *Paleoclimate Modeling Intercomparison Project (PMIP): proceedings of the third PMIP workshop, Canada, 4-8 October 1999*, edited by P. Braconnot, WCRP-111, WMO/TD-1007, pp. 9–24, World Meteorological Organization, 2000.

Kim, S.-J., G. M. Flato, G. J. Boer, and N. McFarlane, A coupled climate model simulation of the Last Glacial Maximum, Part 1: transient multi-decadal response, *Climate Dynamics*, *19*, 515–537, 2002.

Kim, S.-J., G. M. Flato, and G. J. Boer, A couple climate model simulation of the Last Glacial Maximum, Part 2: approach to equilibrium, *Climate Dynamics*, *20*, 635–661, 2003.

Kitoh, A., and S. Murakami, Tropical Pacific climate at the mid-Holocene and the Last Glacial Maximum simulated by a coupled atmosphere-ocean general circulation model, *Paleoceanography*, *17*, doi:10.1029/2001PA000,724, 2002.

Kleidon, A., and S. J. Lorenz, Deep roots sustain Amazonian rainforest in climate model simulations of the last ice age, *Geophysical Research Letters*, *28*, 2425–2428, 2001.

Klotz, S., J. Guiot, and V. Mosbrugger, Continental European Eemian and early Würmian climate evolution: comparing signals using different quantitative reconstruction approaches based on pollen, *Global and Planetary Change*, *36*, 277–294, 2003.

Kohfeld, K., and S. P. Harrison, How well can we simulate past climates? Evaluating the models using global palaeoenvironmental data sets, *Quaternary Science Reviews*, *19*, 321–346, 2000.

Kucharski, F., F. Molteni, and A. Bracco, Decadal interactions between the western tropical Pacific and the

North Atlantic Oscillation, *Climate Dynamics*, *26*, 79–91, 2006.

Kukla, G. J., M. L. Bende, J.-L. de Beaulie, G. Bon, W. S. Broecke, P. Clevering, J. E. Gavi, T. D. Herber, and J. Imbri and J. Jouzel et al., Last interglacial climates, *Quaternary Research*, *58*, 2–13, 2002.

Lean, J., and D. Rind, Climate forcing by changing solar radiation, *Journal of Climate*, *11*, 3069–3094, 1998.

Lee, K. E., and N. C. Slowey, Cool surface waters of the subtropical North Pacic Ocean during the last glacial, *Nature*, *397*, 512–514, 1999.

Legutke, S., and R. Voss, The Hamburg atmosphere-ocean coupled circulation model ECHO-G, *Technical Report 18*, Deutsches Klimarechenzentrum, Hamburg, Germany, 1999.

Liu, Z., S. Shin, P. Behling, W. Prell, M. Trend-Staid, S. P. Harrison, and J. E. Kutzbach, Dynamical and observational constraints on tropical Pacific sea surface temperature at the last glacial maximum, *Geophysical Research Letters*, *27*, 105–108, 2000.

Lohmann, G., and S. J. Lorenz, The hydrological cycle under paleoclimatic conditions as derived from AGCM simulations, *Journal of Geophysical Research*, *105*, 17,417–17,436, 2000.

Lohmann, G., and S. J. Lorenz, Orbital forcing on atmospheric dynamics during the last interglacial and glacial inception, in *The climate of past interglacials*, edited by F. Sirocko, T. Litt, M. Claussen, and F. Sanchez-Goni, Development in Paleoenvironmental Research, Elsevier, accepted, Berlin, 2006.

Lohmann, G., S. J. Lorenz, and M. Prange, Northern high-latitude climate changes during the Holocene as simulated by circulation models, in *The Nordic Seas: An Integrated Perspective*, edited by H. Drange, T. Dokken, T. Furevik, R. Gerdes, and W. Berger, no. 158 in Geophys. Monogr., pp. 273–288, American Geophysical Union, Washington DC, 2005.

Lorenz, S. J., and G. Lohmann, Acceleration technique for Milankovitch type forcing in a coupled atmosphere-ocean circulation model: method and application for the Holocene, *Climate Dynamics*, *23*, 727–743, 2004.

Lorenz, S. J., and G. Lohmann, On a critical reassessment of glacial snow lines with tropical sea surface temperatures, *Geochemistry Geophysics Geosystems*, *submitted, revised form*, 2006.

Lorenz, S. J., J.-H. Kim, N. Rimbu, R. R. Schneider, and G. Lohmann, Orbitally driven insolation forcing on Holocene climate trends: evidence from alkenone records and climate modeling, *Paleoceanography*, *21*, PA1002, 2006.

Mann, M. E., and P. D. Jones, Global surface temperatures over the past two millennia, *Geophysical Research Letters*, *30*, doi:10.1029/2003GL017,814, 2003.

Mann, M. E., R. S. Bradley, and M. K. Hughes, Global-scale temperature patterns and climate forcing over the past six centuries, *Nature*, *392*, 779–787, 1998.

Mann, M. E., R. S. Bradley, and M. K. Hughes, Northern Hemisphere temperature during the past millennium: inferences, uncertainties, and limitations, *Geophysical Research Letters*, *26*, 759–762, 1999.

Milankovič, M., *Kanon der Erdbestrahlung und seine Anwendung auf das Eiszeitenproblem*, 132, Königlich Serbische Akademie, Sektion der Naturwissenschaften und der Mathematik, Spezielle Ausgabe, Belgrad, 1941.

Mix, A. C., Chilled out in the ice-age Atlantic, *Nature*, *425*, 32–33, 2003.

Mix, A. C., E. Bard, and R. Schneider, Environmental processes of the ice age: land, oceans, glaciers (EPILOG), *Quaternary Science Reviews*, *20*, 627–657, 2001.

Moberg, A., D. M. Sonechkin, K. Holmgren, N. M. Datsenko, and W. Karlén, Highly variable Northern Hemisphere temperatures reconstructed from low- and high-resolution proxy data, *Nature*, *433*, 613–617, 2005.

Montoya, M., H. von Storch, and T. J. Crowley, Climate simulation for 125 kyr BP with a coupled ocean-atmosphere general circulation model, *Journal of Climate*, *15*, 1057–1072, 2000.

Müller, P. J., G. Kirst, G. Ruhland, I. von Storch, and A. Rosell-Melé, Calibration of the alkenone palaeotemper-

ature index (UK'37) based on core-tops from the eastern South Atlantic and the global ocean (60 °N-60°S), *Geochimica et Cosmochimica Acta*, *62*, 1757–1772, 1998.

Paul, A., and C. Schäfer-Neth, Modeling the water masses of the Atlantic Ocean at the Last Glacial Maximum, *Paleoceanography*, *18*, doi:10.1029/2002PA000,783, 2003.

Petit, J. R., J. Jouzel, D. Raynaud, N. I. Barkov, J.-M. Barnola, I. Basile, M. Bender, J. Chappellaz, M. Davis, G. Delaygue, M. Delmotte, V. M. Kotlyakov, M. Legrand, V. Y. Lipenkov, C. Lorius, L. Pépin, C. Ritz, E. Saltzman, and M. Stievenard, Climate and atmospheric history of the past 420,000 years from the Vostok ice core, Antarctica, *Nature*, *399*, 429–436, 1999.

Pinot, S., G. Ramstein, S. P. Harrison, I. C. Prentice, J. Guiot, S. Joussaume, M. Stute, and PMIP participating groups, Tropical paleoclimates at the Last Glacial Maximum: comparison of paleoclimate modeling intercomparison project (PMIP) simulations and paleodata, *Climate Dynamics*, *15*, 857–874, 1999.

Porter, S. C., Snowline depression in the tropics during the last glaciation, *Quaternary Science Reviews*, *20*, 1067–1091, 2001.

Renssen, H., H. Goosse, T. Fichefet, V. Brovkin, E. Driesschaert, and F. Wolk, Simulating the holocene climate evolution at northern high latitudes using a coupled atmosphere-sea ice-ocean-vegetation model, *Climate Dynamics*, *24*, 23–43, 2005.

Romanova, V., M. Prange, and G. Lohmann, Stability of the glacial thermohaline circulation and its dependence on the background hydrological cycle, *Climate Dynamics*, *22*, 527–538, 2004.

Sachs, J. P., R. R. Schneider, T. I. Eglinton, K. H. Freeman, G. Ganssen, J. F. McManus, and D. W. Oppo, Alkenones as paleoceanographic proxies, *Geochemistry Geophysics Geosystems*, *1*, 2000GC000,059, 2000.

Sarnthein, M., R. Gersonde, H.-S. Niebler, U. Pflaumann, R. Spielhagen, J. Thiede, G. Wefer, and M. Weinelt, Overview of glacial Atlantic Ocean mapping (GLAMAP 2000), *Paleoceanography*, *18*, 2003.

Schmittner, A., M. Yoshimori, and A. J. Weaver, Instability of glacial climate in a model of the ocean-atmosphere-cryosphere system, *Science*, *295*, 1489–1493, 2002.

Shin, S.-I., Z. Liu, B. Otto-Bliesner, E. C. Brady, J. E. Kutzbach, and S. P. Harrison, A simulation of the Last Glacial Maximum climate using the NCAR-CCSM, *Climate Dynamics*, *20*, 127–151, 2003.

Shindell, D. T., G. A. Schmidt, R. L. Miller, and M. E. Mann, Volcanic and solar forcing of climate change during the preindustrial era, *Journal of Climate*, *16*, 4094–4107, 2003.

Solanki, S. K., I. G. Usoskin, B. Kromer, M. Schussler, and J. Beer, Unusual activity of the Sun during recent decades compared to the previous 11,000 years, *Nature*, *431*, 1084–1087, 2004.

SRES, *Special Report on Emission Scenarios. A special report of IPCC Working Group III*, edited by N. Nakicenovic and R. Swart, Cambridge University Press, Cambridge, UK, 2000.

Stocker, T. F., D. Wright, and L. Mysak, A zonally averaged, coupled ocean-atmosphere model for paleoclimate studies, *Journal of Climate*, *5*, 773–797, 1992.

Thompson, L., E. Mosley-Thompson, M. E. Davis, P. N. Lin, K. A. Henderson, J. Cole-Dai, J. F. Bolzai, and K.-B. Liu, Late glacial stage and Holocene tropical ice core records from Huascaran, Peru, *Science*, *269*, 46–50, 1995.

Timmermann, A., F. B. Justino, F.-F. Jin, and H. Goosse, Surface temperature control in the North and tropical Pacific during the last glacial maximum, *Climate Dynamics*, *23*, 353–370, 2004.

von Storch, H., E. Zorita, J. M. Jones, Y. Dimitriev, J. F. González-Rouco, and S. F. B. Tett, Reconstructing past climate from noisy data, *Science*, *306*, 679–682, 2004.

Weaver, A. L., M. Eby, A. F. Fanning, and E. C. Wiebe, Simulated influence of carbon dioxide, orbital forcing and ice sheets on the climate of the Last Glacial Maximum, *Nature*, *394*, 847–853, 1998.

Weber, S. L., T. Crowley, and G. van der Schrier, Solar irradiance forcing of centennial climate variability

during the Holocene, *Climate Dynamics*, *22*, 539–553, 2004.

Winguth, A., D. Archer, E. Maier-Reimer, U. Mikolajewicz, and J.-C. Duplessy, Sensitivity of the paleonutrient tracer distribution and deep-sea circulation to glacial boundary conditions, *Paleoceanography*, *14*, 304–323, 1999.

Wunsch, C., Determining paleoceanographic circulations, with emphasis on the Last Glacial Maximum, *Quaternary Science Reviews*, *22*, 371–385, 2003.

Zeng, N., J. D. Neelin, K.-M. Lau, and C. J. Tucker, Enhancement of interdecadal climate variability in the Sahel by vegetation interaction, *Science*, *286*, 1537–1540, 1999.

Appendix A

Reconstructing and Modelling the Last Glacial Maximum: Beyond CLIMAP

Abstract.

The update and extension of the CLIMAP data set - preliminarily called “CLIMAP 2000” - is discussed. Although newer data exist, CLIMAP (1981) is still the most widely used source of boundary conditions for modelling the last glacial maximum. Besides the new data, CLIMAP 2000 should also incorporate climate models to create global fields of sea surface temperatures (SSTs) and other climate parameters. Atmospheric general circulation models can be used to check the consistency of SSTs and sea ice margins with data on certain land conditions. In a similar way tracer concentrations resulting from ocean models including biogeochemical processes can be compared with marine proxy data. Coupled atmosphere-ocean models applicable to paleoclimate, which are still under development, would yield complete SST fields. The reconstruction of ice-sheets and vegetation zones can be improved by considering corresponding models. Inverse models can be used to extend sparse data sets by integrating various types of data. From this review, a three-step concept for CLIMAP 2000 is suggested and the key points of the new CLIMAP 2000 data base and maps are listed.

Coupled atmosphere-ocean modelling

Recently, coupled models of atmosphere and ocean have been developed to investigate the effect of an anthropogenic increase of greenhouse gases on the general circulation [*Meehl et al.*, 1993; *Manabe and Stouffer*, 1994; *Cubasch et al.*, 1994; *Murphy*, 1995; *Lunkeit et al.*, 1996]. Model initialization is based on stand-alone runs of the submodels which have been spun up using accurately collected modern data sets at the atmosphere-ocean interface. A typical simulation time for these climate change experiments with coupled models is 200 years.

Herterich et al., in *Use of Proxies in Paleoceanography: Examples from the South Atlantic*, S. 687-714,

Simulation of paleoclimatic states using coupled atmosphere-ocean models can be approached by two different strategies. Similar to the climate change experiments a coupled simulation of a paleoclimate can be initialized with an equilibrium circulation resulting from separate runs of the submodels. Because these results have been generated without feedback between the submodels, they are strongly dependent on our knowledge of the paleoclimatic boundary conditions at the interface, such as the CLIMAP reconstruction (cf. section "Atmospheric modelling" and "Ocean modelling" of this article). Another approach is to integrate a coupled model until a new equilibrium circulation of atmosphere and ocean is achieved. This has the potential to make boundary conditions at the interface superfluous. Driven by paleoclimatic boundary conditions far away from the ocean surface (i. e.solar radiation and land surface characteristics) coupled models should be able to derive independent sea surface data (SST, SSS).

Unfortunately, current general circulation models have two major shortcomings: (1) An atmospheric model with a time step in the range of minutes is too computation expensive to extend the length of a model run to the range of the response time of the deep ocean, which is at least 1000 years. (2) The accuracy of both atmospheric and oceanic submodels is not yet sufficient to directly couple the fluxes at the interface on such a long time scale. Small errors in the surface fluxes of both models lead to an artificial drift towards an unrealistic state of the global ocean circulation. Presently, so-called flux adjustments are used to avoid such a drift [*Sausen et al.*, 1988; *Sausen and Lunkeit*, 1990], but they restrict the application of the coupled model to simulations of a general circulation similar to the modern one.

In order to reduce the excessive computing time required for running a synchronously coupled

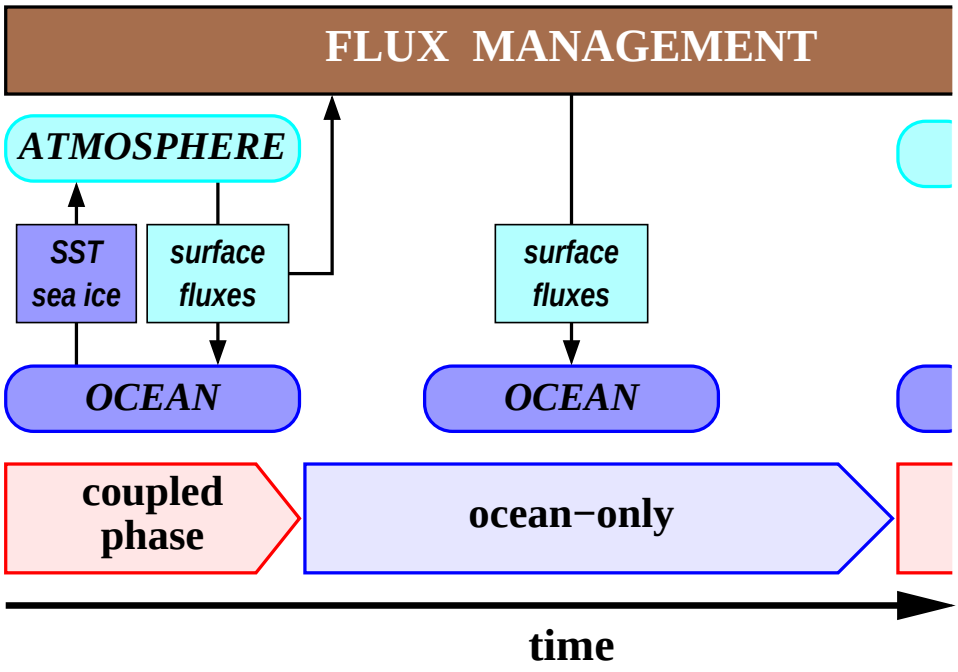

Figure A.1: *Scheme of the periodically-synchronous coupling method: Ocean forcing fluxes (annual cycle and annual mean of heat flux, fresh water flux and wind stress) are calculated during each synchronously coupled phase. These fluxes drive the ocean during the longer ocean-only phases.*

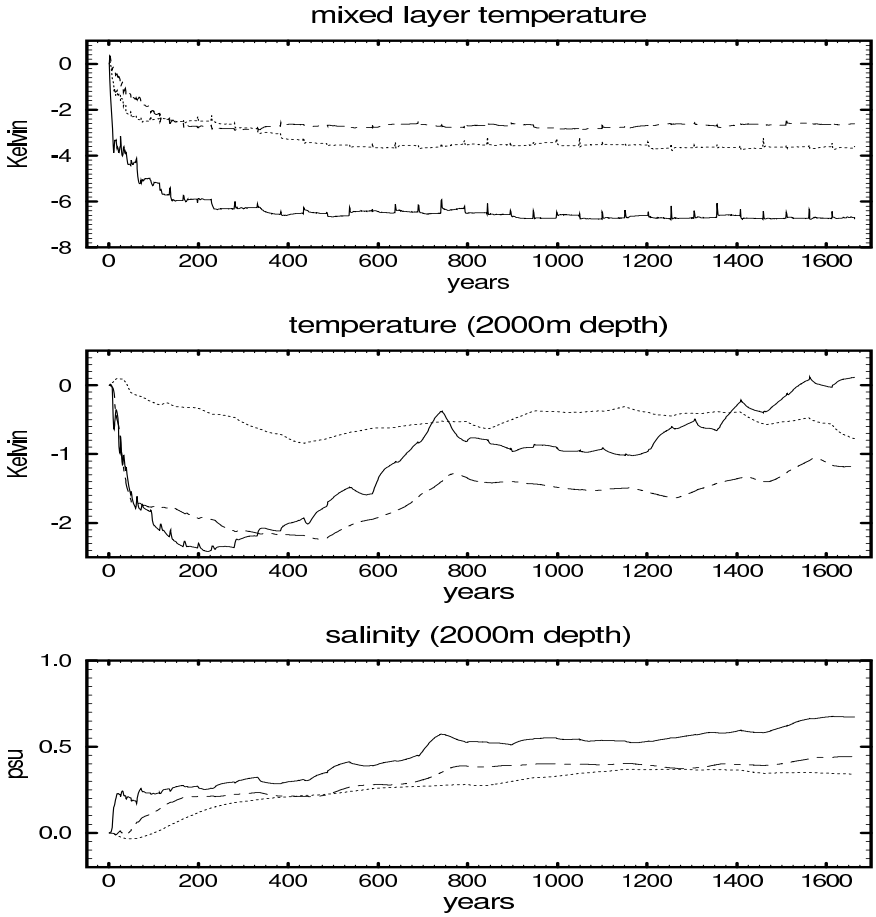

Figure A.2: *Time series of mean ocean temperature and salinity in the mixed layer (25 m depth) and at 2000 m depth of the North Atlantic Ocean (north of 30° N,* solid curve*), the central Atlantic between 30° N and 30° S (*dashed curve*) and the Southern Oceans south of 30° S (*dotted curve*). Shown are differences between the spinup ocean model run and an experiment with the periodically-synchronously coupled model simulating the recent climate without flux adjustments.*

model, the method of periodically-synchronous coupling, suggested by Gates [*Schlesinger*, 1979], has been applied to the coupled ECHAM-LSG model [*Cubasch et al.*, 1992; *Sausen and Voss*, 1996; *Voss and Sausen*, 1996]. Short periods of synchronous coupling alternate with long ocean-only periods. During the latter periods the ocean is forced by the surface boundary conditions generated during previous synchronously coupled periods (Fig. A.1). from a first long term experiment with the coupled model under modern boundary conditions. This run has been performed without flux adjustments over a simulation period of 1600 years with synchronously coupled periods of 15 months. During the first 230 years of simulation time the ocean-only phases were successively extended, starting with a length of 3 years at the beginning of the simulation, up to a length of 50 years. The time series of ocean layer temperatures (Fig. A.2) mark a strong drift of the model towards a cooler climate during the first 100 years of coupling, which is mainly the result of the different representation of surface fluxes in the submodels. The small peaks of the upper layer temperatures show the onsets of the synchronously coupled phases, when the atmosphere responds to the new distribution of SSTs and sea ice, which were calculated during the former ocean-only phase without feedback from the

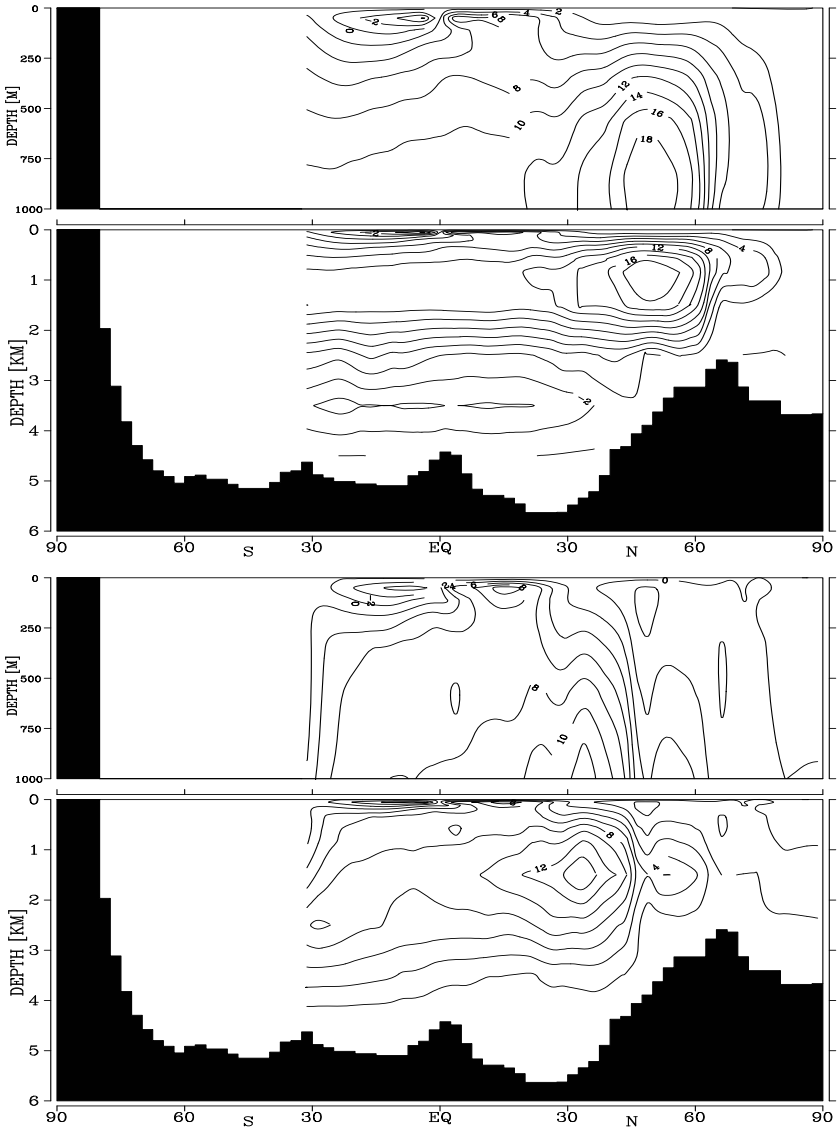

Figure A.3: *Atlantic Ocean meridional stream function (Sv) of ocean model spinup run after 4000 years of simulation time under restoring boundary conditions (*top*) and of the coupled model after 1600 years of periodically-synchronously coupled run, simulating the recent climate without flux adjustments (*bottom*).*

atmosphere model. The deep ocean temperatures and salinities (Fig. A.2) indicate that an equilibrium ocean circulation has not yet been reached. The meridional stream function of the ocean model spinup run (Fig. A.3, top) shows a reasonable circulation with formation of North Atlantic Deep Water and export into the Southern Ocean. The long term integration (over 1600 years) of the coupled model without flux adjustments exhibits also a conveyor-type thermohaline circulation, with a weaker formation of NADW but lacking any AABW (Fig. A.3, bottom).

This coupled model is now fast enough to perform a complete series of experiments with an integration time of several thousand model years for each run. The objective is to determine the required minimum flux adjustment which might be unavoidable to prevent this unrealistic climate drift. If an adjustment can be found which depends on systematic deficiencies of the model components but is mostly independent of the simulated climate, then the model is able to simulate paleoclimate states

like the LGM which may strongly deviate from the modern one. The resultant global data sets at the atmosphere-ocean interface would be a valuable contribution to CLIMAP 2000.

References

Cubasch, U., K. Hasselmann, H. Höck, E. Maier-Reimer, U. Mikolajewicz, B. D. Santer, and R. Sausen, Time-dependent greenhouse warming computations with a coupled ocean-atmosphere model, *Climate Dynamics*, *8*, 55–69, 1992.

Cubasch, U., B. D. Santer, A. Hellbach, G. Hegerl, H. Höck, E. Maier-Reimer, U. Mikolajewicz, A. Stössel, and R. Voss, Monte Carlo climate change forcasts with a global coupled ocean-atmosphere model, *Climate Dynamics*, *10*, 1–19, 1994.

Lunkeit, F., R. Sausen, and J. M. Oberhuber, Climate simulations with the global coupled atmosphere-ocean model ECHAM2/OPYC. Part I: present-day climate and ENSO events, *Climate Dynamics*, *12*, 195–212, 1996.

Manabe, S., and R. J. Stouffer, Multiple-century response of a coupled ocean-atmosphere model to an increase of the atmospheric carbon dioxide, *Journal of Climate*, *7*, 5–23, 1994.

Meehl, G. A., W. M. Washington, and T. R. Karl, Low-frequency variability and CO_2 transient climate change. Part 1. Time-averaged differences, *Climate Dynamics*, *8*, 117–133, 1993.

Murphy, J. M., Transient response of the Hadley centre coupled ocean-atmosphere model to increasing carbon dioxide. Part I: control climate and flux adjustment, *Journal of Climate*, *8*, 36–56, 1995.

Sausen, R., and F. Lunkeit, Some remarks on the cause of the climate drift of coupled ocean-atmosphere models, *Beitr. Phys. Atmosph.*, *63*, 141–146, 1990.

Sausen, R., and R. Voss, Techniques for asynchronous and periodically synchronous coupling of atmosphere and ocean models. Part I: general strategy and application to cyclo-stationary case, *Climate Dynamics*, *12*, 313–323, 1996.

Sausen, R., K. Barthel, and K. Hasselmann, Coupled ocean-atmosphere models with flux correction, *Climate Dynamics*, *2*, 145–163, 1988.

Schlesinger, M. E., Discussion of “A global ocean-atmosphere model with seasonal variation for future studies of climate sensitivity”, *Dynamics of Atmosphere and Oceans*, *3*, 427–432, 1979.

Voss, R., and R. Sausen, Techniques for asynchronous and periodically synchronous coupling of atmosphere and ocean models. Part II: impact of variability, *Climate Dynamics*, *12*, 605–614, 1996.

Danksagung

Meinen besonderen Dank möchte ich Herrn Prof. Dr. Gerrit Lohmann ausprechen für seine unermüdliche Gesprächsbereitschaft und hervorragende Betreuung während meiner Arbeit. Sein Vertrauen, seine Zuversicht und Ermutigung waren mir von unschätzbaren Wert und haben erheblich zum Erfolg dieser Arbeit beigetragen.

Herrn Prof. Dr. Martin Claußen danke ich für die Möglichkeit, die Dissertation in Hamburg einzureichen und für seine Bereitschaft, die Begutachtung der Dissertation zu übernehmen sowie für sein Interesse an meiner Arbeit. Den Teilnehmern des Prüfungsausschusses möchte ich für Ihre Arbeit danken.

Einen speziellen Dank möchte ich an Herrn Prof. Dr. Klaus Herterich richten, der mit seinem Vertrauen in mich die Grundlagen für diese Arbeit geschaffen hat.

Herrn Prof. Dr. Klaus Fraedrich danke ich für die interessante Arbeitsumgebung und für seine Unterstützung, die Arbeit abschliessen zu können.

Für die vielen Anregungen, Ermutigungen und Gespräche mit vielen Kollegen möchte ich mich hiermit bedanken, insbesondere bei Dr. Ute Merkel, Dr. Gregor Knorr, Prof. Dr. Axel Timmermann und Dr. Richard Blender. Außerdem habe ich immer wieder Unterstützung von Freunden und Kollegen erfahren, die einen wichtigen Beitrag zum Erfolg der Arbeit, gerade auch in schwierigen Zeiten, geleistet haben. Für ihre Geduld und ihr Verständnis bedanke ich mich sehr herzlich.

Publikationsreihe des MPI-M
„Berichte zur Erdsystemforschung“ , „*Reports on Earth System Science*“, ISSN 1614-1199
Sie enthält wissenschaftliche und technische Beiträge, inklusive Dissertationen.

Berichte zur Erdsystemforschung Nr.1 Juli 2004	**Simulation of Low-Frequency Climate Variability in the North Atlantic Ocean and the Arctic** Helmuth Haak
Berichte zur Erdsystemforschung Nr.2 Juli 2004	**Satellitenfernerkundung des Emissionsvermögens von Landoberflächen im Mikrowellenbereich** Claudia Wunram
Berichte zur Erdsystemforschung Nr.3 Juli 2004	**A Multi-Actor Dynamic Integrated Assessment Model (MADIAM)** Michael Weber
Berichte zur Erdsystemforschung Nr.4 November 2004	**The Impact of International Greenhouse Gas Emissions Reduction on Indonesia** Armi Susandi
Berichte zur Erdsystemforschung Nr.5 Januar 2005	**Proceedings of the first HyCARE meeting, Hamburg, 16-17 December 2004** Edited by Martin G. Schultz
Berichte zur Erdsystemforschung Nr.6 Januar 2005	**Mechanisms and Predictability of North Atlantic - European Climate** Holger Pohlmann
Berichte zur Erdsystemforschung Nr.7 November 2004	**Interannual and Decadal Variability in the Air-Sea Exchange of CO2 - a Model Study** Patrick Wetzel
Berichte zur Erdsystemforschung Nr.8 Dezember 2004	**Interannual Climate Variability in the Tropical Indian Ocean: A Study with a Hierarchy of Coupled General Circulation Models** Astrid Baquero Bernal
Berichte zur Erdsystemforschung Nr9 Februar 2005	**Towards the Assessment of the Aerosol Radiative Effects, A Global Modelling Approach** Philip Stier
Berichte zur Erdsystemforschung Nr.10 März 2005	**Validation of the hydrological cycle of ERA40** Stefan Hagemann, Klaus Arpe and Lennart Bengtsson
Berichte zur Erdsystemforschung Nr.11 Februar 2005	**Tropical Pacific/Atlantic Climate Variability and the Subtropical-Tropical Cells** Katja Lohmann
Berichte zur Erdsystemforschung Nr.12 Juli 2005	**Sea Ice Export through Fram Strait: Variability and Interactions with Climate**- Torben Königk
Berichte zur Erdsystemforschung Nr.13 August 2005	**Global oceanic heat and fresh water forcing datasets based on ERA-40 and ERA-15** Frank Röske
Berichte zur Erdsystemforschung Nr.14 August 2005	**The** HAM**burg** O**cean** C**arbon** C**ycle Model HAMOCC5.1 - Technical Description Release 1.1** Ernst Maier-Reimer, Iris Kriest, Joachim Segschneider, Patrick Wetzel
Berichte zur Erdsystemforschung Nr.15 Juli 2005	**Long-range Atmospheric Transport and Total Environmental Fate of Persistent Organic Pollutants - A Study using a General Circulation Model** Semeena Valiyaveetil Shamsudheen

Publikationsreihe des MPI-M
„Berichte zur Erdsystemforschung“ , „*Reports on Earth System Science*“, ISSN 1614-1199
Sie enthält wissenschaftliche und technische Beiträge, inklusive Dissertationen.

Publikationsreihe des MPI-M
„Berichte zur Erdsystemforschung“ , „*Reports on Earth System Science*“, ISSN 1614-1199
Sie enthält wissenschaftliche und technische Beiträge, inklusive Dissertationen.

Berichte zur Erdsystemforschung Nr.30 November 2006	**Long-term interactions between ice sheets and climate under anthropogenic greenhouse forcing Simulations with two complex Earth System Models** Miren Vizcaino
Berichte zur Erdsystemforschung Nr.31 November 2006	**Effect of Daily Surface Flux Anomalies on the Time-Mean Oceanic Circulation** Balan Sarojini Beena
Berichte zur Erdsystemforschung Nr.32 November 2006	**Managing the Transition to Hydrogen and Fuel Cell Vehicles – Insights from Agent-based and Evolutionary Models –** Malte Schwoon
Berichte zur Erdsystemforschung Nr.33 November 2006	**Modeling the economic impacts of changes in thermohaline circulation with an emphasis on the Barents Sea fisheries** Peter Michael Link
Berichte zur Erdsystemforschung Nr.34 November 2006	**Indirect Aerosol Effects Observed from Space** Olaf Krüger
Berichte zur Erdsystemforschung Nr.35 Dezember 2006	**Climatological analysis of planetary wave propagation in Northern Hemisphere winter** Qian Li
Berichte zur Erdsystemforschung Nr.36 Dezember 2006	**Ocean Tides and the Earth’s Rotation - Results of a High-Resolving Ocean Model forced by the Lunisolar Tidal Potential** Philipp Weis
Berichte zur Erdsystemforschung Nr.37 Dezember 2006	**Modelling the Global Dynamics of Rain-fed and Irrigated Croplands** Maik Heistermann
Berichte zur Erdsystemforschung Nr.38 Dezember 2006	**Monitoring and detecting changes in the meridional overturning circulation at 26°N in the Atlantic Ocean- The simulation of an observing array in numerical models** Johanna Baehr
Berichte zur Erdsystemforschung Nr.39 Februar 2007	**Low Frequency Variability of the Meridional Overturning Circulation** Xiuhua Zhu
Berichte zur Erdsystemforschung Nr.40 März 2007	**Aggregated Carbon Cycle, Atmospheric Chemistry, and Climate Model (ACC2) – Description of the forward and inverse modes –** Katsumasa Tanaka, Elmar Kriegler
Berichte zur Erdsystemforschung Nr.41 März 2007	**Climate Change and Global Land-Use Patterns — Quantifying the Human Impact on the Terrestrial Biosphere** Christoph Müller
Berichte zur Erdsystemforschung Nr.42 April 2007	**A Subgrid Glacier Parameterisation for Use in Regional Climate Modelling** Sven Kotlarski



ISSN 1614-1199